Systematic Synthesis of Multicyclic Polystyrenes toward Understanding Topology–property Relationship

A Dissertation for the Degree of Doctor of Philosophy

Yamato Ebii

Hokkaido University

March, 2026

Acknowledgements

The study presented in this dissertation has been performed under the direction of Professor Toshifumi Satoh, Division of Applied Chemistry, Faculty of Engineering, Hokkaido University, from 2021 to 2025. The author wishes to express his sincere gratitude to Professor Toshifumi Satoh for his kind instruction, helpful advice, and unstinting encouragement throughout the course of this work.

The author is also deeply grateful to Associate Professor Takuya Isono, Associate Professor Kenji Tajima, Associate Professor Takuya Yamamoto, Assistant Professor Feng Li, and Specially Appointed Assistant Professor Tianle Gao. Division of Applied Chemistry, Faculty of Engineering, Hokkaido University, for their helpful and valuable suggestions with continuous encouragement throughout this work.

The author also would like to show my deep appreciation to Professor Tetsuo

Deguchi, Department of Physics, Faculty of Core Research, Ochanomizu University, for the collaborative works, in which the broad insights for understanding polymer properties were provided.

The author is further indebted to Drs. Yoshinobu Mato and Tomohisa Watanabe, and Ryota Suzuki for their patient teaching and fruitful daily discussion. The author thanks all of the members of Professor Satoh's group.

The author is very grateful to the Hokkaido University DX Doctoral Fellowship during 2023–2024 and the Research Fellowships of the Japan Society for the Promotion of Science (JSPS) for Young Scientists during 2024–2025.

Finally, the author would like to express his utmost gratitude to family for their understanding, support, and continuous encouragement throughout his research and daily life.

March, 2026 Yamato Ebii

Contents

Chapter 1

General Introduction

1.1 Polymer topology

Precise architectural control of polymer molecules has long been one of the central challenges in synthetic polymer chemistry, as the creation of novel polymer topologies offers great potential to endow polymeric materials with unique physical properties and functions. Historically, the molecular architectures of synthetic polymers were largely limited to linear or randomly branched topologies. However, with the advent of advanced synthetic methodologies, particularly living polymerization techniques and highly efficient coupling reactions, a broad variety of topologically distinct polymers, including star-shaped, graft, and cyclic polymers, have been successfully synthesized over the past few decades (**Figure 1.1**).[1] These advances have not only provided fundamental insights into polymer chemistry and physics but have also created unprecedented opportunities to tailor macroscopic properties and functions through precise control of molecular topology.

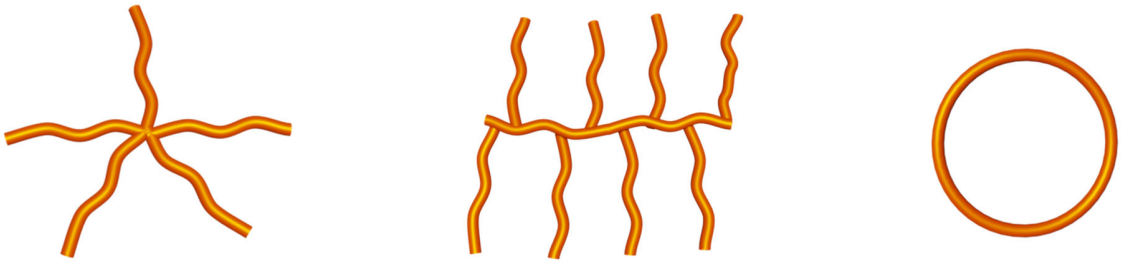

Figure 1.1. Schematic representations of polymer topologies: (a) star, (b) graft, and (c) cyclic architectures.

Cyclic polymers, characterized by a closed-ring molecular architecture, exhibit properties that are fundamentally distinct from those of their linear counterparts. The earliest synthetic cyclic species were detected only as minor oligomeric byproducts formed during step-growth polymerizations, and were regarded primarily as subjects of academic curiosity at that time.[2–4] This was largely due to the inherent difficulties associated with their large-scale synthesis and precise purification, which hindered systematic investigations for decades. Over the past few years, however, various cyclic biomacromolecules have been identified, revealing that their unique topologies confer remarkable thermal and chemical stability as well as strong intramolecular interactions.[5–9] These findings have highlighted that cyclic architectures are not merely of theoretical interest but can also serve as powerful design frameworks for developing advanced functional materials. Furthermore, the advent of living polymerization techniques and the progress in end-group transformation chemistry have enabled the efficient synthesis of structurally well-defined cyclic polymers. More recently, growing attention has also been directed toward industrial applications, where the unique structural features and physical properties of cyclic polymers are being actively exploited for the development of advanced functional materials.[10–12]

Against this background, growing attention has been directed toward the synthesis of multicyclic polymers, which possess multiple cyclic units within a single macromolecular architecture. Multicyclic polymers are generally classified into three types based on the structures of their main rings, branching points, and bridges. Specifically, they can be categorized as fused-type (e.g., θ-shaped), bridged-type (e.g., manacle-shaped), and spiro-type (e.g., figure-8-shaped) topologies, each exhibiting distinct physical properties (**Figure 1.2**). For fused- and spiro-type cyclic polymers, variations in cyclic topology have been shown to exert a

pronounced influence on their physical properties, including hydrodynamic volume, melting temperature, and critical micelle concentration.[13–15] These multicyclic architectures are also promising as design platforms for advanced functional materials. In addition, the use of entanglement structures, in which linear chains penetrate into cyclic chains, has been proposed as an additive to modify bulk material properties (**Figure 1.3**). Such applications are beyond the reach of conventional low-molecular-weight (multi)cyclic compounds.

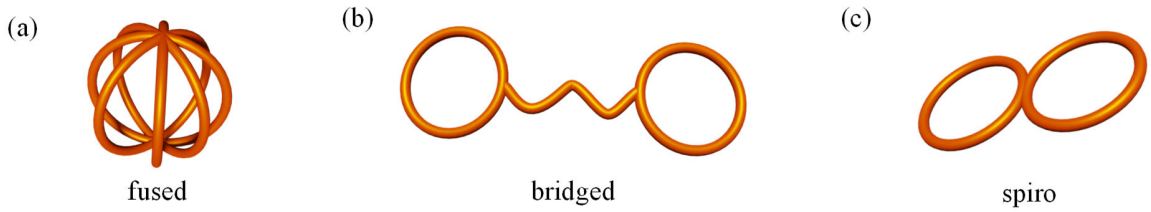

Figure 1.2. Examples of diverse multicyclic topologies.

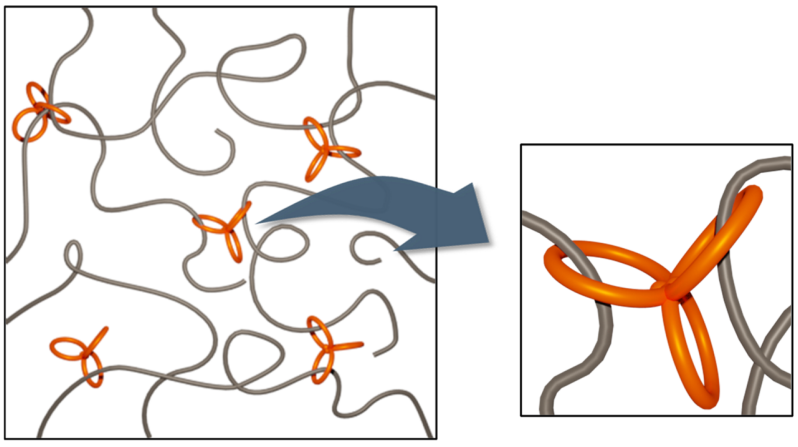

Figure 1.3. Potential applications of multicyclic polymers. Multicyclic polymers could serve as additives for tuning bulk material properties by exploiting the entanglement structure formed through the penetration of linear chains into cyclic chains, as illustrated in the inset.

1.2 Synthesis of monocyclic polymers

The earliest synthetic approaches to monocyclic polymers relied on the ring–chain equilibrium of poly(dimethylsiloxane) (PDMS) and related polyester, where small amounts of cyclic species were generated together with linear chains.[2–4] Although these methods allowed the first experimental studies of cyclic polymer properties, their applicability was limited by low efficiency and poor structural precision. Subsequent breakthroughs in polymer synthesis, most notably the advent of living polymerization techniques and advances in end-group transformation and coupling chemistry, enabled the deliberate construction of structurally well-defined cyclic polymers with minimal linear impurities. Today, well-defined monocyclic polymers are generally synthesized via (a) ring-closure reactions, (b) ring-expansion polymerization, or (c) topology transformation (**Figure 1.4**).

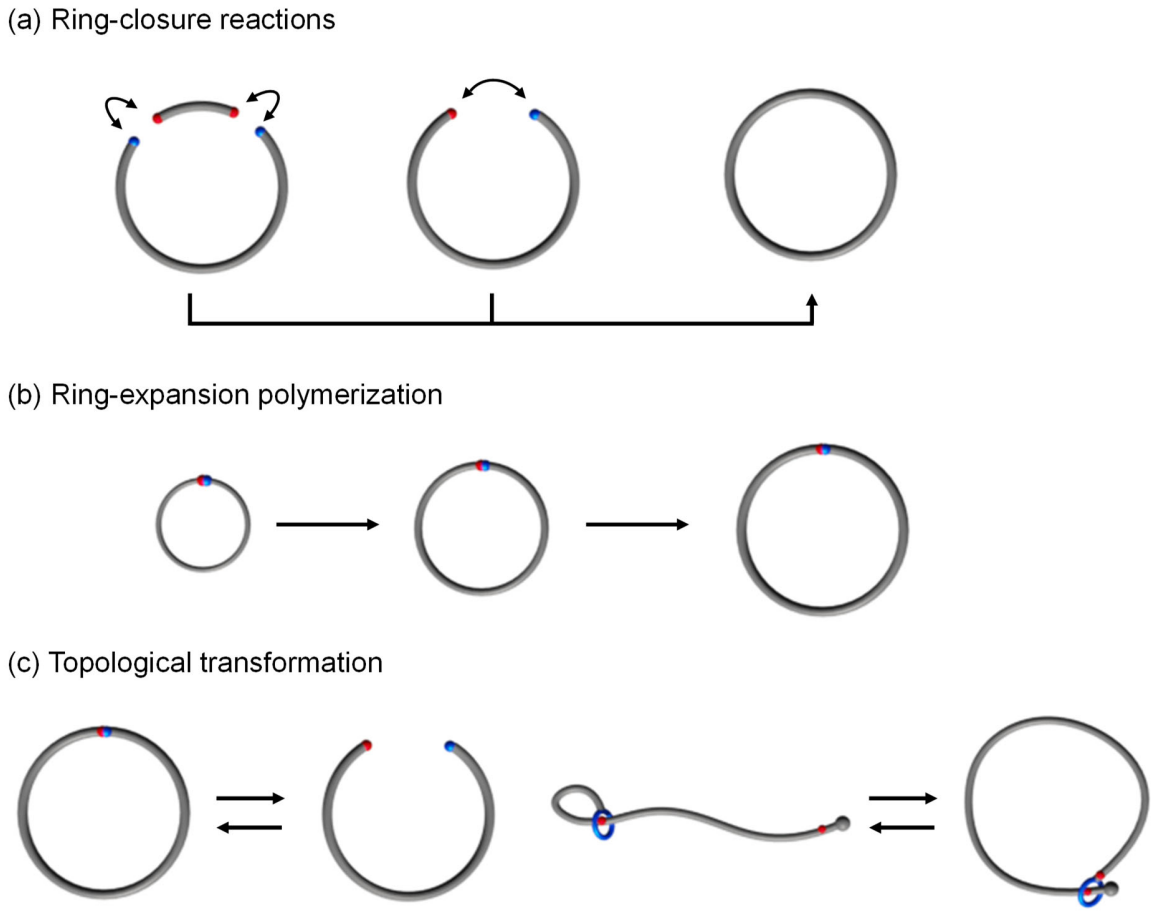

Figure 1.4. Synthetic pathways to monocyclic polymers via (a) ring-closure reactions, (b) ring-expansion polymerization, and (c) topological transformations

The ring-closure reaction represents the most fundamental and straightforward synthetic strategy for the preparation of monocyclic polymers. This approach can be broadly classified into bimolecular ring-closure and unimolecular ring-closure processes. In either case, dilute conditions are essential to preferentially promote intramolecular cyclization over intermolecular coupling. In bimolecular ring-closure, a selective intermolecular coupling reaction occurs between the polymer chain end and a bifunctional linker, leading to the formation of a cyclic structure. For the representative example, Hocker et al. synthesized monocyclic polystyrene (PS) by combining anionic polymerization with a bimolecular coupling reaction using dichloro-*p*-xylene as the coupling agent (**Scheme 1.1a**).[16] Sun et al. developed a novel bimolecular ring-closure pathway based on the double strain-promoted azide–alkyne click (DSPAAC) reaction and reported an efficient method for synthesizing monocyclic PS with a narrow molecular weight distribution (**Scheme 1.1b**).[17] In this approach, a linear PS precursor bearing *α*,*ω*-diazide termini was first prepared via atom transfer radical polymerization (ATRP) of styrene followed by end-group transformation. Subsequent reaction of this precursor with sym-dibenzo-1,5-cyclooctadiene-3,7-diyne (DBA) enabled intramolecular cyclization through the DSPAAC reaction under ambient conditions.

Scheme 1.1. Synthesis of cyclic polymers via intermolecular cyclization, based on bimolecular coupling

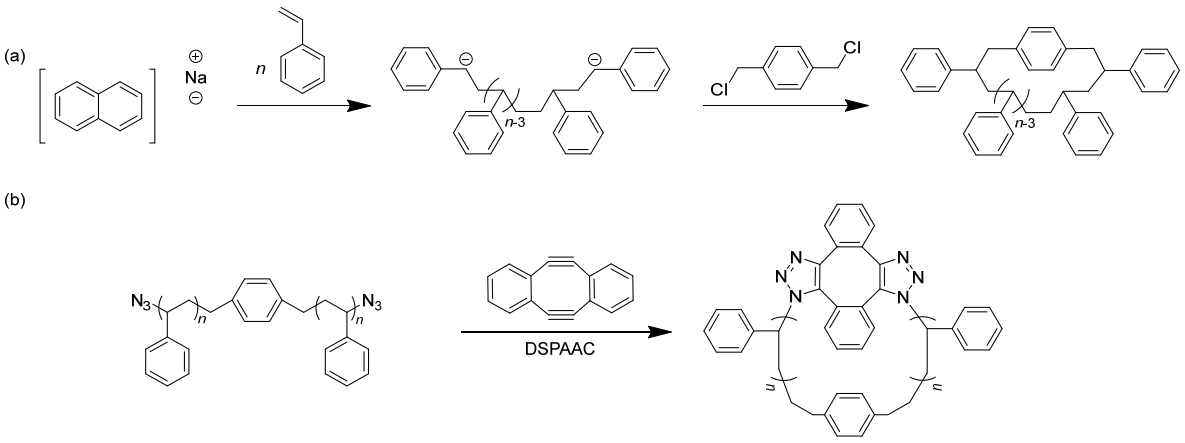

Meanwhile, unimolecular ring-closure reactions (i.e., intramolecular cyclization) have also been widely employed for the synthesis of monocyclic polymers. In numerous studies, highly efficient click reactions have been utilized to construct monocyclic polymer architectures. Grayson et al. demonstrated the synthesis of monocyclic PS by intramolecular cyclization of a linear PS bearing α-ethynyl and ω-azide end groups under Cu-catalyzed azide–alkyne cycloaddition (CuAAC) conditions (**Scheme 1.2**).[18] This approach is now widely recognized as one of the most reliable strategies for the ring-closure of polymers. The CuAAC reaction offers several advantages, including quantitative yields, excellent functional group tolerance, and mild reaction conditions. These characteristics make it particularly well-suited for the efficient intramolecular cyclization of polymer chains without inducing undesired side reactions. However, the possible contamination of the resulting polymers with residual copper catalyst has raised concerns, particularly in applications that require metal-free or highly purified materials. In consideration of the potential toxicity of copper catalysts, various alternative click reactions

have been explored for cyclization as substitutes for CuAAC. As one representative example, Tang et al. developed a light-triggered, catalyst-free ring-closure strategy based on a light-induced Diels–Alder click reaction to achieve rapid and efficient formation of high-purity cyclic PS under mild conditions (Scheme 1.2b).[19]

Scheme 1.2. Synthesis of monocyclic polymers via intramolecular cyclization based on (a) CuAAC reaction and (b) light-induced Diels–Alder click reaction

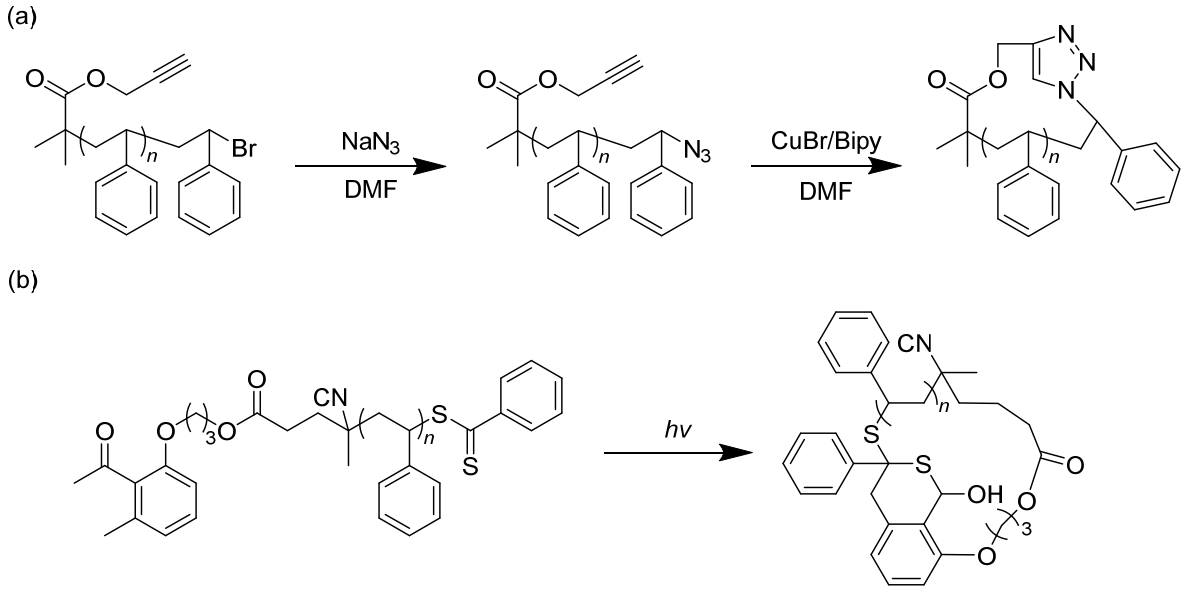

Ring-expansion polymerization is another efficient approach for the synthesis of monocyclic polymers. In early studies, Lee et al. demonstrated that ring-opening polymerization of lactones initiated by cyclic tin alkoxide catalysts afforded monocyclic polyesters, as illustrated in **Scheme 1.3a**.[20] Grubbs et al. reported the synthesis of high-molecular-weight monocyclic polybutadiene from 1,5-cyclooctadiene via ring-expansion metathesis polymerization (REMP) using a ruthenium-based metathesis catalyst.[21] In this mechanism,

successive insertion of monomer units into a cyclic initiator takes place, followed by catalyst elimination through a backbiting process, ultimately yielding a cyclic polymer (Scheme 1.3b). During the ring-expansion process, the cyclic topology of the growing polymer chain is preserved throughout the reaction, allowing REMP to proceed without the need for high-dilution conditions. Consequently, this method enables the efficient synthesis of cyclic polymers over a wide molecular-weight range, even in concentrated solutions or under bulk conditions. In addition to the REMP methodology, several new approaches utilizing ring-expansion processes have recently been proposed for the synthesis of cyclic polymers. Representative examples include the zwitterionic polymerization of lactide initiated by *N*-heterocyclic carbenes reported by Waymouth et al.[22] and the γ-ray-induced radical polymerization of methyl acrylate developed by Pan et al.[23]

Scheme 1.3. Synthesis of monocyclic polymers by (a) tin-catalyzed ring-expansion polymerization of the lactone and (b) ruthenium-catalyzed REMP of cycloalkene.

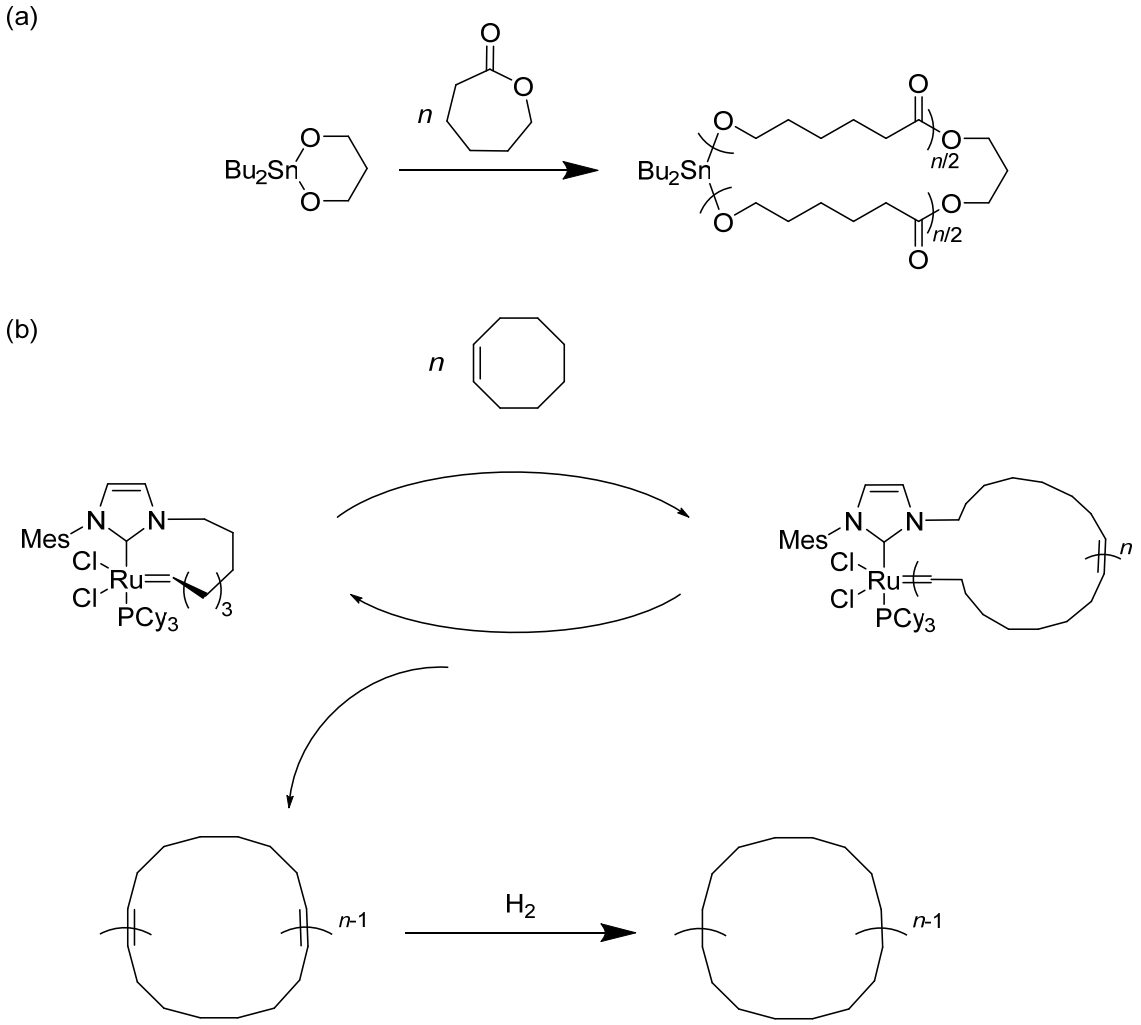

In addition to the aforementioned synthetic routes, topology transformation systems, which enable the conversion from linear to cyclic topologies, have also attracted significant attention owing to their potential applications in stimuli-responsive polymers and for elucidating structure–property relationships. The general concept of a topology transformation system is based on the design principle that polymer segments are connected via reversible linkages, allowing efficient assembly and disassembly processes. By introducing thermoresponsive, photoresponsive, or redox-active functional groups into polymer chains, external stimuli can trigger topological interconversion, providing a versatile platform to investigate dynamic covalent chemistry and polymer topology control. A representative example is the reversible topology transformation system developed by Yamamoto et al., which is based on the photodimerization of anthracene moieties.[24] They synthesized telechelic linear polymers bearing anthryl end groups at both chain termini and subjected them to UV irradiation under highly dilute conditions to induce intramolecular [4+4] photocycloaddition, thereby affording the corresponding cyclic polymers (**Scheme 1.4a**). The resultant cyclic polymers could be quantitatively converted back to their linear precursors upon heating at approximately 150 °C, owing to the thermal cleavage of the anthracene dimer. Over the past two decades, the concept of topology transformation systems has been extended to rotaxane chemistry. Takata et al. demonstrated a rotaxane-driven topology transformation in which *N*-acetylation of the terminal ammonium group suppressed the ammonium–crown ether interaction and induced the migration of the crown ether wheel to the carbamate station, thereby converting linear polymer into its cyclic analogue (Scheme 1.4b).[25] In summary, a variety of synthetic strategies have been established for the precise preparation of monocyclic polymers, including ring-closure reactions, ring-expansion polymerizations, and topology transformation systems. In recent years, the

development of diverse synthetic approaches has greatly broadened the range of polymer backbones amenable to cyclization, encompassing a wide variety of monomer types and compositions.

Scheme 1.4. Synthesis of monocyclic polymers via topology transformation based on (a) anthracene and (b) rotaxane chemistries

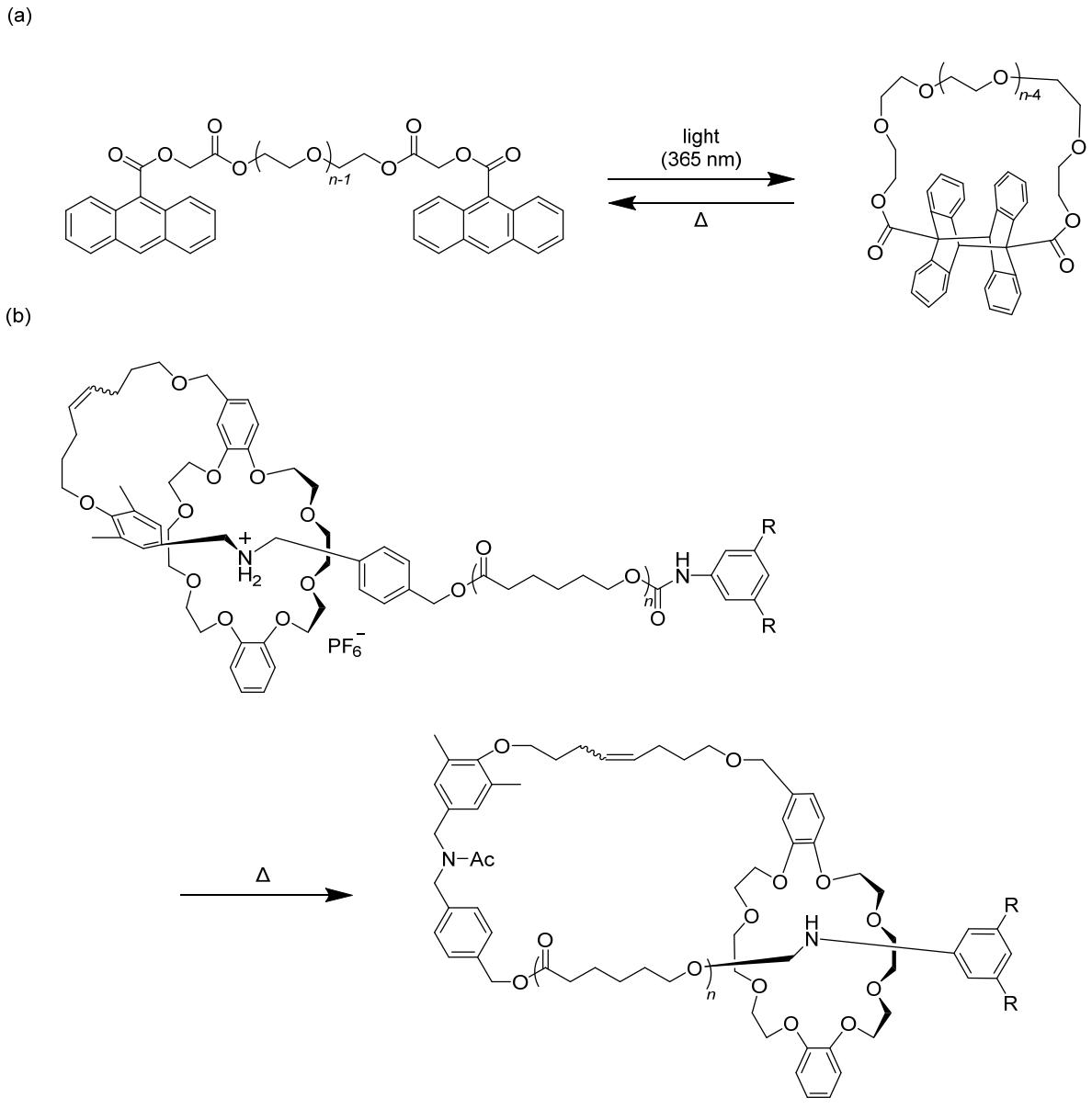

1.3 Synthesis of multicyclic polymers

As the precise synthesis of monocyclic polymers has been achieved, increasing attention has been directed toward the synthesis of multicyclic polymers, which feature more complex topological architectures. Among the various synthetic methodologies developed for monocyclic polymers, as discussed in the previous section, highly efficient and selective ring-closure reactions have been most widely employed for the synthesis of multicyclic polymers. This is because the strategy of connecting reactive functional groups located within a single macromolecule provides the most straightforward and direct approach to constructing complex multicyclic architectures. On the other hand, other synthetic approaches such as ring-expansion polymerization and topology transformation have rarely been employed for the general synthesis of multicyclic polymers, mainly because the synthesis of specifically designed initiators or catalysts is often challenging and the range of applicable monomers remains limited.[20,26,27] To date, several synthetic routes have been developed for the construction of multicyclic polymers, which can be broadly categorized into three representative strategies (**Schemes 1.5–1.7**): (i) intermolecular coupling of monocyclic constituents, (ii) intermolecular cyclization of linear or star-shaped polymers using multifunctional linkers, and (iii) intramolecular cyclization of linear or star-shaped polymer precursors bearing functional groups at predetermined positions.

Strategy (i), namely the direct linking of functionalized monocyclic polymers, represents one of the most straightforward and direct approaches for constructing multicyclic polymer architectures. However, the efficient synthesis of multicyclic polymers requires highly efficient and selective covalent bond-forming reactions. In this regard, the CuAAC click reaction has proven to be an extremely powerful and widely used chemical tool for the

interconnection of multiple polymer chains. Through intermolecular coupling of monocyclic precursors via the CuAAC reaction, various multicyclic polymers, such as figure-8-shaped, trefoil-shaped, quatrefoil-foil-shaped, and even more complex architectures, have been successfully synthesized.[28–30] For example, figure-8-shaped polymers can be obtained by CuAAC coupling between azide-functionalized and ethynyl-functionalized monocyclic polymers, while trefoil-shaped polymers are produced through the CuAAC reaction of monocyclic polymers bearing azide and diethynyl functional groups, respectively (**Scheme 1.5a**).[28] Despite these achievements, several challenges remain. The synthesis of appropriately functionalized monocyclic precursors typically involves multiple synthetic steps, often resulting in overall low yields. Furthermore, Monteiro et al. reported that stepwise CuAAC polymerization of bifunctional monocyclic PS bearing both azide and ethynyl termini enabled the formation of multicyclic polymers containing up to 20 cyclic units (Scheme 1.5b).[31] Nevertheless, this method still requires complex and time-consuming procedures, and suffers from poor control over the number of cyclic units, owing to the step-growth nature of the polymerization, which leads to broad distributions in the number of ring units.

Scheme 1.5. Synthesis of multicyclic polymers via intermolecular coupling of monocyclic constituents based on CuAAC click reaction

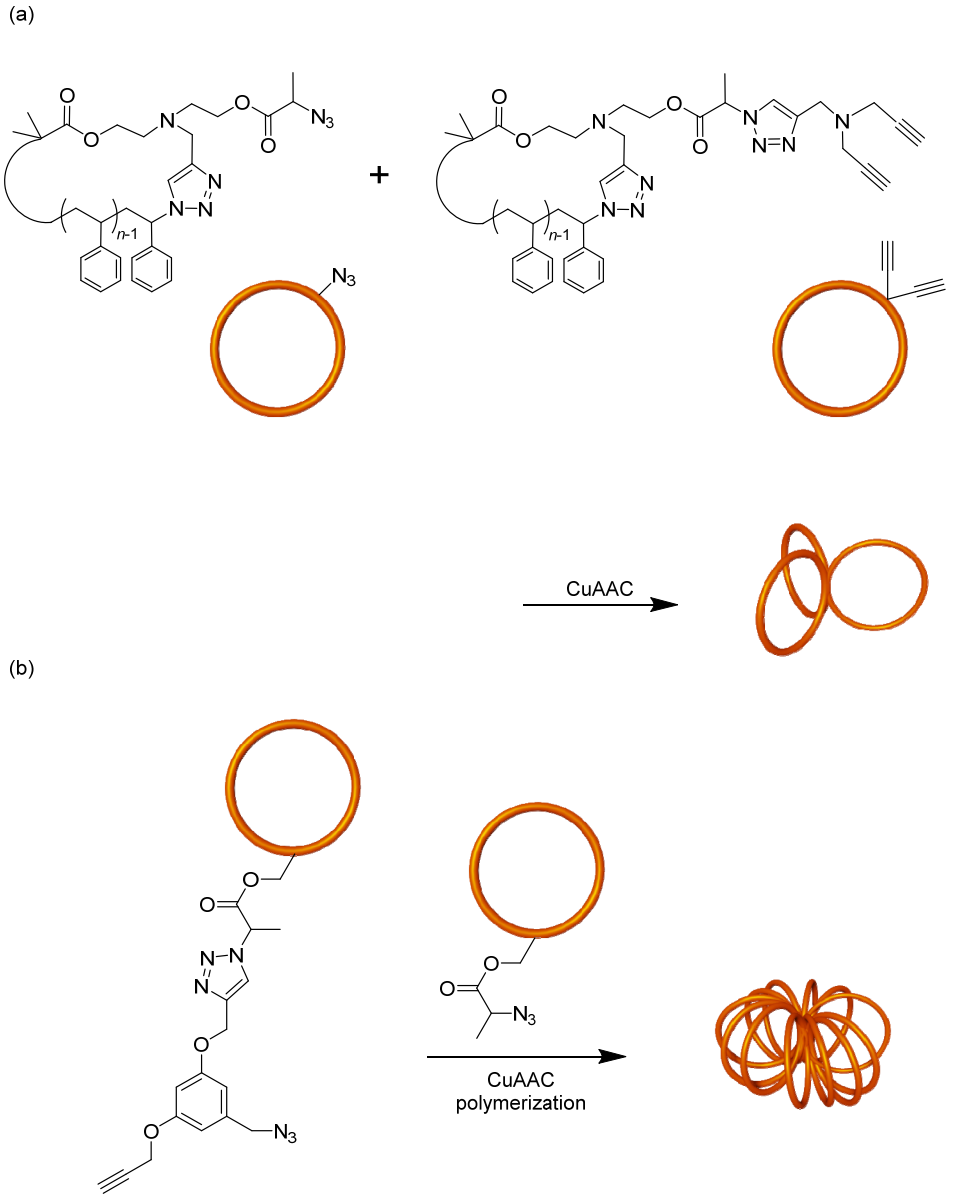

The end-to-end coupling reaction between functionalized linear polymer precursors and coupling agents (strategy (ii)) has also been employed to construct multicyclic polymer architecture. For example, figure-8-shaped multicyclic polymers have been synthesized by the CuAAC click reaction between azide-functionalized star-shaped polymers and ethynyl-functionalized linkers (**Scheme 1.6a**).[32] Furthermore, Tezuka et al. developed an efficient method for the synthesis of multicyclic polymers via electrostatic self-assembly and covalent fixation (ESA-CF) (Scheme 1.6b).[30,33,34] In this approach, electrostatic self-assembly first occurs between telechelic precursors bearing cyclic ammonium salt groups and multifunctional carboxylate anions. Subsequent ring-opening or ring-releasing reactions of the cyclic ammonium groups, triggered by the counter carboxylate anions, lead to covalent fixation of the assembled structure. Notably, this methodology enables the high-yield synthesis of multicyclic polymers with diverse topological architectures. However, because these strategies generally require a custom-made precursor to construct each specific topology, their application to the synthesis of multicyclic polymers containing a larger number of cyclic units remains challenging.

Scheme 1.6. Synthesis of multicyclic polymers via intermolecular cyclization of linear or star-shaped polymers using multifunctional linkers based on (a) CuAAC click reaction and (b) ESA-CF protocol

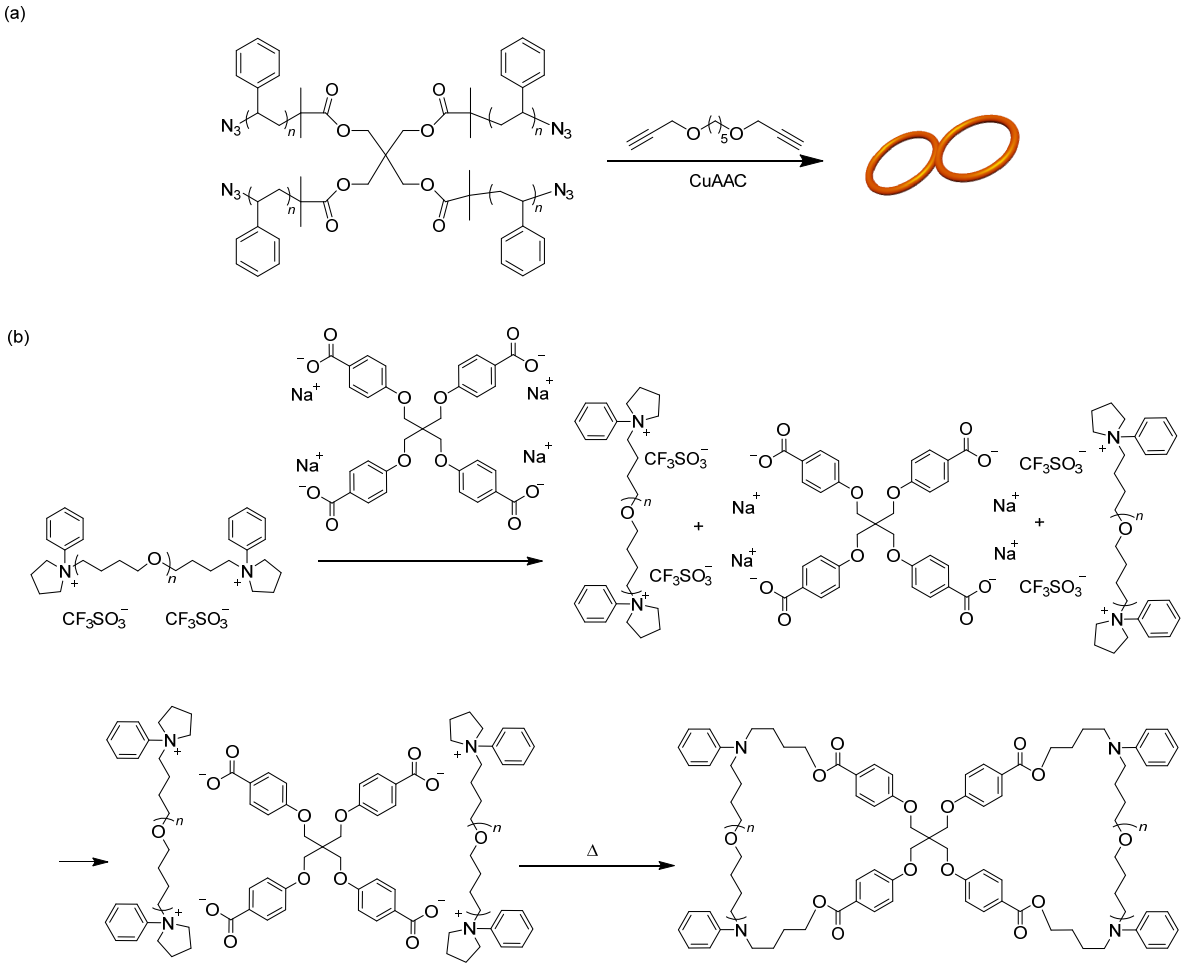

The intramolecular cyclization of linear or star-shaped polymer precursors bearing functional groups at predetermined positions (strategy (iii)) is also an effective approach for the synthesis of multicyclic polymers. For example, figure-8-shaped multicyclic polymers can be synthesized by performing a CuAAC click reaction on a linear polymer containing two ethynyl groups at the center and azide groups at both chain ends (**Scheme 1.7a**).[35] Furthermore, Satoh et al. reported the synthesis of trefoil-shaped and quatrefoil-shaped multicyclic polymers via intramolecular cyclization, followed by topological transformation into three-armed and four-armed cage-like polymers, respectively, through selective hydrogenolysis of the benzyl ether junctions (Scheme 1.7b).[13] The same group also synthesized figure-8-, trefoil-, and quatrefoil-shaped multicyclic polymers via the ring-opening metathesis oligomerization (ROMO) of PCL bearing norbornenyl groups at the chain center and at each end (Scheme 1.7c).[15] This strategy enabled the facile synthesis of multicyclic polymers evidenced by narrow dispersity ($Đ < 1.1$). Despite these advances, all of these approaches share a common limitation: the molecular design required to introduce different functional groups at specific positions within linear or star-shaped precursors is highly complex and synthetically demanding.

As discussed above, current synthetic routes toward multicyclic polymers often involve elaborate molecular design and challenging precursor synthesis, which has limited the number of systematic studies on the fundamental physical properties arising from multicyclic topologies. Therefore, the development of new cyclization methodologies that are simple, efficient, and broadly applicable, based on novel reaction mechanisms, remains a critical challenge for the future synthesis of multicyclic polymers.

Scheme 1.7. Synthesis of multicyclic polymers via intramolecular cyclization of linear/star polymer precursors based on (a–b) CuAAC click reaction and (c) ROMO

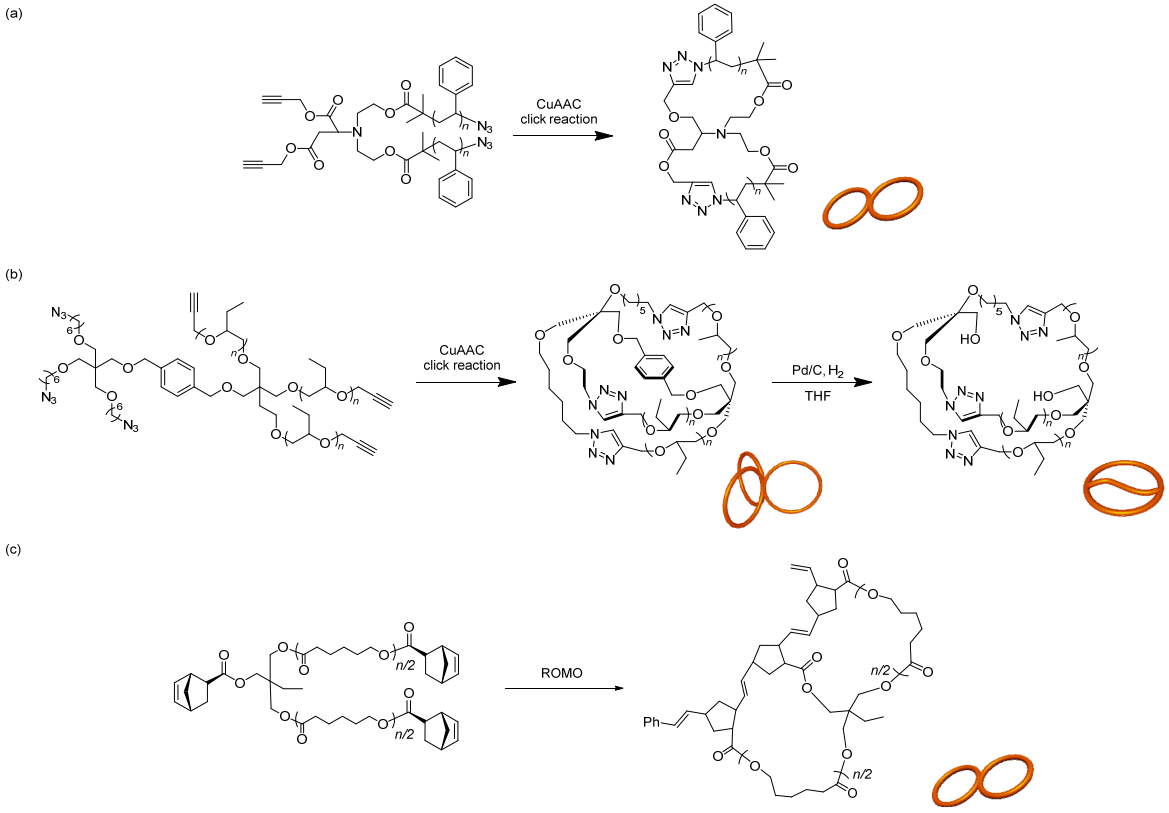

Recently, Satoh et al. established a robust and versatile synthetic route to multicyclic polymers.[36,37] They obtained well-defined multicyclic polymers through cyclopolymerization based on ring-opening metathesis polymerization (ROMP), employing α,ω-norbornenyl-terminated bifunctional linear macromonomers as precursors (**Figure 1.5**). In contrast to conventional multicyclic polymer syntheses, which rely on the stepwise coupling of cyclic units, this method enables the sequential formation of multiple rings in a chain-growth manner. Under dilute conditions, intramolecular cyclization proceeds preferentially and rapidly compared with intermolecular propagation, thereby realizing efficient cyclopolymerization. In this approach, the number of cyclic units in the resulting multicyclic polymer can be readily controlled by simply adjusting the initial feed ratio $[\text{macromonomer}]_0/[\text{G3}]_0$. Moreover, by varying the molecular weight (i.e., ring size) of the macromonomer, the size of each cyclic unit can be independently designed. Notably, this method requires only a norbornenyl group as the reactive site, making the precursor synthesis simple and scalable. These features render this methodology particularly valuable for the systematic investigation of topology–property relationships in multicyclic polymers.

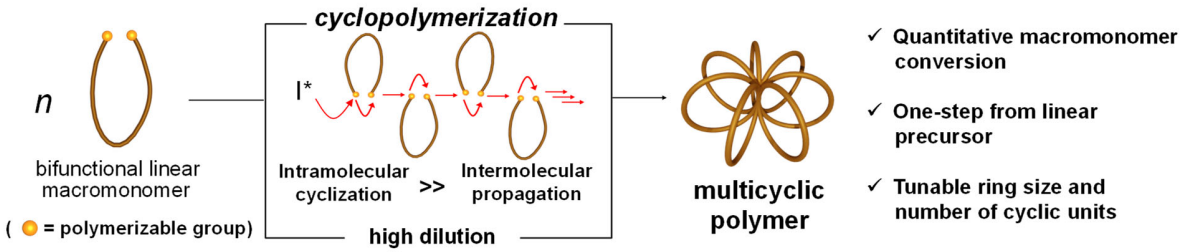

Figure 1.5. Synthesis of multicyclic polymers via cyclopolymerization.

1.4 Influence of polymer topology on physical properties

Polymer topology exerts a profound influence on the physical properties of polymers by altering chain conformation, segmental dynamics, and intermolecular interactions. Understanding these effects is of great importance, as molecular topology provides a direct structural means to precisely control macroscopic properties, such as viscosity, T_g, and mechanical strength, without changing the chemical composition of the polymer.[1] Such insights enable materials design through architectural control, rather than by simple compositional modification, thereby offering a powerful framework for optimizing performance. Ultimately, the elucidation of topology–property relationships serves as a critical bridge between molecular-level design and the bulk or solution properties of polymeric materials. To illustrate these concepts in greater detail, the following section summarizes the representative physical characteristics of various topological architectures, including cyclic, star, bottlebrush, and multicyclic polymers, highlighting how their distinct chain connectivity manifest in macroscopic behavior.

1.4.1 Physical properties of monocyclic polymer

Monocyclic polymers, which lack chain ends, exhibit unique conformational, dynamical, and thermodynamic behaviors distinct from those of their linear analogues.[38–43] The absence of chain termini fundamentally alters the entropic elasticity, diffusion, and entanglement characteristics of the polymer chains, leading to distinctive solution, melt, and solid-state properties (**Table 1.1**). For example, monocyclic polymers exhibit higher T_g than their linear counterparts because the absence of chain ends restricts segmental mobility and reduces free volume.[44] However, as the molecular weight approaches infinity, the end-group effects become negligible, and the T_g values of cyclic and linear polymers converge to the same value.[45] For crystallizable polymers, monocyclic polymers often display higher melting temperatures (T_m) than the corresponding linear analogues.[46] In dilute solution, cyclic polymers generally exhibit lower hydrodynamic volume (R_h)[47] and intrinsic viscosity ([η])[48] than their linear analogues of equivalent molecular weight. This behavior arises from the entropic constraint imposed by ring closure, which reduces the conformational freedom of the chain and eliminates terminal backfolding, leading to a more compact conformation. Monocyclic polymers also exhibit interesting rheological properties owing to their reduced chain entanglement density. For example, monocyclic polymers have been reported to show significantly lower melt viscosity compared with their linear counterparts.[49] Rheological studies on cyclic PS further revealed the absence of a rubbery plateau and a faster terminal relaxation process relative to linear analogues, reflecting the fundamental influence of the closed-ring topology on chain dynamics in the melt state.[49]

Table 1.1. Comparison of physical properties between linear and monocyclic polymers

Topology	Linear 	Monocyclic 
T_g, T_m	Lower	Higher
R_h, $[\eta]$, melt viscosity	Higher	Lower
T_g in the limit of infinite molecular weight	Similar	Similar
Rubbery plateau	Present	Absent
Terminal relaxation	Slower	Faster

1.4.2 Physical properties of star polymer

Star polymers, characterized by multiple linear arms radiating from a central branching point (core), represent a broad class of branched macromolecular architectures.[50–52] In recent decades, the development of controlled/living polymerization techniques and highly efficient coupling reactions has enabled the precise synthesis of star polymers with well-defined molecular architectures. These advances have revealed that star polymers exhibit physical properties distinct from those of their linear analogues (**Table 1.2**). For instance, when compared at identical total molecular weight, the reduced interpenetration and entanglement among arms result in a lower effective entanglement density, leading to significantly reduced $[\eta]$[53] and leading compared[54] with linear counterparts. From a thermal perspective, star polymers showed a lower T_g and T_m values than their linear analogues of equivalent total molecular weight.[55] This behavior is generally attributed to the decreased free volume and suppressed crystallization arising from the large number of chain ends and the steric restriction of arm folding around the core. In contrast, when compared at identical molecular weight, the plateau modulus of star polymers has been reported to be nearly identical to that of their linear counterparts, indicating that the entanglement strength per network strand remains essentially unchanged despite the architectural differences.[56] One of the remarkable features of star polymers lies in their tunable physical properties, which can be precisely controlled by adjusting the number of arms. Kim et al. synthesized a series of poly(ethylene oxide) (PEO) stars containing three to eight arms and systematically analyzed their thermal properties.[57] By varying the number of arms while keeping the total molecular weight nearly constant, they observed a progressive decrease in the T_m with increasing arm number (**Figure 1.6**). Furthermore, the melting peak width, enthalpy of fusion (ΔH_m), and degree of crystallinity (X_c)

also decreased with increasing arm number.[57] These tendencies were attributed to the disturbance of the crystalline folding structure caused by the shorter arm length and the larger number of chain ends.

Table 1.2. Comparison of physical properties between linear and star polymers

Topology	Linear 	Star 
$[\eta]$, melt viscosity	Higher	Lower
T_g, T_m	Higher	Lower
Plateau modulus	Identical	Identical

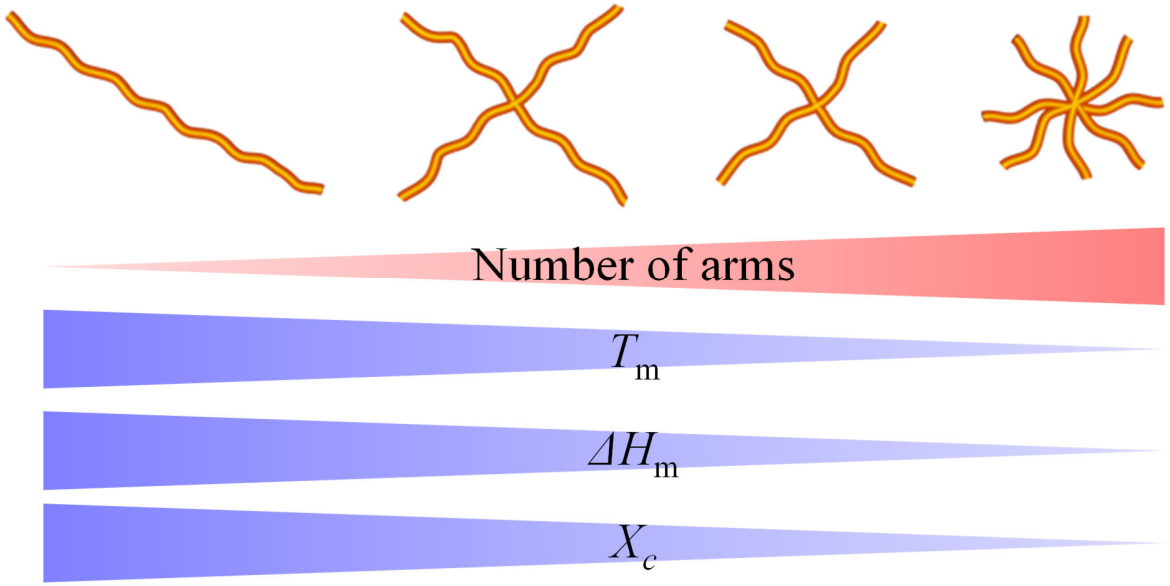

Figure 1.6. Schematic summary of the arm-number dependence of physical properties in star polymers.

1.4.3 Physical properties of bottlebrush polymer

Bottlebrush polymers are a class of branched macromolecules in which numerous polymeric side chains are densely grafted along a linear backbone.[58–60] Their molecular architecture partially resembles that of star polymers, which consist of multiple arms radiating from a central core. However, the position and spatial arrangement of these branches differ significantly: whereas star polymers extend their arms radially from a single core, bottlebrush polymers incorporate side chains periodically along the entire backbone. Owing to this regularly branched architecture, bottlebrush polymers exhibit several characteristic features distinct from their linear analogues of comparable molecular weight: (i) a compact molecular size, (ii) a cylindrically elongated conformation arising from steric repulsion between densely grafted side chains, and (iii) pronounced chain-end effects originating from the large number of chain termini per molecule.

Extensive studies have been conducted to elucidate the structure–property relationships of bottlebrush polymers in both bulk and solution states. The effects of architectural parameters such as side-chain length, backbone length, and concentration have been systematically investigated by means of experimental measurements and computer simulations. Tsukahara et al. revealed that the T_g of PS bottlebrush polymers is primarily governed by the excess free volume associated with chain ends per unit molecular weight.[61,62] Unlike linear polymers, the T_g of bottlebrush polymers does not simply scale with the total molecular weight (**Table 1.3**). When the side-chain length is fixed, T_g remains nearly constant over a wide range of backbone lengths, whereas it increases with increasing side-chain length.[61,62] In solution, bottlebrush polymers are known to undergo a spherical-to-cylindrical conformational transition with increasing backbone degree of polymerization (DP). Sing et al.

systematically investigated the [η] of a series of poly(lactide) (PLA)-based bottlebrush polymers with varying backbone lengths.[63] At low backbone DP, the molecules adopt a nearly spherical conformation, resulting in negligible changes in intrinsic viscosity [η] upon increasing backbone length (**Figure 1.7**). In contrast, at higher backbone DP, the molecular conformation transforms into a cylindrically elongated structure, leading to a marked increase in [η]. A similar trend has been confirmed for PS-based bottlebrush polymers through small-angle neutron scattering (SANS) analysis. Verduzco et al. demonstrated that molecules with short backbones exist as spherical conformation, whereas those with longer backbones adopt cylindrical conformations due to the combined effects of excluded-volume interactions among side chains and the reduced influence of chain-end effects.[64]

Table 1.3. Summary of the effects of backbone and side-chain DP on the T_g of bottlebrush polymers compared with linear analogues

Topology	Linear 	Bottlebrush 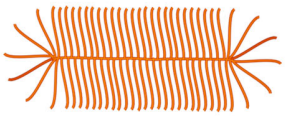
Increase in backbone DP	↑ T_g	Nearly constant
Increase in Side-chain DP	-	↑ T_g

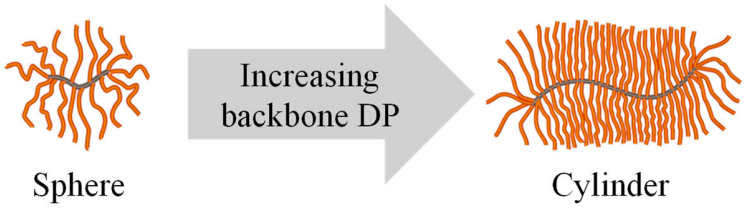

Figure 1.7. Schematic representation of effect of backbone DP on the chain conformation of bottlebrush polymers in solution.

1.4.4 Physical properties of multicyclic polymer

As outlined in Section 1.1, multicyclic polymers can be classified according to their molecular topology based on the presence of main rings, branching points, and bridges, and are typically divided into fused-type (e.g., θ-type), bridged-type (e.g., manacle-type), and spiro-type (e.g., figure-eight-shaped) architectures. As summarized in Section 1.3, several synthetic approaches for multicyclic polymers have been proposed to date, yet systematic studies on their synthesis and physical properties remain scarce. Against this background, Satoh et al. systematically evaluated the solution and thermal properties of spiro-type multicyclic PCLs with two (figure-eight), three (trefoil-shaped), and four (quatrefoil-shaped) rings synthesized via ROMO, as illustrated in Scheme 1.7a (**Figure 1.8**).[15] They found that the R_h and $[\eta]$ decreased in the order linear > monocyclic > figure-eight > trefoil > quatrefoil, indicating that the overall chain dimensions become progressively more compact as the number of cyclic units increases at a fixed total molecular weight. Interestingly, the figure-eight-shaped PCL exhibited the highest T_m among this series. The same group also investigated the physical properties of cage-shaped PCLs synthesized by ROMO while systematically varying the number and length of the arms.[14] In this study, the total molecular weight was held constant, enabling a direct comparison of the influence of cage architecture on the hydrodynamic diameter, viscosity, and crystallization behavior of these polymer cages were found to be strongly dependent on both parameters. For example, they demonstrated that the three-armed cage-type PCL exhibited a T_m comparable to that of the linear PCL, which was lower than that of the monocyclic PCL. Moreover, the T_m progressively decreased with increasing arm number, and the 8-armed cage-type PCL did not exhibit any detectable melting transition. Doi et al. examined dumbbell-shaped PS composed of two small rings connected by a short linear segment.[65] In blends of these

dumbbell-shaped PS with long linear chains, the dumbbell species acted as pseudo-entanglement points, exhibiting characteristic relaxation times longer than those of the host linear chains. Macromolecules bearing densely grafted cyclic side chains have also attracted attention as unique hybrid architectures combining features of both cyclic and branched polymers. Structurally, such polymers resemble star-like architectures when the number of cyclic units is small, but approach bottlebrush-like architectures as the number of rings increases. Monteiro et al. investigated the T_g and conformation of multicyclic PSs containing up to twenty cyclic units synthesized according to Scheme 1.5b.[31] In their study, the ring size of each cyclic unit was kept constant, enabling the isolated effect of the number of cyclic units to be evaluated. They reported that T_g increased with the number of cyclic units but reached a plateau beyond a certain threshold. Moreover, the T_g values of multicyclic PSs were consistently higher than those of the corresponding graft and linear PSs. In good solvents, the overall coil dimensions of the multicyclic PSs became progressively more compact up to approximately twelve cyclic units and remained nearly constant thereafter. Despite these advances, experimental synthesis of well-defined multicyclic polymers remains challenging, and systematic investigations of how the number of cyclic units influences molecular structure and physical properties are still very limited. Furthermore, to deepen the understanding of structural and physical characteristics arising from multicyclic topology, it is essential to perform direct comparisons with the corresponding acyclic counterparts.

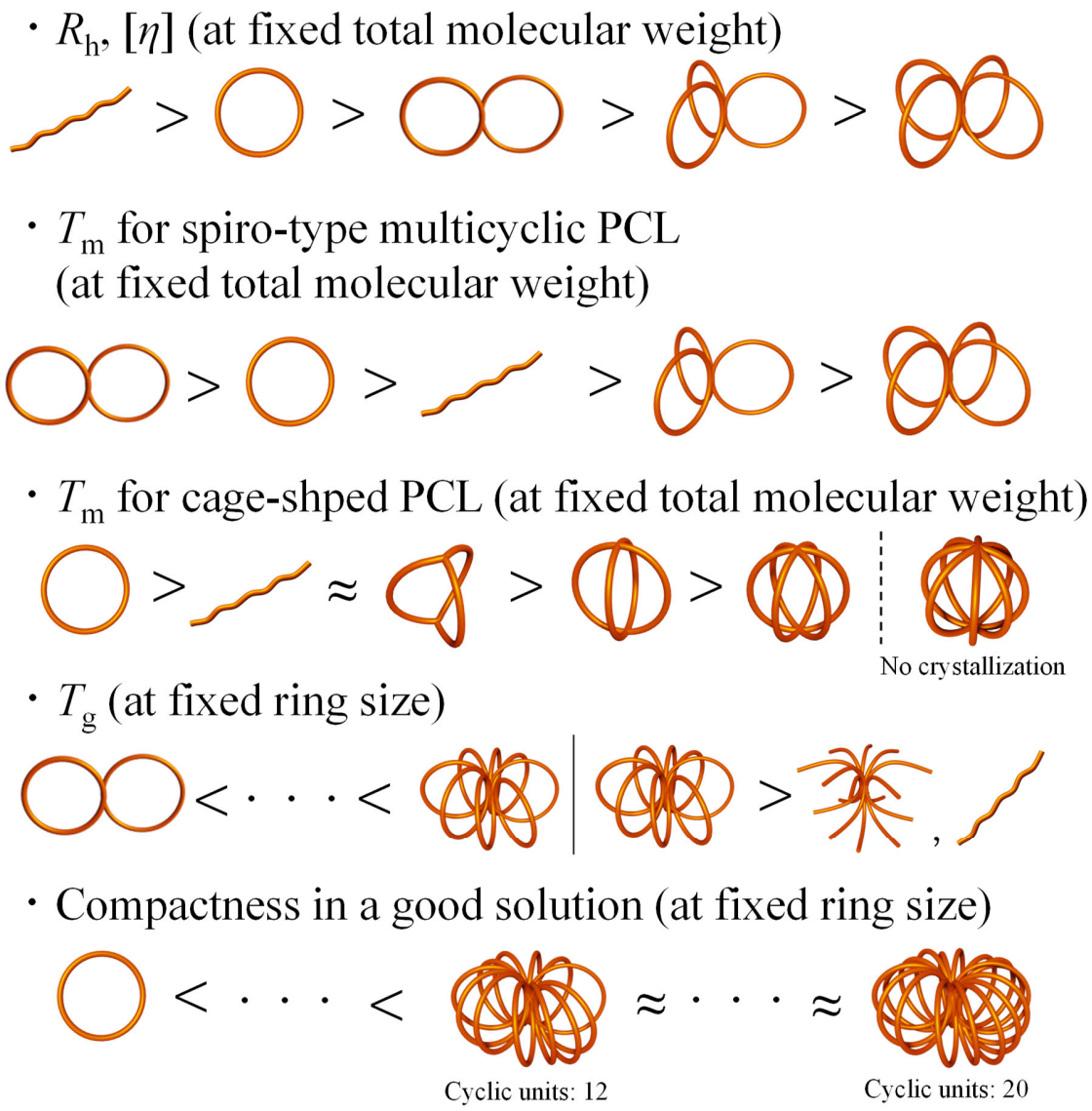

Figure 1.8. Visual representation of the physical properties of multicyclic polymers.

1.5 Threading phenomena in cyclic polymer blends with linear chains

Early rheological studies on cyclic polymers occasionally reported weak plateau-like features in the melt state, suggesting that ring polymers might form entangled networks similar to their linear counterparts.[66] Subsequent advances in purification and characterization, however, revealed that these signatures did not originate from the intrinsic dynamics of the rings themselves but instead arose from trace amounts of linear contaminants, which, even at levels well below 1 wt %, dominate the viscoelastic response of nominally cyclic samples.[67] Consequently, research attention shifted from pure cyclic polymers to cyclic/linear blends. Against this background, a wide range of experimental and theoretical studies have been devoted to elucidating the structural and dynamical consequences of mixing cyclic and linear polymers (**Figure 1.9a**). For example, in monocyclic/linear polybutadiene blends, the melt viscosity was reported to be up to 2.3 times higher than that of the corresponding linear polymer.[66] In blends of monocyclic and linear PLLA, the addition of monocyclic PLLA was found to suppress crystallization and alter the thermal behavior.[68] Among the various phenomena observed in such systems, one of the most important is threading, the penetration of a linear chain through the interior of a cyclic chain, which markedly affects the conformation and mobility of the cyclic component.[69–73] This phenomenon induces topology-dependent intermolecular interactions that do not exist in pure cyclic polymer systems and has therefore been recognized as a key concept for understanding and controlling the structure and properties of cyclic/linear blends. The existence of threading is not merely a conceptual hypothesis but has been demonstrated experimentally. Iwamoto et al. investigated blends composed of highly purified monocyclic PS dispersed in linear poly(styrene-*r*-styrene-d_8) copolymer matrices using SANS.[74] They showed that the radius of gyration (R_g) of the monocyclic component increases

with the volume fraction of the linear component. Interestingly, this size change was found to be almost independent of the molecular weight of the linear chains, suggesting that the expansion of the cyclic chains is governed predominantly by threading interactions. Furthermore, Kruteva *et al.* combined SANS measurements with analyses based on the random phase approximation to quantify the interactions in monocyclic/linear PEO blends in terms of an effective Flory–Huggins parameter, obtaining a negative value.[75] This result indicates that mixing in such blends is thermodynamically favorable and entropically driven, accompanied by active penetration of linear chains into the interiors of monocyclic ones. Consistent with this view, molecular dynamics (MD) simulations have also revealed that monocyclic/linear blends exhibit entropically favorable mixing behavior characterized by a negative Flory–Huggins parameter, whereas such a tendency is absent in monocyclic/monocyclic and linear/linear blends.[76]

Building on these findings, researchers have extended their interest toward more complex architectures, namely multicyclic polymers (Figure 1.9b). The entanglement behavior between linear and multicyclic chains has been analyzed in several MD simulations.[77–79] Hagita et al. reported that, when compared at equal ring-unit degree of polymerization, multicyclic polymers are more susceptible to threading by linear chains than monocyclic polymers.[79] These findings highlight the importance of topological design in governing blend interactions and underscore the need for systematic structural investigations of multicyclic/linear polymer systems. Recently, Satoh et al. synthesized cyclic poly(dimethylsiloxane) (PDMS) with different numbers of rings and experimentally examined the influence of ring topology on threading behavior.[80] They found that multicyclic PDMS is more readily trapped within linear PDMS networks than monocyclic PDMS, exhibiting a higher tendency toward interpenetration.

This observation provides direct experimental evidence that increasing the number of rings enhances chain threading. Nevertheless, experimental studies in this field remain limited, primarily due to the synthetic challenges associated with structurally precise multicyclic polymers. In particular, the ability to independently control both the size and number of cyclic units is indispensable for disentangling the effects of individual topological parameters on macromolecular behavior. Therefore, the establishment of an experimental platform enabling the precise synthesis and structural characterization of multicyclic polymers is of critical importance for advancing our understanding of topology-driven phenomena.

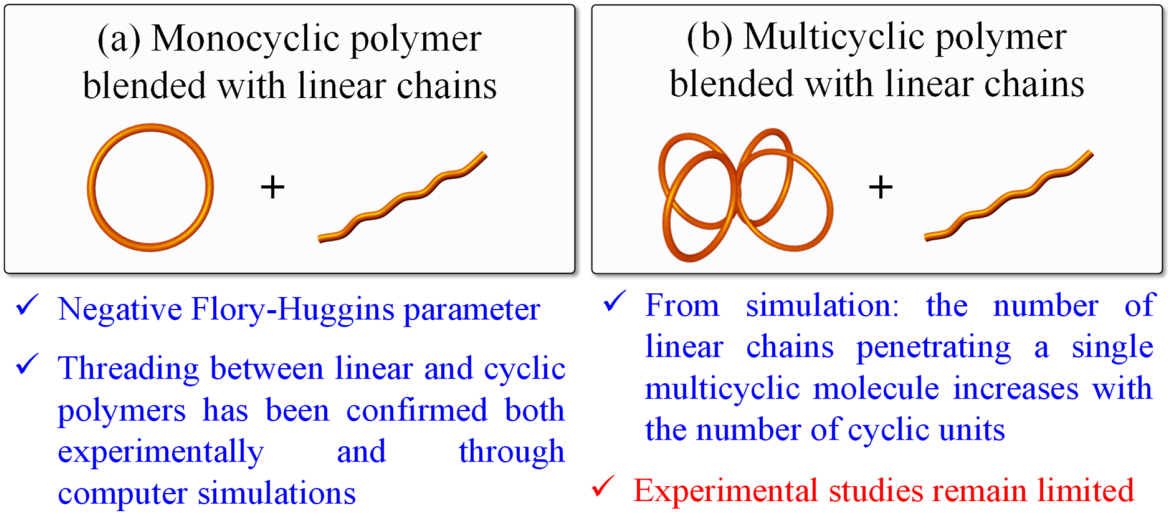

Figure 1.9. Schematic summary of the current research progress on (a) monocyclic/linear and (b) multicyclic/linear blends.

1.6 Objective and outline of this thesis

The topology of polymers refers to the spatial connectivity and arrangement of the polymer backbone, and, as described in Section 1.1, it plays a crucial role in determining and controlling polymer properties. In particular, the topological effects of multicyclic polymers are of great significance in creating novel and advanced material functions that cannot be achieved by monocyclic or other branched architectures such as star or bottlebrush polymers. However, most multicyclic polymers reported to date have been composed of polyether- or polyester-based backbones, primarily because of their synthetic accessibility. In contrast, studies on PS-based multicyclic polymers, despite the fact that PS is one of the most thoroughly characterized general-purpose polymers, remain extremely limited. This scarcity mainly arises from the synthetic challenges associated with constructing well-defined multicyclic topologies on PS frameworks. Consequently, systematic investigations into the structure–property relationships of PS-based multicyclic polymers have scarcely been conducted.

Considering that PS serves as a fundamental platform material for plastics and elastomers, this represents a noteworthy gap in the current understanding of topology-driven polymer behavior.

Accordingly, the primary objective of this study is to establish a systematic synthetic strategy for multicyclic PS (mc-PS) and thereby develop an experimental platform for elucidating the unique physical properties of multicyclic polymers. Specifically, attention was directed toward the cyclopolymerization approach, a versatile synthetic methodology for multicyclic architectures originally reported by Satoh et al.,[36] which was adapted and applied to the synthesis of mc-PS. Furthermore, the physical properties of the synthesized mc-PS were systematically compared with those of their acyclic counterparts, and the structural characteristics of both the neat mc-PS and those dispersed in linear polymer matrices. This

doctoral work developed a versatile cyclopolymerization platform that enables the precise and systematic synthesis of mc-PS with independently tunable ring size and number, thereby addressing long-standing synthetic challenges associated with these topologies. The resulting mc-PSs displayed characteristic bulk and solution properties that are governed by their multicyclic topology and clearly differentiate them from their linear and graft analogues. Furthermore, SANS experiments demonstrated that these topology-driven effects occur in both neat bulk materials and blends with linear chains, providing fundamental insight into how architectural complexity influences polymer structure. Taken together, the findings of this work deepen our fundamental understanding of how multicyclic topology governs the physical properties and structure of polymers, while at the same time offering broadly applicable design principles for exploiting polymer architecture in the development of functional materials.

As outline of the thesis is described in bellow:

In Chapter 2, mc-PSs were systematically synthesized by cyclopolymerization of α,ω-dinorbornenyl-terminated PS macromonomers under dilute conditions in the presence of G3. By varying the initial feed ratio of macromonomer to G3, the number of cyclic units incorporated into the resulting mc-PSs was precisely controlled, reaching up to 239 rings per molecule, which is more than an order of magnitude higher than those reported previously for multicyclic PS systems (**Figure 1.10**). Furthermore, by employing macromonomers with different number-average molecular weights, the molecular weight of each cyclic unit was tuned from 1,640 to 52,100. In addition, block-type macromonomers composed of PS and PLA were successfully subjected to cyclopolymerization, as well as statistical cyclocopolymerization of PS and PLA macromonomers, affording a variety of PS-containing multicyclic copolymers with diverse architectures. The cyclopolymerization strategy established in this study is significantly

simpler and more versatile than previously reported methods for synthesizing multicyclic PS and PS-containing multicyclic polymers. This methodology is therefore expected to open new avenues for both fundamental studies and material development based on polymer topology.

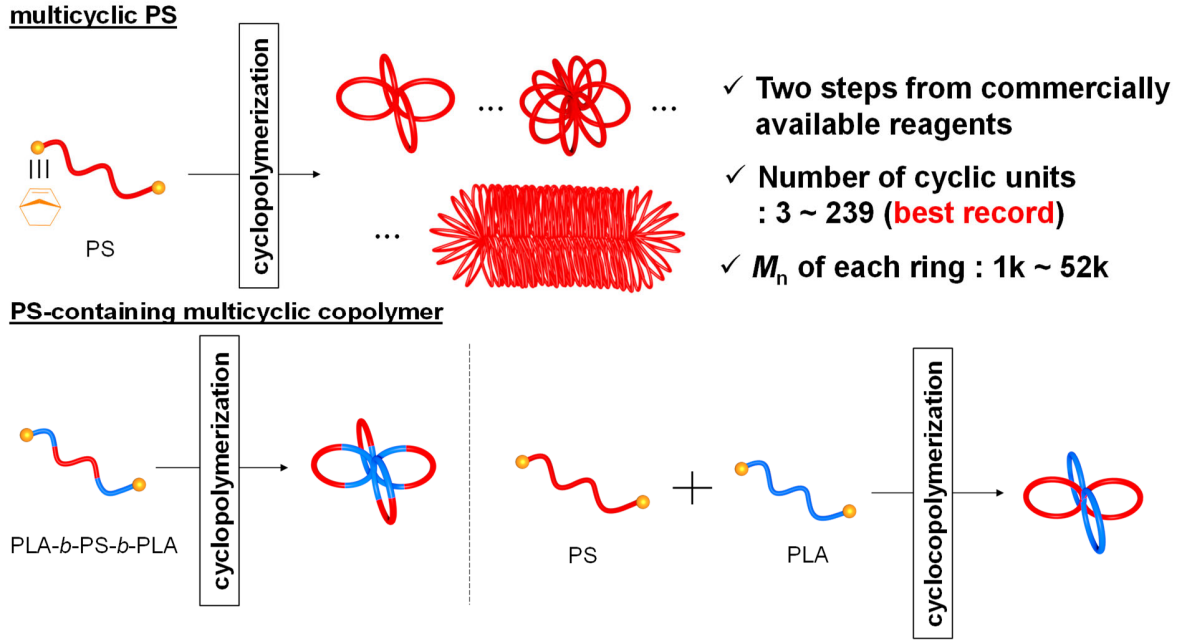

Figure 1.10. Illustration of the Chapter 2 outline.

In Chapter 3, mc-PSs with different numbers of cyclic units were synthesized according to the cyclopolymerization method established in Chapter 2, and their structure–property relationships were investigated in detail. To clearly evaluate the effect of the cyclic topology, graft polymers bearing linear PS side chains (g-PSs) were also synthesized and compared with the corresponding mc-PSs (**Figure 1.11**). The mc-PS samples exhibited higher T_g, superior thermal stability, lower [η], and more compact R_h than the corresponding g-PSs. Moreover, as the number of cyclic units increased, mc-PSs were found to undergo a structural transition from a spherical to a cylindrical conformation. In addition, mc-PSs exhibited slightly

larger Kuhn lengths than the corresponding g-PSs, suggesting that the cyclic topology of the side chains influences the apparent stiffness of the norbornene backbone. These findings provide important insights into the structure–property relationships of topologically complex polymers and offer a new design principle for polymer materials based on topological control.

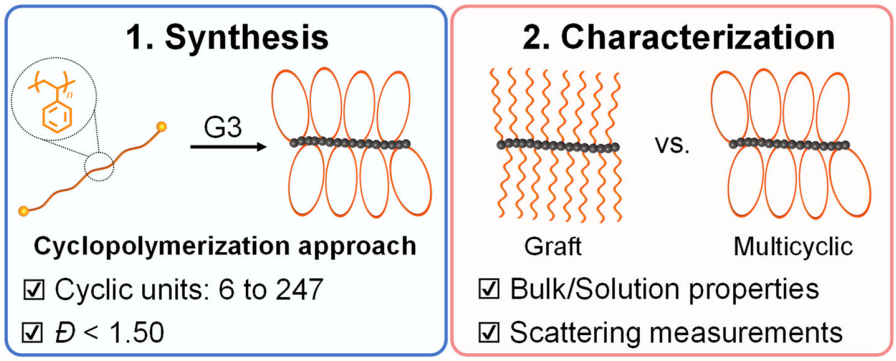

Figure 1.11. Illustration of the Chapter 3 outline.

In Chapter 4, the structures of mc-PSs were investigated in both the neat bulk state and blends with linear PS by SANS. In this study, the author established a versatile experimental platform for the synthesis of structurally well-defined mc-PS and deuterated multicyclic PS (mc-dPS) by cyclopolymerization of atom transfer radical polymerization-based macromonomer (**Figure 1.12**). In the neat bulk state, mc-PS exhibited smaller radii of R_g than the corresponding linear and monocyclic analogues, indicating enhanced chain compaction arising from the multicyclic topology. The scattering data further revealed the presence of strong inter-ring correlations, reflecting the coupled conformations among neighboring cyclic units. In contrast, in blend systems, ring swelling was observed when the ring size exceeded the entanglement molecular weight, and the degree of swelling became more pronounced with

increasing number of cyclic units. Overall, the experimental platform established in this study provides a powerful framework for elucidating topology-governed structures in multicyclic polymers and opens new avenues for understanding their structural characteristics in both bulk and blended states.

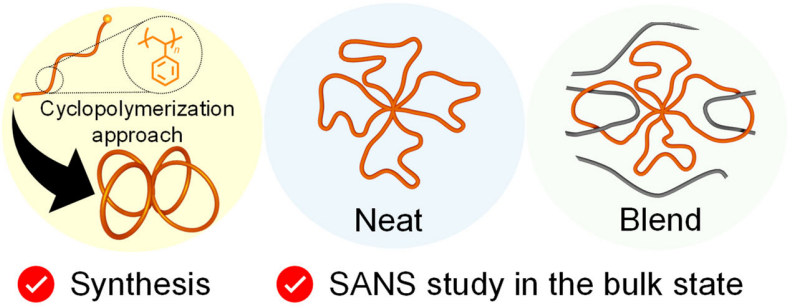

Figure 1.12. Illustration of the Chapter 4 outline.

In Chapter 5, the systematic synthetic strategy for mc-PSs established in this study, together with the structure–property relationships governed by the multicyclic topology, are summarized as the overall conclusions of this thesis.

1.7 References

(1) Polymeropoulos, G.; Zapsas, G.; Ntetsikas, K.; Bilalis, P.; Gnanou, Y.; Hadjichristidis, N. 50th Anniversary Perspective: Polymers with Complex Architectures. *Macromolecules* **2017**, *28*, 1253–1290.

(2) Scott, D. W. Equilibria between Linear and Cyclic Polymers in Methylpolysiloxanes. *J. Am. Chem. Soc.* **1946**, *68*, 2294–2298.

(3) Carothers, W. H.; Arvin, J. A.; Dorough, G. L. *J. Am. Chem. Soc.* **1930**, *52*, 3292–3300.

(4) Carothers, W. H.; Natta, F. J. V. Studies on Polymerization and Ring Formation. Iii. Glycol Esters of Carbonic Acid. *J. Am. Chem. Soc.* **1930**, *52*, 314–326.

(5) El-Sagheer, A. H.; Brown, T. Synthesis, Serum Stability and Cell Uptake of Cyclic and Hairpin Decoy Oligonucleotides for TCF/LEF and GLI Transcription Factors. *Int. J. Pept. Res. Ther.* **2008**, *14*, 367–372.

(6) Saether, O.; Craik, D. J.; Campbell, I. D.; Sletten, K.; Juul, J.; Norman, D. G. Elucidation of the Primary and Three-Dimensional Structure of the Uterotonic Polypeptide Kalata B1. *Biochemistry* **1995**, *34*, 4147–4158.

(7) Vinograd, J.; Lebowitz, J. Physical and Topological Properties of Circular DNA. *J. Gen. Physiol.* **1966**, *49*, 103–125.

(8) Sprott, G. D. Structures of Archaebacterial Membrane Lipids. *J. Bioenerg. Biomembr.* **1992**, *24*, 555–566.

(9) Ireland, D. C.; Clark, R. J.; Daly, N. L.; Craik, D. J. Isolation, Sequencing, and Structure - Activity Relationships of Cyclotides. *J. Nat. Prod.* **2010**, *73*, 1610–1622.

(10) Morgese, G.; Trachsel, L.; Romio, M.; Divandari, M.; Ramakrishna, S. N.; Benetti, E. M. Topological Polymer Chemistry Enters Surface Science: Linear versus Cyclic

Polymer Brushes. *Angew. Chemie* **2016**, *128*, 15812–15817.

(11) Honda, S.; Yamamoto, T.; Tezuka, Y. Topology-Directed Control on Thermal Stability: Micelles Formed from Linear and Cyclized Amphiphilic Block Copolymers. *J. Am. Chem. Soc.* **2010**, *132*, 10251–10253.

(12) Poelma, J. E.; Ono, K.; Miyajima, D.; Aida, T.; Satoh, K.; Hawker, C. J. Cyclic Block Copolymers for Controlling Feature Sizes in Block Copolymer Lithography. *ACS Nano* **2012**, *6*, 10845–10854.

(13) Satoh, Y.; Matsuno, H.; Yamamoto, T.; Tajima, K.; Isono, T.; Satoh, T. Synthesis of Well-Defined Three- and Four-Armed Cage-Shaped Polymers via "Topological Conversion" from Trefoil- and Quatrefoil-Shaped Polymers. *Macromolecules* **2017**, *50*, 97–106.

(14) Mato, Y.; Honda, K.; Tajima, K.; Yamamoto, T.; Isono, T.; Satoh, T. A Versatile Synthetic Strategy for Macromolecular Cages: Intramolecular Consecutive Cyclization of Star-Shaped Polymers. *Chem. Sci.* **2019**, *10*, 440–446.

(15) Mato, Y.; Honda, K.; Ree, B. J.; Tajima, K.; Yamamoto, T.; Deguchi, T.; Isono, T.; Satoh, T. Programmed Folding into Spiro-Multicyclic Polymer Topologies from Linear and Star-Shaped Chains. *Commun. Chem.* **2020**, *3*, 1–7.

(16) Geiser, D.; Hócker, H. Synthesis and Investigation of Macrocyclic Polystyrene. *Macromolecules* **1980**, *13*, 653–656.

(17) Sun, P.; Chen, J.; Liu, J.; Zhang, K. Self-Accelerating Click Reaction for Cyclic Polymer. *Macromolecules* **2017**, *50*, 1463–1472.

(18) Laurent, B. A.; Grayson, S. M. An Efficient Route to Well-Defined Macrocyclic Polymers via "Click" Cyclization. *J. Am. Chem. Soc.* **2006**, *128*, 4238–4239.

(19) Tang, Q.; Wu, Y.; Sun, P.; Chen, Y.; Zhang, K. Powerful Ring-Closure Method for Preparing Varied Cyclic Polymers. *Macromolecules* **2014**, *47*, 3775–3781.

(20) Kricheldorf, H. R.; Lee, S. R. Polylactones. 40. Nanopretzels by Macrocyclic Polymerization of Lactones via a Spirocyclic Tin Initiator Derived from Pentaerythritol. *Macromolecules* **1996**, *29*, 8689–8695.

(21) Bielawski, C. W.; Benitez, D.; Grubbs, R. H. An "Endless" Route to Cyclic Polymers. *Science* **2002**, *297*, 2041–2044.

(22) Culkin, D. A.; Jeong, W.; Csihony, S.; Gomez, E. D.; Balsara, N. P.; Hedrick, J. L.; Waymouth, R. M. Zwitterionic Polymerization of Lactide to Cyclic Poly(Lactide) by Using N-Heterocyclic Carbene Organocatalysts. *Angew. Chem. Int. Ed.* **2007**, *46*, 2627–2630.

(23) He, T.; Zheng, G. H.; Pan, C. Y. Synthesis of Cyclic Polymers and Block Copolymers by Monomer Insertion into Cyclic Initiator by a Radical Mechanism. *Macromolecules* **2003**, *36*, 5960–5966.

(24) Yamamoto, T.; Yagyu, S.; Tezuka, Y. Light- and Heat-Triggered Reversible Linear-Cyclic Topological Conversion of Telechelic Polymers with Anthryl End Groups. *J. Am. Chem. Soc.* **2016**, *138*, 3904–3911.

(25) Ogawa, T.; Nakazono, K.; Aoki, D.; Uchida, S.; Takata, T. Effective Approach to Cyclic Polymer from Linear Polymer: Synthesis and Transformation of Macromolecular [1]Rotaxane. *ACS Macro Lett.* **2015**, *4*, 343–347.

(26) Zhang, Z.; Nie, X.; Wang, F.; Chen, G.; Huang, W. Q.; Xia, L.; Zhang, W. J.; Hao, Z. Y.; Hong, C. Y.; Wang, L. H.; You, Y. Z. Rhodanine-Based Knoevenagel Reaction and Ring-Opening Polymerization for Efficiently Constructing Multicyclic Polymers. *Nat.*

Commun. **2020**, *11*, 3654.

(27) Chen, J.; Li, H.; Zhang, H.; Liao, X.; Han, H.; Zhang, L.; Sun, R.; Xie, M. Blocking-Cyclization Technique for Precise Synthesis of Cyclic Polymers with Regulated Topology. *Nat. Commun.* **2018**, *9*, 1–9.

(28) Lonsdale, D. E.; Monteiro, M. J. Various Polystyrene Topologies Built from Tailored Cyclic Polystyrene via CuAAC Reactions. *Chem. Commun.* **2010**, *46*, 7945–7947.

(29) Ko, Y. S.; Yamamoto, T.; Tezuka, Y. Click Construction of Spiro- and Bridged-Quatrefoil Polymer Topologies with Kyklo-Telechelics Having an Azide Group. *Macromol. Rapid Commun.* **2014**, *35*, 412–416.

(30) Sugai, N.; Heguri, H.; Ohta, K.; Meng, Q.; Yamamoto, T.; Tezuka, Y. Effective Click Construction of Bridged-and Spiro-Multicyclic Polymer Topologies with Tailored Cyclic Prepolymers (Kyklo-Telechelics). *J. Am. Chem. Soc.* **2010**, *132*, 14790–14802.

(31) Gavrilov, M.; Amir, F.; Kulis, J.; Hossain, M. D.; Jia, Z.; Monteiro, M. J. Densely Packed Multicyclic Polymers. *ACS Macro Lett.* **2017**, *6*, 1036–1041.

(32) Jeong, J.; Kim, K.; Lee, R.; Lee, S.; Kim, H.; Jung, H.; Kadir, M. A.; Jang, Y.; Jeon, H. B.; Matyjaszewski, K.; Chang, T.; Paik, H. J. Preparation and Analysis of Bicyclic Polystyrene. *Macromolecules* **2014**, *47*, 3791–3796.

(33) Sugai, N.; Heguri, H.; Yamamoto, T.; Tezuka, Y. A Programmed Polymer Folding: Click and Clip Construction of Doubly Fused Tricyclic and Triply Fused Tetracyclic Polymer Topologies. *J. Am. Chem. Soc.* **2011**, *133*, 19694–19697.

(34) Tezuka, Y. Topological Polymer Chemistry for Designing Multicyclic Macromolecular Architectures. *Polym. J.* **2012**, *44*, 1159–1169.

(35) Shi, G. Y.; Pan, C. Y. Synthesis of Well-Defined Figure-of-Eight-Shaped Polymers by a

Combination of ATRP and Click Chemistry. *Macromol. Rapid Commun.* **2008**, *29*, 1672–1678.

(36) Isono, T.; Sasamori, T.; Honda, K.; Mato, Y.; Yamamoto, T.; Tajima, K.; Satoh, T. Multicyclic Polymer Synthesis through Controlled/Living Cyclopolymerization of α,ω-Dinorbornenyl-Functionalized Macromonomers. *Macromolecules* **2018**, *51*, 3855–3864.

(37) Ebii, Y.; Ebe, M. Multicyclic Polymer Synthesis via a Consecutive Cyclization Approach. *Polym. J.* **2025**, 1–17.

(38) Haque, F. M.; Grayson, S. M. The Synthesis, Properties and Potential Applications of Cyclic Polymers. *Nature Chemistry* **2020**, *12*, 433–444.

(39) Golba, B.; Benetti, E. M.; De Geest, B. G. Biomaterials Applications of Cyclic Polymers. *Biomaterials* **2021**, *267*, 120468.

(40) Yamamoto, T.; Tezuka, Y. Topological Polymer Chemistry: A Cyclic Approach toward Novel Polymer Properties and Functions. *Polym. Chem.* **2011**, *2*, 1930–1941.

(41) Yamamoto, T.; Tezuka, Y. Cyclic Polymers Revealing Topology Effects upon Self-Assemblies, Dynamics and Responses. *Soft Matter* **2015**, *11*, 7458–7468.

(42) Jia, Z.; Monteiro, M. J. Cyclic Polymers: Methods and Strategies. *J. Polym. Sci. Part A Polym. Chem.* **2012**, *50*, 2085–2097.

(43) Laurent, B. A.; Grayson, S. M. Synthetic Approaches for the Preparation of Cyclic Polymers. *Chem. Soc. Rev.* **2009**, *38*, 2202–2213.

(44) Schappacher, M.; Deffieux, A. α-Acetal-ω-Bis(Hydroxymethyl) Heterodifunctional Polystyrene: Synthesis, Characterization, and Investigation of Intramolecular End-to-End Ring Closure. *Macromolecules* **2001**, *34*, 5827–5832.

(45) Gao, L.; Oh, J.; Tu, Y.; Chang, T.; Li, C. Y. Glass Transition Temperature of Cyclic

Polystyrene and the Linear Counterpart Contamination Effect. *Polymer* **2019**, *170*, 198–203.

(46) Schäler, K.; Ostas, E.; Schröter, K.; Thurn-Albrecht, T.; Binder, W. H.; Saalwächter, K. Influence of Chain Topology on Polymer Dynamics and Crystallization. Investigation of Linear and Cyclic Poly(ε-Caprolactone)s by 1H Solid-State NMR Methods. *Macromolecules* **2011**, *44*, 2743–2754.

(47) Zimm, B. H.; Stockmayer, W. H. The Dimensions of Chain Molecules Containing Branches and Rings. *J. Chem. Phys.* **1949**, *17*, 1301–1314.

(48) Jeong, Y.; Jin, Y.; Chang, T.; Uhlik, F.; Roovers, J. Intrinsic Viscosity of Cyclic Polystyrene. *Macromolecules* **2017**, *50*, 7770–7776.

(49) Doi, Y.; Matsubara, K.; Ohta, Y.; Nakano, T.; Kawaguchi, D.; Takahashi, Y.; Takano, A.; Matsushita, Y. Melt Rheology of Ring Polystyrenes with Ultrahigh Purity. *Macromolecules* **2015**, *48*, 3140–3147.

(50) Cameron, D. J. A.; Shaver, M. P. Aliphatic Polyester Polymer Stars: Synthesis, Properties and Applications in Biomedicine and Nanotechnology. *Chem. Soc. Rev.* **2011**, *40*, 1761–1776.

(51) Ren, J. M.; McKenzie, T. G.; Fu, Q.; Wong, E. H. H.; Xu, J.; An, Z.; Shanmugam, S.; Davis, T. P.; Boyer, C.; Qiao, G. G. Star Polymers. *Chem. Rev.* **2016**, *116*, 6743–6836.

(52) Higashihara, T.; Hayashi, M.; Hirao, A. Synthesis of Well-Defined Star-Branched Polymers by Stepwise Iterative Methodology Using Living Anionic Polymerization. *Prog. Polym. Sci.* **2011**, *36*, 323–375.

(53) Van Aert, H. A. M.; Van Genderen, M. H. P.; Meijer, E. W. Star-Shaped Poly(2,6-Dimethyl-1,4-Phenylene Ether). *Polym. Bull.* **1996**, *37*, 273–280.

(54) Utracki, L. A.; Roovers, J. E. L. Viscosity and Normal Stresses of Linear and Star Branched Polystyrene Solutions. I. Application of Corresponding States Principle to Zero-Shear Viscosities. *Macromolecules* **1973**, *6*, 366–372.

(55) Zhao, Y. L.; Cai, Q.; Jiang, J.; Shuai, X. T.; Bei, J. Z.; Chen, C. F.; Xi, F. Synthesis and Thermal Properties of Novel Star-Shaped Poly(L-Lactide)s with Starburst PAMAM-OH Dendrimer Macroinitiator. *Polymer* **2002**, *43*, 5819–5825.

(56) Graessley, W. W.; Roovers, J. Melt Rheology of Four-Arm and Six-Arm Star Polystyrenes. *Macromolecules* **1979**, *12*, 959–965.

(57) Choi, Y. K.; Bae, Y. H.; Kim, S. W. Star-Shaped Poly(Ether-Ester) Block Copolymers: Synthesis, Characterization, and Their Physical Properties. *Macromolecules* **1998**, *31*, 8766–8774.

(58) Saha, D.; Witt, C. L.; Fatima, R.; Uchiyama, T.; Pande, V.; Song, D. P.; Fei, H. F.; Yavitt, B. M.; Watkins, J. J. Opportunities in Bottlebrush Block Copolymers for Advanced Materials. *ACS Nano* **2025**, *19*, 1884–1910.

(59) Li, Z.; Tang, M.; Liang, S.; Zhang, M.; Biesold, G. M.; He, Y.; Hao, S. M.; Choi, W.; Liu, Y.; Peng, J.; Lin, Z. Bottlebrush Polymers: From Controlled Synthesis, Self-Assembly, Properties to Applications. *Prog. Polym. Sci.* **2021**, *116*, 101387.

(60) Verduzco, R.; Li, X.; Pesek, S. L.; Stein, G. E. Structure, Function, Self-Assembly, and Applications of Bottlebrush Copolymers. *Chem. Soc. Rev.* **2015**, *44*, 2405–2420.

(61) Tsukahara, Y.; Namba, S. I.; Iwasa, J.; Nakano, Y.; Kaeriyama, K.; Takahashi, M. Bulk Properties of Poly(Macromonomer)s of Increased Backbone and Branch Lengths. *Macromolecules* **2001**, *34*, 2624–2629.

(62) Tsukahara, Y.; Tsutsumi, K.; Okamoto, Y. Makromol. Chem., Rapid Commun. **1992**, 13,

409–413.

(63) Dutta, S.; Wade, M. A.; Walsh, D. J.; Guironnet, D.; Rogers, S. A.; Sing, C. E. Dilute Solution Structure of Bottlebrush Polymers. *Soft Matter* **2019**, *15*, 2928–2941.

(64) Pesek, S. L.; Li, X.; Hammouda, B.; Hong, K.; Verduzco, R. Small-Angle Neutron Scattering Analysis of Bottlebrush Polymers Prepared via Grafting-through Polymerization. *Macromolecules* **2013**, *46*, 6998–7005.

(65) Doi, Y.; Takano, A.; Takahashi, Y.; Matsushita, Y. Terminal relaxation behavior of entangled linear polymers blended with ring and dumbbell-shaped polymers in melts. *Rheol. Acta* **2022**, *61*, 681–688.

(66) Roovers, J. Viscoelastic Properties of Polybutadiene Rings. *Macromolecules* **1988**, *21*, 1517–1521.

(67) Kapnistos, M.; Lang, M.; Vlassopoulos, D.; Pyckhout-Hintzen, W.; Richter, D.; Cho, D.; Chang, T.; Rubinstein, M. Unexpected Power-Law Stress Relaxation of Entangled Ring Polymers. *Nat. Mater.* **2008**, *7*, 997–1002.

(68) Ruiz, M. B.; Pérez-Camargo, R. A.; López, J. V.; Penott-Chang, E.; Múgica, A.; Coulembier, O.; Müller, A. J. Accelerating the Crystallization Kinetics of Linear Polylactides by Adding Cyclic Poly (L-Lactide): Nucleation, Plasticization and Topological Effects. *Int. J. Biol. Macromol.* **2021**, *186*, 255–267.

(69) Widin, J. M.; Schmitt, A. K.; Schmitt, A. L.; Im, K.; Mahanthappa, M. K. Unexpected Consequences of Block Polydispersity on the Self-Assembly of ABA Triblock Copolymers. *J. Am. Chem. Soc.* **2012**, *134*, 3834–3844.

(70) Tsalikis, D. G.; Mavrantzas, V. G. Threading of Ring Poly(Ethylene Oxide) Molecules by Linear Chains in the Melt. *ACS Macro Lett.* **2014**, *3*, 763–766.

(71) Michieletto, D.; Marenduzzo, D.; Orlandini, E.; Alexander, G. P.; Turner, M. S. Threading Dynamics of Ring Polymers in a Gel. *ACS Macro Lett.* **2014**, *3*, 255–259.

(72) Rosa, A.; Smrek, J.; Turner, M. S.; Michieletto, D. Threading-Induced Dynamical Transition in Tadpole-Shaped Polymers. *ACS Macro Lett.* **2020**, *9*, 743–748.

(73) Michieletto, D.; Marenduzzo, D.; Orlandini, E.; Alexander, G. P.; Turner, M. S. Dynamics of Self-Threading Ring Polymers in a Gel. *Soft Matter* **2014**, *10*, 5936–5944.

(74) Iwamoto, T.; Doi, Y.; Kinoshita, K.; Ohta, Y.; Takano, A.; Takahashi, Y.; Nagao, M.; Matsushita, Y. Conformations of Ring Polystyrenes in Bulk Studied by SANS. *Macromolecules* **2018**, *51*, 1539–1548.

(75) Kruteva, M.; Monkenbusch, M.; Allgaier, J.; Pyckhout-Hintzen, W.; Porcar, L.; Richter, D. Structure of Polymer Rings in Linear Matrices: SANS Investigation. *Macromolecules* **2023**, *56*, 4835–4844.

(76) Grest, G. S.; Ge, T.; Plimpton, S. J.; Rubinstein, M.; O'Connor, T. C. Entropic Mixing of Ring/Linear Polymer Blends. *ACS Polym. Au* **2023**, *3*, 209–216.

(77) Murashima, T.; Hagita, K.; Kawakatsu, T. Topological Transition in Multicyclic Chains with Structural Symmetry Inducing Stress-Overshoot Phenomena in Multicyclic/Linear Blends under Biaxial Elongational Flow. *Macromolecules* **2022**, *55*, 9358–9372.

(78) Hagita, K.; Murashima, T.; Ebe, M.; Isono, T.; Satoh, T. Trapping Probabilities of Multiple Rings in End-Linked Gels. *Polymer* **2022**, *245*, 124683.

(79) Hagita, K.; Murashima, T. Multi-Ring Configurations and Penetration of Linear Chains into Rings on Bonded Ring Systems and Polycatenanes in Linear Chain Matrices. *Polymer* **2021**, *223*, 123705.

(80) Ebe, M.; Soga, A.; Fujiwara, K.; Ree, B. J.; Marubayashi, H.; Hagita, K.; Imasaki, A.;

Baba, M.; Yamamoto, T.; Tajima, K.; Deguchi, T.; Jinnai, H.; Isono, T.; Satoh, T. Rotaxane Formation of Multicyclic Polydimethylsiloxane in a Silicone Network: A Step toward Constructing “Macro-Rotaxanes” from High-Molecular-Weight Axle and Wheel Components. *Angew. Chem. Int. Ed.* **2023**, *62*, e202304493.

Chapter 2

Versatile Approach toward Multicyclic Polystyrene and Polystyrene-containing Multicyclic Copolymers via Cyclopolymerization

2.1 Introduction

Macromolecules with cyclic architectures have attracted significant attention because of their interesting properties stemming from the absence of polymer chain ends. For example, cyclic polymers have higher glass transition temperatures, higher densities, smaller hydrodynamic volumes and lower viscosities than their linear counterparts.[1–6] Moreover, their cyclic polymer architecture is highly valuable for functional material applications, such as decreasing domain spacing for block copolymers,[7] enabling superlubricity at interfaces[8] and improving thermal stability of micelles.[9] Therefore, interest in the synthesis, physical properties and functions of multicyclic polymers composed of two or more cyclic units has been increasing.

Multicyclic polymers are typically classified into three categories based on their topology: fused-type, bridged-type and spiro-type (**Figure 2.1**). For fused- and spiro-type cyclic polymers, differences in the cyclic topology type were found to significantly affect their physical properties, such as hydrodynamic volume, melting temperature and critical micelle concentration.[10–12] As summarized in chapter 1, several synthetic strategies have been proposed for the construction of different types of multicyclic polymers.[10–20] The majority of reported multicyclic polymers are composed of polyethers and polyesters, most likely because of their synthetic accessibility. Multicyclic polymers composed of general-purpose polymers, such as polystyrene (PS), with well-known fundamental characteristics, have been understudied despite their practical importance in plastics and elastomers.

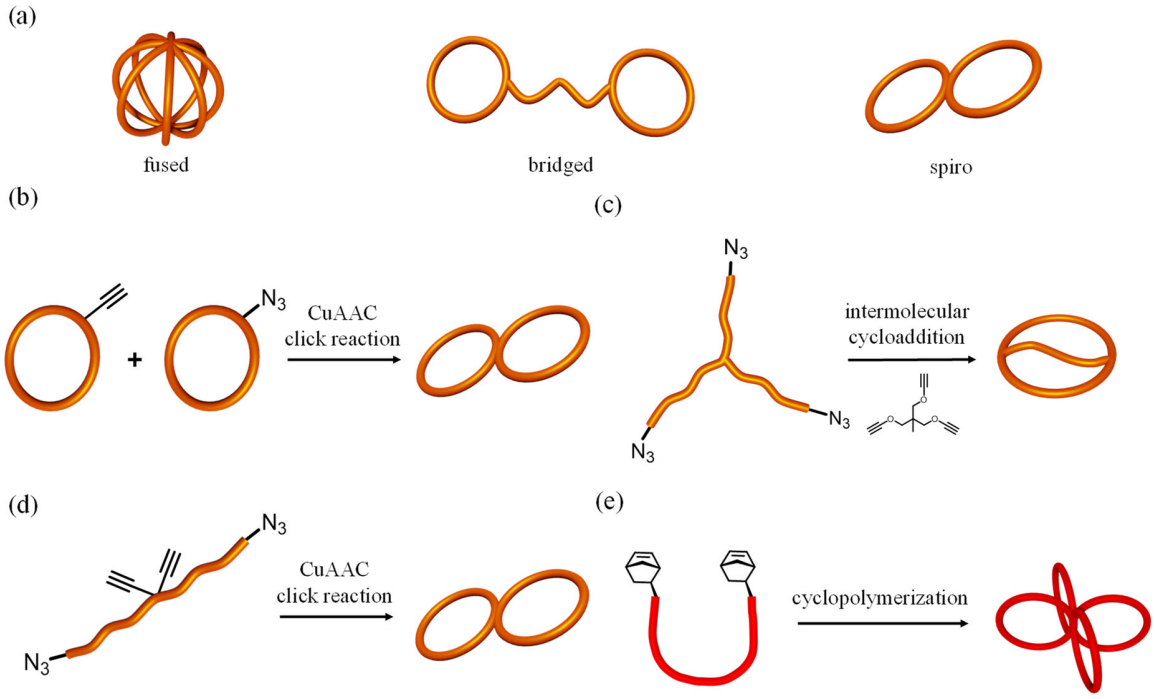

Figure 2.1. (a) Examples of diverse multicyclic topologies. Synthetic strategies for multicyclic PS: (b) intermolecular coupling of monocyclic PS (strategy (i)); (c) intermolecular cyclization of linear/star PS with a multifunctional linker (strategy (ii)); (d) intramolecular cyclization of linear/star PS precursors bearing functional groups at predetermined positions (strategy (iii)). (e) The cyclopolymerization of *α*,*ω*-dinorbornenyl end-functionalized PS described in this chapter.

To date, several synthetic pathways for multicyclic PS (mc-PS) have been developed: (i) intermolecular coupling of monocyclic constituents,[21–25] (ii) intermolecular cyclization of linear/star PS with a multifunctionalized linker,[26–28] and (iii) intramolecular cyclization of linear/star PS precursors bearing functional groups at predetermined positions,[29,30] as shown in Figures 2.1b–2.1d. As discussed in Chapter 1, the current synthetic methods for mc-PS present issues in terms of difficulty in precursor preparation, inefficiency in ring formation and synthetic

complexity due to multistep reactions, which make systematic mc-PS synthesis unrealistic. Therefore, establishing a synthetic approach to systematically produce mc-PS and elucidate the relationship between structure and properties and its industrial application is significant.

In addition to multicyclic homopolymers, the interest in the synthesis of multicyclic copolymers is increasing. Hawker *et al.* reported that a monocyclic polymer consisting of PS-*block*-polyethylene exhibited a microphase-separated structure with a smaller domain-spacing than that in its linear counterpart.[7] Borsali *et al.* revealed drastic differences in the morphologies of micelles made from linear and monocyclic PS-*block*-polyisoprene.[31–34] Yamamoto *et al.* reported that a self-assembled micelle from cyclic poly(butyl acrylate)-*block*-poly(ethylene oxide) displayed significantly improved thermal stability compared to that of its linear counterpart.[9] Even though research focused on monocyclic copolymers is promising for industrial applications, research on multicyclic copolymers is lacking. This is attributable to the complexity of current multicyclic polymer synthetic approaches, which impedes their application to the synthesis of even more complex multicyclic copolymers. Thus, the development of a versatile mc-PS synthetic approach that can be easily applied to the synthesis of PS-containing multicyclic copolymers is of great interest.

Herein, the author reports a versatile synthetic approach for mc-PS and PS-containing multicyclic copolymers based on cyclopolymerization. The synthesis of multicyclic polymers by the cyclopolymerization of α,ω-dinorbornenyl end-functionalized linear macromonomers via ring-opening metathesis polymerization (ROMP) using the Grubbs' 3rd generation catalyst (G3) has been previously reported by Satoh et al.[35] When applying highly diluted conditions, the intramolecular cyclization process surpasses the intermolecular propagation, realizing multicyclic polymer formation in a chain growth manner virtually without intermolecular

crosslinking. Although the systematic synthesis of multicyclic polymers with polyester and polyether main chains, such as polylactide, poly(ε-caprolactone), poly(ethylene glycol) and poly(tetrahydrofuran), has been achieved, the application of the cyclopolymerization approach for the synthesis of multicyclic polymers consisting of more common polymer main chains, such as polystyrene, remains unexplored. Herein, the author demonstrates the effectiveness of the cyclopolymerization approach for the systematic synthesis of mc-PS with varying numbers and sizes of cyclic units (Figures. 2.1e and **Scheme 2.1a**). Several mc-PSs were synthesized and the relationships between the structure and the viscosity, hydrodynamic volume and glass transition temperature were comprehensively examined. Furthermore, the applicability of the developed approach for the synthesis of PS-containing multicyclic copolymers with various architectures was proven (Scheme 2.1b and 2.1c).

Scheme 2.1. Synthesis of (a) mc-PS, (b) mc-(PLA-*b*-PS), and (c) poly(*c*PLA-*st*-*c*PS)

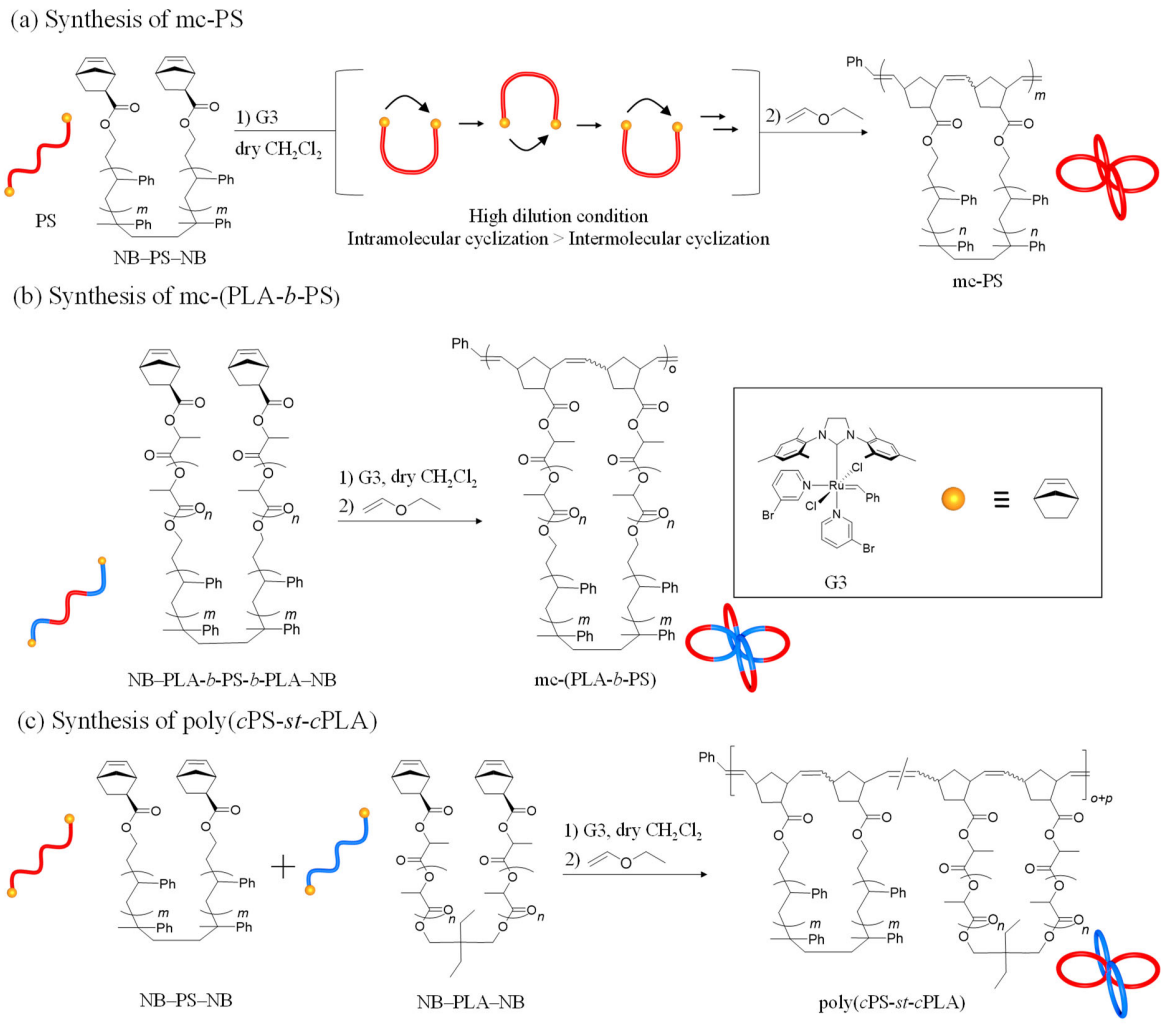

2.2 Experimental section

2.2.1 Materials

Grubbs' 3rd generation catalyst (G3) was prepared according to previously reported method.[36] *N*,*N*-Dimethyl-4-aminopyridine (DMAP; Tokyo Chemical Industry Co., Ltd. (TCI), >99.0%), 1-ethyl-3-(3-(dimethylamino)-propyl)carbodiimide hydrochloride (EDC; TCI, >98.0%), ethyl vinyl ether (TCI, >98.0%), (±)-*exo*-5-norbornenecarboxylic acid (*exo*-NB–COOH; Aldrich, 97%), *rac*-lactide (LA; TCI, >98.0%), 1,8-diazabicyclo[5.4.0]-7-undecene (DBU; TCI, >98.0%), 1-butanol (Wako Pure Chemical Industry Co. Ltd., >99.0%), CH_2Cl_2 (Junsei Chemical Co., Ltd., >99.0%), methanol (Aldrich, >99.8, dry methanol (Kanto Chemical Co., Inc., >99.5%), *sec*-butyllithium (*sec*-BuLi; Kanto Chemical Co., Inc., 1.23 mol L^{-1} in cyclohexane/*n*-hexane (v/v = 24/1)), and dry CH_2Cl_2 (Kanto Chemical Co., Inc., >99.5%, water content, 99%), propylene oxide (PO; TCI, >99.0%), and cyclohexane (Kanto Chemical Co., Inc., >99.5%) were purified by distillation over CaH_2 under reduced pressure. Linear polystyrenes with different molecular weights, synthesized by anionic polymerization with *sec*-BuLi as an initiator, were obtained from Shodex and used as received.

2.2.2 Instruments

The polymerization experiments were carried out in an MBRAUN stainless steel glovebox equipped with a gas purification system (molecular sieves and copper catalyst) in a dry argon atmosphere (H_2O, O_2<0.1 ppm). The moisture and oxygen contents in the glovebox were monitored by an MB-MO-SE 1 moisture sensor and an MB-OX-SE 1 oxygen sensor, respectively. The ^1H (400 MHz) spectra were recorded using a JEOL JNM-ECS400 instrument at room temperature in $CDCl_3$. The size exclusion chromatography (SEC) was performed at 40 °C in THF (flow rate, 1.0 mL min^{-1}) using a Shodex GPC-101 gel permeation chromatography system (Shodex DU-2130 dual pump, Shodex RI-71-S reflective index detector, and Shodex ERC-3125SN degasser) equipped with a Shodex KF-G guard column (4.6 mm × 10 mm; particle size, 8 μm) and two Shodex KF-804L columns (linear, 8 mm × 300 mm) or Jasco high-performance liquid chromatography system (PU-3 980 Intelligent HPLC Pump, CO-2065 Plus Intelligent Column Oven, RI-2031 Plus Intelligent RI Detector, and DG2080-53 Degasser) equipped with a Shodex KF-G guard column (4.6 mm × 10 mm; particle size, 8 μm) and two Shodex KF-804L columns (linear; particle size 7 μm; 8.0 mm × 300 mm; exclusion limit, 4×10^4) or Jasco high-performance liquid chromatography system (PU-4180 HPLC pump, AS-4550 auto sampler, and CO-4060 column oven) equipped with a Shodex K-800D guard column (8.0 mm × 100 mm; particle size, 10 μm), two Shodex columns (K-806L and K-804L; linear, 8.0 mm × 100 mm; particle size, 10 μm) (which was only used for the measurement of NB–PS_{52k}–NB and mc-PS_{52k}) . The absolute number-averaged molecular weight ($M_{n,MALS}$) and polydispersity ($Đ_{MALS}$) of the samples were determined by SEC with multiangle light scattering detection (SEC-MALS-Visco) in $CHCl_3$ (flow rate, 1.0 mL min^{-1}) at 40 °C using a Jasco high-performance liquid chromatography system (PU-4180 HPLC pump, AS-4550 auto sampler, and

CO-4060 column oven) equipped with a Shodex K-800D guard column (8.0 mm × 100 mm; particle size, 10 μm), two Shodex columns (K-806L and K-804L; linear, 8.0 mm × 100 mm; particle size, 10 μm), a DAWN 8 multiangle laser light scattering detector (Wyatt Technology), a Viscostar viscosity detector (Wyatt Technology), and an RI-501 refractive index detector (Shodex). The preparative GPC was performed at room temperature in $CHCl_3$ (flow rate, 10.0 mL min^{-1}) using LaboACE LC-7080 liquid chromatography system (Japan Analytical Industry Co. Ltd.) equipped with a P-LA80 pump, a RI-700LA RI detector, JAIGEL-HR-P guard column (8 mm × 40 mm; Japan Analytical Industry Co. Ltd.), JAIGEL-2HR column (linear, 20.0 mm × 600 mm; exclusion limit, 5.0×10^3), JAIGEL-2.5HR column (linear, 20.0 mm × 600 mm; exclusion limit, 2.0×10^4), and JAIGEL-3HR column (linear, 20.0 mm × 600 mm; exclusion limit, 7.0×10^4).

Differential scanning calorimetry (DSC) measurement

The DSC experiments were performed using a Hitachi DSC 7000X under a nitrogen atmosphere. The samples of mc-PS were heated to 150 °C, cooled to 30 °C, and heated again to 150 °C at the heating and cooling rate of 10 °C min^{-1} and 20 °C min^{-1}, respectively. The samples of PS-containing multicyclic copolymers were heated to 150 °C, cooled to −10 °C, and heated again to 150 °C at the heating and cooling rate of 10 °C min^{-1} and 20 °C min^{-1}, respectively.

Matrix-assisted laser desorption ionization time-of-flight mass spectrometry (MALDI-TOF MS)

The MALDI-TOF MS measurement of the obtained products was performed using an Bruker Daltonics (Germany) Ultraflex MALDI-TOF/TOF mass spectrometer equipped with a 355-nm Nd:YAG laser. PS samples were prepared by depositing a mixture of the polymer, matrix, and cationic agent in THF onto a sample plate. A 10:10:1 (v/v) ratio of [PS (1 g L^{-1} in THF)]/[*trans*-2-[3-(4-tertbutylphenyl)-2-methyl-propenylidene]malononitrile (DCTB; 20 g L^{-1} in THF)]/[silver trifluoroacetate (2.0 g L^{-1} in THF)] was used.

2.2.3 Synthetic details

Synthesis of *α*, *ω*-end norbornenyl-functionalized PS (NB–PS$_{1k}$–NB)

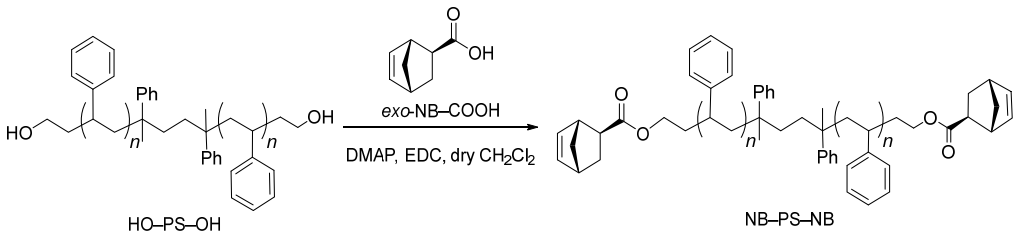

A typical procedure for the condensation reaction is as follows (Method A): In a round-bottom flask, HO–PS$_{1k}$–OH ($M_{n,NMR}$ = 1,100, 2.00 g, 1.82 mmol), *exo*-NB–COOH (1.02 g, 7.38 mmol), EDC (2.11 g, 11.0 mmol), and DMAP (1.33 mg, 10.9 mmol) were dissolved in CH_2Cl_2 (25.0 mL), and the mixture was stirred at r.t. for 96 h. The polymer crude was purified by silica gel column chromatography (CH_2Cl_2/Methanol = 19/1 (v/v), R_f = 0.29) to give NB–PS$_{1k}$–NB as a white solid. Note that higher molecular weight NB–PS$_x$–PS (x = 6k, 12k, 13k, and 52k) were purified by the reprecipitation from the CH_2Cl_2 solution into methanol. Yield: 1.58 g (79.0%)

$M_{n,NMR}$ = 1,640, $M_{n,SEC}$ = 1,220, $Đ$ = 1.55

^{1}H NMR ($CDCl_3$, 400 MHz): δ (ppm) 7.40–6.17 (m, *aromatic*), 6.18–6.00 (m, 4H, –C*H*=C*H*– in norbornene ring), 3.93–3.60 (m, 4H, –CH_2C*H*$_2$OCO–), 3.14–2.91 (m, 4H, –C*H*–CH_2–CH–CO– in norbornene ring, –C*H*–CH–CO– in norbornene ring), 2.53–1.69 (m, –CH_2C*H*Ph–, *endo*-C*H*– of –CH–CH_2–CH–C*H*CO– in norbornene ring, *exo*-C*H*– of –CH–C*H*$_2$–CH–CO– in norbornene ring), 1.69–1.13 (m, –C*H*$_2$CHPh–, –CH_2CC*H*$_3$(Ph)–, –C*H*$_2$CCH$_3$(Ph)–, –C*H*$_2$CH$_2$OCO–, *endo*-C*H*– of –CH–C*H*$_2$–CH–CO– in norbornene ring, bridge head –C*H*$_2$– in norbornene ring).

Method A was used for the reaction of HO–PS_{6k}–OH ($M_{n,NMR}$ = 6,000, 2.50 g, 417 μmol) with *exo*-NB–COOH (231 mg, 1.67 mmol), DMAP (485 mg, 2.53 mmol), and EDC (485 mg, 2.53 mmol) in CH_2Cl_2 (25.0 mL) for 91 h to give NB–PS_{6k}–NB as a white solid. Yield: 2.45 g (98.0%)

$M_{n,NMR}$ = 6,000, $M_{n,SEC}$ = 5,800, $Đ$ = 1.09, $M_{n,MALS}$ = 6,470, $Đ_{MALS}$ = 1.04

Method A was used for the reaction of HO–PS_{12k}–OH ($M_{n,NMR}$ = 12,000, 2.50 g, 208 μmol) with *exo*-NB–COOH (111 mg, 803 μmol), DMAP (148 mg, 1.21 mol), and EDC (232 mg, 1.21 mol) in CH_2Cl_2 (25.0 mL) for 72 h to give NB–PS_{12k}–NB as a white solid. Yield: 1.99 g (79.6%)

$M_{n,NMR}$ = 11,600, $M_{n,SEC}$ = 11,500, $Đ$ = 1.07, $M_{n,MALS}$ = 12,300, $Đ_{MALS}$ = 1.05

Method A was used for the reaction of HO–PS_{13k}–OH ($M_{n,NMR}$ = 11,600, 2.50 g, 216 μmol) with *exo*-NB–COOH (136 mg, 984 μmol), DMAP (181 mg, 1.48 mol), and EDC (284 mg, 1.48 mol) in CH_2Cl_2 (25.0 mL) for 72 h to give NB–PS_{13k}–NB as a white solid. Yield: 2.24 g (89.6%)

$M_{n,NMR}$ = 12,300, $M_{n,SEC}$ = 12,500, $Đ$ = 1.22, $M_{n,MALS}$ = 13,400, $Đ_{MALS}$ = 1.19

Method A was used for the reaction of HO–PS_{52k}–OH ($M_{n,NMR}$ = 55,600, 1.00 g, 17.8 μmol) with *exo*-NB–COOH (15.3 mg, 111 μmol), DMAP (20.3 mg, 166 μmol), and EDC (32.1 mg, 167 μmol) in CH_2Cl_2 (10.0 mL) for 168 h to give NB–PS_{52k}–NB as a white solid. Yield: 837 mg (83.7%)

$M_{n,NMR}$ = 55,600, $M_{n,SEC}$ = 54,400, $Đ$ = 1.06, $M_{n,MALS}$ = 52,100, $Đ_{MALS}$ = 1.01

Synthesis of multicyclic-polystyrene (mc-PS)

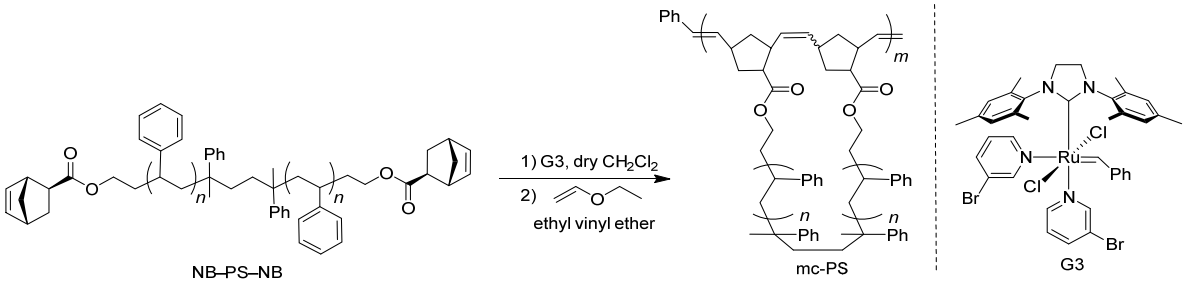

A typical procedure for the ring-opening metathesis polymerization (ROMP) is as follows (Method B): In a three-necked flask, a stock solution of Grubbs third-generation catalyst (G3; 2.54 mL, 20.3 μmol as a 8.0 mol L^{-1} in dry CH_2Cl_2, 1.0 eq.) was quickly added to a stirred mixture of *α*,*ω*-dinorbornenyl-functionalized linear polystyrene (NB–PS_{1k}–NB; $M_{n,NMR}$ = 1,640, 100 mg, 61.0 μmol, 3.0 eq.) in dry CH_2Cl_2 (122 mL) under an argon atmosphere. After 10 min, an excess amount of ethyl vinyl ether was added to the reacting mixture to terminate the ROMP. The crude product was purified by preparative GPC to remove the catalyst residue, affording mc-PS_{1k} as a brown solid. Yield: 82.0 mg (82.0%)

$M_{n,SEC}$ = 3,870, $Đ$ = 1.28, $M_{n,MALS}$ = 5,300, $Đ_{MALS}$ = 1.22, average number of cyclic units = 3.2

^{1}H NMR ($CDCl_3$, 400 MHz): δ (ppm) 7.23–6.12 (m, *aromatic*), 5.79–4.78 (br, alkenyl of poly(norbornene) backbone), 4.31–2.35 (br, alkenyl of poly(norbornene) backbone), 2.44–1.69 (m, –CH_2CHPh–), 1.69–0.99 (m, –CH_2CHPh–, –CH_2CCH_3(Ph)–, –CH_2CCH_3(Ph)–, –CH_2CH_2OCO–)

Gram-Scale Synthesis of mc-PS

Method A was used for the ROMP of NB–PS_{13k}–NB ($M_{n,MALS}$ = 13,400, 1.50 g, 112 μmol) with G3 (4.66 mL, 37.3 μmol as a 8.0 mmol L^{-1} solution in CH_2Cl_2) in dry CH_2Cl_2 (746 mL) for 1.5 h to give mc-PS_{13k} as a brown solid. Yield: 1.39 g (92.7%)

$M_{n,SEC}$ = 29,900, $Đ$ = 1.52, $M_{n,MALS}$ = 51,100, $Đ_{MALS}$ = 1.41, average number of cyclic units = 3.8

^{1}H NMR ($CDCl_3$, 400 MHz): δ (ppm) 7.24–6.11 (m, *aromatic*), 5.81–4.78 (br, alkenyl of poly(norbornene) backbone), 3.94–3.36 (br, alkenyl of poly(norbornene) backbone), 2.99–2.72 (br, alkenyl of poly(norbornene) backbone), 2.44–1.67 (m, –CH_2CHPh–), 1.67–0.99 (m, –CH_2CHPh–, –CH_2CCH_3(Ph)–, –CH_2CCH_3(Ph)–, –CH_2CH_2OCO–).

Synthesis of *α*, *ω*-end hydroxy-functionalized PLA-*block*-PS-*block*-PLA (HO–PLA-*b*-PS-*b*-PLA–OH)

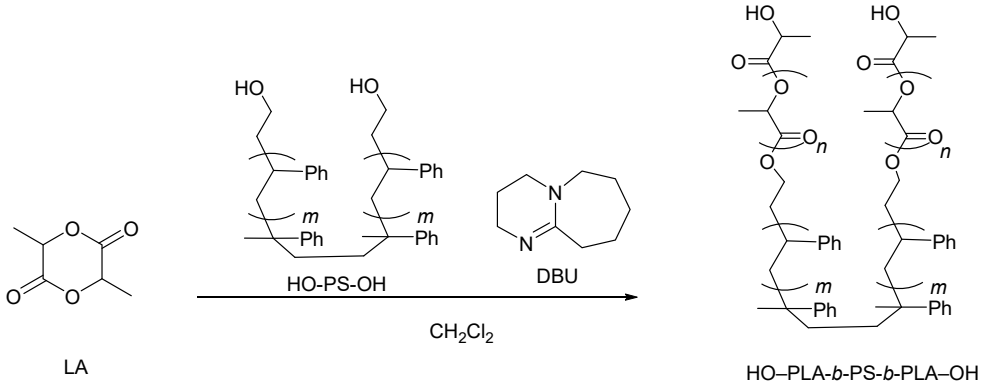

Typical procedure for the ring-opening polymerization of LA is as follows (method C): In a glovebox, HO–PS_{6k}–OH ($M_{n,NMR}$ = 6,000, 579 mg, 96.5 μmol) and LA (1.20 g, 8.32 mmol) were dissolved in CH_2Cl_2 (10.1 mL). 1,8-Diazabicyclo[5.4.0]undec-7-ene (DBU; 8.0 μL, 52 μmol) was then added to the CH_2Cl_2 solution to initiate the polymerization. After 50 sec, the polymerization was quenched by the addition of excess amount of benzoic acid. The mixture was purified by reprecipitation from CH_2Cl_2 to cold methanol to give HO–PLA-*b*-PS-*b*-PLA–OH as a white solid. Yield: 1.56 g (86.7%)

$M_{n,NMR}$ = 16,000, $M_{n,SEC}$ = 21,100, $Đ$ = 1.04

^{1}H NMR ($CDCl_3$, 400 MHz): δ (ppm) 7.24–6.26 (m, *aromatic*), 5.28–5.08 (m, methine of PLA backbone), 3.88–3.63 (m, 4H, –CH_2CH_2OCO–), 2.77–2.60 (m, –O*H*), 2.23–1.72 (m, –CH_2CHPh–), 1.72–1.16 (m, –CH_2CHPh–, –CH_2CCH_3(Ph)–, –CH_2CCH_3(Ph)–, –CH_2CH_2OCO, $CH_3CH_2)_2C(CH_2)$O–, $(CH_3CH_2)_2C(CH_2)$O–).

Synthesis of *α*, *ω*-end norbornenyl-functionalized PLA-*block*-PS-*block*-PLA (NB–PLA-*b*-PS-*b*-PLA–NB)

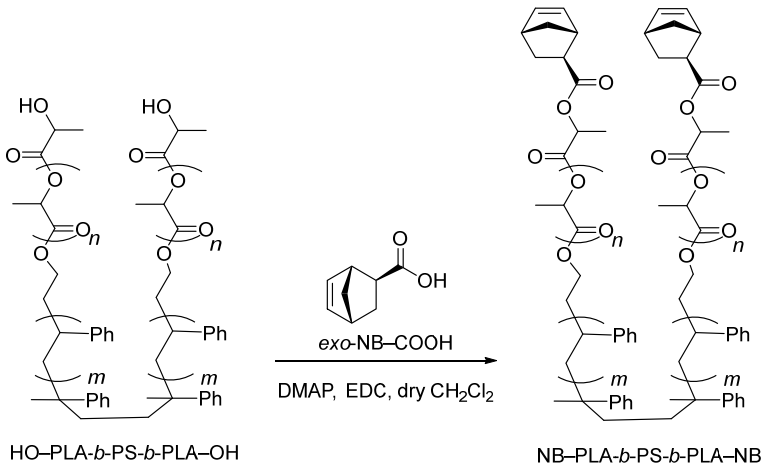

Method A was used for the reaction of HO–PLA-*b*-PS-*b*-PLA–OH ($M_{n,NMR}$ = 16,000, 1.00 g, 62.5 μmol) with *exo*-NB–COOH (34.5 mg, 249 μmol), DMAP (45.8 mg, 375 μmol), and EDC (485 mg, 375 μmol) in CH_2Cl_2 (10.0 mL) for 81 h to give NB–PLA-*b*-PS-*b*-PLA–NB as a white solid. Yield: 831 mg (83.1%)

$M_{n,NMR}$ = 15,900, $M_{n,SEC}$ = 22,700, $Đ$ = 1.03, $M_{n,MALS}$ = 12,700, $Đ_{MALS}$ = 1.01

^{1}H NMR ($CDCl_3$, 400 MHz): δ (ppm) 7.24–6.26 (m, *aromatic*), 6.16–6.07 (m, 4H, –C*H*=C*H*– in norbornene ring), 5.28–5.08 (m, methine of PLA backbone), 3.88–3.63 (m, 4H, –CH_2CH_2OCO–), 2.96–2.77 (m, 4H, –C*H*–CH_2–CH–CO– in norbornene ring, –C*H*–CH–CO– in norbornene ring), 2.23–1.72 (m, –CH_2C*H*Ph–, *endo*-C*H*– of –CH–CH_2–CH–C*H*CO– in norbornene ring, *exo*-C*H*– of –CH–C*H*$_2$–CH–CO– in norbornene ring), 1.72–1.16 (m, –C*H*$_2$CHPh–, –CH_2CC*H*$_3$(Ph)–, –C*H*$_2$CCH$_3$(Ph)–, –C*H*$_2$CH$_2$OCO, $CH_3CH_2)_2C(CH_2)$O–, $(CH_3CH_2)_2C(CH_2)$O–, –C*H*$_2$CH$_2$OCO–, *endo*-C*H*– of –CH–C*H*$_2$–CH–CO– in norbornene ring, bridge head –C*H*$_2$– in norbornene ring).

Synthesis of multicyclic PLA-*block*-PS (mc-(PLA-*b*-PS))

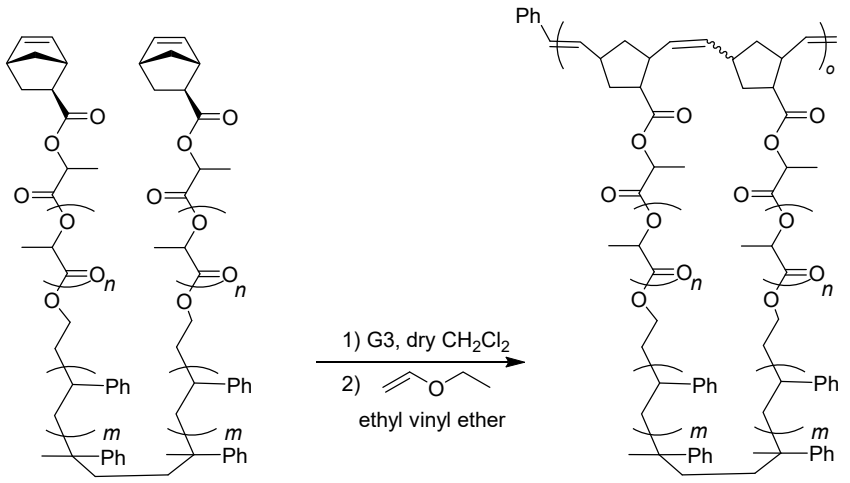

NB–PLA-*b*-PS-*b*-PLA–NB mc-(PLA-*b*-PS)

Method B was used for the ROMP of NB–PLA-*b*-PS-*b*-PLA–NB ($M_{n,NMR}$ = 15,900, 50.0 mg, 3.14 μmol) with G3 (131 μL, 1.04 μmol as a 8.0 mmol L^{-1} solution in CH_2Cl_2) in dry CH_2Cl_2 (21.0 mL) for 1.5 h to give mc-(PLA-*b*-PS) as a brown solid. Yield: 49.8 mg (99.6%) $M_{n,SEC}$ = 55,200, $Đ$ = 1.82, $M_{n,MALS}$ = 66,400, $Đ_{MALS}$ = 1.44, average number of cyclic units = 5.2

^{1}H NMR ($CDCl_3$, 400 MHz): δ (ppm) 7.24–6.26 (m, *aromatic*), 5.28–5.08 (m, methine of PLA backbone), 4.05–2.52 (br, alkenyl of poly(norbornene), 3.88–3.63 (m, 4H, –CH_2CH_2OCO–), 2.23–1.72 (m, –CH_2CHPh–), 1.72–1.16 (m, –CH_2CHPh–, –CH_2CCH_3(Ph)–, –CH_2CCH_3(Ph)–, –CH_2CH_2OCO, $CH_3CH_2)_2C(CH_2)$O–, $(CH_3CH_2)_2C(CH_2)$O–).

Synthesis of *α*, *ω*-end hydroxy-functionalized PLA (HO–PLA–OH)

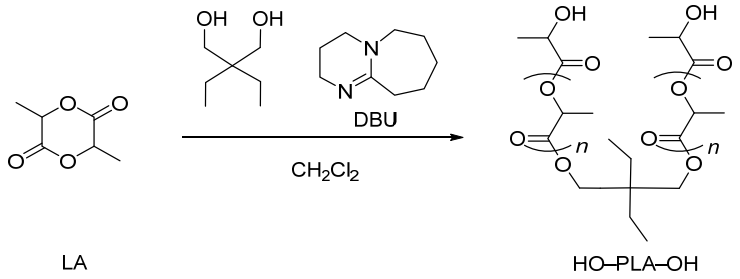

Method C was used for the polymerization of LA (1.50 g, 10.4 mmol) with 2,2-diethyl-1,3-propanediol (29.8 mg, 226 μmol) and DBU (15.9 μL, 104 μmol) in CH_2Cl_2 (10.4 mL) for 4 min to give HO–PLA_{6k}–OH as a white solid. Yield: 1.46 g (97.3%)

$M_{n,NMR}$ = 6,400, $M_{n,SEC}$ = 12,000, $Đ$ = 1.07

^{1}H NMR ($CDCl_3$, 400 MHz): δ (ppm) 5.29–5.04 (m, methine of PLA backbone), 4.42–4.28 (m, methine of *α*, *ω*-chain end lactyl unit), 4.04–3.86 (m, $(CH_3CH_2)_2C(CH_2)O$–) 2.73–2.63 (m, –O*H*), 1.79–1.44 (methyl of PLA backbone), 1.35–1.17 (m, $(CH_3CH_2)_2C(CH_2)O$–), and 0.92–0.75 (m, $(CH_3CH_2)_2C(CH_2)O$–).

Method C was used for the polymerization of LA (1.50 g, 10.4 mmol) with 2,2-diethyl-1,3-propanediol (11.0 mg, 83.1 μmol) and DBU (15.9 μL, 104 μmol) in CH_2Cl_2 (10.4 mL) for 4 min to give HO–PLA_{13k}–OH as a white solid. Yield: 1.25 g (83.3%)

$M_{n,NMR}$ = 12,700, $M_{n,SEC}$ = 19,300, $Đ$ = 1.04

Synthesis of *α*, *ω*-end norbornenyl-functionalized PLA (NB–PLA–NB)

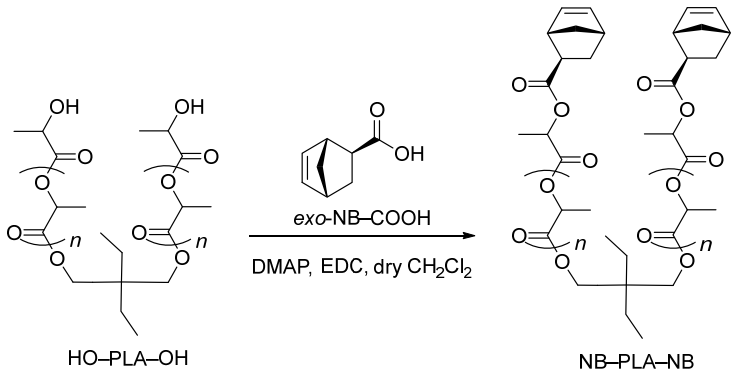

Method A was used for the reaction of HO–PLA$_{6k}$–OH ($M_{n,NMR}$ = 6,700, 1.00 g, 149 μmol) with *exo*-NB–COOH (44.3 mg, 321 μmol), DMAP (58.6 mg, 493 μmol), and EDC (94.6 mg, 480 μmol) in CH_2Cl_2 (10.0 mL) for 2 days to give NB–PLA$_{6k}$–NB as a white solid. Yield: 930 mg (93.0%)

$M_{n,NMR}$ = 6,700, $M_{n,SEC}$ = 12,100, $Đ$ = 1.08

^{1}H NMR ($CDCl_3$, 400 MHz): δ (ppm) 6.15–6.00 (m, 4H, –C*H*=C*H*– in norbornene ring), 5.02-4.49 (m, methine of PLLA backbone), 3.90–3.54 (m, 4H, –CH_2CH_2OCO–), 2.94–2.83 (m, 4H, –C*H*–CH_2–CH–CO– in norbornene ring, –C*H*–CH–CO– in norbornene ring), 2.48–1.66 (*endo*-C*H*– of –CH–CH_2–CH–C*H*CO– in norbornene ring, *exo*-C*H*– of –CH–CH_2–CH–CO– in norbornene ring), 1.66–1.15 (m, –C$H_2$$CH_2$OCO–, *endo*-C*H*– of –CH–CH_2–CH–CO– in norbornene ring, bridge head –CH_2– in norbornene ring, methyl of PLA backbone), and 0.92–0.75 (m, (C$H_3$$CH_2$)$_2$C($CH_2$)O–).

Method B was used for the reaction of HO–PLA$_{13k}$–OH ($M_{n,NMR}$ = 12,700, 1.00 g, 78.7 μmol) with *exo*-NB–COOH (48.5 mg, 351 μmol), DMAP (59.0 mg, 483 μmol), and EDC (95.1 mg, 496 μmol) in CH_2Cl_2 (10.0 mL) for 2 days to give NB–PLA$_{13k}$–NB as a white solid. Yield: 911 mg (91.1%)

$M_{n,NMR}$ = 13,200, $M_{n,SEC}$ = 19,800, $Đ$ = 1.03

Statistical cyclocopolymerization of NB–PS–NB and NB–PLA–NB

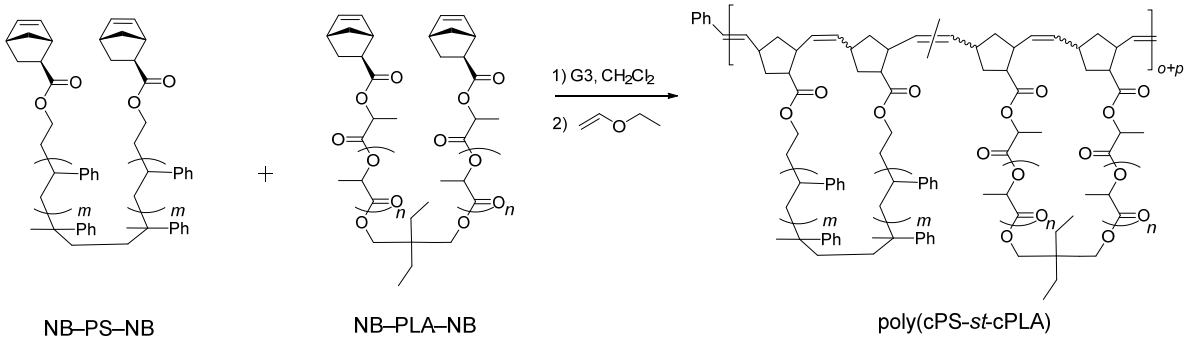

Method B was used for the ROMP of NB–PS$_{6k}$–NB ($M_{n.NMR}$ = 5,700, 50.0 mg, 8.77 μmol) and NB–PLA$_{6k}$–NB ($M_{n,NMR}$ = 6,700, 50.0 mg, 7.46 μmol) with G3 (1.01 mL, 8.06 μmol as a 8.0 mmol L^{-1} solution in CH_2Cl_2) in dry CH_2Cl_2 (129 mL) for 3 h to give poly(*c*PS-*st*-*c*PLA) as a brown solid. Yield: 81.7 mg (81.7%)

$M_{n,SEC}$ = 15,300, $Đ$ = 1.34, $M_{n,MALS}$ = 23,800, $Đ_{MALS}$ = 1.07, average number of cyclic units = 3.8

^{1}H NMR ($CDCl_3$, 400 MHz): δ (ppm) 7.38–6.25 (m, *aromatic*), 5.02-4.49 (m, methine of PLLA backbone), 4.31–2.48 (br, alkenyl of poly(norbornene), 2.44–0.75 (m, –CH_2CHPh–, –CH_2CHPh–, –$CH_2CCH_3(Ph)$–, –$CH_2CCH_3(Ph)$–, –CH_2CH_2OCO–, –CH_2CH_2OCO–, methyl of PLA backbone, $(CH_3CH_2)_2C(CH_2)O$–).

Synthesis of *ω*-end hydroxy-functionalized PS (PS_{3k}–OH)

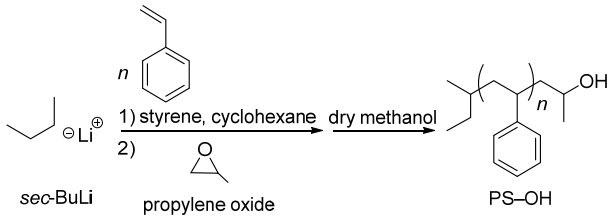

Under Ar atmosphere, cyclohexane (24.0 mL) was placed in a round-bottom flask equipped with a greaseless valve and then heated to 40 °C in an oil bath. *sec*-BuLi (953 μL, 857 μmol) was added to the solution. Styrene (2.76 mL, 24.0 mmol) was added to the solution, and the mixture was stirred for 2 h. Propylene oxide (600 μL, 8.57 mmol) was then added to the solution at 40 °C, and the mixture was stirred for 2 h. Excess dry methanol was added to terminate the polymerization. The product was purified by reprecipitation in methanol to give PS_{3k}–OH as a white solid. Yield: 2.49 g (99.6%)

$M_{n,NMR}$ = 2,900, $M_{n,SEC}$ = 3,200, $Đ$ = 1.10

^{1}H NMR ($CDCl_3$, 400 MHz): δ (ppm) 7.22–6.22 (m, *aromatic*), 3.61–3.16 (s, 1H, –$CH_2CH(CH_3)OH$), 2.44–1.66 (m, –CH_2CHPh–), 1.66–1.21 (m, –CH_2CHPh–, –$CH_2CH(CH_3)OH$, –$CH_2CH(CH_3)OH$), 1.14–0.51 (m, –*sec*-butyl).

Synthesis of *ω*-end norbornenyl-functionalized PS (PS_{3k}–NB)

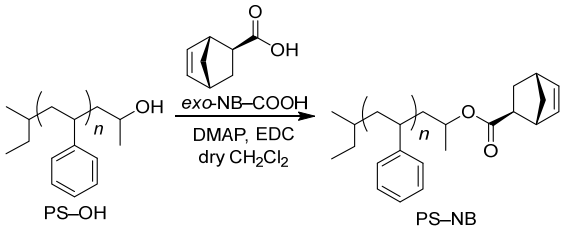

Method B was used for the reaction of PS–OH ($M_{n,NMR}$ = 2,900, 2.30 g, 793 μmol) with *exo*-NB–COOH (268 mg, 1.94 mmol), DMAP (351 mg, 2.87 mmol), and EDC (559 mg, 2.92 mmol) in CH_2Cl_2 (24 mL) for 4 days to give PS_{3k}–NB as a white solid. Yield: 1.73 g (75.2%)

$M_{n,NMR}$ = 3,300, $M_{n,SEC}$ = 3,300, $Đ$ = 1.04, $M_{n,MALS}$ = 5,100, $Đ_{MALS}$ = 1.01

^{1}H NMR ($CDCl_3$, 400 MHz): δ (ppm) 7.22–6.19 (m, *aromatic*), 6.19–5.96 (m, 2H, –C*H*=C*H*– in norbornene ring), 4.78–4.34 (s, 1H, –CH_2C*H*(CH_3)O–), 2.97–2.72 (m, 2H, –C*H*–CH_2–CH–CO– in norbornene ring, –C*H*–CH–CO– in norbornene ring), 2.44–1.68 (m, –CH_2C*H*Ph–, *endo*-C*H*– of –CH–CH_2–CH–C*H*CO– in norbornene ring, *exo*-C*H*– of –CH–C*H*$_2$–CH–CO– in norbornene ring, bridge head –C*H*$_2$– in norbornene ring), 1.68–1.09 (m, –C*H*$_2$CHPh–, –C*H*$_2$CH(CH_3), –CH_2CH(C*H*$_3$), *endo*-C*H*– of –CH–C*H*$_2$–CH–CO– in norbornene ring), 1.08–0.51 (m, –*sec*-butyl).

Synthesis of *ω*-end norbornenyl-functionalized PLA (PLA_{3k}–OH)

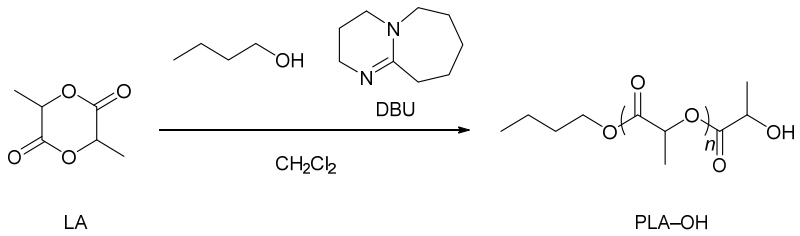

Method C was used for the polymerization of LA (1.50 g, 10.4 mmol) with 1-butanol (29.6 mg, 399 μmol) and DBU (15.9 μL, 104 μmol) in CH_2Cl_2 (10.4 mL) for 1 min to give PLA_{3k}–OH as a white solid. Yield: 859 mg (69.3%)

$M_{n,NMR}$ = 2,700, $M_{n,SEC}$ = 4,700, $Đ$ = 1.10

^{1}H NMR ($CDCl_3$, 400 MHz): δ (ppm) 5.27–5.04 (m, methine of PLA backbone), 4.41–4.29 (m, methine of *ω*-chain end lactyl unit), 2.74–2.62 (m, –O*H*), 1.79–1.44 (methyl of PLA backbone), 1.35–1.17 (m, $CH_3CH_2CH_2CH_2O$–), 1.35–1.17 (m, $CH_3CH_2CH_2CH_2O$–), 1.35–1.17 (m, $CH_3CH_2CH_2CH_2O$–), and 0.97–0.75 (m, $CH_3CH_2CH_2CH_2O$–).

Synthesis of *ω*-end norbornenyl-functionalized PLA (PLA_{3k}–NB)

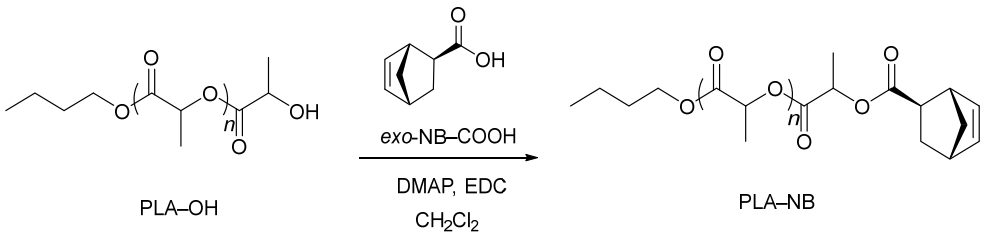

Method A was used for the reaction of PLA_{3k}–OH ($M_{n,NMR}$ = 2,700, 500 mg, 185 μmol) with *exo*-NB–COOH (53.4 mg, 387 μmol), DMAP (68.7 mg, 562 μmol), and EDC (112 mg, 583 μmol) in CH_2Cl_2 (5.0 mL) for 2 days to give PLA_{3k}–NB as a white solid. Yield: 491 mg (98.2%)

$M_{n,NMR}$ = 3,000, $M_{n,SEC}$ = 5,300, $Đ$ = 1.08

^{1}H NMR ($CDCl_3$, 400 MHz): δ (ppm) 6.19–6.08 (m, 2H, –C*H*=C*H*– in norbornene ring), 5.27–5.04 (m, methine of PLA backbone), 4.41–4.29 (m, methine of *ω*-chain end lactyl unit), 3.19–2.89 (m, 2H, –C*H*–CH_2–CH–CO– in norbornene ring, –C*H*–CH–CO– in norbornene ring), 2.38–1.90 (*endo*-C*H*– of –CH–CH_2–CH–C*H*CO– in norbornene ring, *exo*-C*H*– of –CH–C*H*$_2$–CH–CO– in norbornene ring), 1.79–1.44 (–C*H*$_2$$CH_2$OCO–, *endo*-C*H*– of –CH–C*H*$_2$–CH–CO– in norbornene ring, bridge head –C*H*$_2$– in norbornene ring, methyl of PLA backbone), 1.35–1.17 (m, CH_3CH_2C*H*$_2$$CH_2$O–), 1.35–1.17 (m, CH_3C*H*$_2$$CH_2CH_2$O–), 1.35–1.17 (m, CH_3CH_2C*H*$_2$$CH_2$O–), and 0.97–0.75 (m, C*H*$_3$$CH_2CH_2CH_2$O–).

Statistical copolymerization of PS–NB and PLA–NB

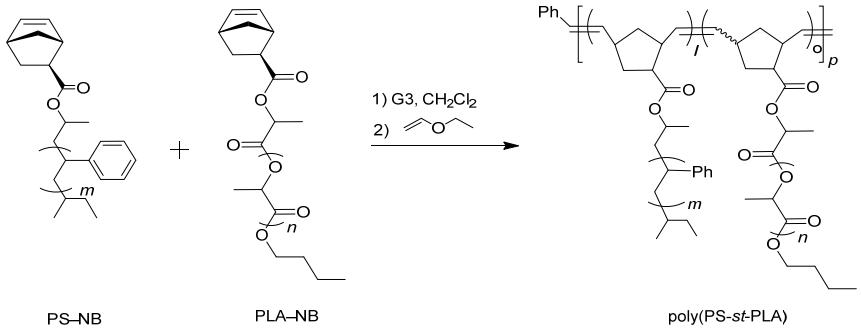

Method B was used for the ROMP of PS_{3k}–NB (50.0 mg, 13.9 μmol) and PLA_{3k}–NB (50.0 mg, 16.7 μmol) with G3 (316 μL, 2.53 μmol as a 8.0 mmol L^{-1} solution in CH_2Cl_2) in dry CH_2Cl_2 (1.52 mL) for 2.0 h to give poly(PS-*st*-PLA) as a brown solid. Yield: 76.7 mg (76.7%) $M_{n,SEC}$ = 28,200, $Đ$ = 1.07, $M_{n,MALS}$ = 33,800, $Đ_{MALS}$ = 1.02, average number of side-chain units = 10.7

^{1}H NMR ($CDCl_3$, 400 MHz): δ (ppm) 7.22–6.19 (m, *aromatic*), 5.27–5.04 (m, methine of PLA backbone), 4.78–4.34 (s, 1H, –$CH_2CH(CH_3)$O–), 4.41–4.29 (m, methine of ω-chain end lactyl unit), 4.32–2.52 (br, alkenyl of poly(norbornene), 2.44–0.51 (m, –CH_2CHPh–, methyl of PLA backbone, –CH_2CHPh–, –$CH_2CH(CH_3)$, –$CH_2CH(CH_3)$, $CH_3CH_2CH_2CH_2$O–, $CH_3CH_2CH_2CH_2$O–, –*sec*-butyl, $CH_3CH_2CH_2CH_2$O–).

2.3 Results and discussion

2.3.1 Synthesis of macromonomers

NB–PS–NB was synthesized via a condensation reaction between commercially available PS diol (HO–PS–OH) and *exo*-5-norbornenecarboxylic acid according to **Scheme 2.1** and was used as the macromonomer (MM) in the cyclopolymerization approach. To synthesize mc-PS with cyclic units of various sizes, five different NB–PS_x–NB macromonomers were prepared (x = 1k, 6k, 12k, 13k and 52k) with molecular weights ranging from 1k to 52k (**Table 2.1**). The quantitative esterification in each NB–PS–NB synthesis was confirmed using ^{1}H NMR spectroscopy (**Figures 2.1–2.5**).

Table 2.1 Molecular characterization of NB–PS–NB

sample (MM)	$M_{n,NMR}$ [a]	$M_{n,SEC}$ [b]	$Đ$ [b]	$M_{n,MALS}$ [c]
NB–PS_{1k}–NB	1,640	1,220	1.55	-
NB–PS_{6k}–NB	6,000	5,800	1.09	6,470
NB–PS_{12k}–NB	11,600	11,500	1.07	12,300
NB–PS_{13k}–NB	12,300	12,500	1.22	13,400
NB–PS_{52k}–NB	55,600	54,400	1.06	52,100

[a] Determined by ^{1}H NMR. [b] Determined by size exclusion chromatography (SEC) equipped with a refractive index detector in THF using PS standards. [c] Determined using triple-detection SEC equipped with multi-angle light scattering, viscosity and refractive index detectors (SEC-MALS-Visco) in chloroform.

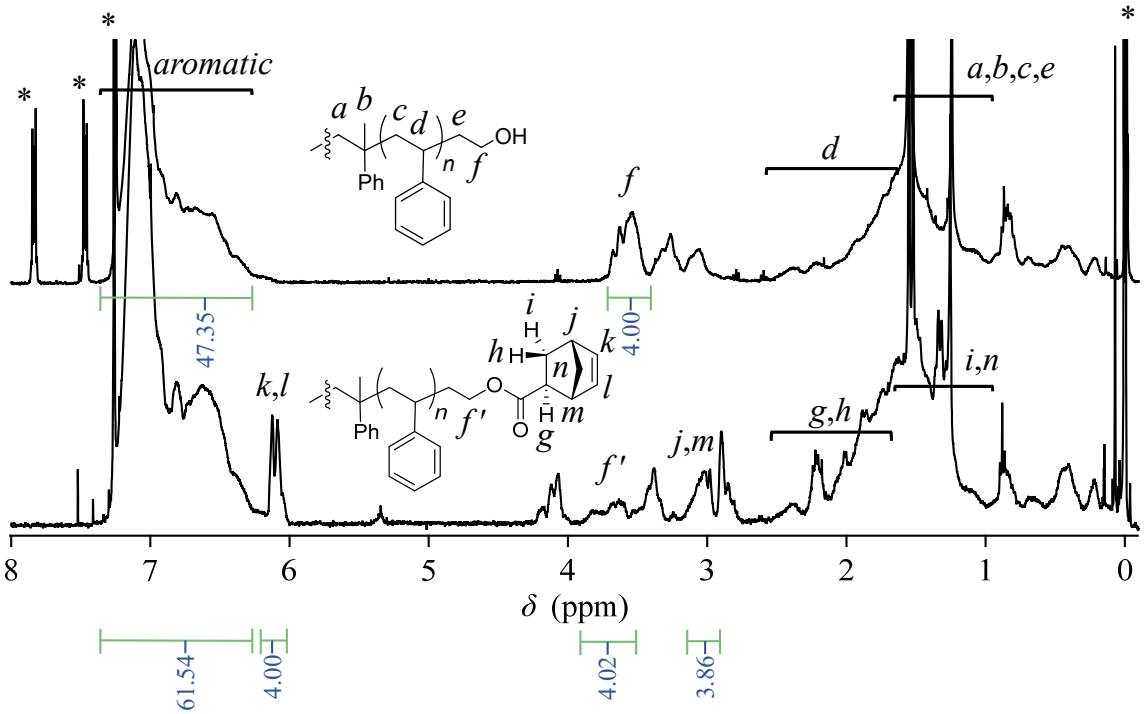

Figure 2.1. ^{1}H NMR spectra of HO–PS$_{1k}$–OH (upper) and NB–PS$_{1k}$–NB (lower) in $CDCl_3$.

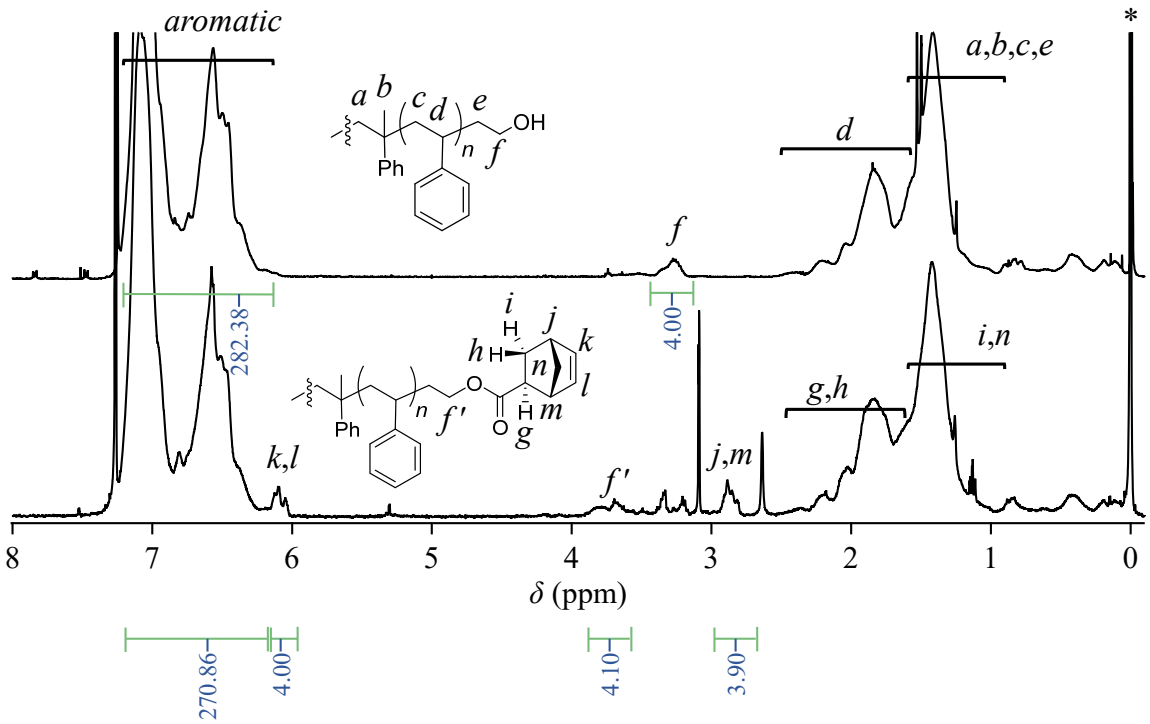

Figure 2.2. ^{1}H NMR spectra of HO–PS$_{6k}$–OH (upper) and NB–PS$_{6k}$–NB (lower) in $CDCl_3$.

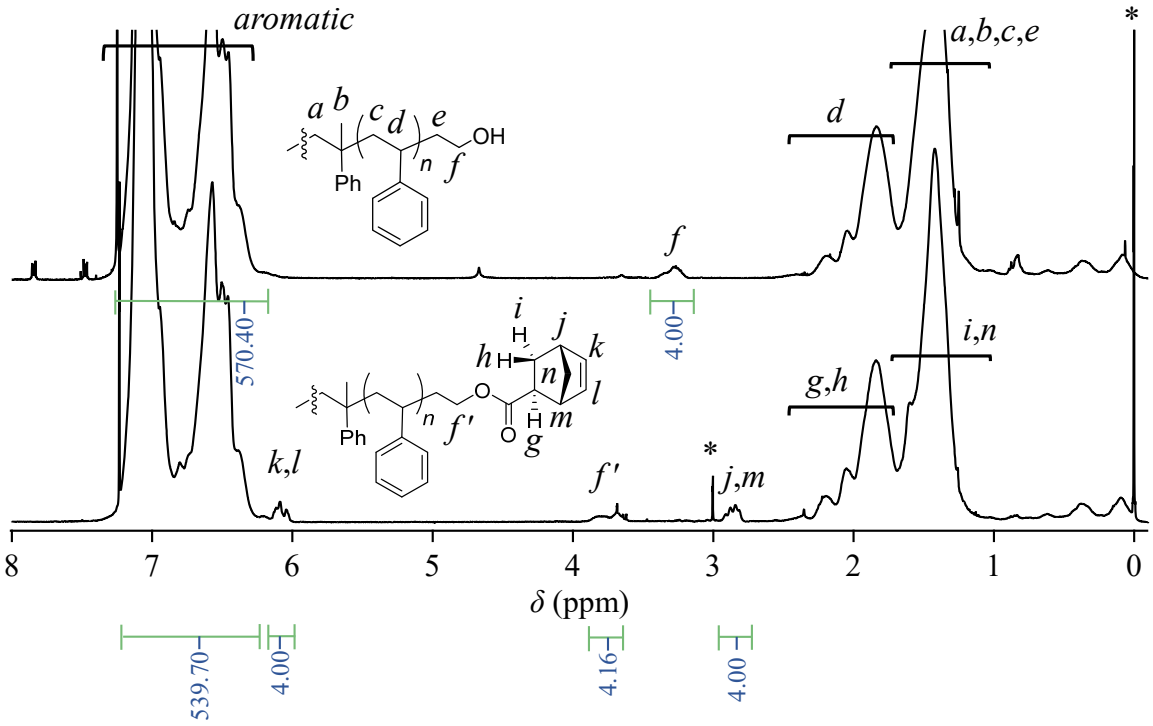

Figure 2.3. ^{1}H NMR spectra of HO–PS$_{12k}$–OH (upper) and NB–PS$_{12k}$–NB (lower) in $CDCl_3$.

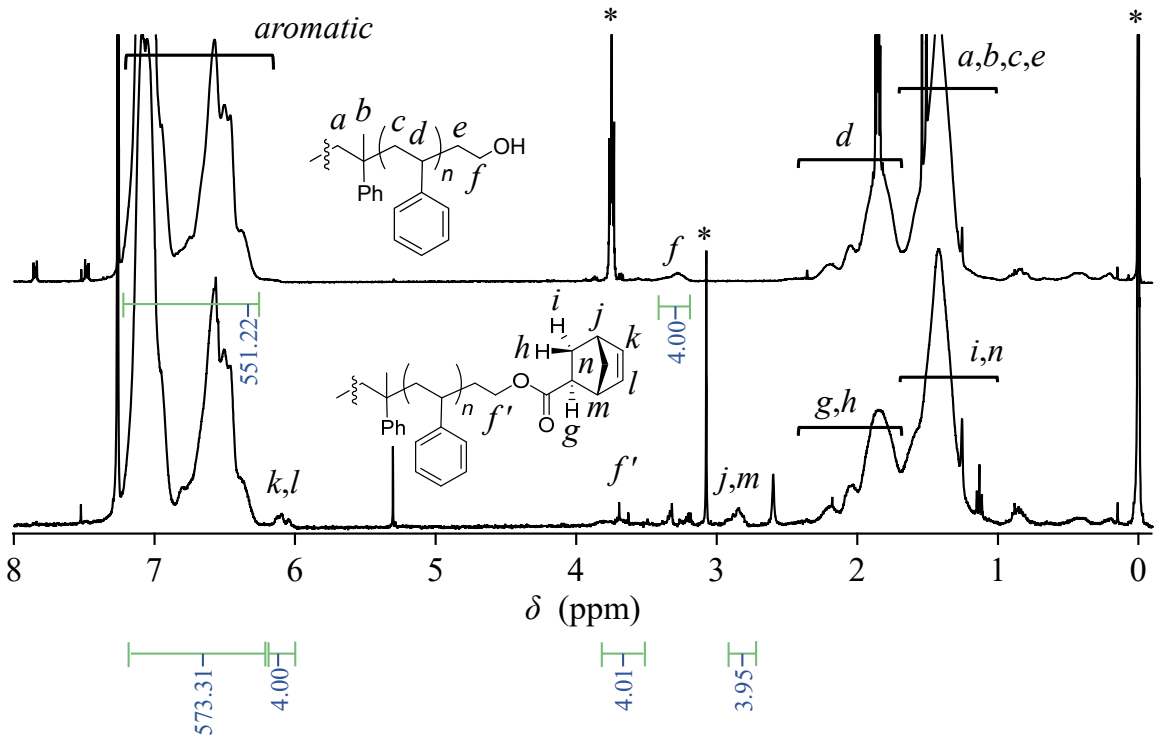

Figure 2.4. ^{1}H NMR spectra of HO–PS_{13k}–OH (upper) and NB–PS_{13k}–NB (lower) in $CDCl_3$.

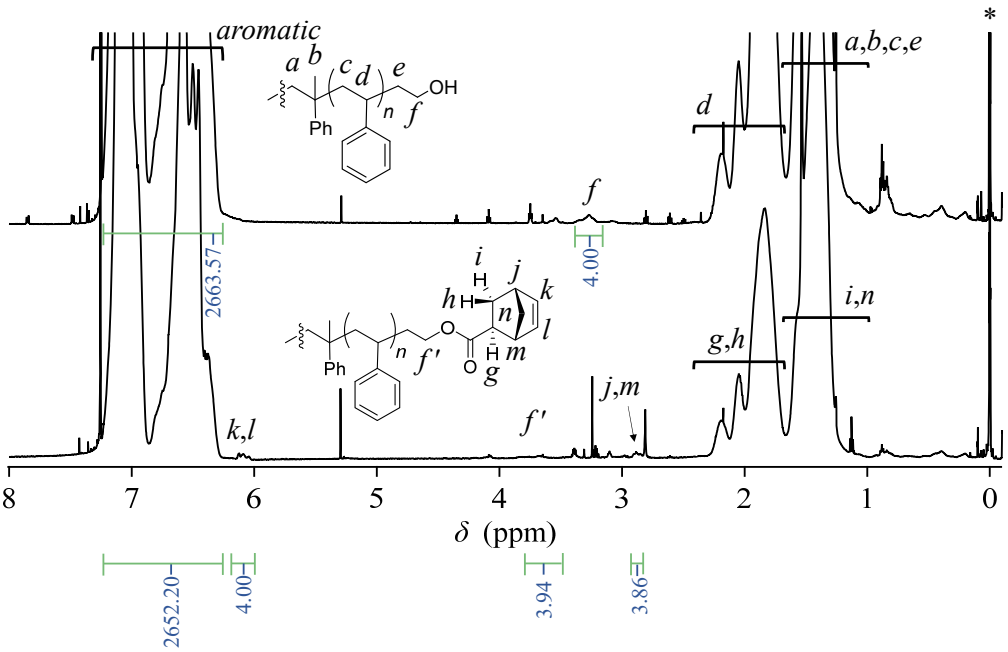

Figure 2.5. ^{1}H NMR spectra of HO–PS_{52k}–OH (upper) and NB–PS_{52k}–NB (lower) in $CDCl_3$.

2.3.2 Synthesis of multicyclic polystyrenes via cyclopolymerization

The synthesis of mc-PS was conducted using the MM with the smallest molecular weight (1k), that is, NB–PS_{1k}–NB. Because the G3-initiated ROMP is known to proceed in a living manner, the initial MM-to-G3 ratio determines the average number of cyclic units of the resulting mc-PS. A $[NB–PS_{1k}–NB]_0/[G3]_0$ ratio of 3/1 was applied to obtain the target mc-PS with three cyclic units (run 1 in **Table 2.2**). Under highly diluted conditions ($[NB–PS_{1k}–NB]_0$ = 0.500 mM) in CH_2Cl_2, the cyclopolymerization proceeded without gelation, affording a soluble product in 82.0% yield. The SEC elution peak of the product clearly shifted to the high molecular weight region compared to that of NB–PS_{1k}–NB, while maintaining the unimodal shape ($M_{n,SEC}$ = 3,870, $Đ$ = 1.28, **Figure 2.6a**). This result indicates that the controlled cyclopolymerization proceeds by suppressing uncontrolled intermolecular reactions. The ^{1}H NMR analysis suggested that the ROMP, the elementary reaction of the cyclopolymerization, proceeded quantitatively, as evidenced by the complete disappearance of the signals due to the norbornenyl group (*a*, *b*: 6.18–6.00; *c*, *d*: 3.14–2.91 ppm) and the emergence of broad signals due to the polynorbornene backbone (Figure 2.6b). Furthermore, the absolute M_n value determined by SEC-MALS-Visco ($M_{n,MALS}$) was 5,850 and the number of cyclic units was calculated to be 3.6, which is close to the theoretical value. Thus, the cyclic units can be controlled by the living manner of the G3-initiated ROMP. Finally, MALDI-TOF MS was employed to reveal further structural details (**Figure 2.7**). The spectra showed a series of repeated peaks with approximately 104 Da unit intervals corresponding to repeating PS. The peaks observed in the range of m/z = 2,000–4,000 Da were assigned to the desired mc-PS containing two cyclic units, whereas those observed in the range of m/z = 4,000–6,000 Da were assigned to the desired mc-PS containing three cyclic units. For example, the peaks at m/z =

2800.88 and 4407.60 (denoted by ○ and Δ, respectively) closely matched the calculated masses for the dimer containing 14 styrene repeating units ($[M + Ag]^+$ = 2800.52) and the trimer containing 24 styrene repeating units ($[M + Ag]^+$ = 4407.49), respectively. No other peaks were present apart from those of the desired mc-PS. This implies that mc-PS was produced through alternating intramolecular cyclization and intermolecular growth reactions. Overall, these structural characterization results confirmed that mc-PS was synthesized via cyclopolymerization as intended. To systematically characterize mc-PS, the author attempted to synthesize mc-PS with more cyclic units by varying the ratio of $[MM]_0/[G3]_0$. Under the established conditions of $[MM]_0/[G3]_0$ = 6/1 or 9/1, the desired mc-PSs with 7.4 and 10.4 cyclic units were obtained (runs 2 and 3 in Table 2.2). To date, the highest number of cyclic units recorded in multicyclic PS is approximately 20, as reported by Monteiro et al.[29] To overcome this limitation, the cyclopolymerization was conducted at $[MM]_0/[G3]_0$ = 20/1, 50/1, 75/1 and 100/1 (runs 4–7 in Table 2.2). The SEC analysis revealed that the cyclopolymerization proceeded without obvious side reactions, even at an $[MM]_0/[G3]_0$ ratio of 100/1 (**Figure 2.8**). Owing to the living polymerization nature, the number of the resulting cyclic units increased upon increasing the $[MM]_0/[G3]_0$ ratio and reached the expected value (= $[MM]_0/[G3]_0$). The highest number of cyclic units was 239, which is more than ten times the number reported by Monteiro et al. Thus, the number of cyclic units could be easily controlled by varying the initial MM-to-G3 ratio, enabling the synthesis of mc-PS with a high number of cyclic units. This enabled us to study the effect of the number of cyclic units on the physical properties of PS.

To elucidate the effect of ring size on the physical properties of PS, mc-PSs with larger ring sizes were synthesized by the cyclopolymerization of NB–PS_{6k}–NB and NB–PS_{12k}–NB (runs 8–13 in Table 2.2). Intermolecular cyclization would be less likely to occur if the

molecular weight of the MM increased; therefore, the cyclopolymerization of NB–PS_{6k}–NB and NB–PS_{12k}–NB was conducted at lower substrate concentrations, at an $[MM]_0/[G3]_0$ ratio of 3/1 where $[MM]_0$ = 0.125 or 0.150 mM (runs 8 and 11 in Table 2.2). Despite the increased molecular weight of the MM, the desired mc-PSs were successfully synthesized without gelation. The SEC elution peak of the products clearly shifted to a higher molecular weight region compared to that of the MM, and the ^{1}H NMR data suggested that the ROMP proceeded quantitatively **(Figures 2.9–2.12**). The synthesized mc-PS_{6k} and mc-PS_{12k} had 3.4 and 4.4 repeating units, respectively, which were close to the theoretical values. Moreover, mc-PSs with more cyclic units were successfully synthesized by applying $[MM]_0/[G3]_0$ = 6/1 and 9/1, while thorough optimization of the substrate concentration and reaction time was necessary (runs 9, 10, 12 and 13 in Table 2.2). However, the author was unable to synthesize mc-PS_x (x = 6k and 12k) composed of a large number of cyclic units (>20) because of the competitive deactivation of G3 during cyclopolymerization when applying a higher $[MM]_0/[G3]_0$ ratio. Nevertheless, the author confirmed that the number of cyclic units could be regulated to some degree.

The cyclopolymerization of a high-molecular-weight MM, NB–PS_{52k}–NB, was also carried out for the synthesis of mc-PS with a ring size of 52k. Surprisingly, mc-PS_{52k} with an average number of cyclic units of 10.2 was obtained without gelation (**Figure 2.13**). The successful cyclopolymerization of such a high-molecular-weight MM demonstrates the versatility of this method for the systematic synthesis of mc-PS.

An attractive aspect of the cyclopolymerization strategy is the possibility of synthesizing multicyclic polymers on a gram scale, which is in contrast with previous synthetic methodologies that require multiple steps and cumbersome processes. Commercial scale-up has been a substantial issue, even for monocyclic polymers;[36] the applicability of the presented

approach to gram-scale synthesis is therefore a critical factor for the practical applications of mc-PS. In this study, the cyclopolymerization of 1.5 g of NB–PS_{13k}–NB with an $[MM]_0/[G3]_0$ ratio of 3/1 where $[MM]_0/[G3]_0 = 0.150$ was conducted successfully. The cyclopolymerization proceeded without gelation, affording 1.39 g of mc-PS_{13k} with 3.8 cyclic units in a 92.7% yield. Again, the SEC elution peak of the product clearly shifted to the higher molecular weight region compared to that of the MM, and the ^{1}H NMR data suggested that the ROMP proceeded quantitatively (**Figures 2.14** and **2.15**).

Table 2.2. Molecular characterization of mc-PS [a]

Run	MM	$[MM]_0/[G3]_0$	$[MM]_0$ (mM)	Time (min)	$M_{n,MALS}$ [b]	$Đ$ [c]	Number of cyclic units [d]	R_h [b] (nm)	$[\eta]$ [b] (mL g^{-1})	T_g (°C)	Yield (%)
1	NB–PS_{1k}–NB ($M_{n,NMR}$ = 1,640)	3/1	0.500	10	5,850	1.28	3.6	1.8	6.4	99.8	82.0
2		6/1	0.500	10	12,200	1.21	7.4	2.5	7.8	105.3	80.3
3		9/1	0.500	10	17,100	1.16	10.4	2.9	8.8	106.1	90.8
4		20/1	0.500	15	72,300	1.14	44.1	5.9	18.0	109.2	78.0
5		50/1	0.500	30	82,200	1.12	53.8	6.5	20.2	110.6	99.6
6		75/1	1.000	60	180,000	1.40	109.8	9.7	32.0	112.0	97.0
7		100/1	1.000	80	392,000	1.42	239.1	15.0	55.7	113.2	68.0
8	NB–PS_{6k}–NB ($M_{n,MALS}$ = 6,470)	3/1	0.125	150	22,000	1.11	3.4	9.6	3.8	103.7	90.1
9		6/1	0.125	180	35,500	1.12	5.5	10.2	4.5	111.2	72.2
10		9/1	0.150	540	50,600	1.07	7.8	11.6	5.0	111.4	72.3
11	NB–PS_{12k}–NB ($M_{n,MALS}$ = 12,300)	3/1	0.150	90	54,400	1.44	4.4	5.5	16.1	105.2	98.0
12		6/1	0.150	540	109,600	1.21	8.9	6.6	17.1	110.9	99.1
13		9/1	0.150	540	155,100	1.36	12.6	7.8	19.2	111.8	79.2
14	NB–PS_{52k}–NB ($M_{n,MALS}$ = 52,100)	3/1	0.100	330	497,400	1.42	10.2	18.0	79.1	106.3	69.4

[a] Polymerization conditions: temperature, room temperature; atmosphere, Ar; solvent, CH_2Cl_2. [b] Determined using SEC-MALS-Visco in chloroform. [c] Determined using SEC in THF using PS as the standard. [d] The average number of cyclic units in the obtained mc-PS was estimated as (M_n of mc-PS)/(M_n of NB–PS–NB).

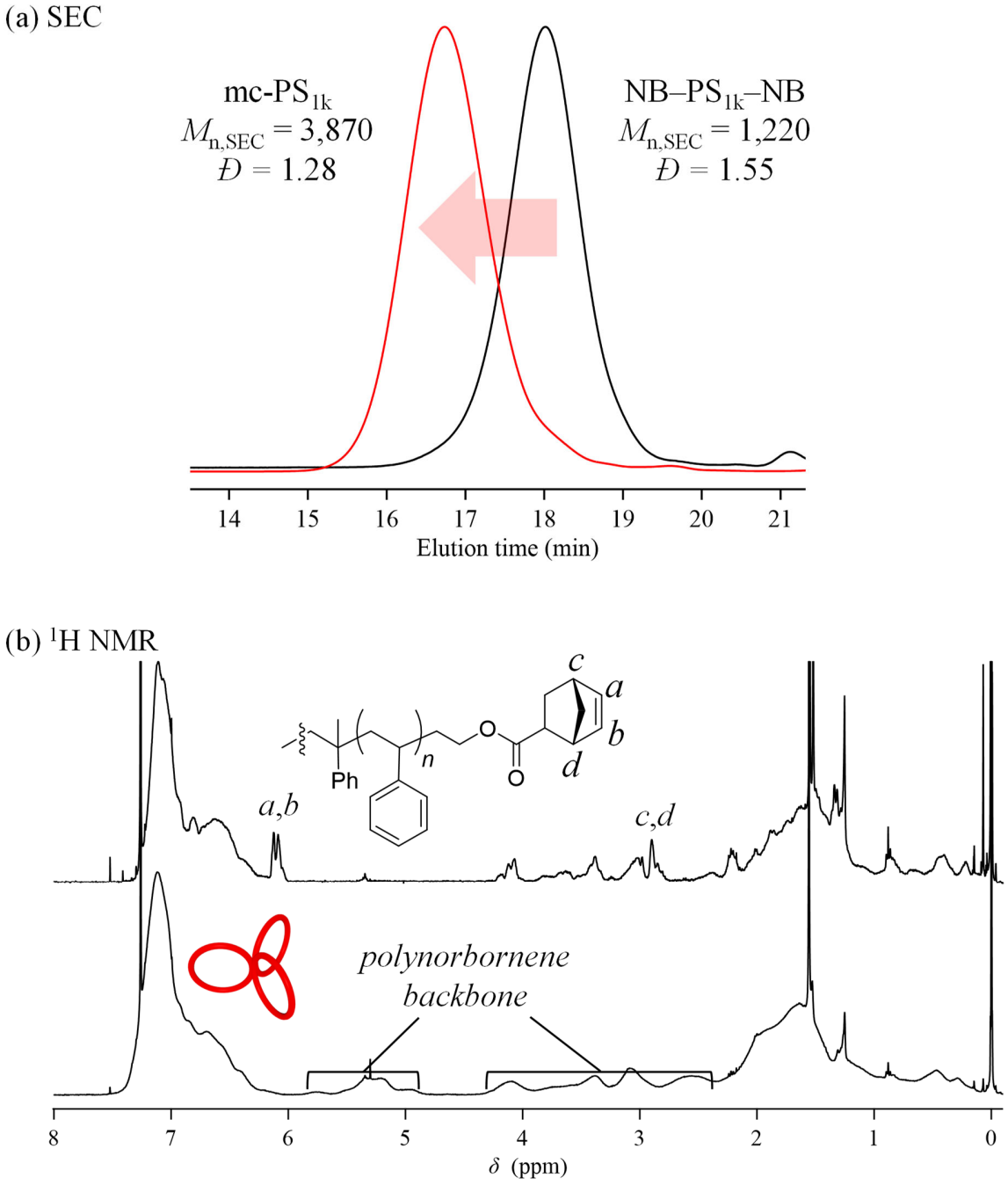

Figure 2.6. (a) SEC traces of NB–PS$_{1k}$–NB and mc-PS$_{1k}$ obtained from run 1 in Table 2.2 (refractive index (RI) detection; eluent, THF; flow rate, 1.0 mL min^{-1}). (b) ^{1}H NMR spectra of NB–PS$_{1k}$–NB (upper) and mc-PS$_{1k}$ (lower, run 1 in Table 2.2) in $CDCl_3$ (400 MHz).

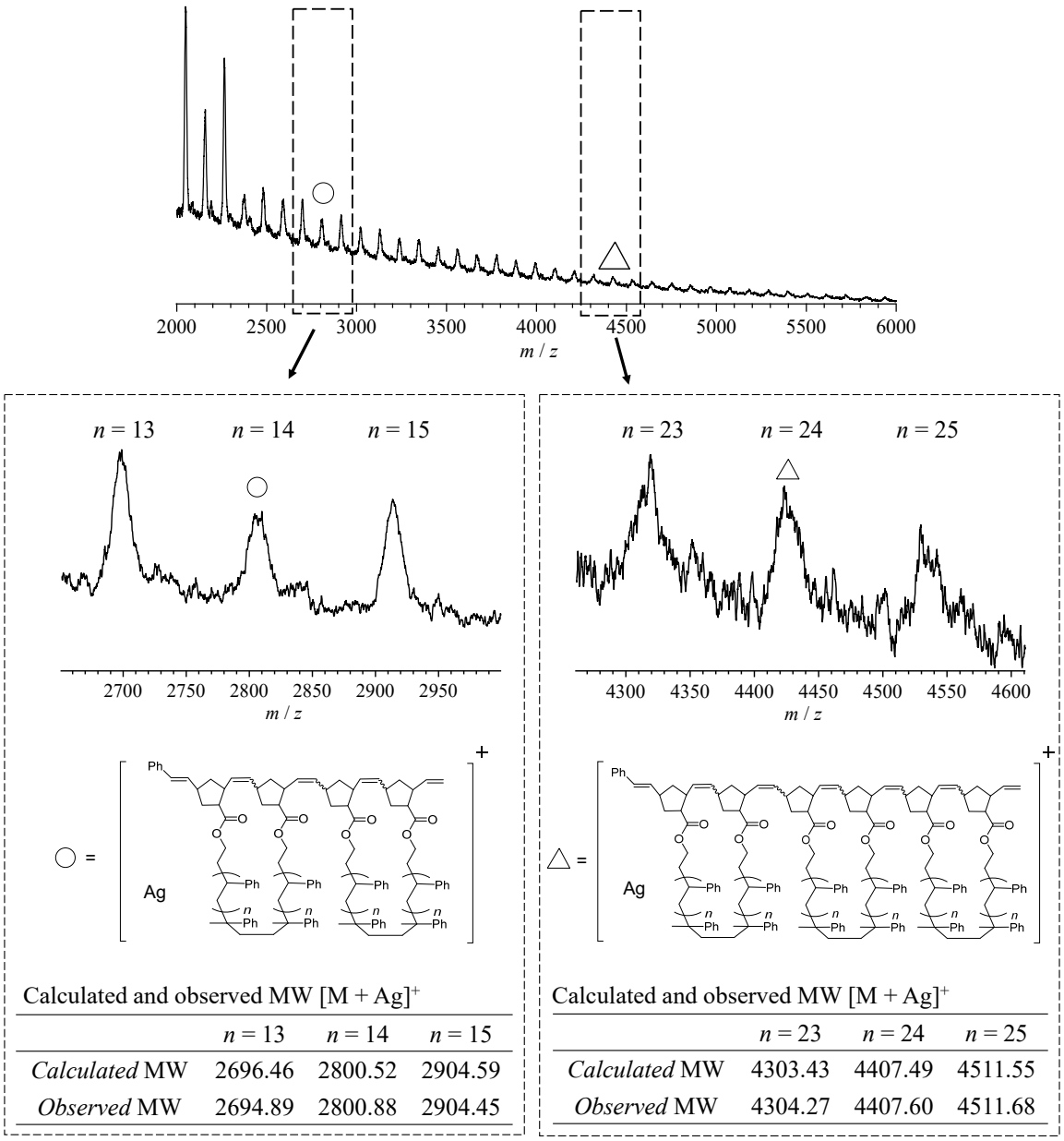

Calculated and observed MW $[M + Ag]^+$

	$n = 13$	$n = 14$	$n = 15$
Calculated MW	2696.46	2800.52	2904.59
Observed MW	2694.89	2800.88	2904.45

Calculated and observed MW $[M + Ag]^+$

	$n = 23$	$n = 24$	$n = 25$
Calculated MW	4303.43	4407.49	4511.55
Observed MW	4304.27	4407.60	4511.68

Figure 2.7. MALDI-TOF-MS analysis of mc-PS_{1k} (run 1 in Table 2.2).

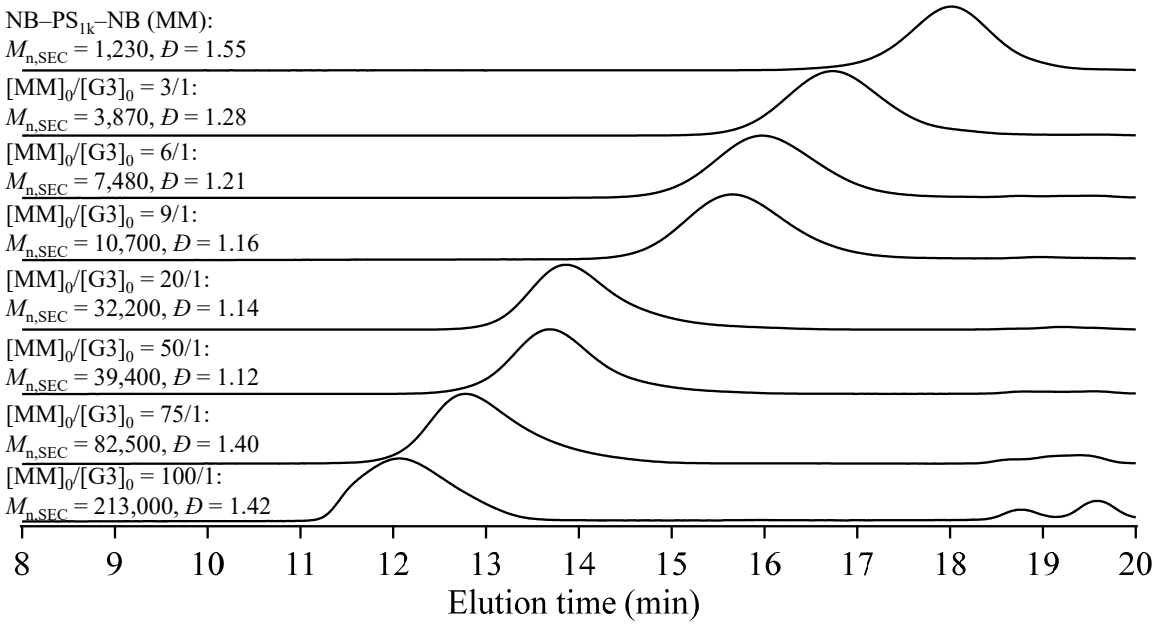

Figure 2.8. SEC traces of NB–PS_{1k}–NB and mc-PS_{1k} obtained from cyclopolymerization (refractive index (RI) detection; eluent, THF; flow rate, 1.0 mL min^{-1}).

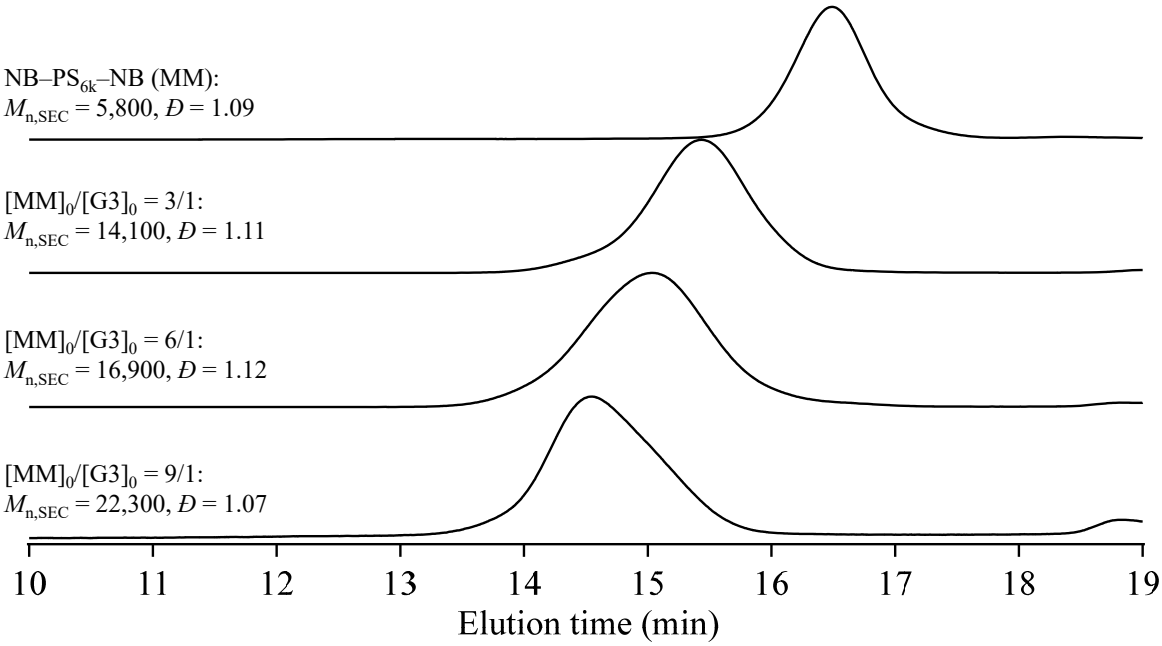

Figure 2.9. SEC traces of NB–PS_{6k}–NB and mc-PS_{6k} obtained from cyclopolymerization (refractive index (RI) detection; eluent, THF; flow rate, 1.0 mL min^{-1}).

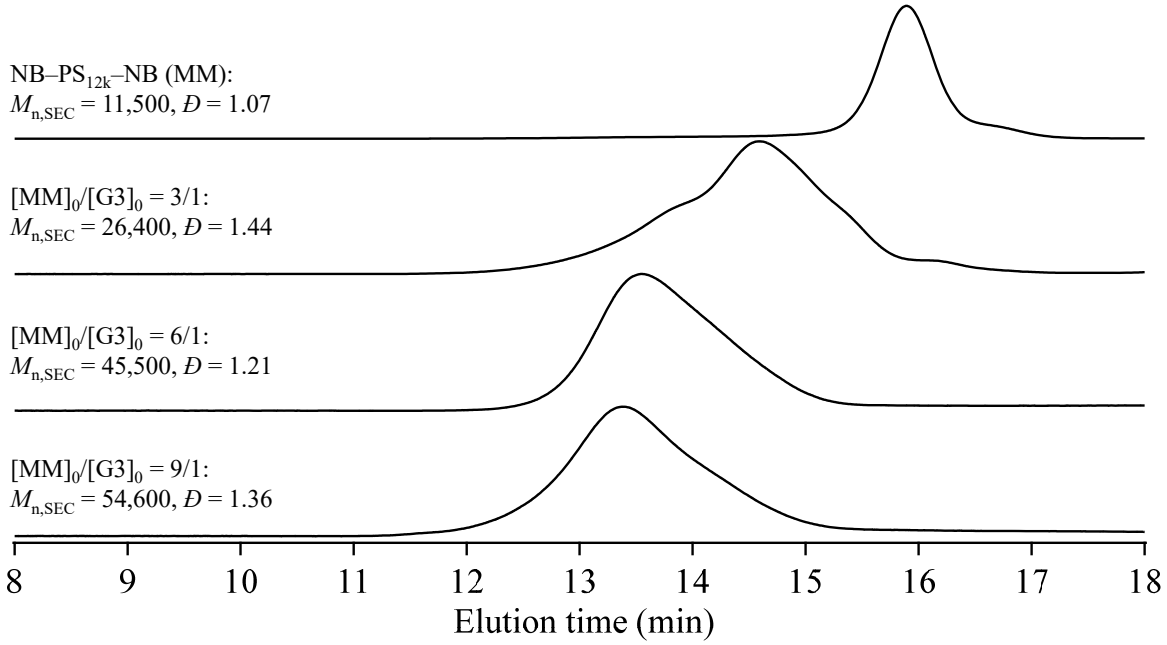

Figure 2.10. SEC traces of NB–PS$_{12k}$–NB and mc-PS$_{12k}$ obtained from cyclopolymerization (refractive index (RI) detection; eluent, THF; flow rate, 1.0 mL min^{-1}).

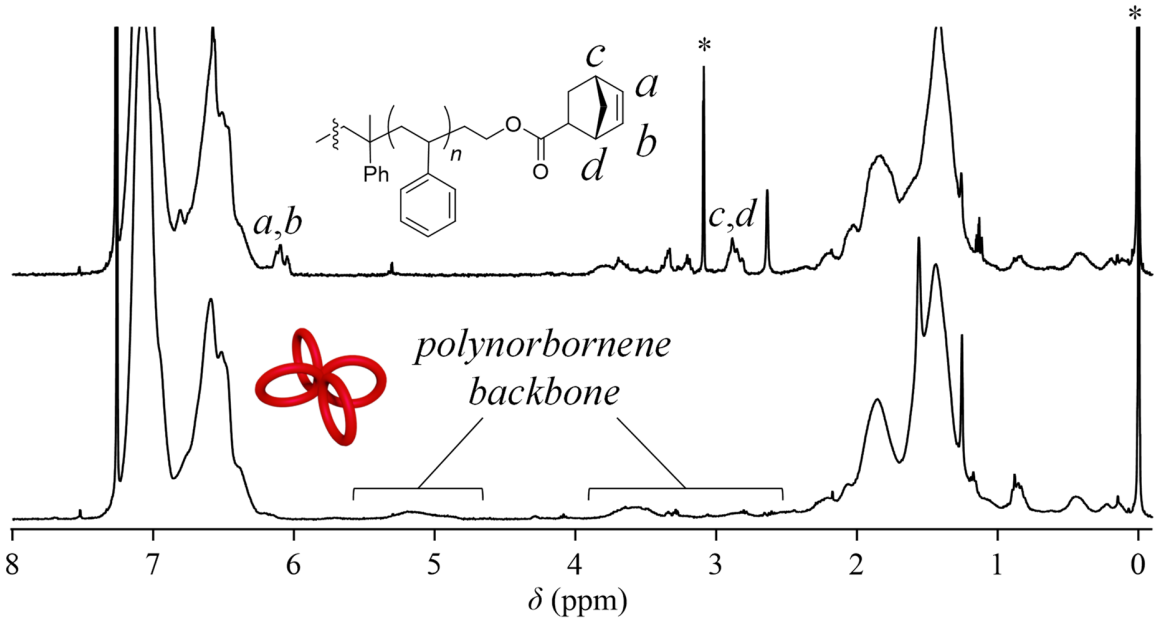

Figure 2.11. ^{1}H NMR spectra of NB–PS$_{6k}$–NB (upper) and mc-PS$_{6k}$ (run 8 in Table 2.2, lower) in $CDCl_3$.

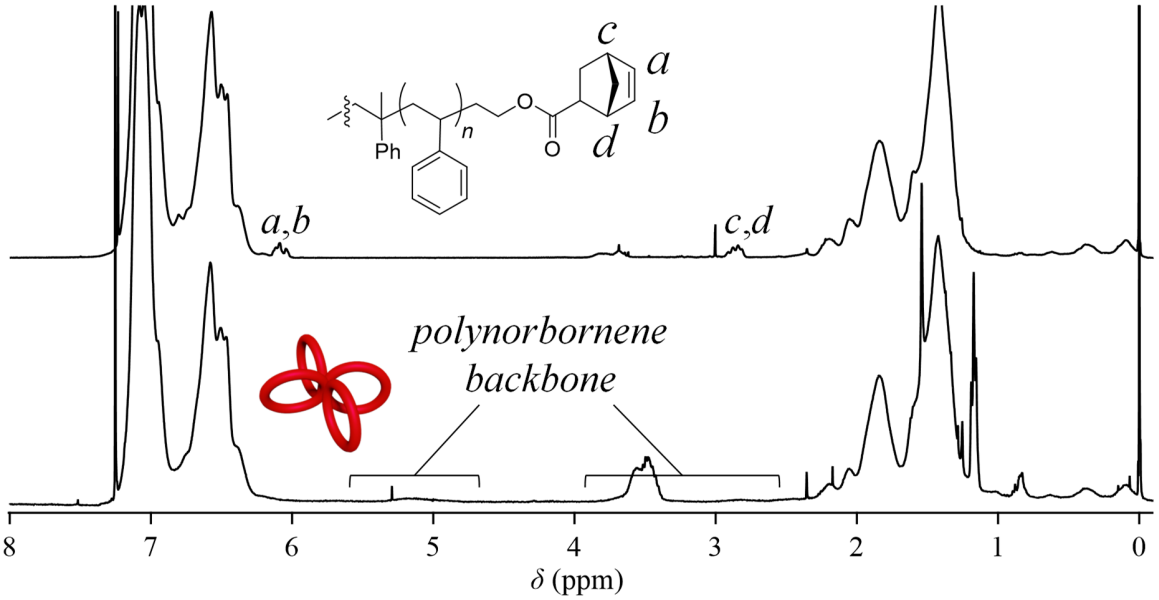

Figure 2.12. ^{1}H NMR spectra of NB–PS$_{12k}$–NB (upper) and mc-PS$_{12k}$ (run 11 in Table 2.2, lower) in $CDCl_3$.

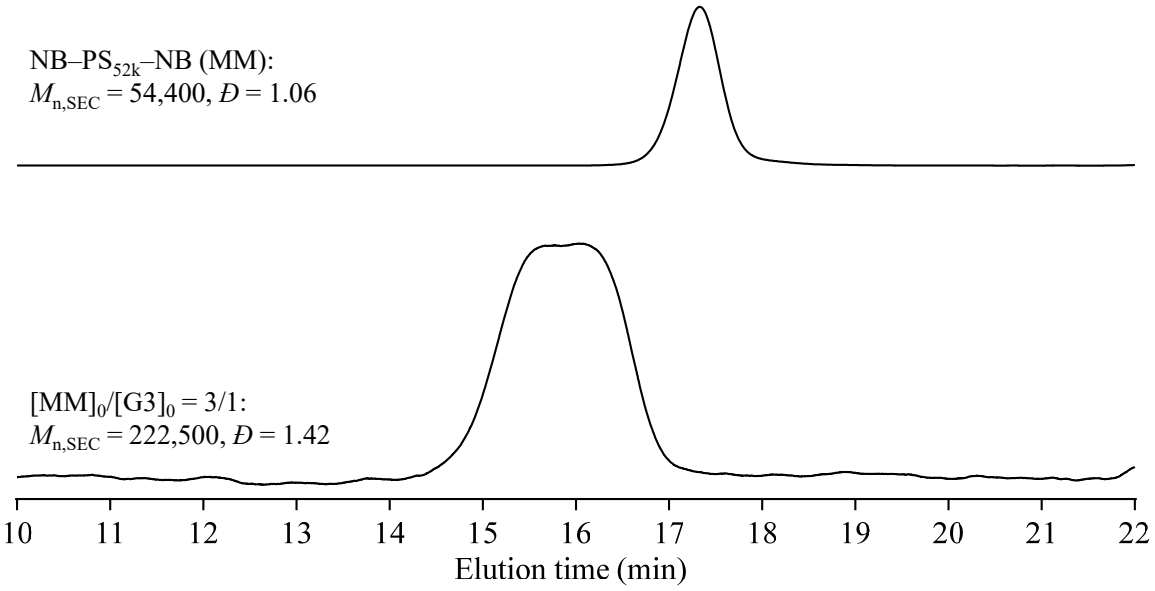

Figure 2.13. SEC traces of NB–PS$_{52k}$–NB and mc-PS$_{52k}$ obtained from SEC with higher exclusion limit (refractive index (RI) detection; eluent, THF; flow rate, 1.0 mL min^{-1})

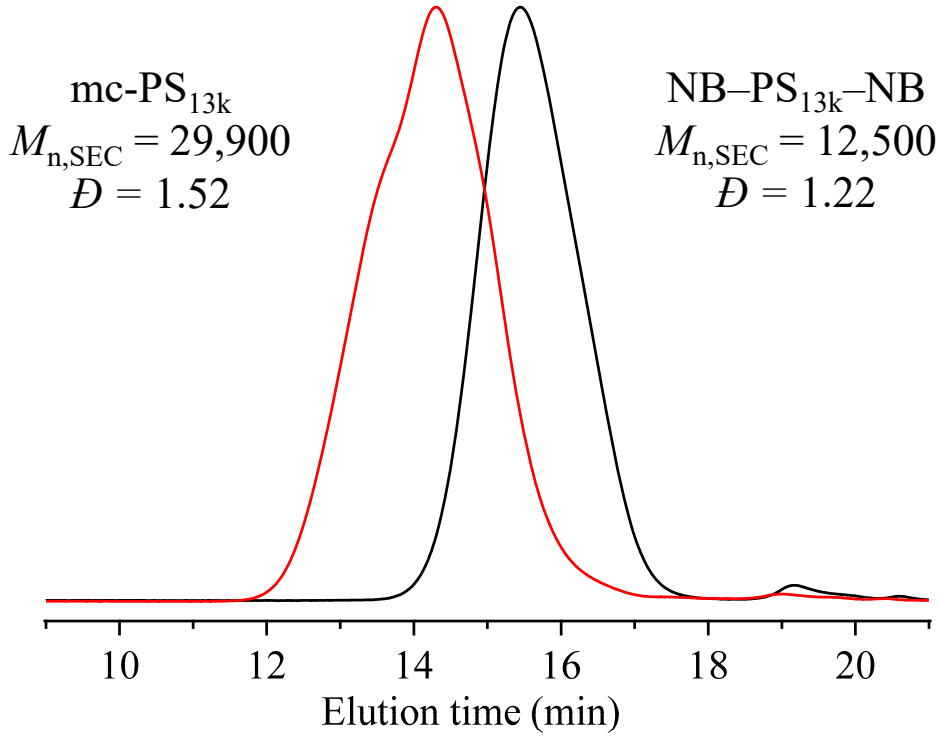

Figure 2.14. SEC traces of NB–PS$_{13k}$–NB (black) and mc-PS$_{13k}$ (red) (RI detection; eluent, THF).

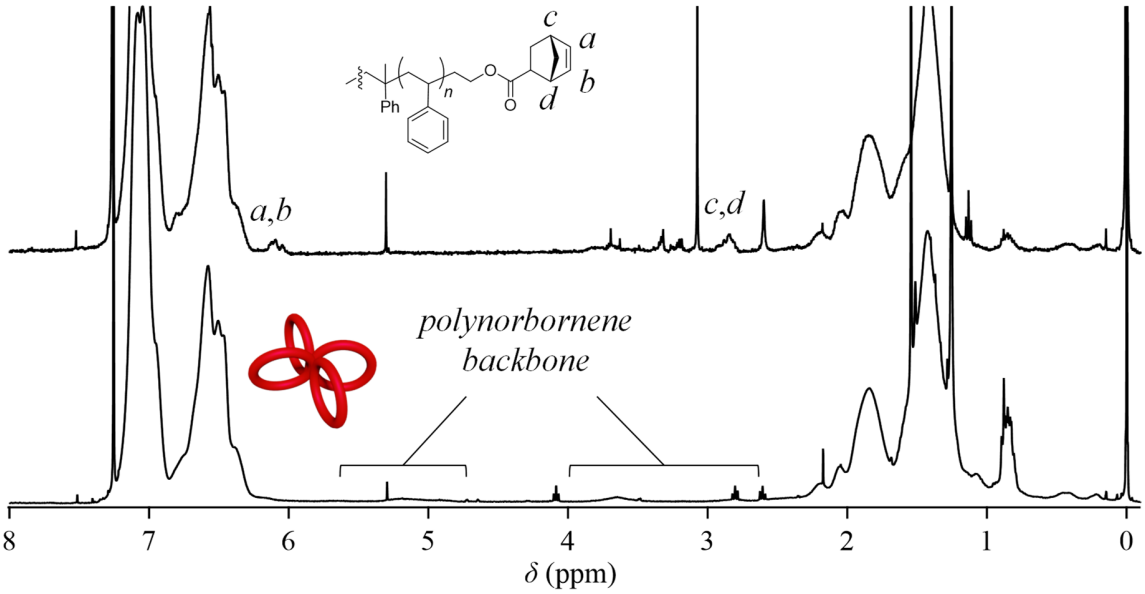

Figure 2.15. ^{1}H NMR spectra of NB–PS$_{13k}$–NB (upper) and mc-PS$_{13k}$ (lower) in $CDCl_3$.

2.3.3 Solution properties of mc-PS

The investigation of the relationship between the number and size of the cyclic units of multicyclic polymers and their physical properties is highly attractive, and acquiring such information is beneficial for materials design based on multicyclic polymers. The hydrodynamic radius (R_h) and intrinsic viscosity ([η]) of the developed mc-PS$_{1k}$ with varied numbers of cyclic units were investigated using SEC-MALS-Visco in chloroform. The [η] and R_h values of mc-PS$_{1k}$ were in the range of 6.4–55.7 mL g^{-1} and 1.8–15.0 nm, respectively, as summarized in Table 3.2. To further analyze the solution conformation of mc-PS$_{1k}$, the [η] and R_h values were normalized by dividing them with the number of cyclic units in the molecules (denoted as [$\eta_{,ring}$] and $R_{h,ring}$). The results showed that [$\eta_{,ring}$] and $R_{h,ring}$ decreased with an increasing number of cyclic units up to approximately 50 and then reached almost constant values (**Figure 2.16a**). This suggests that the conformation of each cyclic unit in solution gradually became more compact after the number of cyclic units reached a certain value. Molecular simulations and experimental studies have demonstrated that the conformation of a bottlebrush polymer changes from spherical to cylindrical as the backbone DP increases.[37–40] Thus, conformational changes similar to those seen in bottlebrush polymers may occur in mc-PS$_{1k}$ upon increasing the number of cyclic units. The degree of shrinkage of mc-PS$_{1k}$ in solution was investigated. The hydrodynamic volume contraction (g_v) was determined from SEC-MALS-Visco using eqn (1).[29]

$$g_v = (M_{n,app}/M_{n,abs})^{1.7} \quad (1)$$

where $M_{n,app}$ and $M_{n,abs}$ are the apparent and absolute molecular weights, respectively. The g_v value is a measure of the compactness of a polymer relative to its linear counterpart in a good solvent. As shown in Figure 2.16b, the g_v decreased upon increasing the number of cyclic units

(up to 50) and then reached a constant value (0.26). Monteiro et al. reported that as the number of cyclic units of multicyclic polystyrene increased, g_v steadily decreased, and its value eventually stabilized at 0.25.[29] Even for the case of mc-PS with more than 200 cyclic units, g_v converged at approximately 0.25, indicating that additional increases in the number of cyclic units does not contribute to the formation of a denser conformation. Similarly, the $[\eta_{,ring}]$ and $R_{h,ring}$ of mc-PSs with large ring sizes (mc-PS_{6k} and mc-PS_{12k}) also decreased upon increasing the number of cyclic units (Figures 2.16c and e). Interestingly, mc-PS_{6k} and mc-PS_{12k} showed a g_v value of approximately 0.25 upon increasing the number of cyclic units, suggesting that the g_v value stabilizes at a certain value regardless of the molecular weight of the cyclic units (Figures 2.16d and f). The compactness of mc-PS is suggested to be unrelated to the molecular weight of the ring units. However, g_v reaches a threshold with fewer cyclic units as the molecular weight of the cyclic units increases.

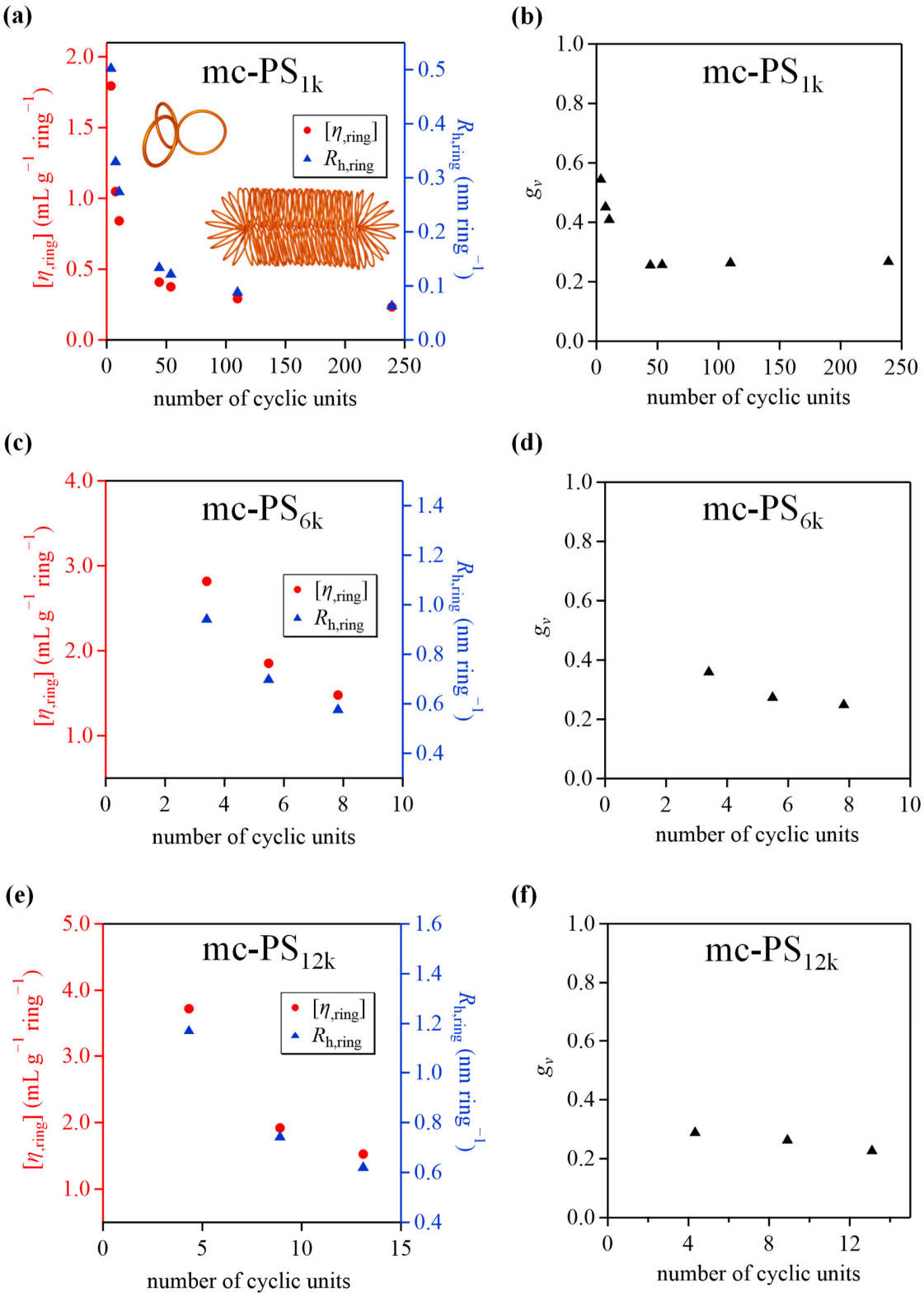
(a)
mc-PS1k
[η,ring] (mL g−1 ring−1)
Rh,ring (nm ring−1)
[η,ring]
Rh,ring
number of cyclic units
(b)
mc-PS1k
gv
number of cyclic units
(c)
mc-PS6k
[η,ring] (mL g−1 ring−1)
Rh,ring (nm ring−1)
[η,ring]
Rh,ring
number of cyclic units
(d)
mc-PS6k
gv
number of cyclic units
(e)
mc-PS12k
[η,ring] (mL g−1 ring−1)
Rh,ring (nm ring−1)
[η,ring]
Rh,ring
number of cyclic units
(f)
mc-PS12k
gv
number of cyclic units

Figure 2.16. (a) Dependence of [η] (red) and R_h (blue) of mc-PS_{1k} on the number of cyclic units (solvent, CHCl3). (b) Dependence of g_v of mc-PS_{1k} on the number of cyclic units. (c) Dependence of [η] (red) and R_h (blue) of mc-PS_{6k} on the number of cyclic units (solvent, $CHCl_3$). (d) Dependence of g_v of mc-PS_{6k} on the number of cyclic units. (e) Dependence of [η] (red) and R_h (blue) of mc-PS_{12k} on the number of cyclic units (solvent, $CHCl_3$). (f) Dependence of g_v of mc-PS_{12k} on the number of cyclic units.

2.3.4 Solid state properties of mc-PS

Differential scanning calorimetry (DSC) was used to determine the T_g of mc-PS$_{1k}$ and linear PS in order to investigate the relationship between structure and T_g (**Figures 2.17** and **2.18**). **Figure 2.19a** presents the T_g values of mc-PS$_{1k}$ and linear PS as a function of M_n. All mc-PS$_{1k}$ polymers showed a higher T_g than their linear counterparts, which can be attributed to their cyclic topology. For both linear and mc-PS$_{1k}$, T_g increased with increasing M_n in the lower molecular weight region and finally converged to a constant value. However, a difference was observed in the M_n at which the T_g reached a constant value, approximately 50,000 for linear PS and 200,000 for mc-PS$_{1k}$.

To further investigate the dependence of the T_g on the molecular weight, the author employed the Flory-Fox equation:[41] $T_g = T_{g,\infty} - AM_n^{-1}$, where $T_{g,\infty}$ is T_g in the limit of infinite M_n and A is an empirical parameter related to the free volume. Figure 2.19b shows the plots of T_g for linear PS and mc-PS against the inverse of M_n, with linear fitting corresponding to the Fox-Flory equation. By extrapolation of T_g to the infinite molecular weight, $T_{g,\infty}$ was determined to be 106.7 and 111.6 °C for linear PS and mc-PS, respectively. This confirms the topological effect on T_g. Monteiro et al. have reported that multicyclic PS shows a higher T_g than linear PS because the linkages between each cyclic unit can be considered as irreversible knots, lowering the conformational entropy of the coil.[29] In contrast to multicyclic PS, the $T_{g,\infty}$ of monocyclic PS is almost identical to that of linear PS.[42] The distinct difference in T_g between linear and monocyclic polymers in the low molecular weight region is attributed to the presence and absence of a terminal structure. Meanwhile, in the high molecular weight range, the terminal contribution of the linear polymer becomes negligible; thus, the T_g of linear and monocyclic

polymers converges to the same value. Therefore, the increased $T_{g,\infty}$ of mc-PS over those of linear and monocyclic PS is a unique characteristic of the multicyclic topology.

The A values for the linear PS and mc-PS$_{1k}$ were 8.9×10^4 and 7.3×10^4, respectively, indicating a strong T_g-M_n dependence. For linear PS, such a strong T_g-M_n dependence can be explained by the free volume around the terminals. In contrast, the T_g–M_n dependence of mc-PS is explained by other factors: the steric repulsion of the cyclic side chains of mc-PS increases upon increasing the norbornene backbone DP, that is, the number of cyclic units, which reduces the free volume of the cyclic chain. Such a scenario is also different from that of the T_g-M_n dependence of monocyclic polymers, where T_g shows a weak dependence on the molecular weight.[43–45]

Next, we investigated the T_g-M_n dependence of mc-PSs with larger numbers of cyclic units (**Figure 2.20**). As expected, mc-PS$_{6k}$ and mc-PS$_{12k}$ also showed an increased T_g compared to that of linear PS with a comparable molecular weight. The $T_{g,\infty}$ values of mc-PS$_{6k}$ and mc-PS$_{12k}$ were 118.7 and 115.5 °C, respectively. These values were higher than that of linear PS (106.7 °C), which implied the topological effect on the T_g, similar to that seen in mc-PS$_{1k}$ (Figure 2.19c and d). Notably, the T_g of mc-PS$_{52k}$ (M_n = 497,400) was determined to be 106.3 °C, which was almost identical to that of its linear PS counterpart (M_n = 275,000, T_g = 107.0 °C). According to a previous study, linear and monocyclic PS with a molecular weight of 42k showed almost the same T_g.[46] In other words, for molecular weights higher than 42k, no terminal effect was observed on T_g. This suggests that when the molecular weight of the cyclic units is greater than a certain value, T_g is not affected, even when the number of cyclic units is increased.

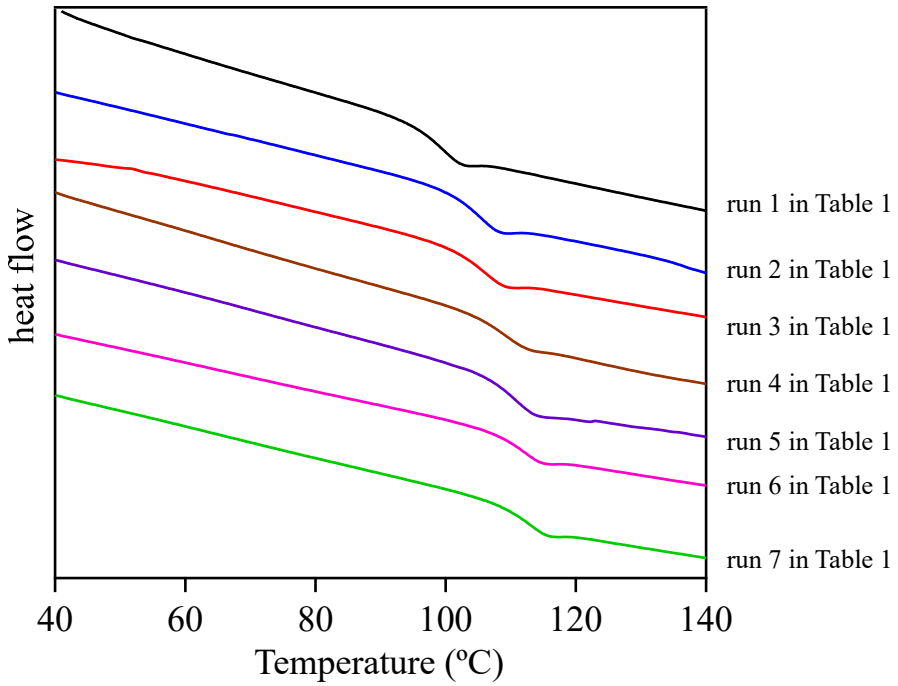

Figure 2.17. DSC curves of mc-PS_{1k} during the second heating (heating rate: 10 °C min^{-1}).

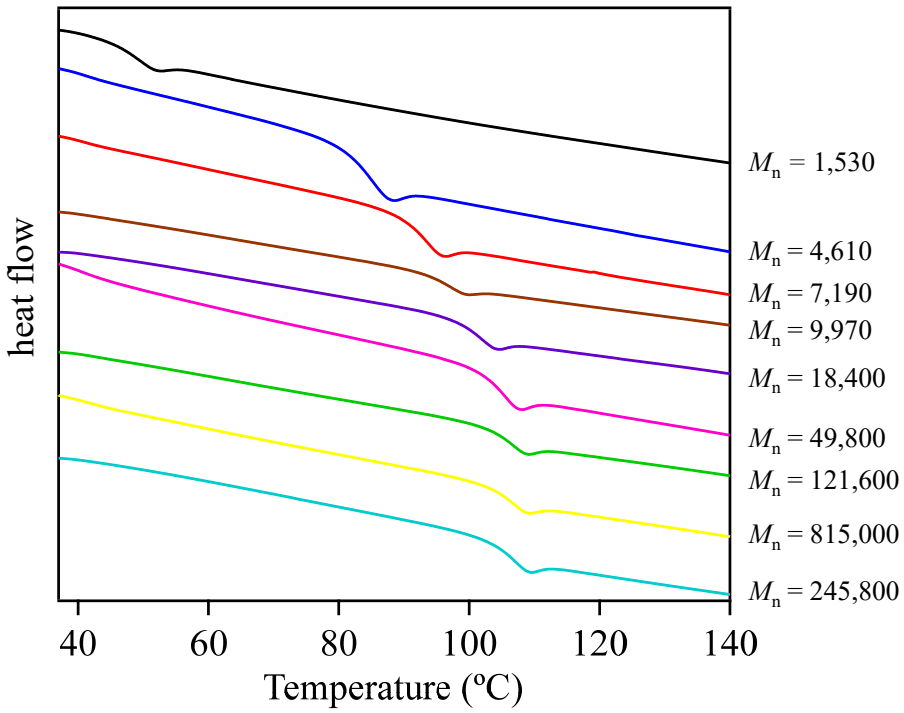

Figure 2.18. DSC curves of linear PS during the second heating (heating rate: 10 °C min^{-1}).

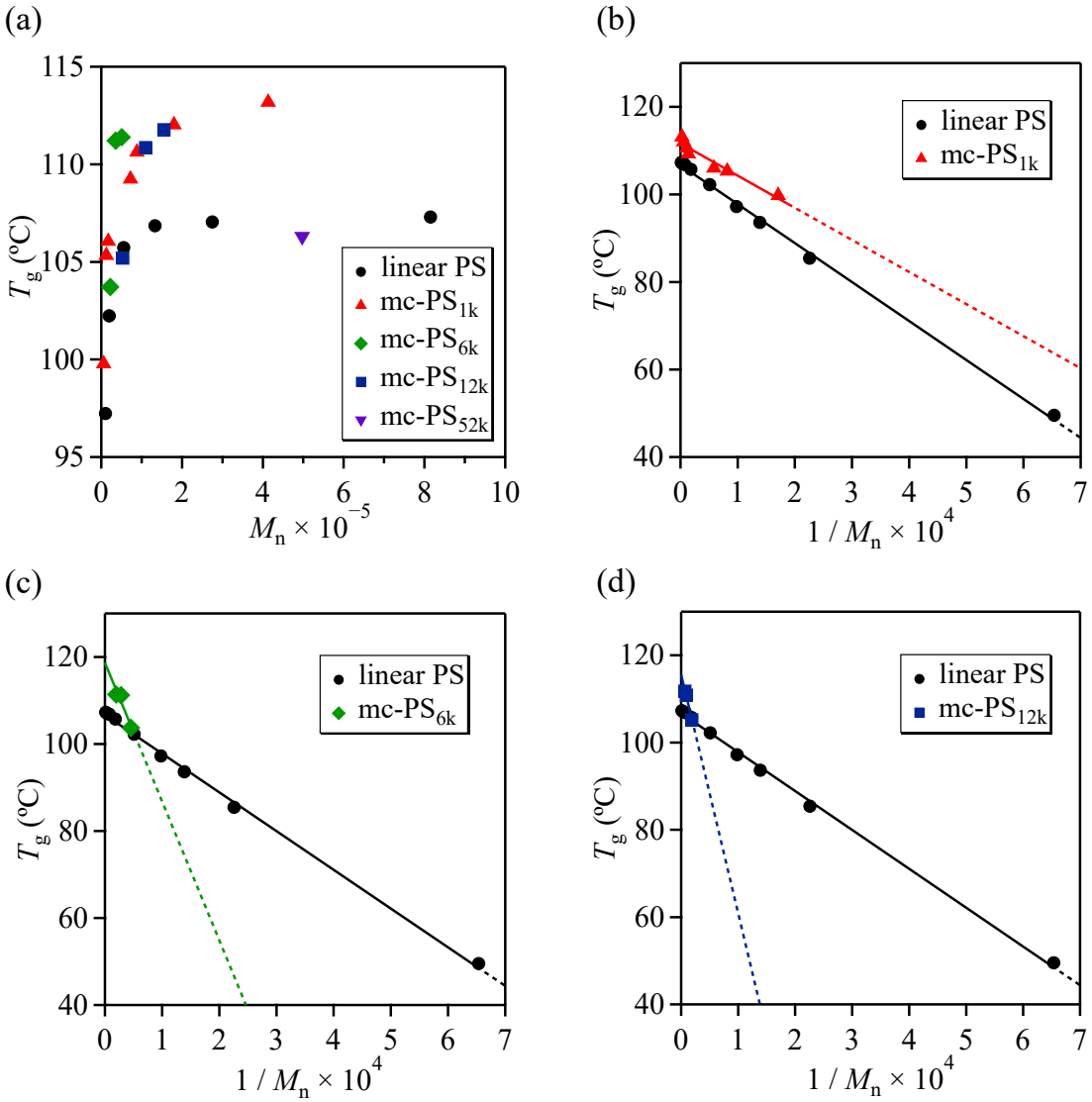

Figure 2.19. (a) Molecular weight dependence of glass transition temperature for mc-PS and linear PS. To fit the Flory-Fox equation, the T_g was plotted against the inverse of molecular weight of (b) mc-PS$_{1k}$, (c) mc-PS$_{6k}$ and (d) mc-PS$_{12k}$, plotted together with linear PS.

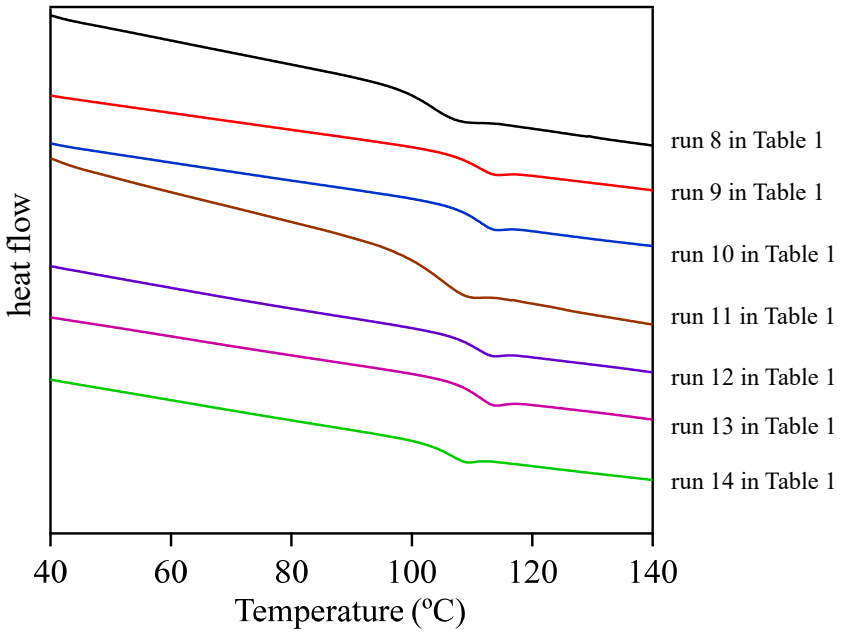

Figure 2.20. DSC curves of mc-PS_{6k}, mc-PS_{12k}, and mc-PS_{52k} during the second heating (heating rate: 10 °C min^{-1}).

Various mc-PSs with comparable cyclic units and different ring sizes were used for investigating the dependence of T_g on the ring size: mc-PS$_{1k}$ (number of cyclic units = 3.6, ring size = 1k, run 1 in Table 2.2), mc-PS$_{6k}$ (number of cyclic units = 3.4, ring size = 6k, run 8 in Table 2.2) and mc-PS$_{12k}$ (number of cyclic units = 4.4, ring size = 12k, run 11 in Table 2.2). The $T_{g,\infty}$ and A parameter were determined to be 105.5 °C and 3.0×10^3 , respectively, using the Flory-Fox equation (**Figure 2.21**). The $T_{g,\infty}$ of mc-PS with a number of cyclic units of approximately 3–4 was close to that of linear PS. Such a finding can be explained by the same reason as that for mc-PS$_{52k}$ showing a comparable T_g to that of linear PS. The estimated A parameter was close to the reported value for monocyclic PS (4.5×10^3), which is about an order of magnitude lower than that of linear PS (8.9×10^4).[47] Such a difference confirmed the smaller free volume of mc-PS compared to that of its linear counterpart.

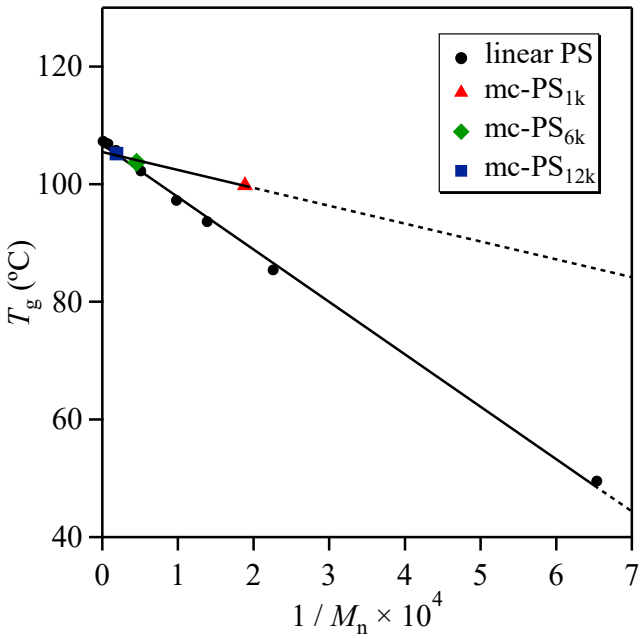

Figure 2.21. Plot of glass transition temperature vs. inverse of molecular weight for linear PS and mc-PS bearing comparable cyclic units: mc-PS$_{1k}$ (number of cyclic units = 3.6, ring size = 1k, run 1 in Table 2.2), mc-PS$_{6k}$ (number of cyclic units = 3.4, ring size = 6k, run 8 in Table 2.2) and mc-PS$_{12k}$ (number of cyclic units = 4.4, ring size = 12k, run 11 in Table 2.2).

2.3.5. Application to PS-containing multicyclic copolymer synthesis

To demonstrate the versatility of the present cyclopolymerization approach, the author synthesized PS-containing multicyclic copolymers with different architectures (Schemes 1.1b and c). The aim was to enrich mc-PS with novel properties that cannot be obtained through its utilization alone, thus, expanding its possible applications. In this study, the author focuses on multicyclic copolymers composed of PS and poly(*rac*-lactide) (PLA) segments. Because the block copolymer consisting of PS and PLA is known to show a high Flory-Huggins interaction parameter, multicyclic copolymers possessing PS and PLA segments are expected to self-assemble into microphase-separated structures.[48–51] First, the author investigated the cyclopolymerization of *α*,*ω*-norbornenyl end-functionalized PLA-*block*-PS-*block*-PLA triblock copolymer (NB–PLA-*b*-PS-*b*-PLA–NB; $M_{n,NMR}$ = 15,900, $M_{n,SEC}$ = 24,300, $Đ$ = 1.04) to synthesize multicyclic PLA-*block*-PS (mc-(PLA-b-PS)) according to Scheme 1.1b. Under established conditions, the cyclopolymerization of NB–PLA-*b*-PS-*b*-PLA–NB ([NB–PLA-*b*-PS-*b*-PLA–NB]$_0$ = 0.15 mM, [MM]$_0$/[G3]$_0$ = 3/1; see the **Table 3.3**) yielded a soluble product. The SEC elution peak of the product clearly shifted to a higher molecular weight region ($M_{n,SEC}$ = 55,200, $Đ$ = 1.82) compared to that of the MM (**Figure 2.22**), and ^{1}H NMR analysis suggested that the ROMP proceeded quantitatively (**Figure 2.23**). Although the T_g of the PS block could not be clearly observed, DSC analysis revealed that the T_g of the PLA segment of mc-(PLA-*b*-PS) was higher than that of the macromonomer (**Figure 2.24**), strongly suggesting the multicyclic architecture of the obtained mc-(PLA-*b*-PS). The number of cyclic units was determined from its $M_{n,MALS}$ as 5.2. These results indicate that the cyclopolymerization strategy can be applied to the synthesis of PS-containing multicyclic copolymers. Furthermore, mc-

(PLA-*b*-PS) copolymers possessing 6.3 and 8.8 cyclic units were successfully obtained by applying the $[MM]_0/[G3]_0$ = 6/1 and 9/1, respectively.

Table 2.3. Molecular characterization of mc-(PLA-*b*-PS) [a]

run	$[MM]_0/[G3]_0$	$[MM]_0$ (mM)	time (min)	$M_{n,MALS}$ [b]	$Đ$ [c]	number of cyclic unit [d]	yield (%)
15	3/1	0.150	90	66,400	1.82	5.2	99.6
16	6/1	0.150	300	80,400	1.61	6.3	97.2
17	9/1	0.150	300	112,100	1.59	8.8	94.4

[a] Polymerization conditions: temperature, r.t.; atmosphere, Ar; solvent, CH_2Cl_2. [b] Determined by SEC-MALS-Visco in chloroform. [c] Determined by SEC in THF using PS as the standard. [d] The average number of cyclic units in the obtained mc-(PLA-*b*-PS) was estimated as (M_n of mc-(PLA-*b*-PS))/(M_n of NB–PLA-*b*-PS-*b*-PLA–NB).

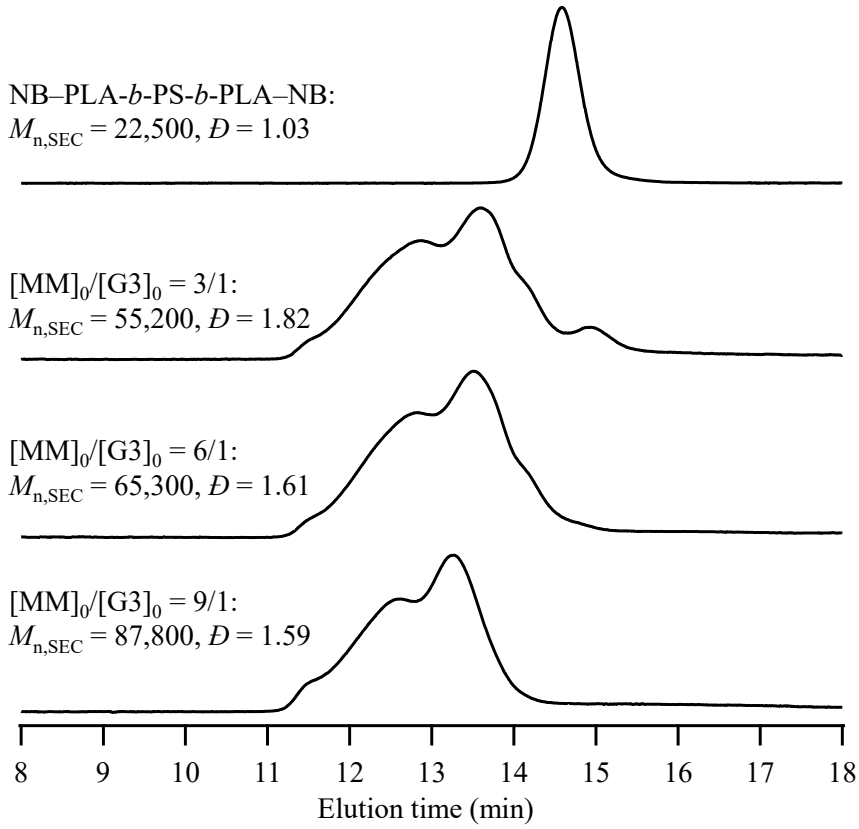

Figure 2.22. SEC traces of NB–PLA-*b*-PS-*b*-PLA–NB and mc-(PLA-*b*-PS) (refractive index (RI) detection; eluent, THF; flow rate, 1.0 mL min^{-1}).

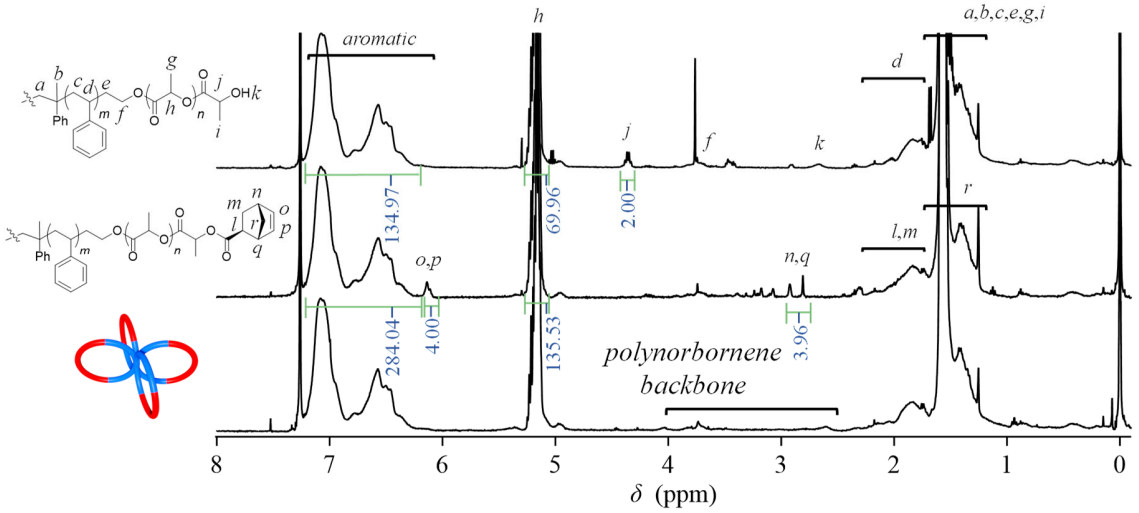

Figure 2.23. ^{1}H NMR spectra of HO–PLA-*b*-PS-*b*-PLA–OH (upper), NB–PLA-*b*-PS-*b*-PLA–NB (middle), and mc-(PLA-*b*-PS) (lower) in $CDCl_3$.

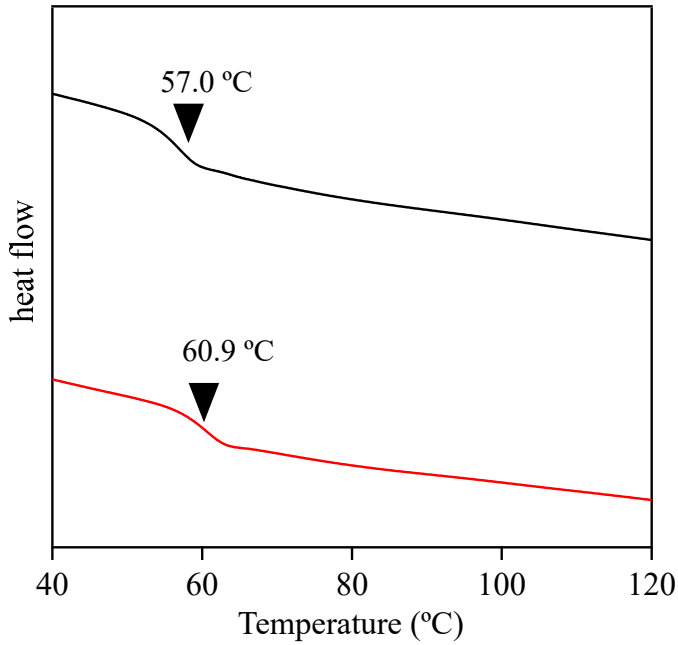

Figure 2.24. DSC curves during second heating process of NB–PLA-*b*-PS-*b*-PLA–NB (black) and mc-(PS-*b*-PLA) (run 15 in Table 2.3, red).

A statistical copolymer of cyclic PS and cyclic PLA (poly(cPS-*st*-cPLA)) was synthesized, as shown in Scheme 1.1c. *α*,*ω*-Norbornenyl end-functionalized PLA (NB–PLA–NB) was synthesized following method reported Satoh et al. (**Figures 2.25** and **2.26**).[35] The cyclocopolymerization of NB–PS_{6k}–NB ($M_{n,NMR}$ = 6,000, $M_{n,SEC}$ = 5,800, $Đ$ = 1.09) and NB–PLA_{6k}–NB ($M_{n,NMR}$ = 6,700, $M_{n,SEC}$ = 12,100, $Đ$ = 1.08) was conducted at $[NB–PS_{6k}–NB]_0/[NB–PLA_{6k}–NB]_0/[G3]_0$ = 1/1/1 to afford a soluble product without gelation ($M_{n,SEC}$ = 15,300, $Đ$ = 1.34, run 18 in **Table 2.4**). The SEC analysis of the product revealed that both macromonomers were quantitatively consumed (**Figure 2.27**), and ^{1}H NMR analysis suggested the quantitative consumption of each norbornenyl group (**Figure 2.28**). Furthermore, the $M_{n,MALS}$ of the products was determined to be 23,800, from which the number of cyclic units was calculated to be 3.8, which is close to the theoretical value. The number of cyclic units and the ring size can also be controlled by changing the $[NB–PS–NB]_0/[NB–PLA–NB]_0/[G3]_0$ ratio or using macromonomers with different M_n values (Figures 2.27 and 2.29). To provide evidence for the multicyclic architecture, the author compared the T_g, R_h and [η] of poly(cPS-*st*-cPLA) ($M_{n,MALS}$ = 40,300, number of cyclic units = 6.5, $Đ$ = 1.29, run 20 in **Table 2.4**) with those of the graft copolymer counterpart composed of linear PS and PLA side chains (poly(PS-*st*-PLA)) with comparable side-chain and main-chain lengths ($M_{n,MALS}$ = 33,800, number of graft units = 10.7, $Đ$ = 1.07; see synthetic details in **Figures 2.30–2.32**). DSC analysis revealed that the T_g of each segment of poly(cPS-*st*-cPLA) was higher than that of poly(PS-*st*-PLA) (**Figure 2.33**). SEC-MALS-Visco measurements revealed the lower R_h and [η] compared to those of poly (PS-*st*-PLA) in the same molecular weight range (**Figures 2.34** and **2.35**). These results strongly suggest the multicyclic architecture of the obtained poly(cPS-*st*-cPLA). Overall, the author

demonstrated that multicyclic copolymers containing cyclic PS units with various architectures can be synthesized via the established cyclopolymerization approach.

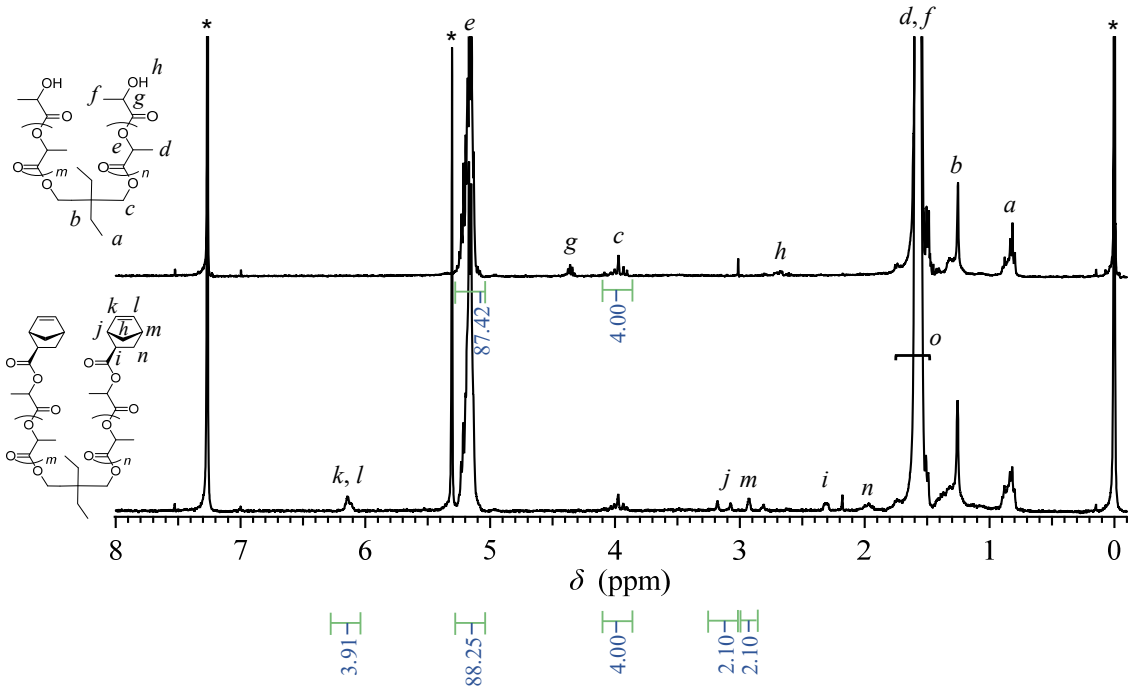

Figure 2.25. ^{1}H NMR spectra of HO–PLA$_{6k}$–OH (upper) and NB–PLA$_{6k}$–NB (lower) in $CDCl_3$.

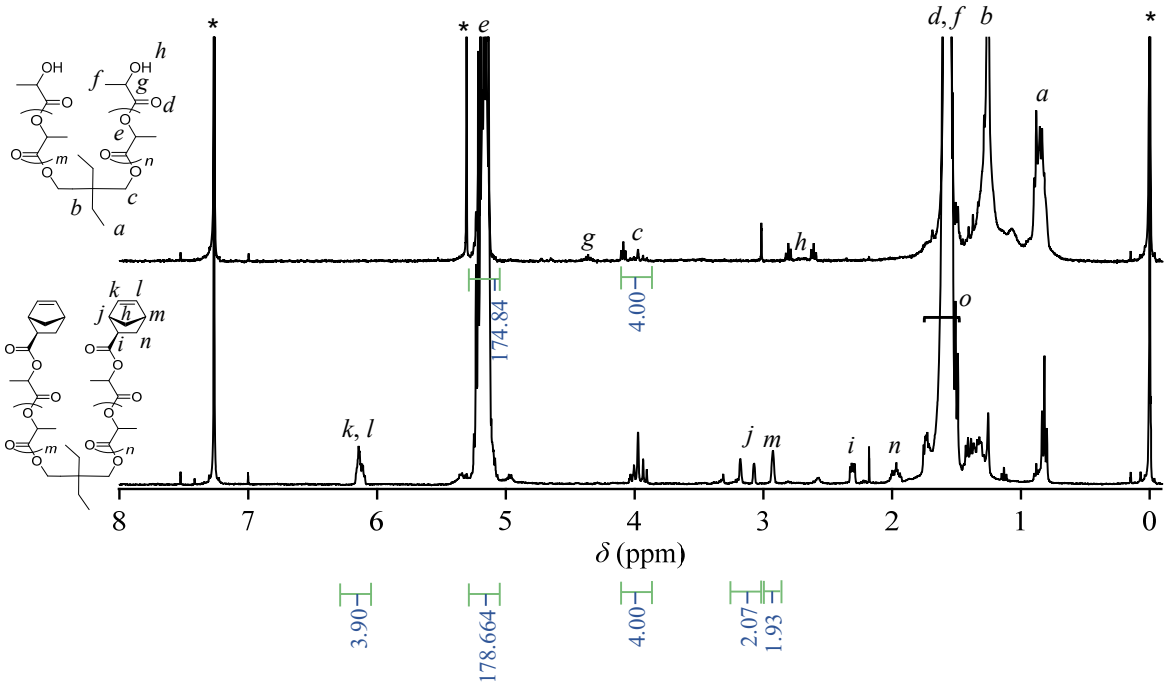

Figure 2.26. ^{1}H NMR spectra of HO–PLA$_{13k}$–OH (upper) and NB–PLA$_{13k}$–NB (lower) in $CDCl_3$.

Table 2.4. Molecular characterization of poly(cPS-*st*-cPLA) [a]

run	MM	$[PS]_0/[PLA]_0/[G3]_0$	$[MM]_0$ (mM)	time (min)	$M_{n,MALS}$ [b]	$Đ$ [c]	number of cyclic unit [d]	yield (%)
18	NB–PS_{6k}–NB ($M_{n,MALS}$ = 6,470)	1/1/1	0.125	120	23,800	1.34	3.8	81.7
19	and	2/2/1	0.125	210	27,000	1.19	4.4	50.4
20	NB–PLA_{6k}–NB ($M_{n,MALS}$ = 6,700)	3/3/1	0.150	120	40,300	1.29	6.5	92.2
21	NB–PS_{13k}–NB ($M_{n,MALS}$ = 13,400)	1/1/1	0.125	180	45,000	1.54	3.5	61.1
22	and	2/2/1	0.150	120	62,700	1.47	4.9	88.2
23	NB–PLA_{13k}–NB ($M_{n,MALS}$ = 13,200)	3/3/1	0.200	300	117,600	1.47	9.2	52.8

[a] Polymerization conditions: temperature, r.t.; atmosphere, Ar; solvent, CH_2Cl_2. [b] Determined by SEC-MALS-Visco in chloroform. [c] Determined by SEC in THF using PS as the standard. [d] The average number of cyclic units in the obtained poly(cPS-*st*-cPLA) was estimated as (M_n of poly(cPS-*st*-cPLA))/(M_n of NB–PS–NB + NB–PLA–NB).

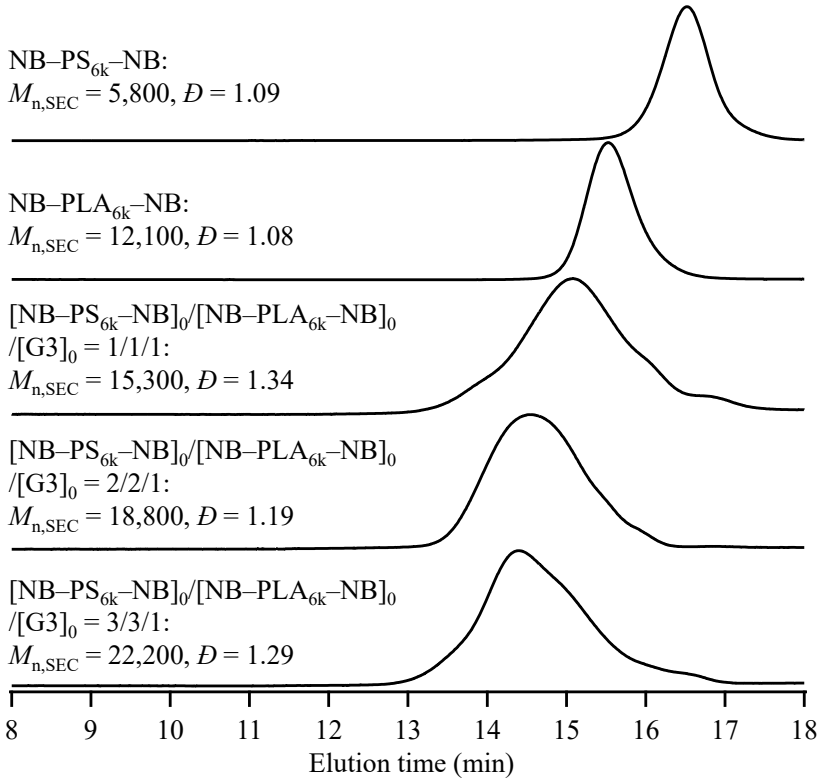

Figure 2.27. SEC traces of poly(cPS$_{6k}$-*st*-cPLA$_{6k}$) and their corresponding macromonomers (refractive index (RI) detection; eluent, THF; flow rate, 1.0 mL min^{-1}).

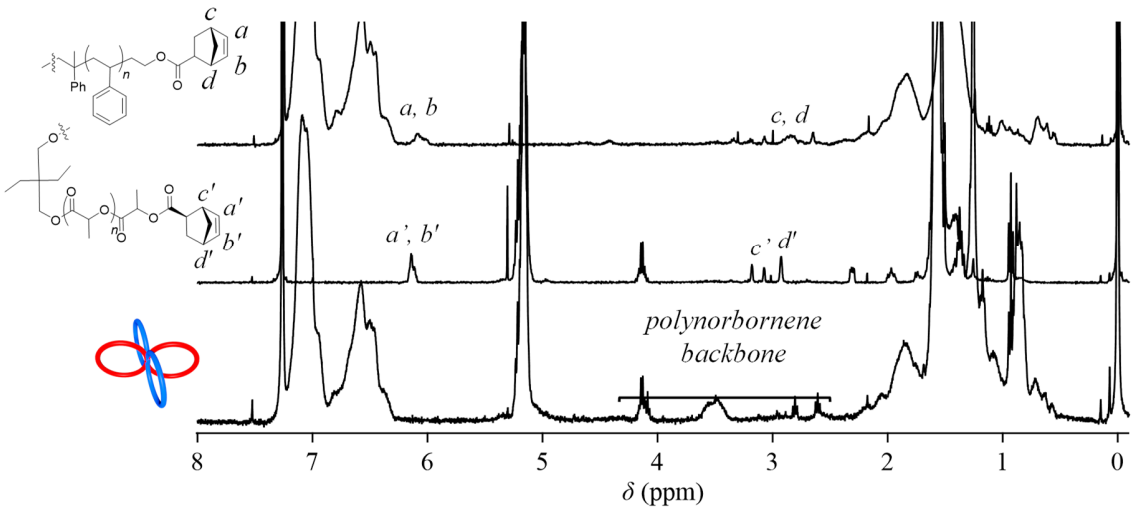

Figure 2.28 ^{1}H NMR spectra of NB–PS$_{6k}$–NB (upper), NB–PLA$_{6k}$–NB (middle), and poly(cPS-*st*-cPLA) (lower) in $CDCl_3$.

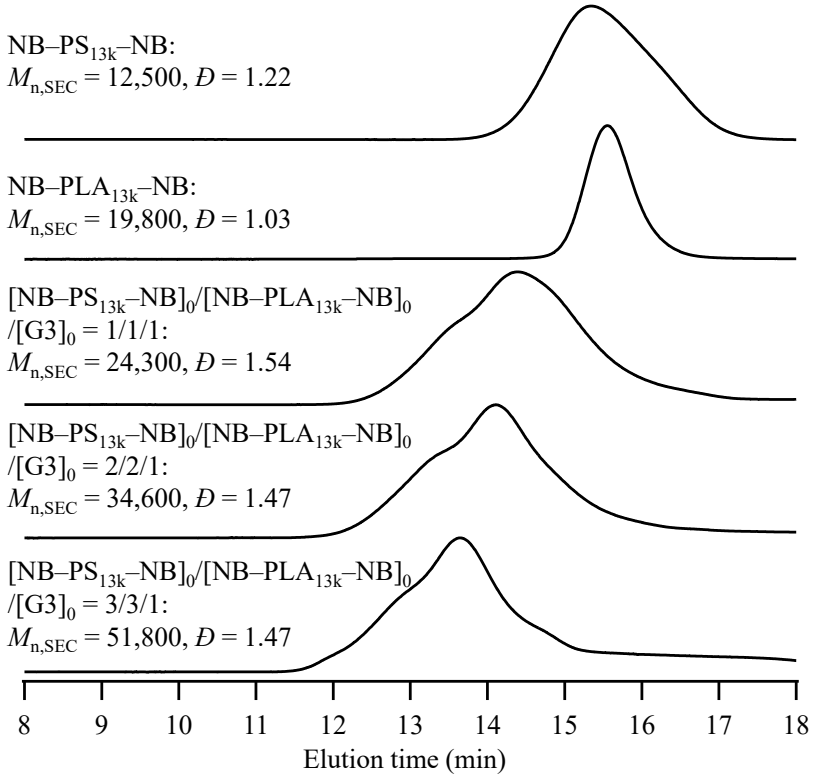

Figure 2.29. SEC traces of poly(cPS$_{13k}$-*st*-cPLA$_{13k}$) and their corresponding macromonomers (refractive index (RI) detection; eluent, THF; flow rate, 1.0 mL min^{-1}).

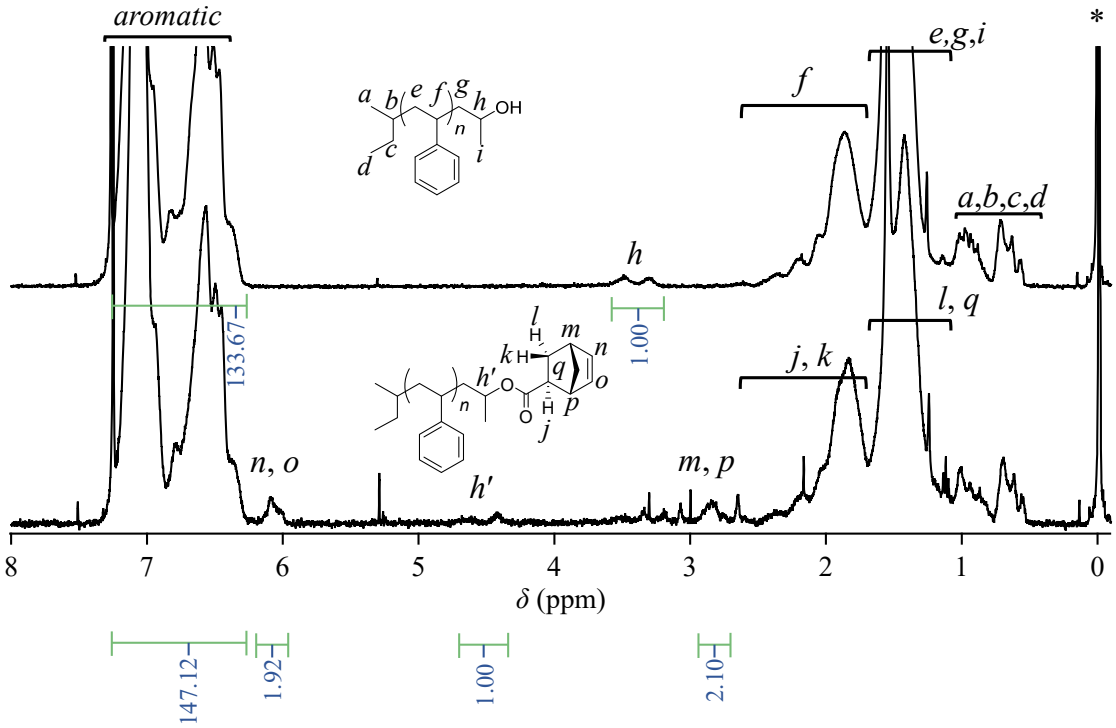

Figure 2.30. ^{1}H NMR spectra of PS_{3k}–OH (upper) and PS_{3k}–NB (lower) in $CDCl_3$.

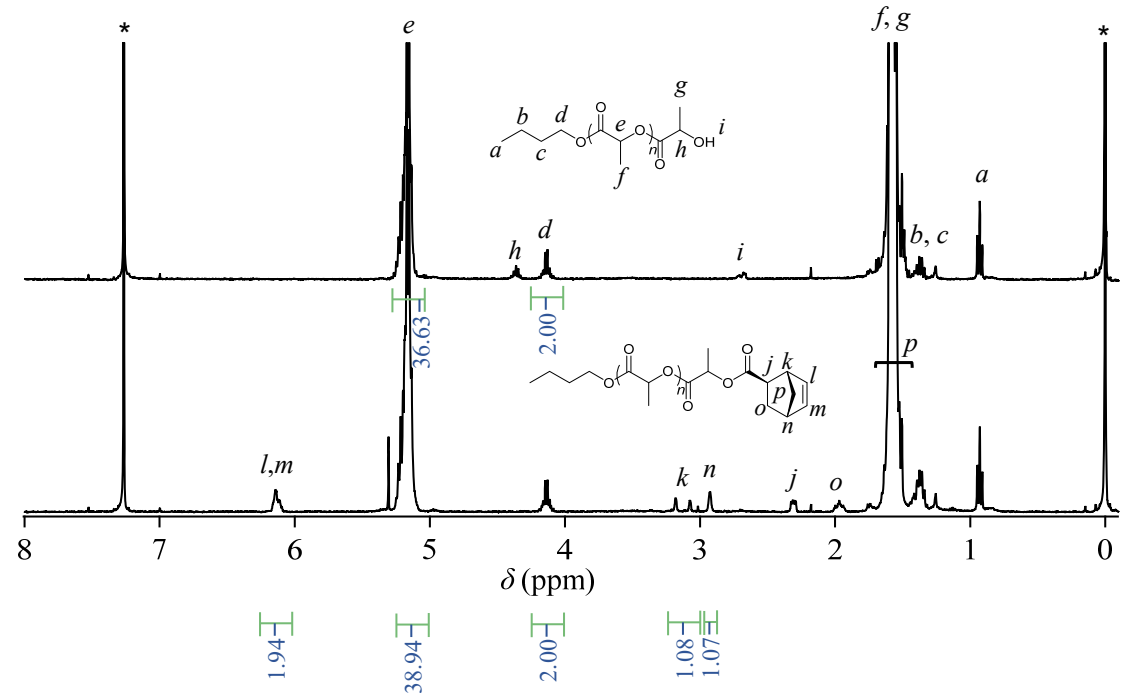

Figure 2.31. ^{1}H NMR spectra of PLA$_{3k}$–OH (upper) and PLA$_{3k}$–NB (lower) in $CDCl_3$.

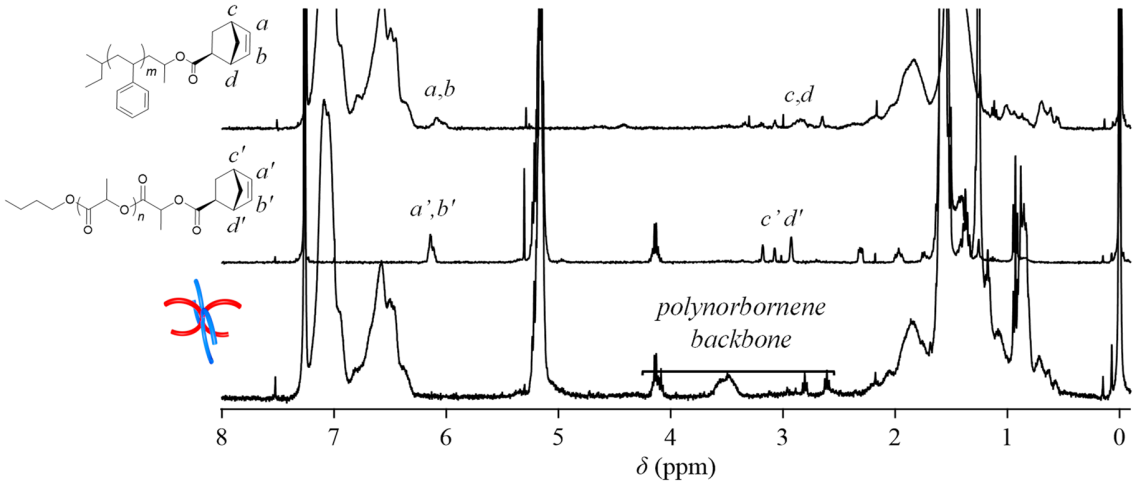

Figure 2.32 ^{1}H NMR spectra of PS$_{3k}$–NB (upper), PLA$_{3k}$–NB (middle), and poly(PS-*st*-PLA) (lower) in $CDCl_3$.

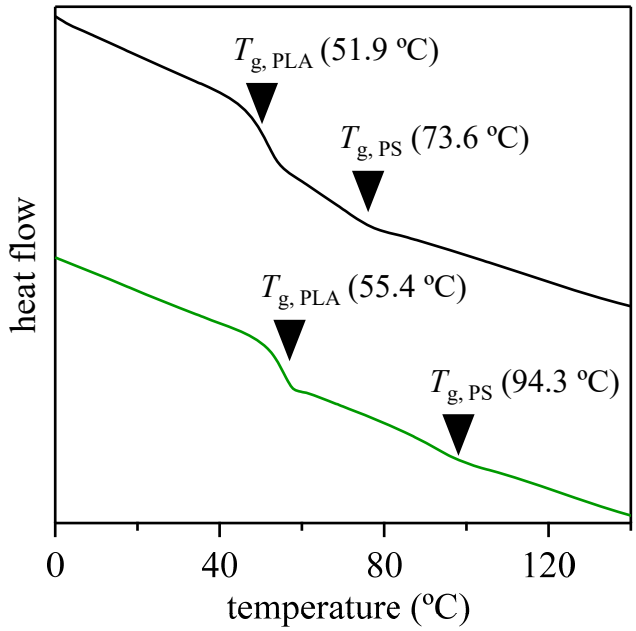

Figure 2.33. DSC curves during the second heating process of poly(PS-*st*-PLA) (black) and poly(cPS-*st*-cPLA) (run 20 in Table 2.4, green).

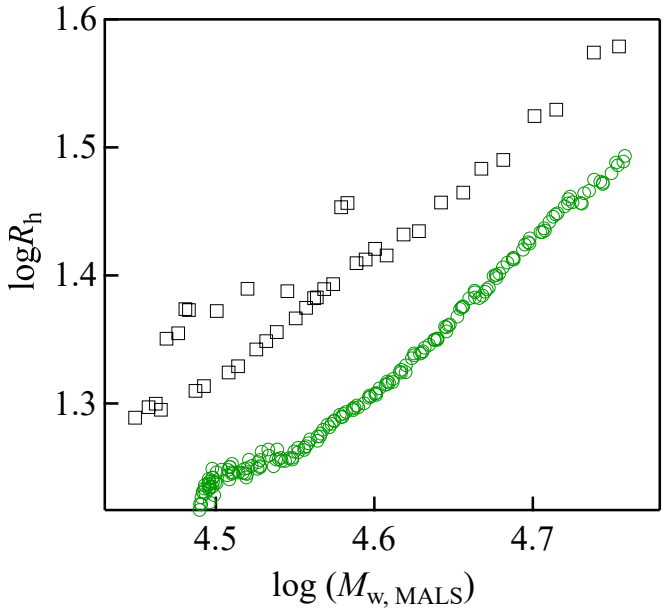

Figure 2.34. R_h conformation plots and for poly(PS-*st*-PLA) (black) and poly(cPS-*st*-cPLA) (run 20 in Table 2.4, green).

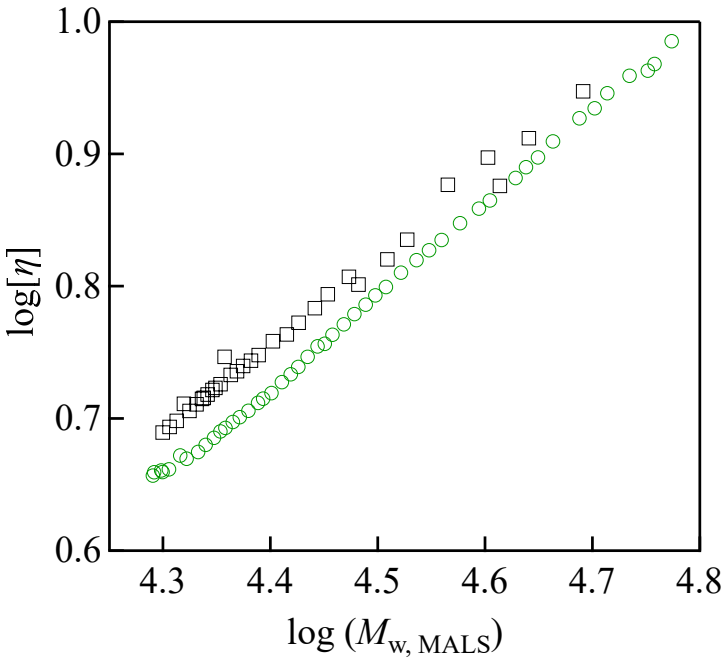

Figure 2.35. Mark-Hauwink-Sakurada plots and for poly(PS-*st*-PLA) (black) and poly(cPS-*st*-cPLA) (run 20 in Table 2.4, green).

2.4 Conclusions

In this study, the author synthesized multicyclic polystyrene (mc-PS) and PS-containing multicyclic copolymers via the cyclopolymerization of *α*,*ω*-dinorbornenyl end-functionalized macromonomers. Owing to the ease of macromonomer preparation (a one-step procedure using a commercially available reagent) and the high efficiency of the cyclopolymerization reaction, the author systematically synthesized a series of mc-PSs, achieving the highest reported number of cyclic units (239) and molecular weight of cyclic units (52,100). Compared to previously reported approaches that require multistep synthesis, the developed synthetic method is highly efficient and straightforward. The presented synthetic approach allowed the systematic evaluation of the effects of structure on the viscosity, hydrodynamic volume, and glass transition temperature. Furthermore, the author successfully synthesized multicyclic copolymers composed of PS and poly(*rac*-lactide) with various architectures via the cyclopolymerization of block copolymer-type macromonomers or the cyclocopolymerization of two macromonomers, further proving the synthetic versatility of the presented approach. Given the industrial importance of PS and PS-containing copolymers, the insights revealed in this study will contribute to both fundamental studies and practical applications of multicyclic polymers.

2.5. References

1. Polymeropoulos, G.; Zapsas, G.; Ntetsikas, K.; Bilalis, P.; Gnanou, Y.; Hadjichristidis, N. 50th Anniversary Perspective: Polymers with Complex Architectures. *Macromolecules*. **2017**, *50*, 1253–1290.
2. Santangelo, P. G.; Roland, C. M.; Chang, T.; Cho, D.; Roovers, J. Dynamics near the Glass Temperature of Low Molecular Weight Cyclic Polystyrene. *Macromolecules* **2001,** *34*, 9002–9005.
3. Clarson, S. J.; Semlyen, J. A. Cyclic Polysiloxanes: 1. Preparation and Characterization of Poly(Phenylmethylsiloxane). *Polymer* **1986**, *27*, 1633–1636.
4. Mckenna, G. B.; Hadziioannou, G.; Lutz, P.; Hild, G.; Strazielle, C.; Straupe, C.; Rempp, P.; Kovacs, A. J. Dilute Solution Characterization of Cyclic Polystyrene Molecules and Their Zero-Shear Viscosity in the Melt. *Maclomolecules* **1987,** 20, 498–512.
5. Bielawski, C. W.; Benitez, D.; Grubbs, R. H. An "Endless" Route to Cyclic Polymers. *Science* **2002**, *297*, 2041–2044.
6. Gauthier-Jaques, M.; Theato, P. Synergy of Macrocycles and Macromolecular Topologies: An Efficient [34]Triazolophane-Based Synthesis of Cage-Shaped Polymers. *ACS Macro Lett.* **2020**, *9*, 700–705.
7. Poelma, J. E.; Ono, K.; Miyajima, D.; Aida, T.; Satoh, K.; Hawker, C. J. Cyclic Block Copolymers for Controlling Feature Sizes in Block Copolymer Lithography. *ACS Nano* **2012**, *6*, 10845–10854.
8. Morgese, G.; Trachsel, L.; Romio, M.; Divandari, M.; Ramakrishna, S. N.; Benetti, E. M. Topological Polymer Chemistry Enters Surface Science: Linear versus Cyclic Polymer Brushes. *Angew. Chemie* **2016**, *128*, 15812–15817.

9. Honda, S.; Yamamoto, T.; Tezuka, Y. Topology-Directed Control on Thermal Stability: Micelles Formed from Linear and Cyclized Amphiphilic Block Copolymers. *J. Am. Chem. Soc.* **2010**, *132*, 10251–10253.

10. Satoh, Y.; Matsuno, H.; Yamamoto, T.; Tajima, K.; Isono, T.; Satoh, T. Synthesis of Well-Defined Three- and Four-Armed Cage-Shaped Polymers via "Topological Conversion" from Trefoil- and Quatrefoil-Shaped Polymers. *Macromolecules* **2017**, *50*, 97–106.

11. Mato, Y.; Honda, K.; Tajima, K.; Yamamoto, T.; Isono, T.; Satoh, T. A Versatile Synthetic Strategy for Macromolecular Cages: Intramolecular Consecutive Cyclization of Star-Shaped Polymers. *Chem. Sci.* **2019**, *10*, 440–446.

12. Mato, Y.; Honda, K.; Ree, B. J.; Tajima, K.; Yamamoto, T.; Deguchi, T.; Isono, T.; Satoh, T. Programmed Folding into Spiro-Multicyclic Polymer Topologies from Linear and Star-Shaped Chains. *Commun. Chem.* **2020**, *3*, 1–7.

13. Isono, T.; Satoh, Y.; Miyachi, K.; Chen, Y.; Sato, S. I.; Tajima, K.; Satoh, T.; Kakuchi, T. Synthesis of Linear, Cyclic, Figure-Eight-Shaped, and Tadpole-Shaped Amphiphilic Block Copolyethers via t-Bu-P4-Catalyzed Ring-Opening Polymerization of Hydrophilic and Hydrophobic Glycidyl Ethers. *Macromolecules* **2014**, *47*, 2853–2863.

14. Kusuyama, N.; Daito, Y.; Kubota, H.; Kametani, Y.; Ouchi, M. Construction of Ring-Based Architectures: Via Ring-Expansion Cationic Polymerization and Post-Polymerization Modification: Design of Cyclic Initiators from Divinyl Ether and Dicarboxylic Acid. *Polym. Chem.* **2021**, *12*, 2532–2541.

15. Zhang, Y.; Wu, Y.; Zhao, Y.; Zhang, L.; Zhang, K. Versatile Bimolecular Ring-Closure Method for Cage-Shaped Polymers. *Macromolecules* **2021**, *54*, 6901–6910.

16. Sugai, N.; Heguri, H.; Ohta, K.; Meng, Q.; Yamamoto, T.; Tezuka, Y. Effective Click Construction of Bridged-and Spiro-Multicyclic Polymer Topologies with Tailored Cyclic Prepolymers (Kyklo-Telechelics). *J. Am. Chem. Soc.* **2010**, *132*, 14790–14802.

17. Sugai, N.; Heguri, H.; Yamamoto, T.; Tezuka, Y. A Programmed Polymer Folding: Click and Clip Construction of Doubly Fused Tricyclic and Triply Fused Tetracyclic Polymer Topologies. *J. Am. Chem. Soc.* **2011**, *133*, 19694–19697.

18. Tezuka, Y. Topological Polymer Chemistry for Designing Multicyclic Macromolecular Architectures. *Polym. J.* **2012**, *44*, 1159–1169.

19. Zhang, H. L.; Xu, W.; Liu, C.; Hong, C. Y. Synthesis of a Bead-like Multicyclic Polymer by UV-Induced Coupling of an Anthracene-Telechelic Monocyclic Precursor and Its Reversible Topological Conversion. *Polym. Chem.* **2021**, *12*, 5357–5363.

20. Ma, C.; Quan, Y.; Liao, X.; Sun, R.; Xie, M. Cyclic-hanging-multicyclic polymer synthesized by ladderphane-mediated blocking-cyclization technique for the direct visualization of cyclic macromolecular topology. *Polym. Chem.* **2023**, *14*, 2072– 2079.

21. Lonsdale, D. E.; Monteiro, M. J. Various Polystyrene Topologies Built from Tailored Cyclic Polystyrene via CuAAC Reactions. *Chem. Commun.* **2010**, *46*, 7945–7947.

22. Hossain, M. D.; Reid, J. C.; Lu, D.; Jia, Z.; Searles, D. J.; Monteiro, M. J. Influence of Constraints within a Cyclic Polymer on Solution Properties. *Biomacromolecules* **2018**, *19*, 616–625.

23. Pipertzis, A.; Hossain, M. D.; Monteiro, M. J.; Floudas, G. Segmental Dynamics in Multicyclic Polystyrenes. *Macromolecules* **2018**, *51*, 1488–1497.

24. Gavrilov, M.; Amir, F.; Kulis, J.; Hossain, M. D.; Jia, Z.; Monteiro, M. J. Densely Packed Multicyclic Polymers. *ACS Macro Lett.* **2017**, *6*, 1036–1041.

25. Yan, Z. C.; Hossain, M. D.; Monteiro, M. J.; Vlassopoulos, D. Viscoelastic Properties of Unentangled Multicyclic Polystyrenes. *Polymers* **2018**, *10*, 1–13.

26. Jeong, J.; Kim, K.; Lee, R.; Lee, S.; Kim, H.; Jung, H.; Kadir, M. A.; Jang, Y.; Jeon, H. B.; Matyjaszewski, K.; Chang, T.; Paik, H. J. Preparation and Analysis of Bicyclic Polystyrene. *Macromolecules* **2014**, *47*, 3791–3796.

27. Mohanty, A. K.; Ye, J.; Ahn, J.; Yun, T.; Lee, T.; Kim, K. S.; Jeon, H. B.; Chang, T.; Paik, H. J. Topologically Reversible Transformation of Tricyclic Polymer into Polyring Using Disulfide/Thiol Redox Chemistry. *Macromolecules* **2018**, *51*, 5313–5322.

28. Jung, J. H.; Kumar Mohanty, A.; Ye, J.; Lee, T.; Ahn, J.; Lim, Y. G.; Chang, T.; Paik, H. J. Covalent Fixed Multicyclic Polystyrene Conformers. *J. Polym. Sci. Part A Polym. Chem.* **2017**, *55*, 4020–4026.

29. Shi, G. Y.; Pan, C. Y. Synthesis of Well-Defined Figure-of-Eight-Shaped Polymers by a Combination of ATRP and Click Chemistry. *Macromol. Rapid Commun.* **2008**, *29*, 1672–1678.

30. Xue, X.; Chen, Y.; Li, Y.; Liang, K.; Huang, W.; Yang, H.; Jiang, L.; Jiang, Q.; Chen, F.; Jiang, T.; Lin, B.; Jiang, B.; Pu, H. Remarkable Untangled Dynamics Behavior of Multicyclic Branched Polystyrenes. *Chem. Commun.* **2021**, *57*, 399–402.

31. Minatti, E.; Borsali, R.; Schappacher, M.; Deffieux, A.; Soldi, V.; Narayanan, T.; Putaux, J. L. Effect of Cyclization of Polystyrene/Polyisoprene Block Copolymers on Their Micellar Morphology. *Macromol. Rapid Commun.* **2002**, *23*, 978–982.

32. Minatti, E.; Viville, P.; Borsali, R.; Schappacher, M.; Deffieux, A.; Lazzaroni, R. Micellar Morphological Changes Promoted by Cyclization of PS-*b*-PI Copolymer: DLS and AFM Experiments. *Macromolecules* **2003**, *36*, 4125–4133.

33. Lecommandoux, S.; Borsali, R. On the physics of block copolymers. *Polym. Int.* **2006**, *55*, 961–969.

34. Di Cola, E.; Lefebvre, C.; Deffieux, A.; Narayanan, T.; Borsali, R. Micellar Transformations of Poly(Styrene-*b*-Isoprene) Block Copolymers in Selective Solvents. *Soft Matter* **2009**, *5*, 1081–1090.

35. Isono, T.; Sasamori, T.; Honda, K.; Mato, Y.; Yamamoto, T.; Tajima, K.; Satoh, T. Multicyclic Polymer Synthesis through Controlled/Living Cyclopolymerization of *α*,*ω*-Dinorbornenyl-Functionalized Macromonomers. *Macromolecules* **2018**, *51* (10), 3855–3864.

36. Choi, T. L.; Grubbs, R. H. Controlled Living Ring-Opening-Metathesis Polymerization by a Fast-Initiating Ruthenium Catalyst. *Angew. Chem. Int. Ed.* **2003**, *42*, 1743–1746.

37. Haque, F. M.; Grayson, S. M. The Synthesis, Properties and Potential Applications of Cyclic Polymers. *Nature Chemistry* **2020**, *12*, 433–444.

38. Li, Z.; Zhang, K. E.; Ma, J.; Chong, C.; Wooley, K. L. Facile Syntheses of Cylindrical Molecular Brushes by a Sequential RAFT and ROMP "Grafting-Through" Methodology. *J. Polym. Sci. Part A Polym. Chem.* **2009**, *47*, 5557–5563.

39. Hsu, H. P.; Paul, W.; Rathgeber, S.; Binder, K. Characteristic Length Scales and Radial Monomer Density Profiles of Molecular Bottle-Brushes: Simulation and Experiment. *Macromolecules* **2010**, *43*, 1592–1601.

40. Li, Z.; Lee, N. S.; Wooley, K. L. Dynamic Cylindrical Assembly of Triblock Copolymers. *J. Am. Chem. Soc.* **2011**, *133*, 1228–1231.

41. Pesek, S. L.; Li, X.; Hammouda, B.; Hong, K.; Verduzco, R. Small-Angle Neutron Scattering Analysis of Bottlebrush Polymers Prepared via Grafting-through

Polymerization. *Macromolecules* **2013**, *46*, 6998–7005.

42. Fox, T. G.; Flory, P. J. Second-Order Transition Temperatures and Related Properties of Polystyrene. I. Influence of Molecular Weight. *J. Appl. Phys.* **1950**, *21*, 581–591.

43. Gao, L.; Oh, J.; Tu, Y.; Chang, T.; Li, C. Y. Glass Transition Temperature of Cyclic Polystyrene and the Linear Counterpart Contamination Effect. *Polymer* **2019**, *170*, 198–203.

44. Clarson, S. J.; Semlyen, J. A.; Dodgson, K. Cyclic Polysiloxanes: 4. Glass Transition Temperatures of Poly(Phenylmethylsiloxanes). *Polymer* **1991**, *32*, 2823–2827.

45. Rique-Lurbet, L.; Schappacher, M.; Deffieux, A. A New Strategy for the Synthesis of Cyclic Polystyrenes: Principle and Application. *Macromolecules* **1994**, *27*, 6318–6324.

46. Kammiyada, H.; Ouchi, M.; Sawamoto, M. A Study on Physical Properties of Cyclic Poly(Vinyl Ether)s Synthesized via Ring-Expansion Cationic Polymerization. *Macromolecules* **2017**, *50*, 841–848.

47. Gan, Y.; Dong, D.; Hogen-esch, T. E. Poly(2-Vinylpyridine). *Macromolelues* **1995**, *28*, 383–385.

48. Zalusky, A. S.; Olayo-Valles, R.; Wolf, J. H.; Hillmyer, M. A. Ordered Nanoporous Polymers from Polystyrene-Polylactide Block Copolymers. *J. Am. Chem. Soc.* **2002**, *124*, 12761–12773.

49. Keen, I.; Cheng, H. H.; Yu, A.; Jack, K. S.; Younkin, T. R.; Leeson, M. J.; Whittaker, A. K.; Blakey, I. Behavior of Lamellar Forming Block Copolymers under Nanoconfinement: Implications for Topography Directed Self-Assembly of Sub-10 Nm Structures. *Macromolecules* **2014**, *47*, 276–283.

50. Li, X.; Liu, Y.; Wan, L.; Li, Z.; Suh, H.; Ren, J.; Ocola, L. E.; Hu, W.; Ji, S.; Nealey, P.

F. Effect of Stereochemistry on Directed Self-Assembly of Poly(Styrene-b-Lactide) Films on Chemical Patterns. *ACS Macro Lett.* **2016**, *5*, 396–401.

51. Watanabe, K.; Katsuhara, S.; Mamiya, H.; Yamamoto, T.; Tajima, K.; Isono, T.; Satoh, T. Downsizing Feature of Microphase-Separated Structures via Intramolecular Crosslinking of Block Copolymers. *Chem. Sci.* **2019**, *10*, 3330–3339.

Chapter 3

Structure-property Relationships in Multicyclic Polystyrenes: Physical Properties and Comparison with Acyclic Counterparts

3.1 Introduction

Complex architectural polymers with well-defined structures have attracted significant attention not only because of their crucial role as model systems for elucidating structure–property relationships, but also because of their promising applications in the development of advanced materials. Recent progress in polymer science has facilitated the synthesis of polymers with diverse architectures, such as cyclic,[1] star-shaped,[2] hyperbranched,[3] and complex hybrid structures.[4] Among these, cyclic polymers stand out because of their unique physical properties and distinct applications compared with those of linear polymers; these properties are primarily attributed to their compact architectures.[5–10] For example, cyclic polymers exhibit higher glass transition temperatures (T_g),[11] higher melting points (T_m),[12] smaller hydrodynamic radii (R_h),[13] and lower intrinsic viscosities ([η])[14] than their linear counterparts with comparable molecular weights (**Figure 3.1a**). Moreover, functional materials derived from cyclic polymers are expected to exhibit superior properties to those derived from linear polymers. These properties include decreased domain spacings for microphase-separated block copolymers,[15] improved thermal stabilities for self-assembled micelles,[16] increased gene delivery efficiencies, and reduced cytotoxicities.[17] Additionally, macromolecules bearing densely grafted side chains (referred to as star-like polymers when the degree of backbone polymerization is low and bottlebrush polymers when it is high) also constitute an interesting class of branched polymers. These branched polymers exhibit unique properties, such as higher backbone stiffnesses[18] and lower T_g, T_m,[19] and [η] values[20] than their corresponding linear polymers (Figure 3.1b). In addition to these physical properties, they are known to exhibit a spherical-to-cylindrical conformational transition in solution upon increasing the degree of

backbone polymerization, thereby rendering them a unique subject of research from both fundamental and application viewpoints.[21]

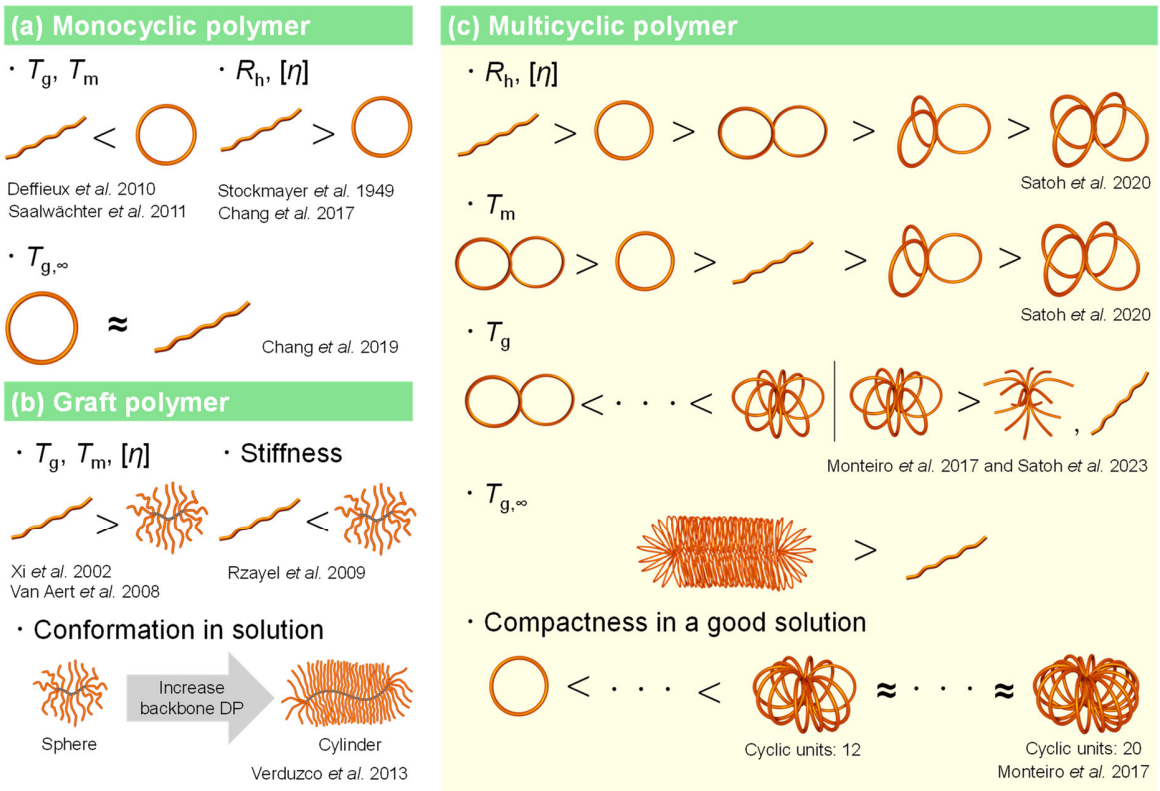

Figure 3.1. Visual representation of the physical properties of monocyclic, bottlebrush, and multicyclic polymers.

Macromolecules bearing backbones that are densely grafted with cyclic polymer chains (multicyclic polymers) are also interesting due to their unique molecular architectures that combine the characteristics of both cyclic and branched structures. Although several synthetic pathways have been developed for the preparation of multicyclic polymers,[22–35] few studies have focused on their syntheses and physical properties (Figure 3.1c). As summarized

in Chapter 1, Satoh et al. prepared spiro-type multicyclic polycaprolactones (PCLs) with two to four rings via intramolecular ring-opening metathesis oligomerization and demonstrated that, at fixed total molecular weight, the hydrodynamic radius (R_h), intrinsic viscosity [η], and chain dimensions decreased with increasing number of cyclic units, while the 8-shaped PCL exhibited the highest T_m in the series.[36] In a related study, Monteiro et al. synthesized multicyclic polystyrenes containing up to 20 cyclic units by click chemistry and showed that their T_g increased with the number of cyclic units, became more compact in solution up to approximately twelve rings, and consistently exceeded the T_g values of the corresponding graft and linear polystyrenes.[29] As described in Chapter 2, this work further extended these concepts by synthesizing multicyclic polystyrenes with up to 250 cyclic units via cyclopolymerization and confirming analogous topology-dependent T_g trends, with Flory–Fox analysis yielding $T_{g,\infty}$ values higher than that of linear polystyrene.

Polystyrene is one of the most commonly used polymers for studying the physical properties of polymers and serves as a standard material for such research. Therefore, multicyclic polystyrenes are particularly important platforms for understanding the unique properties arising from various topologies. However, owing to the challenges associated with their syntheses, several aspects remain unexplored. In particular, no systematic studies have investigated how the number of cyclic units influences the molecular structures and physical properties of multicyclic polymers. Such systematic investigations are scarce not only for polystyrene but also for other polymer systems, despite their importance for establishing general structure–property relationships. Furthermore, only a few studies have systematically compared the physical properties of multicyclic polymers with those of their acyclic

counterparts. Such a comparison would provide further insight into the unique structures and properties arising from the cyclic topology.

In the chapter, multicyclic polystyrene (mc-PS) species containing different numbers of cyclic units were synthesized via cyclopolymerization method established in Chapter 2 to investigate the correlation between the multicyclic structure and various physical properties (i.e., T_g, degradation temperature, R_h, viscosity, and Kuhn length), and also to provide a comparison with a series of graft PS (g-PS) and linear PS (l-PS) systems. Furthermore, small-angle neutron scattering (SANS) and small-angle X-ray scattering (SAXS) measurements were performed in solution to reveal the conformational transition of mc-PS upon increasing the number of cyclic units. Additionally, SAXS analysis was carried out using a flexible cylinder model to evaluate the Kuhn lengths of the polymers and determine the backbone rigidity. The cyclopolymerization approach enabled, for the first time, a systematic investigation of how the number of cyclic units affects the physical properties and molecular structures of multicyclic polymers, as well as a direct comparison with their acyclic counterparts.

3.2 Experimental section

3.2.1 Materials

Grubbs' 3rd generation catalyst (G3) was prepared according to previously reported method.[37] *N*,*N*-Dimethyl-4-aminopyridine (DMAP; Tokyo Chemical Industry Co., Ltd. (TCI), >99.0%), 1-ethyl-3-(3-(dimethylamino)-propyl)carbodiimide hydrochloride (EDC; TCI, >98.0%), ethyl vinyl ether (TCI, >98.0%), (±)-*exo*-5-norbornenecarboxylic acid (*exo*-NB-COOH; Aldrich, 97%), CH_2Cl_2 (Junsei Chemical Co., Ltd., >99.0%), methanol (Aldrich, >99.8, dry methanol (Kanto Chemical Co., Inc., >99.5%), *sec*-butyllithium (*sec*-BuLi; Kanto Chemical Co., Inc., 1.23 mol L^{-1} in cyclohexane/*n*-hexane (v/v = 24/1)), dry CH_2Cl_2 (Kanto Chemical Co., Inc., >99.5%, water content, <0.001%), deuterated toluene (toluene-d_8, Aldrich, >99.0%, >99.96 atom% D) were used as received. HO–PS–OH samples were obtained from Polymer Source and used as received. Linear polystyrene (l-PS) samples were obtained from Shodex and used as received. Styrene (TCI, >99%), propylene oxide (PO; TCI, >99.0%), and cyclohexane (Kanto Chemical Co., Inc., >99.5%) were purified by distillation over CaH_2 under reduced pressure.

3.2.2 Instruments

The polymerization experiments were carried out in an MBRAUN stainless steel glovebox equipped with a gas purification system (molecular sieves and copper catalyst) in a dry argon atmosphere (H_2O, O_2<0.1 ppm). The moisture and oxygen contents in the glovebox were monitored by an MB-MO-SE 1 moisture sensor and an MB-OX-SE 1 oxygen sensor, respectively. The ^1H (400 MHz) spectra were recorded using a JEOL JNM-ECS400 instrument at room temperature in $CDCl_3$. The size exclusion chromatography (SEC) was performed at 40 °C in THF (flow rate, 1.0 mL min^{-1}) using a Jasco high-performance liquid chromatography system (PU-4180 HPLC pump, AS-4550 auto sampler, and CO-4060 column oven) equipped with a Shodex K-800D guard column (8.0 mm × 100 mm; particle size, 10 μm), two Shodex columns (K-806L and K-804L; linear, 8.0 mm × 100 mm; particle size, 10μm). The absolute number-averaged molecular weight ($M_{n,MALS}$) and polydispersity ($Đ_{MALS}$) of the samples were determined by SEC with multiangle light scattering detection (SEC-MALS-Visco) in $CHCl_3$ (flow rate, 1.0 mL min^{-1}) at 40 °C using a Jasco high-performance liquid chromatography system (PU-4180 HPLC pump, AS-4550 auto sampler, and CO-4060 column oven) equipped with a Shodex K-800D guard column (8.0 mm × 100 mm; particle size, 10 μm), two Shodex columns (K-806L and K-804L; linear, 8.0 mm × 100 mm; particle size, 10μm), a DAWN 8 multiangle laser light scattering detector (Wyatt Technology), a Viscostar viscosity detector (Wyatt Technology), and an RI-501 refractive index detector (Shodex). The preparative SEC was performed at room temperature in $CHCl_3$ (flow rate, 10.0 mL min^{-1}) using LaboACE LC-7080 liquid chromatography system (Japan Analytical Industry Co. Ltd.) equipped with a P-LA80 pump, a RI-700LA RI detector, JAIGEL-HR-P guard column (8 mm × 40 mm; Japan Analytical Industry Co. Ltd.), JAIGEL-2HR column (linear, 20.0 mm × 600 mm; exclusion

limit, 5.0×10^3), JAIGEL-2.5HR column (linear, 20.0 mm × 600 mm; exclusion limit, 2.0×10^4), and JAIGEL-3HR column (linear, 20.0 mm × 600 mm; exclusion limit, 7.0×10^4).

Differential scanning calorimetry (DSC) measurement

The DSC experiments were performed using a Hitachi DSC 7000X under a nitrogen atmosphere. The polystyrene samples were heated to 150 °C, cooled to 30 °C, and heated again to 150 °C at the heating and cooling rate of 10 °C min^{-1} and 20 °C min^{-1}, respectively.

Thermogravimetric analysis (TGA)

The TGA analysis was performed using Hitachi STA200RV under nitrogen atmosphere. The polystyrene samples were heated to 120 °C, cooled to 30 °C, and heated to 550 °C at the heating and cooling rate of 10 °C min^{-1}.

Small-angle Neutron Scattering (SANS) Measurements.

SANS measurements were performed at C1-2: SANS-U in JRR-3M, Japan. The incident beam wavelength was set to 0.70 nm. A detector was placed 1.0 m or 8.0 m from the sample. The measurement setup provided the q range of 0.04–3.4 nm^{-1}, where q is the magnitude of the scattering vector defined by $q = 4\pi/\lambda \sin(\theta)$, with the incident beam length denoted as λ, and the scattering angle of 2θ. The samples were loaded into quartz cylindrical cells with a path length of 1 mm and measured at 25 °C. Sample solutions were measured at a beam exposure time of 120 min, and the resulting two-dimensional SANS images was converted to one-dimensional $I(q)$ versus q profiles via circular averaging.

Small-angle X-ray Scattering (SAXS) Measurements.

SAXS measurements were performed at the beamline BL40B2 in SPring-8, Japan. The incident beam wavelength was set to 0.10 nm. A detector was placed 4.0 m from the sample, and ion chambers were placed in front and behind the sample to determine the X-ray transmittance. The measurement setup provided the q range of 0.02–2.0 nm^{-1}, where q is the magnitude of the scattering vector defined by $q = 4\pi/\lambda \sin(\theta)$, with the incident beam length denoted as λ, and the scattering angle of 2θ. The sample solutions were packed in a quartz capillary (2 mm Φ, Hilgenberg GmbH) and set in the sample chamber controlled by a INSTEC HCS-302 temperature control system to a temperature of 25.0 ºC. Sample solutions were measured at a beam exposure time of 3 min, and the resulting two-dimensional SAXS images was converted to one-dimensional $I(q)$ versus q profiles via circular averaging. Here, $I(q)$ is the scattering intensity at q, and the background scattering from the solvent and the cell was subtracted to obtain the reduced excess scattering intensity ($\Delta I(q)$) of the sample using the following equation,

$$\Delta I(q) = \frac{I_{soln}(q)}{T_{soln} - T_{dark}} - \frac{I_{solv}(q)}{T_{solv} - T_{dark}} \qquad (1)$$

where $I_{soln}(q)$ and $I_{solv}(q)$ are the scattering intensity of the sample solution and the solvent, respectively, and the T_{soln}, T_{solv} and T_{dark} each represent the X-ray transmittance of the sample solution, solvent, and the background from the environment without any beam exposure, respectively. $\Delta I(q)$ was further corrected into absolute intensity values through the use of water (MilliQ water) as a secondary standard.[38]

3.2.3 Synthetic details

Synthesis of *α*, *ω*-end norbornenyl-functionalized PS (NB–PS–NB)

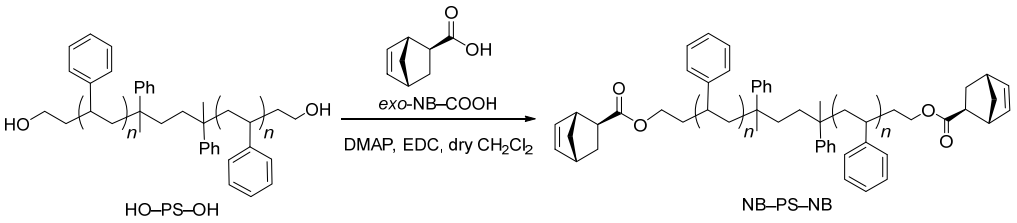

A typical procedure for the condensation reaction is as follows (Method A): In a round-bottom flask, HO–PS–OH ($M_{n,NMR}$ = 3,500, 5.06 g, 1.45 mmol), *exo*-NB–COOH (817 mg, 5.91 mmol), EDC (1.68 g, 8.76 mmol), and DMAP (1.08 mg, 8.84 mmol) were dissolved in CH_2Cl_2 (50.0 mL), and the mixture was stirred at r.t. for 72 h. The polymer crude was purified by reprecipitation in methanol to give NB–PS–NB as a white solid. Yield: 5.05 g (99.9%)

$M_{n,NMR}$ = 3,700, $M_{n,SEC}$ = 3,100, $Đ$ = 1.30

^{1}H NMR ($CDCl_3$, 400 MHz): δ (ppm) 7.40–6.17 (m, *aromatic*), 6.17–6.00 (m, 4H, –C*H*=C*H*– in norbornene ring), 3.93–3.60 (m, 4H, –CH_2C*H*$_2$OCO–), 3.17–2.94 (m, 4H, –C*H*–CH_2–CH–CO– in norbornene ring, –C*H*–CH–CO– in norbornene ring), 2.53–1.69 (m, –CH_2C*H*Ph–, *endo*-C*H*– of –CH–CH_2–CH–C*H*CO– in norbornene ring, *exo*-C*H*– of –CH–C*H*$_2$–CH–CO– in norbornene ring), 1.69–1.13 (m, –C*H*$_2$CHPh–, –CH_2CC*H*$_3$(Ph)–, –C*H*$_2$CCH$_3$(Ph)–, –C*H*$_2$CH$_2$OCO–, *endo*-C*H*– of –CH–C*H*$_2$–CH–CO– in norbornene ring, bridge head –C*H*$_2$– in norbornene ring).

Synthesis of mc-PS

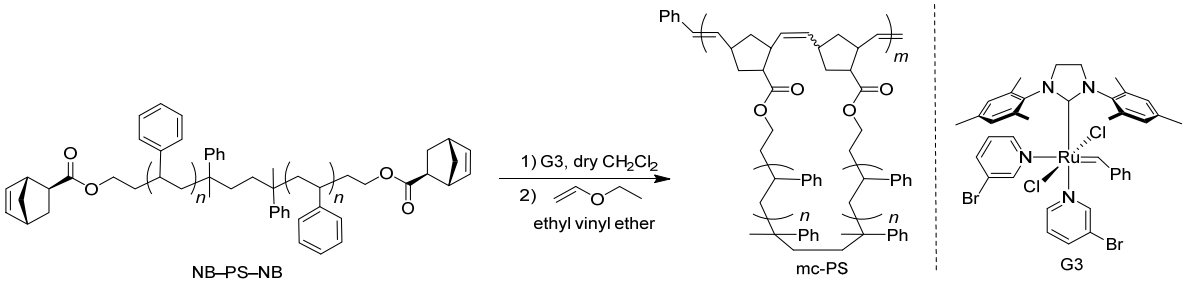

A typical procedure for the ring-opening metathesis polymerization (ROMP) is as follows (Method B): In a three-necked flask, a stock solution of Grubbs third-generation catalyst (G3; 540 μL, 16.2 μmol as a 8.0 mol L^{-1} in dry CH_2Cl_2, 1.0 eq.) was quickly added to a stirred mixture of *α*,*ω*-dinorbornenyl-functionalized linear polystyrene (NB–PS–NB; 300 mg, 81.1 μmol, 5.0 eq.) in dry CH_2Cl_2 (541 mL) under an argon atmosphere. After 1.0 h, an excess amount of ethyl vinyl ether was added to the reacting mixture to terminate the ROMP. The crude product was purified by preparative GPC to remove the catalyst residue, affording mc-PS as a brown solid. Yield: 288 mg (96.0%)

$M_{n,SEC}$ = 10,400, $Đ$ = 1.15, $M_{n,MALS}$ = 20,300, $Đ_{MALS}$ = 1.15, average number of cyclic units = 5.5

^{1}H NMR ($CDCl_3$, 400 MHz): δ (ppm) 7.23–6.12 (m, *aromatic*), 5.79–4.78 (br, alkenyl of poly(norbornene) backbone), 4.31–2.35 (br, alkenyl of poly(norbornene) backbone), 2.44–1.69 (m, –CH_2CHPh–), 1.69–0.99 (m, –CH_2CHPh–, –CH_2CCH_3(Ph)–, –CH_2CCH_3(Ph)–, –CH_2CH_2OCO–).

Synthesis of *ω*-end hydroxy-functionalized PS (PS–OH)

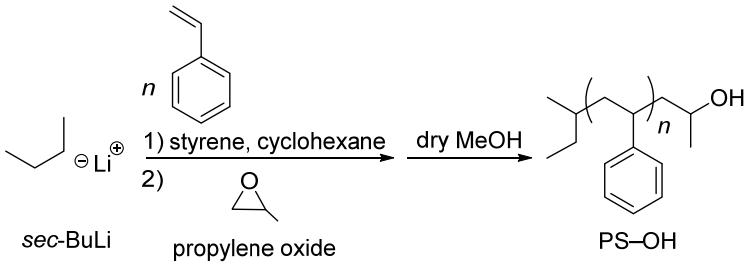

Under Ar atmosphere, cyclohexane (86.4 mL) was placed in a round-bottom flask equipped with a greaseless valve and then heated to 40 °C in an oil bath. *sec*-BuLi (4.68 mL, 5.61 mmol) was added to the solution. Styrene (9.93 mL, 86.4 mmol) was added to the solution, and the mixture was stirred for 2 h. Propylene oxide (3.93 mL, 56.1 mmol) was then added to the solution at 40 °C, and the mixture was stirred for 2 h. Excess dry MeOH was added to terminate the polymerization. The product was purified by reprecipitation in MeOH to give PS–OH as a white solid. Yield: 8.06 g (89.6%)

$M_{n,NMR}$ = 1,600, $M_{n,SEC}$ = 1,600, $Đ$ = 1.16

^{1}H NMR ($CDCl_3$, 400 MHz): δ (ppm) 7.22–6.22 (m, *aromatic*), 3.61–3.16 (s, 1H, –$CH_2CH(CH_3)OH$), 2.44–1.66 (m, –CH_2CHPh–), 1.66–1.21 (m, –CH_2CHPh–, –$CH_2CH(CH_3)OH$, –$CH_2CH(CH_3)OH$), 1.14–0.51 (m, –*sec*-butyl).

Synthesis of *ω*-end norbornenyl-functionalized PS (PS–NB)

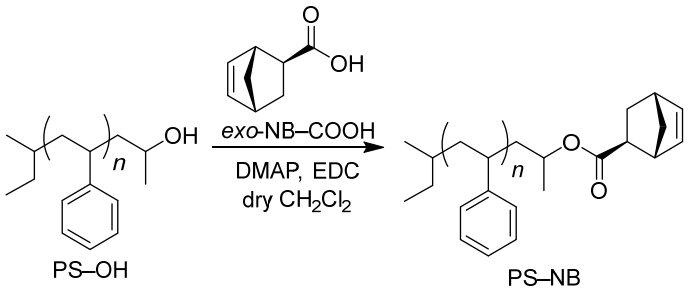

Method A was used for the reaction of PS–OH ($M_{n,NMR}$ = 1,600, 7.54 g, 4.71 mmol) with *exo*-NB–COOH (1.31 g, 9.48 mmol), DMAP (1.73 g, 14.2 mmol), and EDC (2.72 mg, 14.2 mmol) in CH_2Cl_2 (75.4 mL) for 2 days to give PS–NB as a white solid. Yield: 7.39 g (98.0%) $M_{n,NMR}$ = 1,900, $M_{n,SEC}$ = 1,400, $Đ$ = 1.20

^{1}H NMR ($CDCl_3$, 400 MHz): δ (ppm) 7.22–6.19 (m, *aromatic*), 6.19–5.96 (m, 2H, –C*H*=C*H*– in norbornene ring), 4.78–4.34 (s, 1H, –CH_2C*H*(CH_3)O–), 2.97–2.72 (m, 2H, –C*H*–CH_2–CH–CO– in norbornene ring, –C*H*–CH–CO– in norbornene ring), 2.44–1.68 (m, –CH_2C*H*Ph–, *endo*-C*H*– of –CH–CH_2–CH–C*H*CO– in norbornene ring, *exo*-C*H*– of –CH–C*H*$_2$–CH–CO– in norbornene ring, bridge head –C*H*$_2$– in norbornene ring), 1.68–1.09 (m, –C*H*$_2$CHPh–, –C*H*$_2$CH(CH_3), –CH_2CH(C*H*$_3$), *endo*-C*H*– of –CH–C*H*$_2$–CH–CO– in norbornene ring), 1.08–0.51 (m, –*sec*-butyl).

Synthesis of graft PS (g-PS)

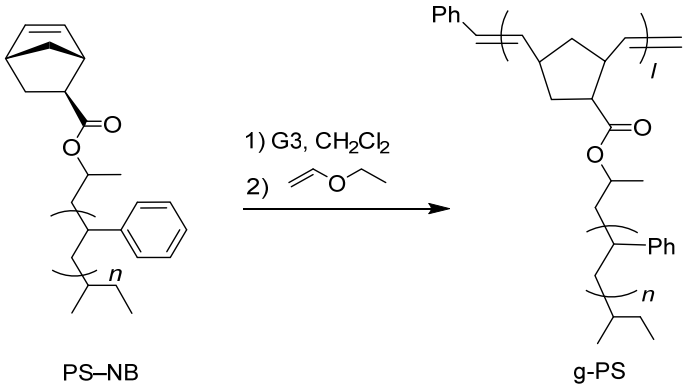

Method B was used for the ROMP of PS–NB (300 mg, 158 μmol) with G3 (1.97 μL, 15.8 μmol as a 8.0 mmol L^{-1} solution in CH_2Cl_2) in dry CH_2Cl_2 (7.89 mL) for 1.0 h to give g-PS as a brown solid. Yield: 248 mg (82.7%)

$M_{n,SEC}$ = 14,200, $Đ$ = 1.04, $M_{n,MALS}$ = 19,800, $Đ_{MALS}$ = 1.03, average number of cyclic units = 10.4

^{1}H NMR ($CDCl_3$, 400 MHz): δ (ppm) 0.49–1.10 (m, –*sec*-butyl), 1.11–1.68 (m, –C*H*$_2$CHPh–, –C*H*$_2$CH(CH_3), –CH_2CH(C*H*$_3$)), 1.68–2.51 (m, –CH_2C*H*Ph–), 2.58–3.90 (br, cyclopentane ring of poly(norbornene) backbone), 4.02–4.73 (s, –CH_2C*H*(CH_3)O–), 4.73–5.42 (br, alkenyl of poly(norbornene) backbone), 6.19–7.22 (m, *aromatic*).

3.3 Results and Discussion

3.3.1 Synthesis of multicyclic polystyrenes

The mc-PS species were synthesized according to the procedure described in Chapter 2, as outlined in **Figure 3.2**. Specifically, the mc-PSs were prepared via the cyclopolymerization of NB–PS–NB ($M_{n,\,NMR}$ = 3,700, $M_{n,\,SEC}$ = 3,700, $Đ$ = 1.30; see **Figure 3.3**). The cyclic units of the resulting mc-PSs possessed number-average molecular weights of 3,700, while the polymers exhibited overall absolute number-average molecular weights ($M_{n,\,MALS}$; determined by multi-angle light scattering) ranging from 20,300 to 917,900. The average number of cyclic units ranged from 6 to 248, as calculated by dividing the mc-PS $M_{n,\,MALS}$ by the $M_{n,\,NMR}$ of the NB–PS–NB (**Tables 3.1**). As each cyclic unit is formed from two norbornene groups, the degree of polymerization of the norbornene backbone (N_{NB}) corresponds to twice the number of cyclic units. Hereafter, the calculated average number of cyclic units is used as a prefix for the designation of the mc-PS species (e.g., 6c-PS denotes an mc-PS with six cyclic units). Importantly, the obtained mc-PSs exhibited narrow $Đ$ values (**Figure 3.4**). For the 6c-PS–72c-PS systems, $Đ$ remained ≤1.20, indicating that the number distribution of cyclic units was well controlled. Notably, a narrow molecular weight distribution ensures a more uniform polymer chain length, rendering it easier to correlate the molecular structure with the material properties. The $Đ$ values of the 105c-PS and 248c-PS systems were relatively broad (i.e., 1.33 and 1.49, respectively), likely due to the partial deactivation of the reactive chain ends during cyclopolymerization. G3 decomposition is known to occur through reactions with trace impurities such as water.[39] Under high macromonomer-to-G3 ratios, the completion of cyclopolymerization requires longer reaction times, during which polymerization and catalyst deactivation compete, resulting in broader $Đ$ values. It should also be considered that if the

synthesized mc-PS contains unexpected structures, such as dangling chains resulting from the reaction of only one norbornene unit, or intermolecular crosslinks resulting from intermolecular reactions of the dangling chain, various physical properties may be affected. Although the direct observation of such defect structures is challenging, their presence can be indirectly inferred through proton nuclear magnetic resonance (^{1}H NMR) spectroscopy. Given that the ^{1}H NMR signals originating from the norbornenyl group disappeared completely after cyclopolymerization, the presence of a dangling chain was considered to be highly unlikely (**Figure 3.5**). Furthermore, in such cases, gelation was expected to occur during cyclopolymerization; however, the obtained mc-PSs were found to be completely soluble. Consistently, SEC traces showed unimodal elution peaks without high-molar-mass shoulders. Together, these observations indicate that highly diluted conditions favored intramolecular cyclization over intermolecular propagation, thereby strongly suppressing intermolecular crosslinking.

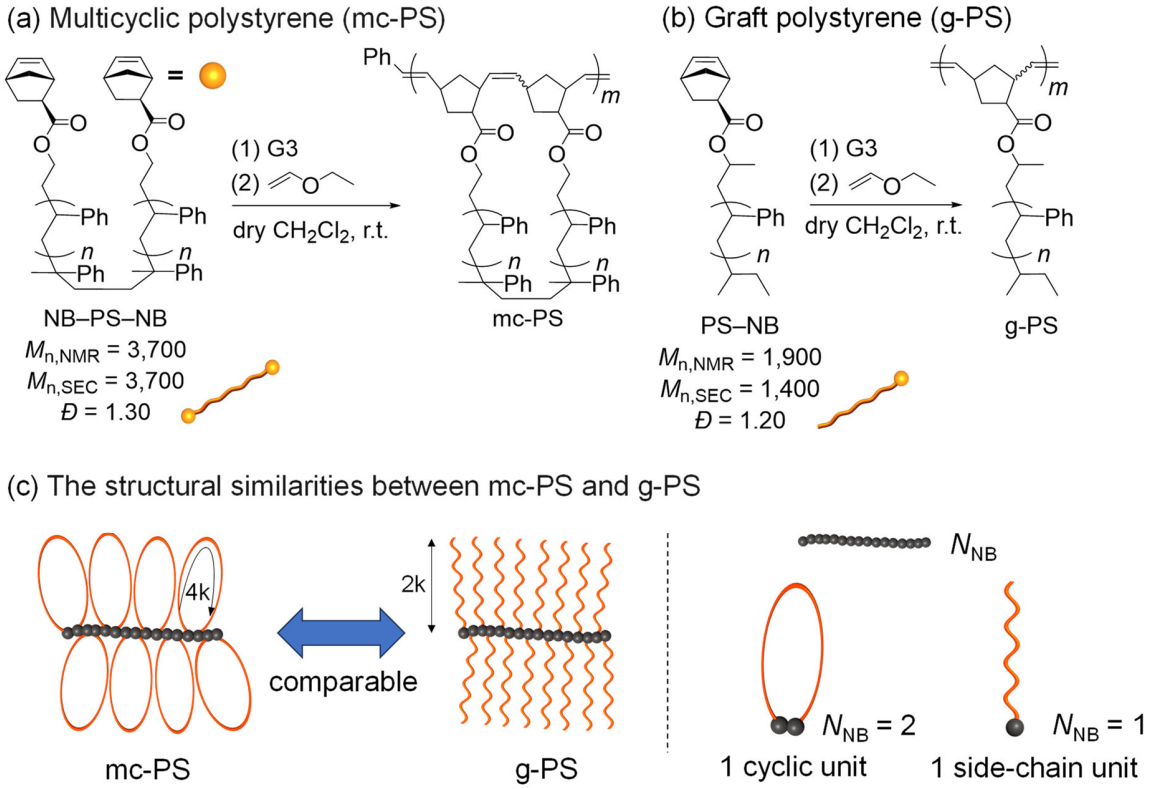

Figure 3.2. (a) Synthesis of mc-PS. (b) Synthesis of g-PS. (c) Illustration of the structural similarities between mc-PS and g-PS.

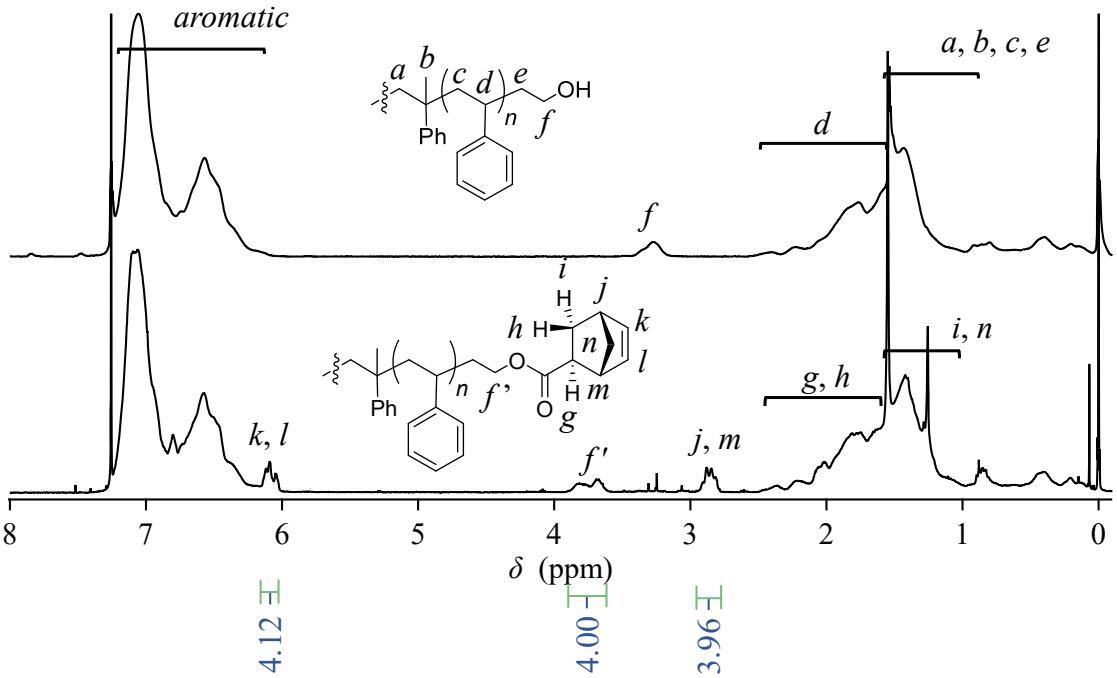

Figure 3.3. ^{1}H NMR spectra of HO–PS–OH (upper) and NB–PS–NB (lower) in $CDCl_3$.

Table 3.1. Molecular characterization of the prepared polystyrenes with different architectures

Topology	Sample	$M_{n,\,SEC}$[a]	$Đ$[a]	$M_{n,\,MALS}$[b]	$M_{w,\,MALS}$[b]	Number of cyclic/side-chain units[c]	N_{NB}[d]	Yield (%)
multicyclic (mc-PS)	6c-PS	11,300	1.20	20,300	23,300	6	12	96.0
	11c-PS	17,400	1.14	40,800	44,900	11	22	91.3
	19c-PS	23,900	1.20	69,700	74,600	19	38	95.3
	28c-PS	35,000	1.16	103,600	110,900	28	56	96.5
	35c-PS	49,700	1.11	128,300	133,400	35	70	83.7
	57c-PS	72,400	1.19	212,400	223,000	57	114	83.0
	63c-PS	82,000	1.16	231,500	238,400	63	126	84.0
	72c-PS	90,800	1.18	268,000	276,000	72	144	85.0
	105c-PS	111,600	1.33	389,200	408,700	105	210	72.3
	248c-PS	153,700	1.49	917,900	973,000	248	596	38.5
graft (g-PS)	10g-PS	14,200	1.04	19,800	20,400	10	10	82.7
	18g-PS	19,800	1.05	33,600	34,900	18	18	91.3
	25g-PS	24,000	1.07	47,800	49,700	25	25	90.7
	42g-PS	38,600	1.08	80,500	83,100	42	42	84.0
	79g-PS	68,400	1.07	149,200	151,600	79	79	72.5
	101g-PS	80,400	1.07	192,600	193,200	101	101	92.0
	122g-PS	96,300	1.10	231,800	233,700	122	122	96.5
	139g-PS	127,000	1.09	264,600	266,500	139	139	87.3
	159g-PS	148,200	1.10	302,900	309,000	159	159	91.8
	215g-PS	201,600	1.09	408,600	411,800	215	215	92.5
	320g-PS	252,500	1.19	607,900	612,900	320	320	87.3
linear (l-PS)	-	17,200	1.03	15,500	16,900	-		
	-	50,400	1.03	45,100	46,500	-		
	-	133,700	1.04	116,500	119,500	-		
	-	259,000	1.06	217,900	221,800	-		
	-	633,600	1.05	492,000	500,000	-		
	-	1,343,500	1.05	1,042,000	1,049,000	-		

[a]Determined by SEC in THF using polystyrene standards. [b]Determined using SEC-MALS-Visco in chloroform. [c]The average number of cyclic units in each mc-PS species was estimated using the expression: (M_n of mc-PS or g-PS)/(M_n of the macromonomer). [d]Degree of polymerization of the norbornene backbone.

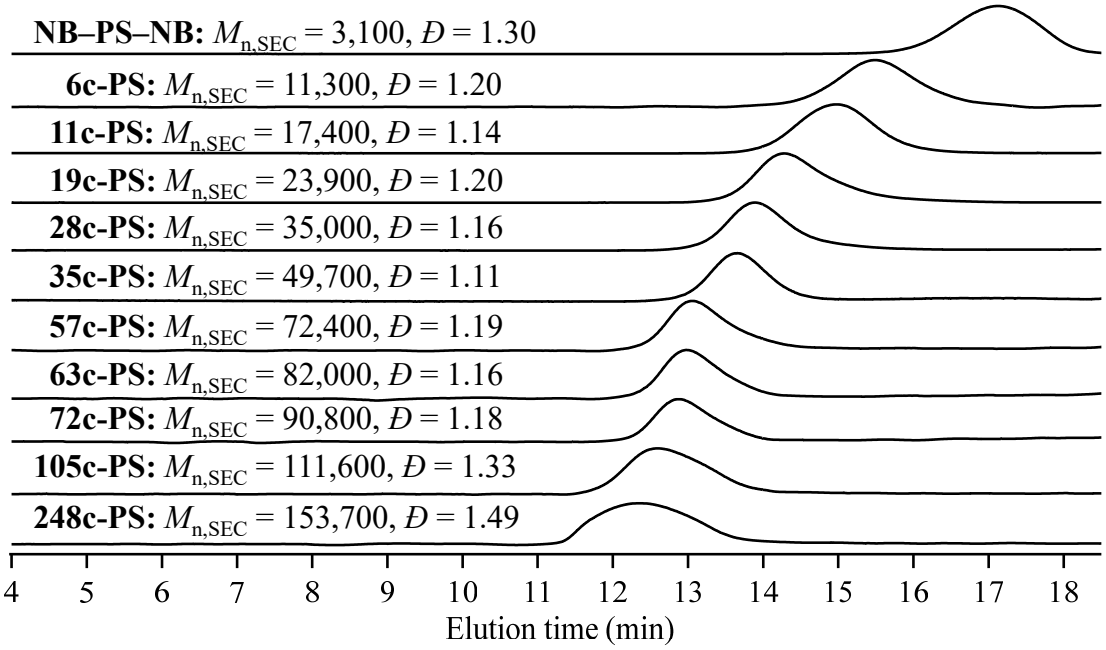

Figure 3.4. SEC traces of the NB–PS–NB and mc-PS specimens synthesized via cyclopolymerization (refractive index detection; eluent, THF; flow rate, 1.0 mL min^{-1}).

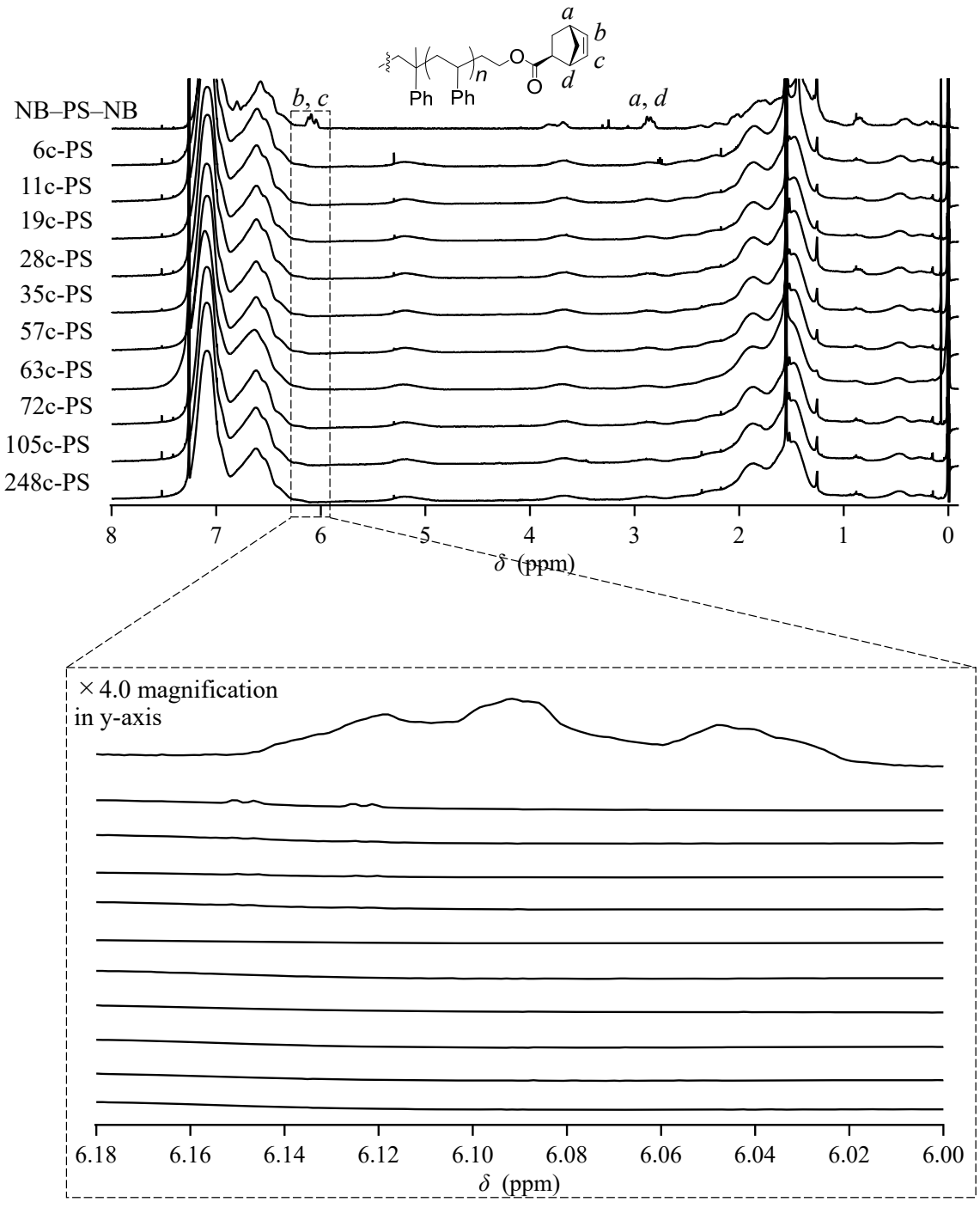

Figure 3.5. ^{1}H NMR spectra recorded for the NB–PS–NB and mc-PS species in $CDCl_3$.

For comparison, g-PS species were prepared via the ROMP of PS–NB ($M_{n,\,NMR}$ = 1,900, $M_{n,\,SEC}$ = 1,400, $Đ$ = 1.20; see **Figure 3.6**) as shown in Figure 3.2b. To compare their properties with those of the mc-PS species, the side chains of the g-PSs were designed to possess a molecular weight of ~1,900, which is approximately half that of the cyclic units in the mc-PS species (Figure 3.2c). Consequently, the resulting g-PSs exhibited overall molecular weights ranging from 19,800 to 607,900, corresponding to an average of 10–320 side-chain units. Since these side-chain units are formed from a single norbornene group, the value of N_{NB} corresponds to the number of side-chain units (Table 3.1 and **Figure 3.7**). Hereafter, the calculated average number of side-chain units is used as a prefix for the g-PS species (e.g., 10g-PS denotes g-PS with 10 side-chain units). Importantly, similar to the mc-PS species, the g-PSs also exhibited narrow $Đ$ values (≤1.19). Polystyrene standards with molecular weights ranging from 15,500 to 1,042,900 were purchased from Shodex (Tokyo, Japan) and were used as linear reference samples (denoted as l-PS).

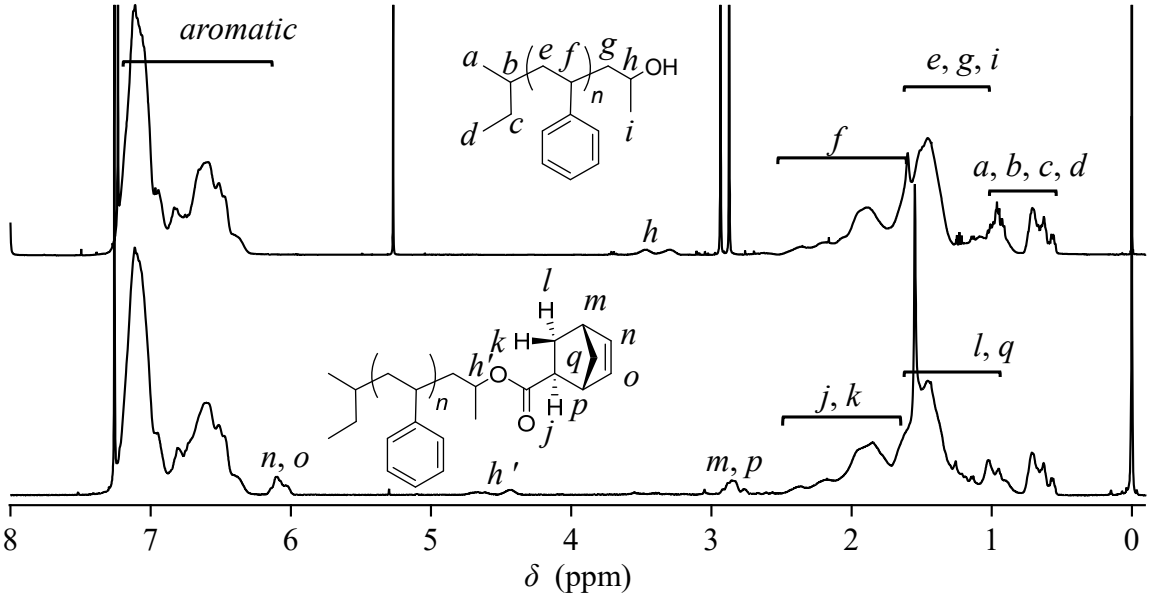

Figure 3.6. ^{1}H NMR spectra of PS–OH (upper) and PS–NB (lower) in $CDCl_3$.

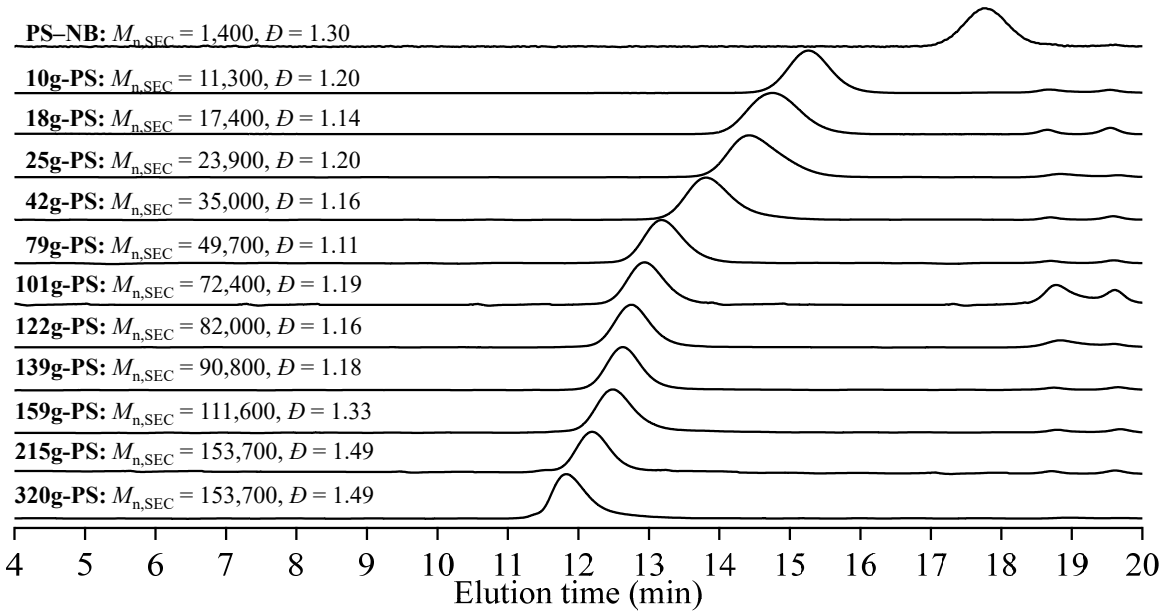

Figure 3.7. SEC traces of PS–NB and g-PS synthesized via ROMP (refractive index (RI) detection; eluent, THF; flow rate, 1.0 mL min^{-1}).

3.3.2 Thermal measurements

Initially, differential scanning calorimetry (DSC) measurements were performed for the mc-PS, g-PS, and l-PS specimens to examine the relationship between the polymer structure and T_g (**Figures 3.8–3.10**). In a previous study, Monteiro et al. reported that multicyclic polystyrene bearing 1–20 cyclic units showed higher T_g values than linear polystyrene and graft polystyrene.[29] Furthermore, they suggested that these higher T_g values compared with those of the linear equivalents were due to the topological constraints imposed by the cyclic architecture, which reduced the conformational entropy. However, no systematic evaluation has been conducted on the T_g values of mc-PSs containing ≥20 cyclic units, and no comparison has been performed with their g-PS counterparts. Moreover, no previous studies have applied the Flory–Fox empirical rule (based on the free volume of polymer chains) to analyze T_g. Therefore, the T_g values were systematically measured for the series of synthesized polystyrene samples and the results were analyzed using the Flory–Fox equation. **Figure 3.11a** illustrates the dependence of T_g on the number-average absolute molecular weight ($M_{n,\,MALS}$) for the polystyrene samples with three different topologies. As indicated, all mc-PS samples exhibited higher T_g values than their g-PS and l-PS counterparts, likely due to their unique multicyclic topologies. Notably, the T_g values of the mc-PS specimens were ~30 °C higher than those of the g-PSs across all molecular weight ranges. According to the Flory–Fox equation[40] ($T_g = T_{g,\infty} - AM_n^{-1}$, where $T_{g,\infty}$ represents the T_g in the limit of infinite M_n, and A is an empirical parameter associated with the free volume), a plot of T_g against the inverse of $M_{n,\,MALS}$ was constructed, wherein the linear fit corresponded to the Flory–Fox equation (Figure 3.11b). By extrapolating T_g to the limit of infinite molecular weight, the $T_{g,\infty}$ values were determined to be 109.6, 87.2, and 116.6 °C for l-PS, g-PS, and mc-PS, respectively (**Table 3.3**). In general, the T_g value of the monocyclic PS

was ~30 °C higher than that of the corresponding l-PS at a molecular weight of ~3,000. However, upon increasing the molecular weight, the difference in T_g became smaller, eventually approaching the same T_g at the limit of the molecular weight (~300,000).[41] The distinct difference in T_g values between the linear and monocyclic polymers in the low-molecular-weight region was attributed to the presence or absence of chain ends. In contrast, at higher molecular weights, the contribution of the chain ends in the linear polymers became negligible, leading to a convergence of the T_g values for the linear and monocyclic polymers. This result indicates that the chain ends possess significantly larger free volumes than the interiors of the chains. Furthermore, the unique chain diffusion modes and intramolecularly constrained structures arising from the cyclic topology have been shown to reduce segment mobility.[42] Consequently, the T_g values of the monocyclic PS samples were significantly higher than those of the l-PS specimens, particularly when considering the low-molecular-weight samples. For the mc-PS specimens, the increase in molecular weight was attributed to the number of cyclic units, wherein the molecular weight of each cyclic unit remained the same. Therefore, even with an increase in the total molecular weight, the influence of the cyclic topology remains significant.

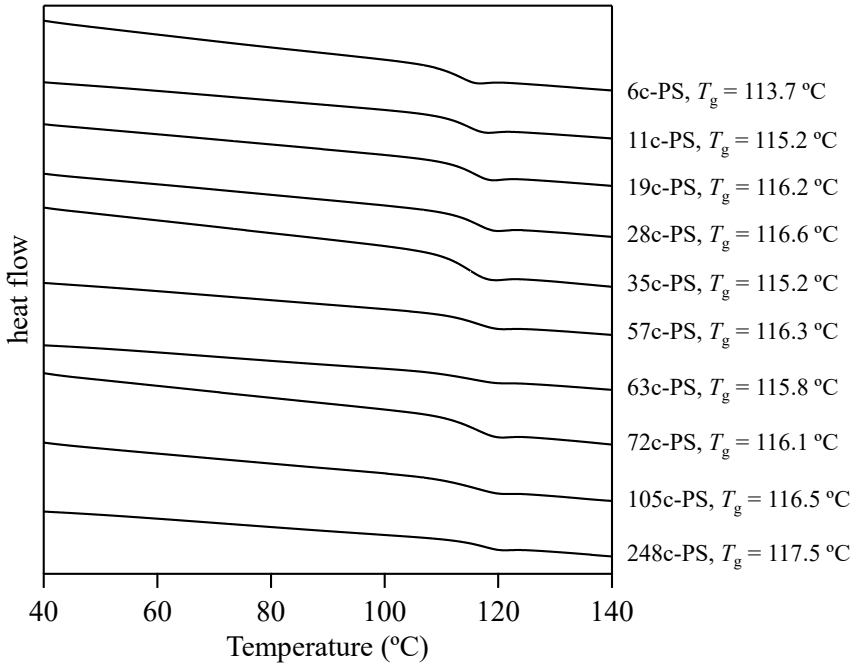

Figure 3.8. DSC curves of mc-PS during the second heating (heating rate: 10 °C min^{-1}).

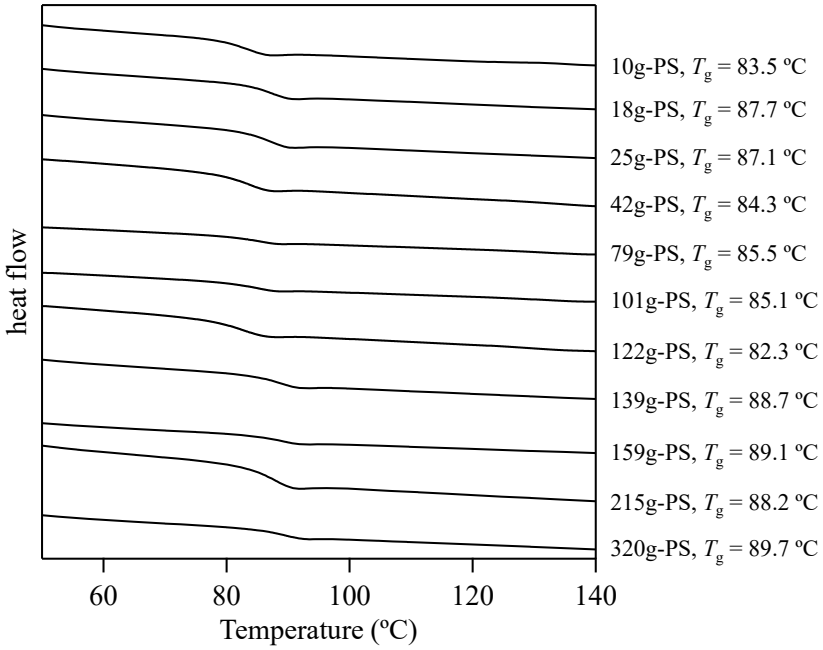

Figure 3.9. DSC curves of g-PS during the second heating (heating rate: 10 °C min^{-1}).

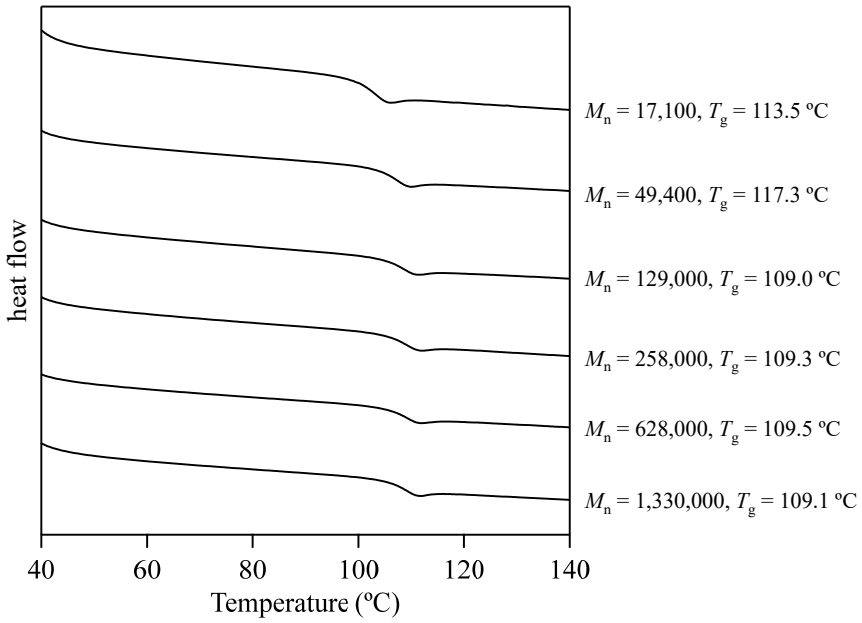

Figure 3.10. DSC curves of l-PS during the second heating (heating rate: 10 °C min^{-1}).

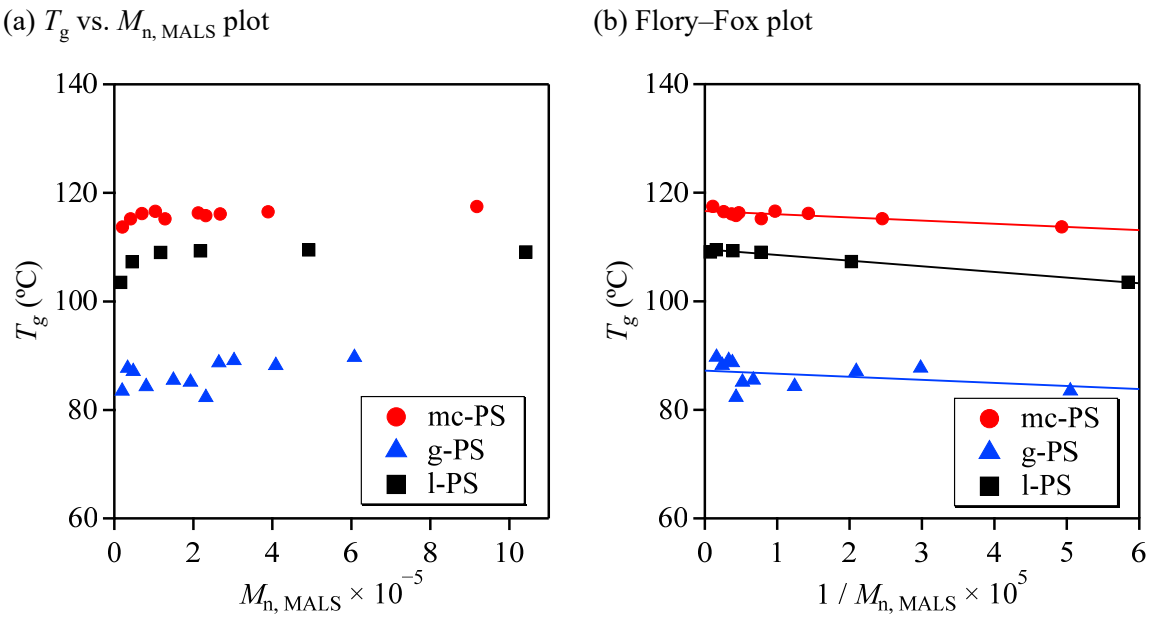

Figure 3.11. (a) T_g vs. $M_{n,\,MALS}$ plots of the topological polystyrene samples. (b) Flory–Fox plots of the polystyrene samples.

Table 3.3. Flory–Fox equation parameters for the PSs with different topologies

Polymer	$T_{g,\infty}$	A
mc-PS	116.6	5.9×10^4
g-PS	87.2	5.5×10^4
l-PS	109.6	1.0×10^5
monocyclic PS	-	4.5×10^3 [34]

Chang et al. previously reported that the monocyclic PS sample exhibited a lower A value than the l-PS sample and that the molecular weight dependence of T_g was relatively weak.[41] This can be attributed to the absence of chain ends, the concentration of which is the primary contributor to the molecular weight dependence of linear polymers. In stark contrast, the A value of the mc-PS system was determined to be 5.9×10^4, which is comparable to those of the l-PS ($A = 1.0 \times 10^5$) and g-PS ($A = 5.5 \times 10^4$) systems, indicating a strong molecular weight dependence for T_g. This result highlights a key difference between the monocyclic and multicyclic architectures. In the mc-PS specimens, this strong dependence of T_g on the molecular weight can be attributed to the steric hindrance imparted by the side chains. As the degree of polymerization (DP) of the norbornene backbone increases, the steric hindrance exerted by the cyclic side chains in mc-PS becomes more pronounced. This increased steric hindrance leads to a smaller free volume in the cyclic chains, which is considered the primary factor underlying the pronounced dependence of T_g on the molecular weight (**Figure 3.12a**). A similar scenario applies to g-PS; as the DP of the backbone increases, the steric hindrance from the linear side chains reduces the free volume (Figure 3.12b). In contrast, the dependence of T_g on the molecular weight is significant for the l-PS systems because as the molecular weight increases, the influence of the terminal free volume on the polymer chain diminishes (Figure 3.12c). This behavior differs from those observed for the mc-PS and g-PS systems.

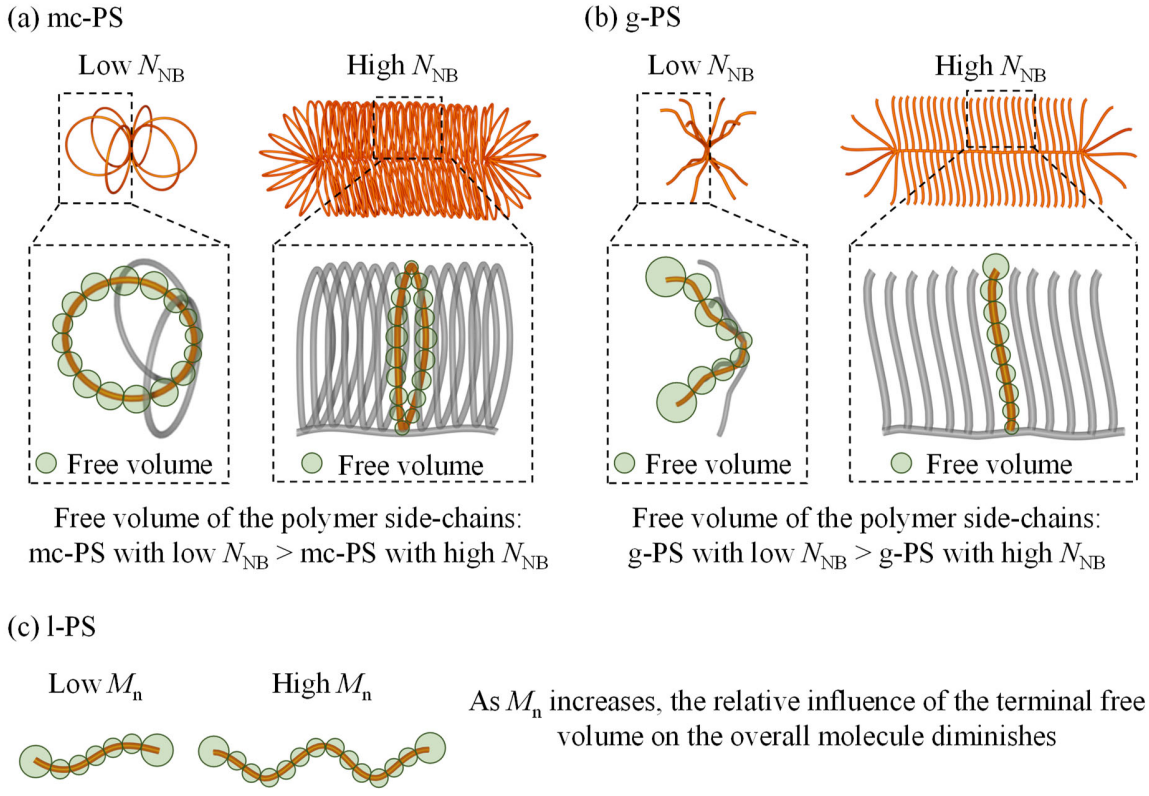

Figure 3.12. Schematic illustration of the free volumes for the (a) mc-PS and (b) g-PS systems with low N_{NB} and high N_{NB} values. (c) Schematic illustration of the free volume for the l-PS system with low M_n and high M_n values.

Subsequently, the thermal degradation behaviors of the mc-PS, g-PS, and l-PS species were evaluated using thermogravimetric analysis by determining the temperatures at which 5 wt% weight loss ($T_{d5\%}$) was reached along with the temperature associated with the maximum weight loss (T_{dMAX}) (**Figures 3.13–3.15** and **Table 3.4**). It was found that $T_{d5\%}$ increased in the order of l-PS < g-PS < mc-PS, whereas T_{dMAX} was nearly identical for g-PS and mc-PS, giving values exceeding that of l-PS (**Figure 3.16**). This trend in $T_{d5\%}$ suggests that the thermal stability depends on the extent of the constraint at the polymer chain ends. During the initial stage of thermal degradation, decomposition occurs preferentially at the chain ends. Given that l-PS has a fully linear structure with two free chain ends, it is expected to degrade the most rapidly. In contrast, in g-PS, one of the chain ends is constrained by the backbone, which delays the onset of thermal degradation and leads to a higher $T_{d5\%}$ than that of l-PS. Furthermore, in mc-PS, both chain ends are fully constrained by the backbone, preventing end-driven degradation and resulting in the highest observed $T_{d5\%}$. No significant difference in T_{dMAX} was observed between mc-PS and g-PS, suggesting that the primary degradation process was governed by the random cleavage of the PS main chain, with minimal influence from the number of constrained ends.[41] In other words, the constraint of the chain ends significantly affected the degradation behavior at the initial stage, whereas at higher temperatures, the degradation of the PS main chain became dominant, and the impact of the cyclic structure diminished.

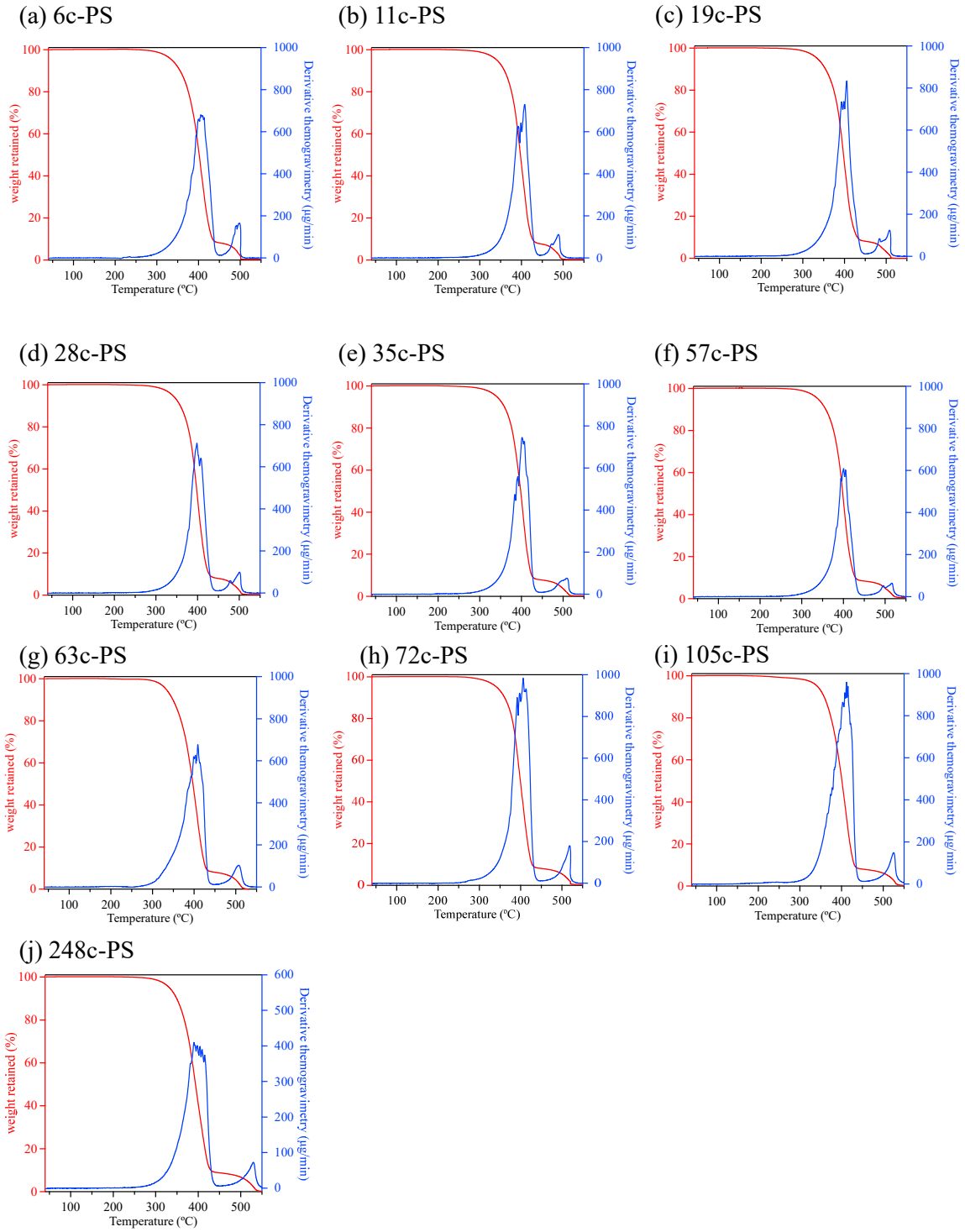

Figure 3.13. TGA and derivative thermogravimetry curves of mc-PS (heating rate: 10 °C min^{-1}).

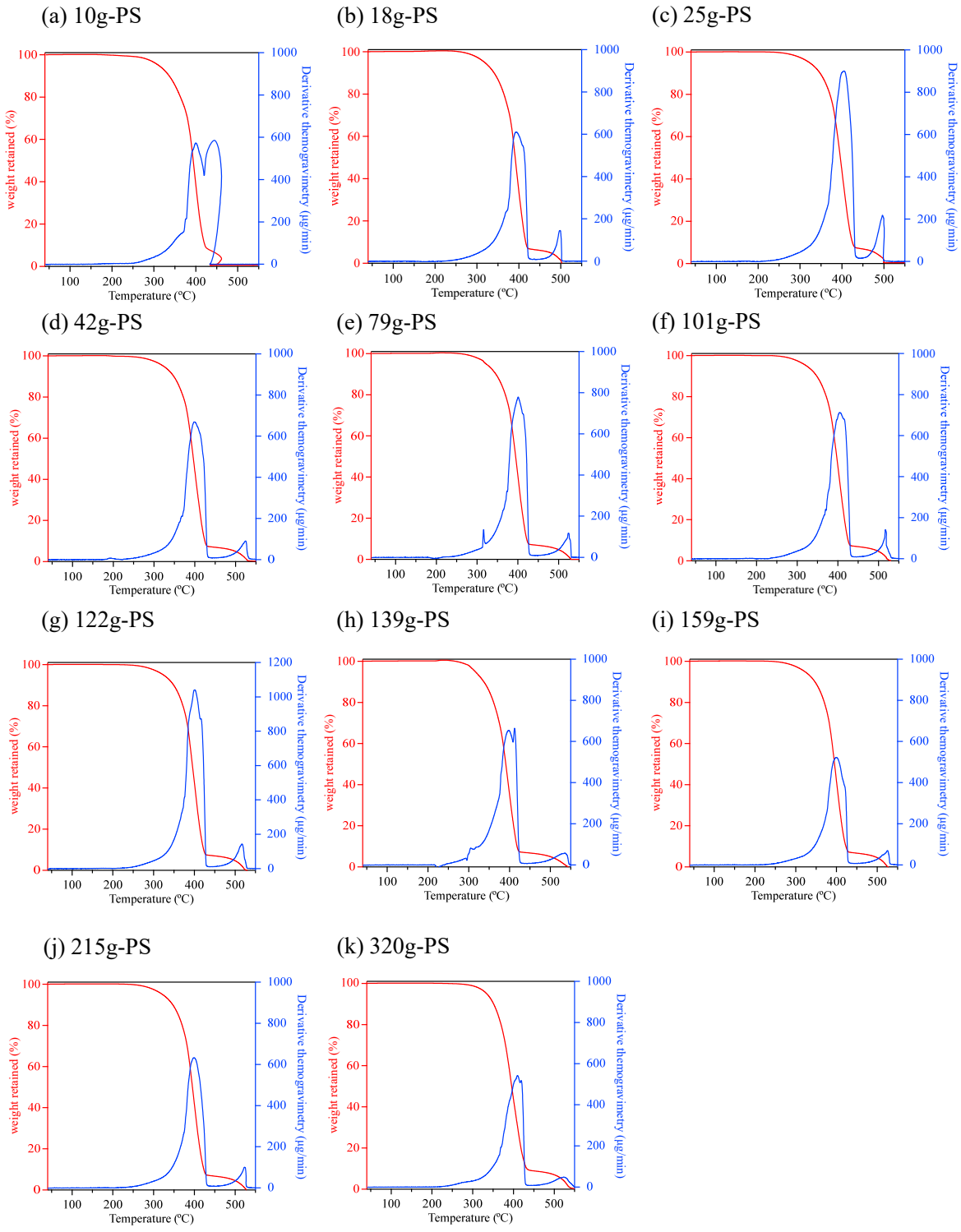

Figure 3.14. TGA and derivative thermogravimetry curves of g-PS (heating rate: 10 °C min^{-1}).

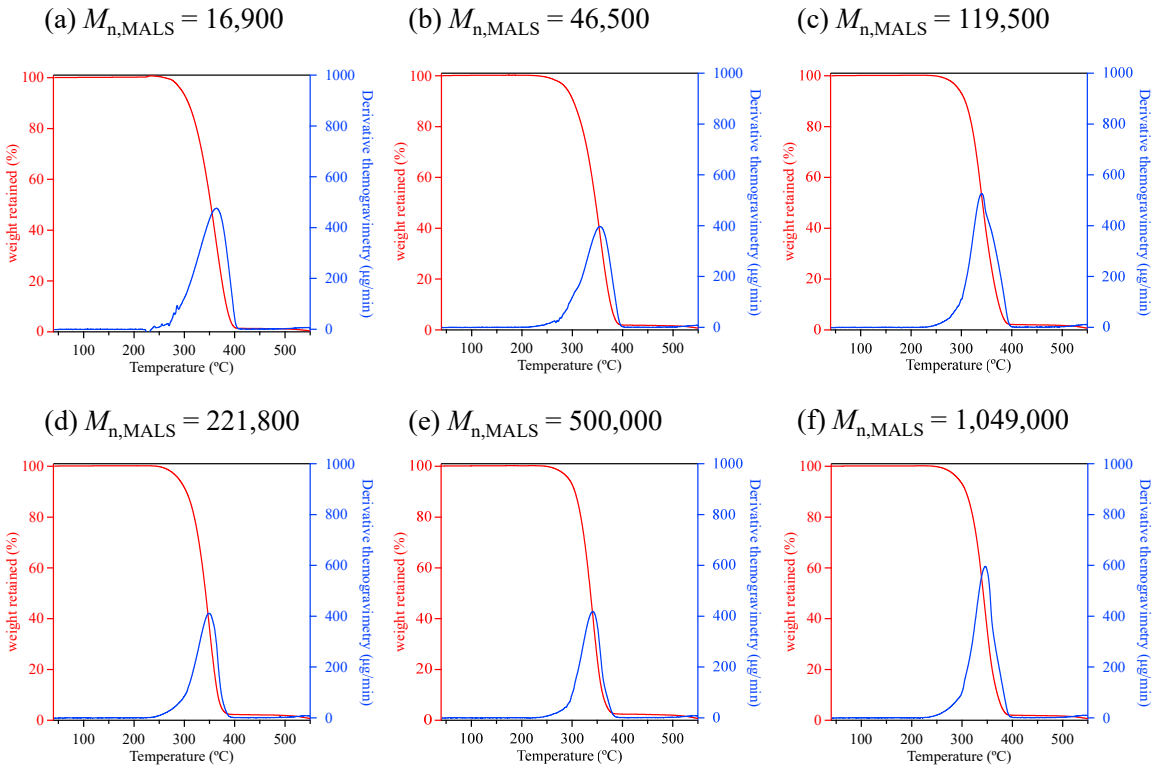

Figure 3.15. TGA and derivative thermogravimetry curves of g-PS (heating rate: 10 °C min^{-1}).

Table 3.4. $T_{d5\%}$ and T_{dMAX} for PSs with different topologies

Topology	sample	$M_{n,MALS}$ [a]	number of cyclic/side-chain unit [c]	$T_{d5\%}$ [b]	T_{dMAX} [c]
multicyclic (mc-PS)	6c-PS	20,300	6	336.6	405.4
	11c-PS	40,800	11	341.4	407.9
	19c-PS	69,700	19	334.9	405.4
	28c-PS	103,600	28	340.1	398.3
	35c-PS	128,300	35	340.5	401.7
	57c-PS	212,400	57	339.0	400.5
	63c-PS	231,500	63	332.8	408.8
	72c-PS	268,000	72	342.1	406.3
	105c-PS	389,200	105	341.7	411.6
	248c-PS	917,900	248	332.6	410.6
graft (g-PS)	10g-PS	19,800	10	311.4	396.6
	18g-PS	33,600	18	318.1	393.6
	25g-PS	47,800	25	322.4	405.5
	42g-PS	80,500	42	323.4	399.3
	79g-PS	149,200	79	321.7	400.6
	101g-PS	192,600	101	322.8	404.0
	122g-PS	231,800	122	323.9	401.0
	139g-PS	264,600	139	315.9	412.2
	159g-PS	302,900	159	318.3	399.4
	215g-PS	408,600	215	322.0	398.8
	320g-PS	607,900	320	314.9	410.0
linear (l-PS)	-	15,500	-	294.7	364.3
	-	45,100	-	288.3	354.7
	-	116,500	-	293.6	340.0
	-	217,900	-	289.0	349.4
	-	492,000	-	293.5	341.3
	-	1,042,000	-	292.7	346.3

[a] Determined by SEC in THF using PS as the standard.[b] Temperature of maximal rate of decomposition determined by TGA. [c] 5% weight loss degradation temperature determined by TGA.

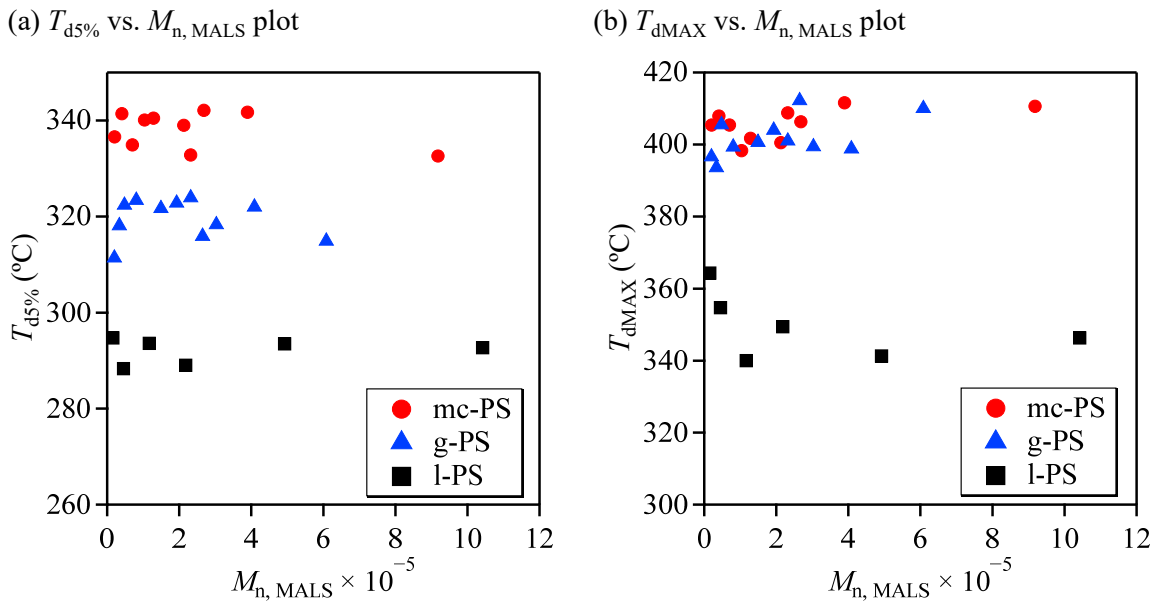

Figure 3.16. (a) $T_{d5\%}$ vs. $M_{n,\,MALS}$ plots and (b) T_{dMAX} vs. $M_{n,\,MALS}$ plots of the various topological polystyrene samples.

3.3.3 Viscosity measurements

The intrinsic viscosity ([η]) is a fundamental property of dilute polymer solutions, reflecting the conformation of the polymer chains. The [η] values of mc-PS, g-PS, and l-PS were measured using size-exclusion chromatography (SEC) in combination with multiangle light scattering and viscosity detection (SEC-MALS-Visco) in chloroform. **Figure 3.17a** presents a double-logarithmic plot of the [η] values of the topological PS samples against their weight-average absolute molecular weights ($M_{w,\,MALS}$). Each set of mc-PS samples exhibited slightly lower [η] values compared to that of g-PS. A similar trend was observed for the monocyclic PS, which showed lower viscosity values than its linear polymer counterpart.[14] Moreover, the R_h value of the mc-PS specimen was smaller than that of the corresponding g-PS specimen, consistent with the trend observed for monocyclic polymers (**Figure 3.18**).[13] Subsequently, based on the Mark–Houwink–Sakurada (MHS) scaling relation, $[\eta] = KM_w^{\alpha}$, the scaling exponent α was determined to obtain insight into the conformations of mc-PS and g-PS in solution (Figure 3.17b). Specifically, an α value close to 0 indicates a solid sphere conformation, while an α value of ~0.5–0.8 suggests a random coil, and values >1 indicate a cylindrical structure.[43] Prior to considering the α values of the mc-PS and g-PS systems, the corresponding value for the l-PS system was obtained and the results were compared with those of previous studies. The value of α obtained for l-PS (0.749) was found to be nearly equivalent to the range observed in previous studies of linear polystyrene in good solvents (0.70–0.76),[44] thereby indicating the reliability of the measurements. Additionally, it was found that the α values for mc-PS and g-PS increased with an increasing molecular weight. This suggests a global conformational shift with an increasing molecular weight (i.e., an increase in the number of cyclic units or linear side-chain units). More specifically, when the number of cyclic units in

mc-PS was low, the molecule adopted a conformation close to spherical (or star-like) owing to the small aspect ratio resulting from the short polynorbornene backbone length. However, as the number of cyclic units was increased, crowding of the cyclic chains became more pronounced, stretching the polynorbornene backbone. It was therefore expected that the global conformation would eventually transition to a cylindrical structure. Such phenomena have been revealed in bottlebrush systems through molecular simulations and experimental studies; as the backbone DP increased, the global conformation transitioned from spherical to cylindrical.[21,45–47] Additionally, Sing et al. confirmed that the α values of bottlebrush polymers increased with an increasing backbone DP, consistent with the trend observed herein.[48] When focusing on the region with fewer cyclic units and side chains ($M_{w,\,MALS} \leq 50{,}000$), it was found that mc-PS tend to show a larger α value than g-PS, indicating that mc-PS adopted a conformation closer to a cylindrical structure. In contrast, for $M_{w,\,MALS} > 50{,}000$, the α values of the mc-PS and g-PS species became almost indistinguishable, indicating that both topologies converged to a similar, cylinder-like global conformation.

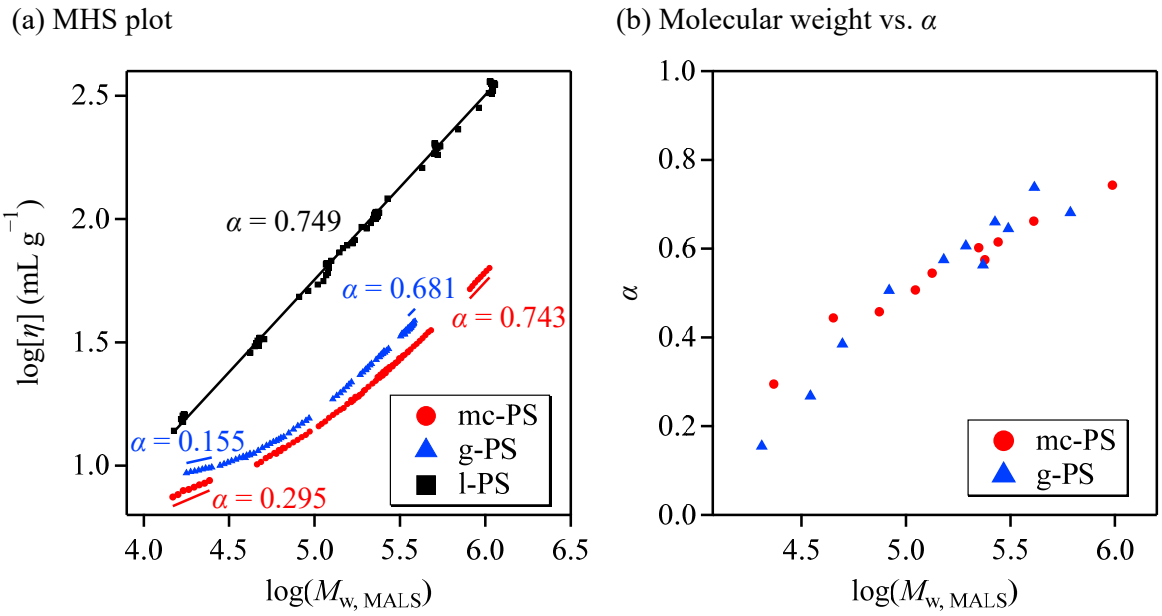

Figure 3.17. (a) MHS plots obtained for the mc-PS (red), g-PS (blue), and l-PS (black) specimens. (b) Plot of α as a function of $\log(M_{w,MALS})$.

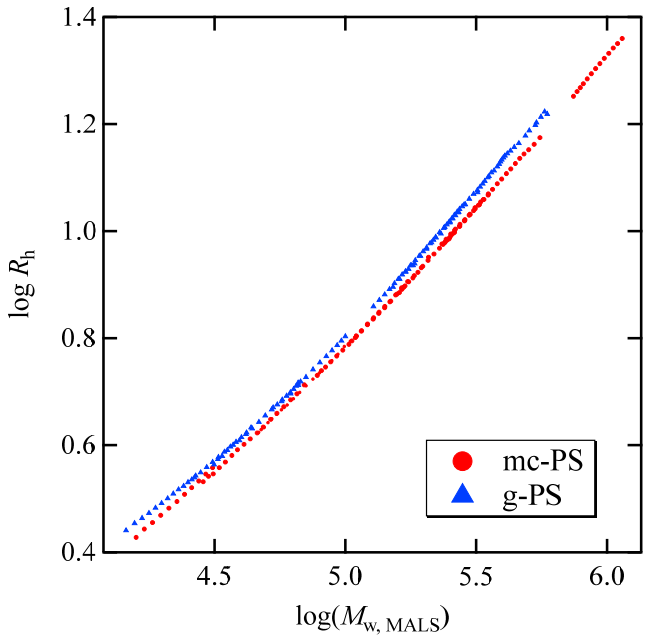

Figure 3.18. Conformation plots of mc-PS (red) and g-PS (blue).

3.3.4 Small angle scattering measurements

To gain a deeper understanding of the effect of the multicyclic topology on the global structure in a good solvent, the chain conformations of mc-PS and g-PS were investigated using SANS and SAXS measurements. While SANS measurements were performed on representative samples owing to limited access to the neutron scattering facility, SAXS measurements were conducted for the entire series of mc-PS and g-PS samples prepared in this study. This comprehensive SAXS analysis enabled a systematic comparison of the global chain conformations across various molecular architectures and sizes under identical solution conditions.

Specifically, the SANS measurements were performed using 8.7 g L^{-1} polymer solutions in deuterated toluene (toluene-d_8) at 25 °C using a q range of 0.004–0.34 $Å^{-1}$ (**Figure 3.19**). The radius of gyration (R_g) was initially evaluated using Guinier analysis, where the low-q scattering intensity $I(q)$ was approximated by the Guinier equation: $\ln I(q) = \ln I(0) - (q^2R_g^2/3)$. In this equation, $I(0)$ represents the forward scattering intensity at $q = 0$. The Guinier plots obtained for mc-PS and g-PS are shown in **Figures 3.20** and **3.21**, demonstrating the high quality of the linear fit. The resulting R_g values revealed distinct trends depending on the molecular weight (**Table 3.5**). For samples with relatively low $M_{n,\,MALS}$ values (i.e., low N_{NB}, <122), the mc-PS specimens exhibited smaller R_g values than the corresponding g-PS samples. This difference was attributed to the topological constraints of the cyclic side chains in mc-PS, which likely led to a more compact overall conformation in solution. In contrast, for samples with relatively high $M_{n,\,MALS}$ values (i.e., high N_{NB}, >122), this trend was no longer observed. In this regime, the polymer chains were presumed to adopt a cylindrical structure, wherein the overall size was dominated by the cross-sectional dimensions of the cylindrical structure rather

than by the side chain topology.[21] This interpretation was further supported by the observation that the increase in R_g with an increasing total molecular weight became less pronounced in this high $M_{n,\,MALS}$ region, indicating a transition toward a more rigid and extended conformation (**Figure 3.22**). Subsequently, the cross-sectional radius (R_c) was evaluated using the cross-sectional Guinier approximation (**Figure 3.23**). This analysis was applied to mc-PS and g-PS samples with high N_{NB} values (≥122), for which a cylindrical conformation was anticipated. R_c was determined by fitting the low-q region of the cross-sectional Guinier plot, $\ln qI(q) - (q^2R_c^2/2)$ (**Figure 3.24**). This approach enabled the estimation of the R_c value, independent of the total chain length, thereby providing a more direct assessment of the lateral dimensions of the polymer. The resulting R_c values remained essentially constant across both the mc-PS and g-PS samples, regardless of N_{NB}. This result suggests that under the present solvent and concentration conditions, the cross-sectional dimensions are predominantly governed by the size and conformation of the individual side chains rather than by their number.

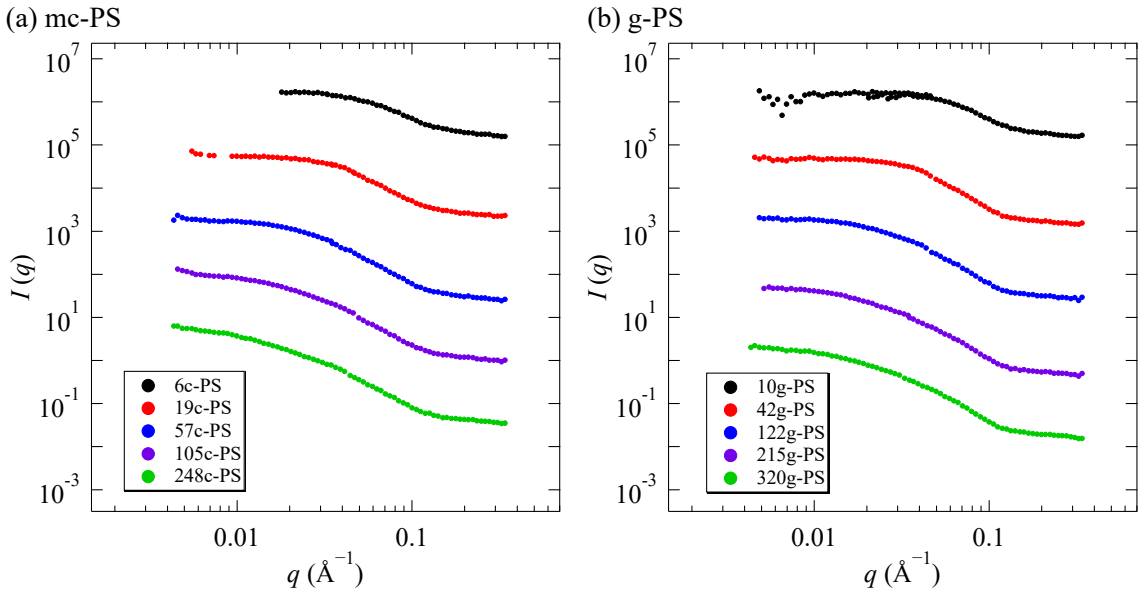

Figure 3.19. SANS scattering intensity profiles for (a) mc-PS and (b) g-PS with varying number of cyclic or side-chain units. The $I(q)$ are shifted along the y-axis for better visibility. All samples were dissolved in toluene-d_8 at a polymer concentration of 8.7 g L^{-1}.

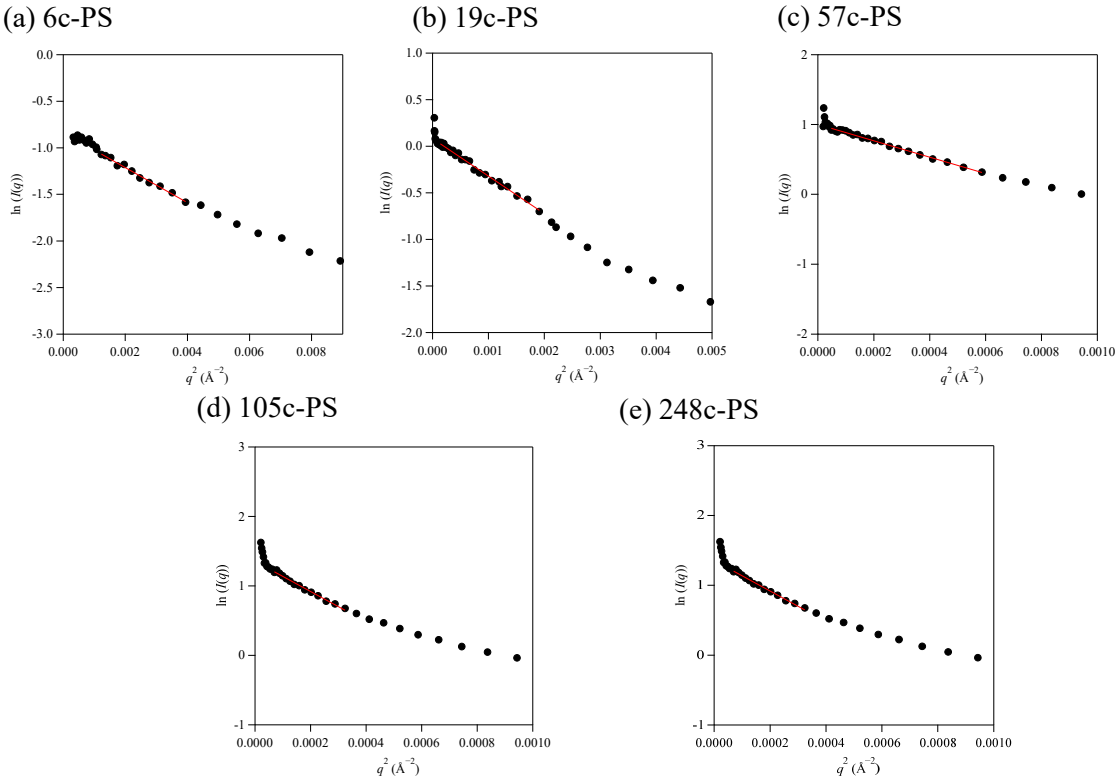

Figure 3.20. Guinier plots obtained from the SANS profiles of the mc-PS samples.

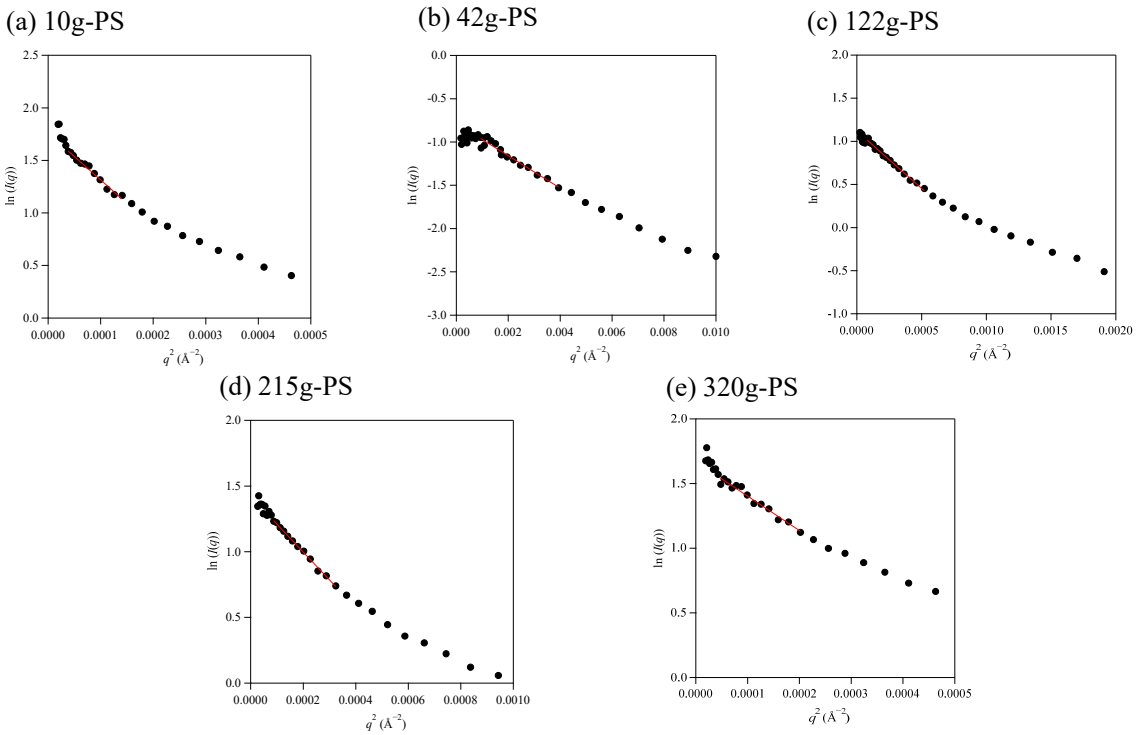

Figure 3.21. Guinier plots obtained from the SANS profiles of the g-PS samples.

Table 3.5. Radii of gyration (R_g) and cross-sectional radii (R_c) for the mc-PS and g-PS specimens, as determined by SANS analysis

Topology	Sample	$M_{n,\,MALS}$[a]	Number of cyclic/side-chain units[b]	N_{NB}[c]	R_g (Å)[d]	R_c (Å)[d]
multicyclic (mc-PS)	6c-PS	20,300	6	12	23.8±0.05	-
	19c-PS	69,700	19	38	34.8±0.10	-
	57c-PS	212,400	57	114	59.4±0.06	24.2±0.09
	105c-PS	389,200	105	210	80.8±0.15	23.8±0.10
	248c-PS	917,900	248	596	115.5±0.30	22.5±0.10
graft (g-PS)	10g-PS	19,800	10	10	24.7±0.09	-
	42g-PS	80,500	42	42	35.4±0.05	-
	122g-PS	231,800	122	122	63.1±0.08	22.4±0.06
	215g-PS	408,600	215	215	79.9±0.08	23.3±0.05
	320g-PS	607,900	320	320	89.4±0.28	22.8±0.06

[a]Determined using SEC-MALS-Visco in chloroform. [b]The average number of cyclic units in the obtained mc-PS was estimated using the expression: (M_n of mc-PS or g-PS)/(M_n of the macromonomer). [c]Degree of polymerization of the norbornene backbone. [d]Determined by SANS analysis.

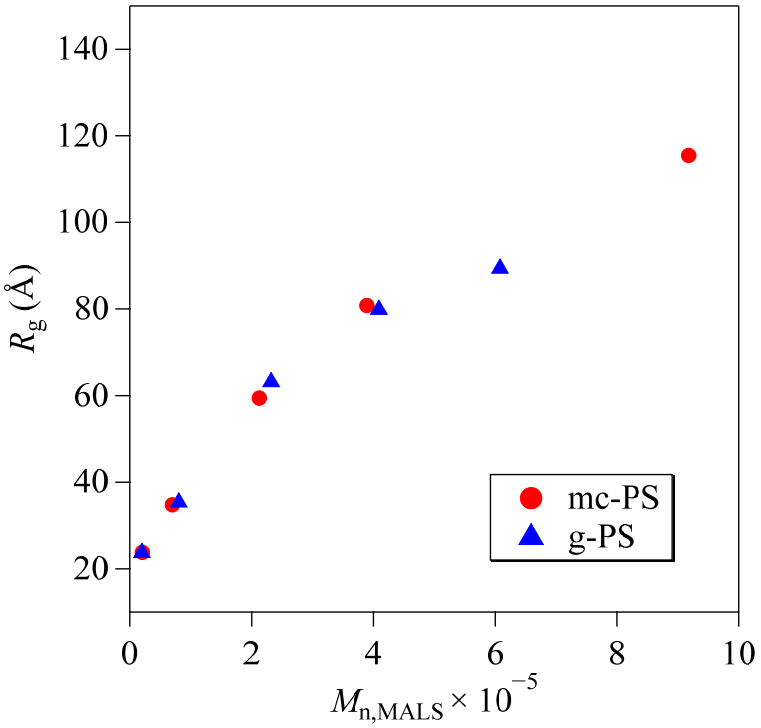

Figure 3.22. Comparison between mc-PS and g-PS for the R_g using the Guinier equation.

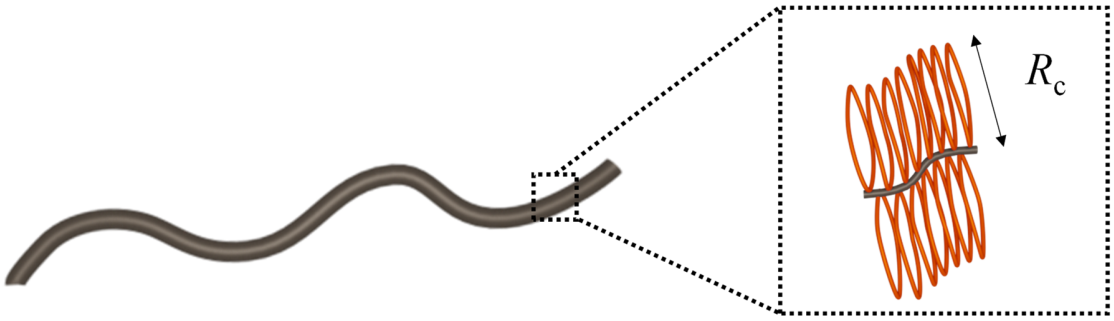

Figure 3.23. Structural parameters used in cross-section Guinier.

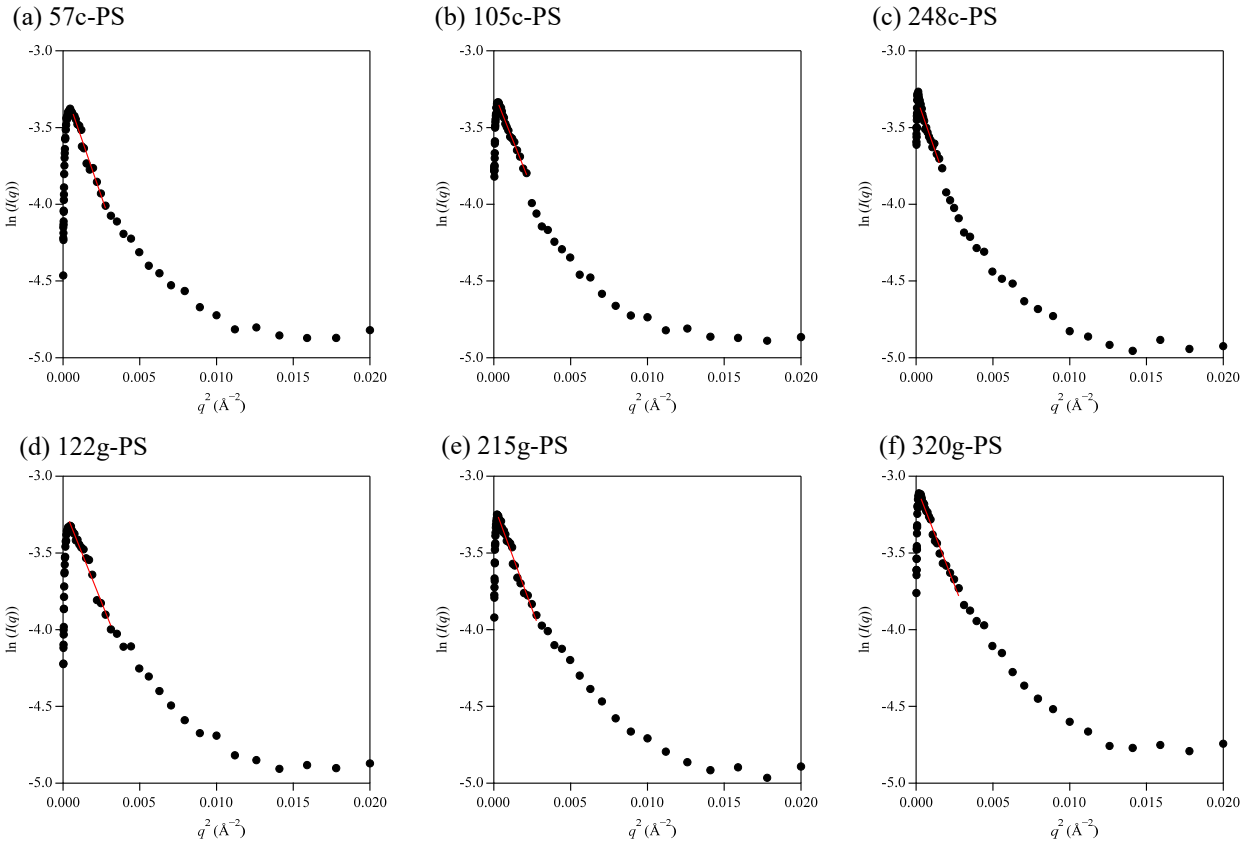

Figure 3.24. Cross-section Guinier plots of (a–c) mc-PS and (d–f) g-PS.

SAXS measurements were then performed on a 2.0 g L^{-1} polymer solution in toluene at 25 ºC with the machine q-range set to 0.002–0.2 $Å^{-1}$. However, taking into account the uncertainty in the scattering data in the low-q region (q < 0.01 $Å^{-1}$) and in the high-q region (q > 0.1 $Å^{-1}$) due to large background scattering and dominant solvent scattering, respectively, further analysis was performed within the q-range of 0.01–0.1 $Å^{-1}$. The Porod exponent [49] was determined from the SAXS profile, and fitting was performed using the flexible cylinder model in the SasView software.[50]

The scattering intensity ($I(q)$) typically followed a power law relationship with q, which can be expressed as: $I(q) = I(0)q^{-P}$.[51] Here, the scaling exponent (P) is related to the shape of the scatterers, which in this case can be regarded as the global conformation of the polymer chains. For example, $P = 4$ is typically observed for spherical structures, $P = 2$ for thin plate- or disk-like structures, and $P = 1$ for rod-shaped structures. The obtained SAXS profiles are summarized in **Figure 3.25**, and the calculated P values are presented in **Figure 3.26** as a function of the number of cyclic or side-chain units. In the low-molecular-weight region, both mc-PS and g-PS exhibited P values ranging from 2 to 3, suggesting that they adopted a sphere- or disk-like conformation. As the number of cyclic or linear side chains increased, the P value decreased. When the molecular weight approached ~200,000, the P value converged to ~1.5, suggesting that the polymer adopted a conformation closer to a cylindrical structure. These findings suggest that as the number of cyclic or linear side chains increased, the conformations of the mc-PS and g-PS systems transitioned from sphere-like (or disk-like) to cylindrical structures. Furthermore, focusing on the low molecular weight region ($M_{w,\,MALS} \leq 50{,}000$), it was observed that in this region, the P value for mc-PS was smaller than that for g-PS,

confirming that mc-PS is more likely to adopt a cylindrical structure than g-PS. These phenomena corroborate the findings of the MHS plots discussed in the previous section.

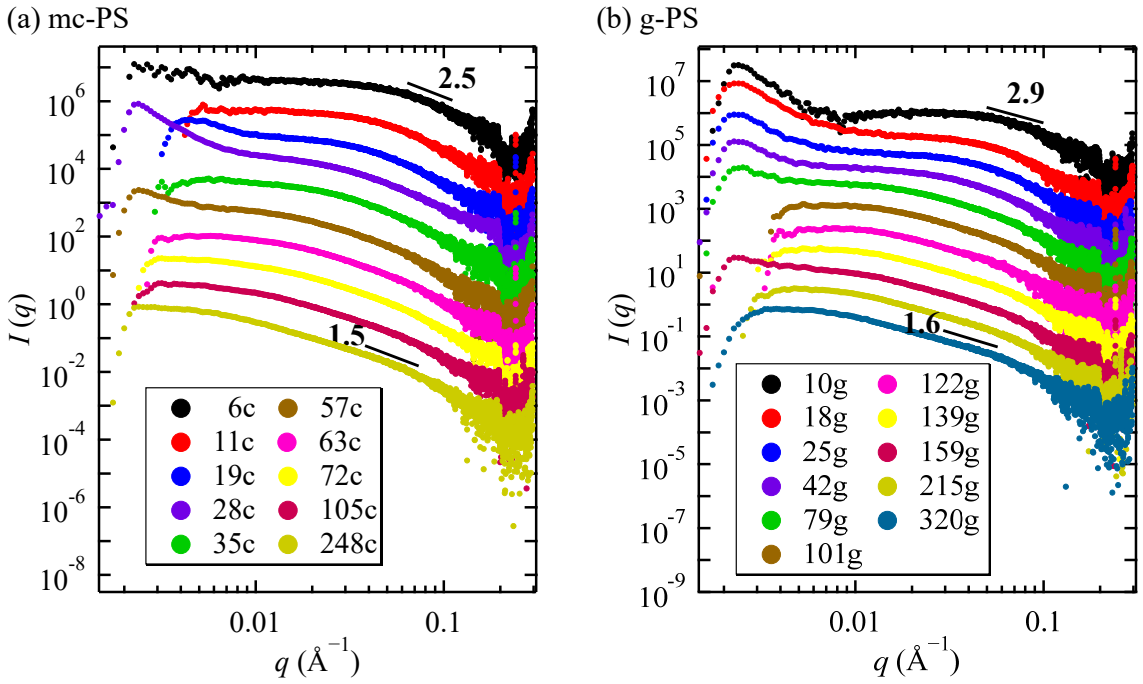

Figure 3.25. SAXS scattering intensities for the (a) mc-PS and (b) g-PS structures bearing varying numbers of cyclic or side-chain units. The $I(q)$ values are shifted along the y-axis for clarity.

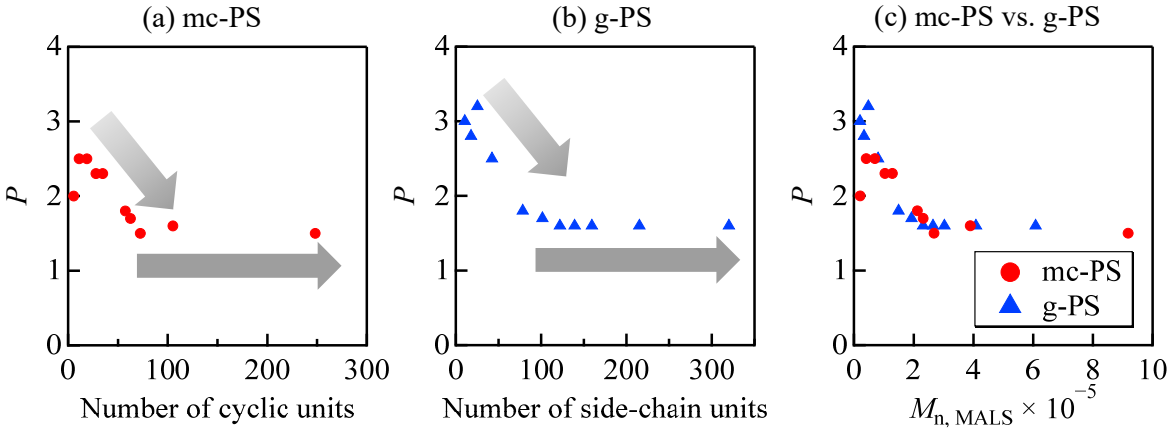

Figure 3.26. The scaling exponent (P) as a function of (a) the number of cyclic units and (b) the number of side-chain units, as obtained from SAXS profiles. (c) Comparison of the scaling exponents between mc-PS and g-PS.

More detailed information regarding the mc-PS species were extracted by fitting the experimental SAXS results using a scattering form factor for a theoretical model; in this case, a flexible cylinder model was employed.[52] In this model, the polymer chains in solution were approximated as flexible cylinders, characterized by the Kuhn length (λ_k), R_c, and the contour length (L) (**Figure 3.27**). Notably, a flexible cylinder model was also employed in previous studies to analyze bottlebrush polymers using SAXS and SANS.[21,53–54] For the mc-PS and g-PS specimens with low N_{NB} values, which were expected to adopt a spherical conformation in solution, an appropriate fit was not obtained using the flexible cylinder model. Thus, the flexible cylinder model was applied to the samples with P values <1.8, which were more likely to adopt a cylindrical structure in solution (**Figures 3.28** and **3.29**). The estimated R_c values ranged from 22.5 to 27.5 Å for both the mc-PS and g-PS systems (Figure 3.27a). Previously, it was reported that the R_c value of a g-PS specimen with a comparable side-chain molecular weight was ~25 Å, which is in good agreement with the current results. Furthermore, these R_c values were in close agreement with those obtained independently from the cross-sectional Guinier analysis of the SANS profiles, confirming the consistency between the SAXS- and SANS-based evaluations. The similar R_c values obtained for the mc-PS and g-PS systems were attributed to the loops formed in mc-PS, which resulted in the chain length of the cyclic polymer being comparable to that of the fully extended chain of the linear polymer, albeit with half the molecular weight (Figure 3.27b). Additionally, because L increases with the total molecular weight (i.e., the number of side chains), the cylinder becomes elongated as the number of side chains increases. Moreover, the λ_k values for the mc-PS specimens were calculated to be in the range of 110.1–147.4 Å, which were considerably larger than those of the g-PS specimens (74.5–105.1 Å) (Figure 3.27c). These results indicate that mc-PS possesses a molecular

backbone with a greater apparent rigidity than g-PS. This apparent backbone stiffening can be attributed to the covalent closure of adjacent side chains into loops, which couples the motions of neighboring side chains and suppresses the local rotational freedom of the backbone near the grafting points.

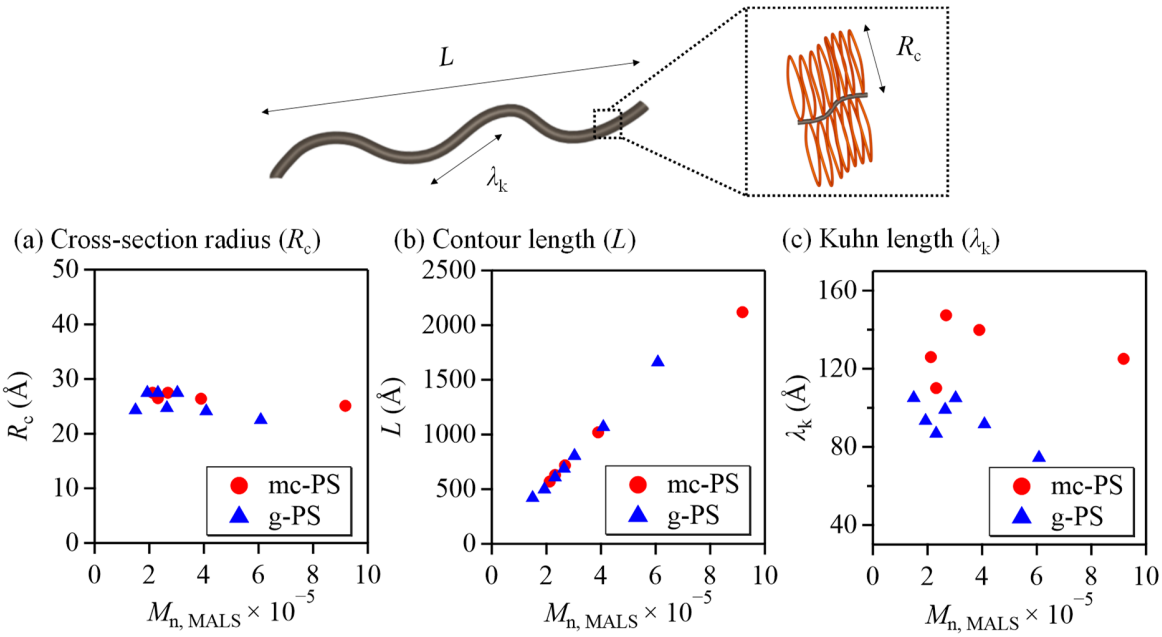

Figure 3.27. Comparison between the fitted parameters obtained for mc-PS and g-PS using the flexible cylinder model.

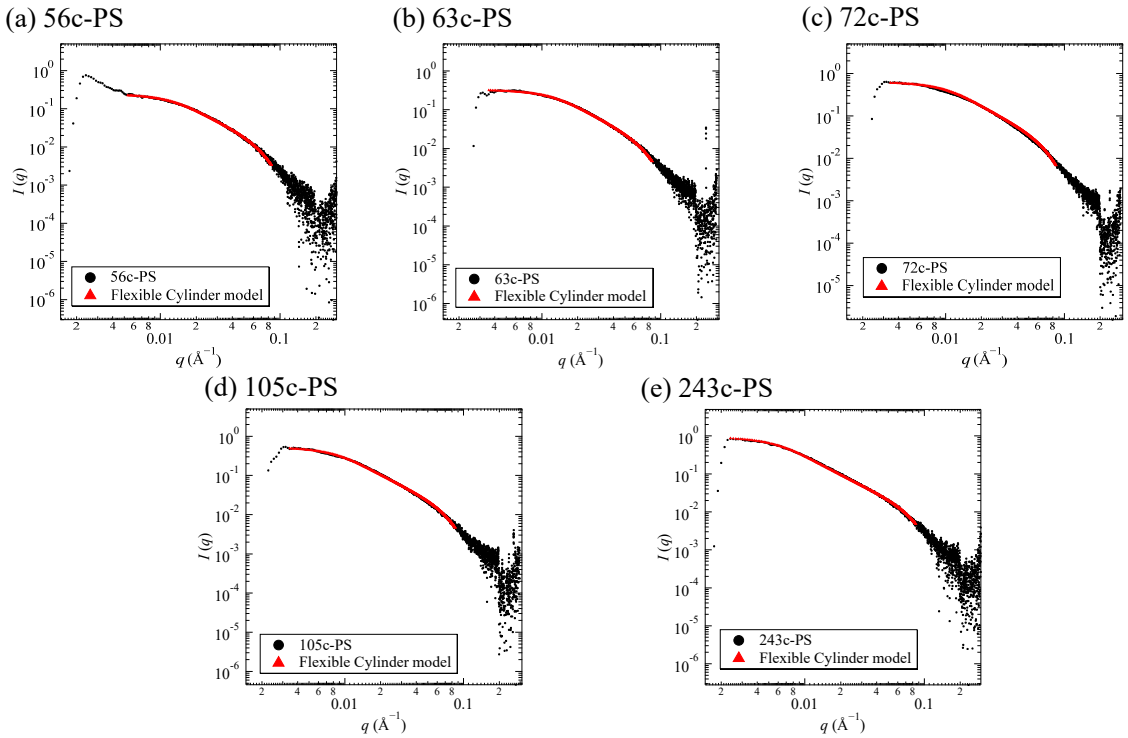

Figure 3.28. mc-PS SAXS data and model fits for flexible cylinder model. All samples were dissolved in toluene at a polymer concentration of 1.0 g L^{-1}.

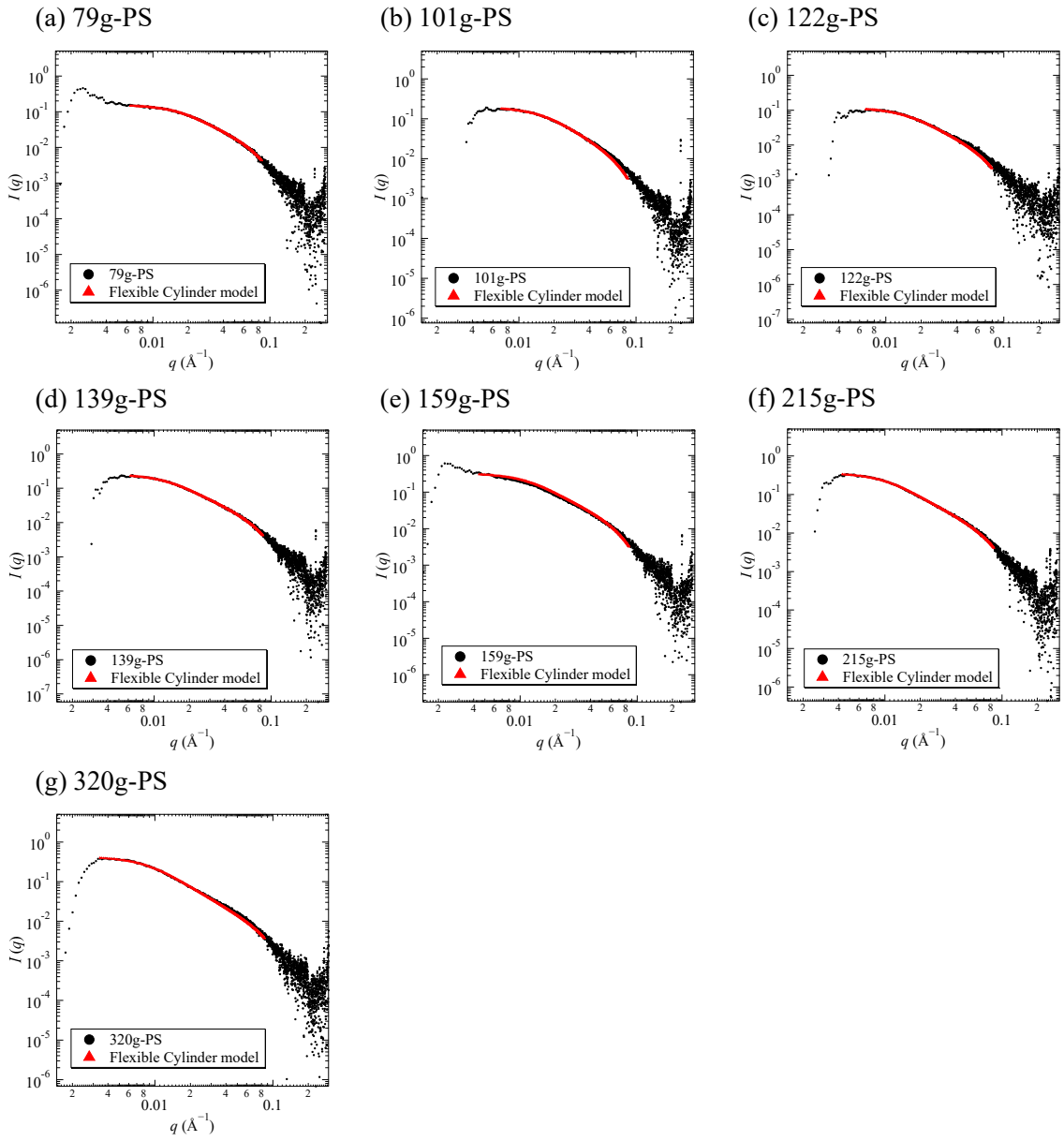

Figure 3.29. g-PS SAXS data and model fits for flexible cylinder model. All samples were dissolved in toluene at a polymer concentration of 1.0 g L^{-1}.

3.4 Conclusions

This chapter quantitatively evaluated the impact of a multicyclic polymer topology on the structural and physical properties of the resulting material by systematically comparing multicyclic polystyrene (mc-PS) with its acyclic counterpart, graft polystyrene (g-PS). Both polymers share a polynorbornene backbone, thereby allowing the influence of the side-chain architecture to be clearly assessed. Cyclopolymerization enabled the synthesis of mc-PS with a narrow dispersity ($Đ \leq 1.50$) and over 20 cyclic units, allowing precise structural and property assessments to be performed. The obtained results highlighted distinct differences in the solution and solid-state properties of the mc-PS and g-PS species, emphasizing their unique multicyclic topology effects. Furthermore, as the number of cyclic units was increased, a transition from spherical-to-cylindrical was observed in solution, representing a transition behavior similar to that of g-PS. However, when the degree of polymerization of the norbornene backbone was low, mc-PS tended to adopt a more cylindrical conformation than g-PS, with the increased apparent rigidity of the norbornene backbone being induced by the cyclic topology of the side chains. Importantly, several unexpected findings were revealed. First, mc-PS exhibited T_g values up to ~30 °C higher than those of g-PS at comparable molecular weights, far exceeding the typical T_g increase (5–10 °C) known for monocyclic polymers. In addition, a clear spherical-to-cylindrical conformational transition was observed in solution as the number of cyclic units increased, indicating topology-driven changes in chain shape. Furthermore, an increase in the apparent Kuhn length was detected for mc-PS relative to g-PS, suggesting that side-chain cyclization leads to a stiffer backbone. The findings of this study not only advance our understanding of the fundamental properties of multicyclic polymers, but they also provide

valuable guidelines for the design of novel polymer materials that leverage these unique properties and facilitate precise structural control through molecular design.

3.5. References

1. Chen, C.; Weil, T. Cyclic Polymers: Synthesis, Characteristics, and Emerging Applications. *Nanoscale Horizons* **2022**, *7*, 1121–1135.
2. Ren, J. M.; McKenzie, T. G.; Fu, Q.; Wong, E. H. H.; Xu, J.; An, Z.; Shanmugam, S.; Davis, T. P.; Boyer, C.; Qiao, G. G. Star Polymers. *Chem. Rev.* **2016**, *116*, 6743–6836.
3. Zheng, Y.; Li, S.; Weng, Z.; Gao, C. Hyperbranched Polymers: Advances from Synthesis to Applications. *Chem. Soc. Rev.* **2015**, *44*, 4091–4130.
4. Polymeropoulos, G.; Zapsas, G.; Ntetsikas, K.; Bilalis, P.; Gnanou, Y.; Hadjichristidis, N. 50th Anniversary Perspective: Polymers with Complex Architectures. *Macromolecules* **2017**, *50*, 1253–1290.
5. Haque, F. M.; Grayson, S. M. The Synthesis, Properties and Potential Applications of Cyclic Polymers. *Nat. Chem*. **2020**, *12*, 433–444.
6. Golba, B.; Benetti, E. M.; De Geest, B. G. Biomaterials Applications of Cyclic Polymers. *Biomaterials* **2021**, *267*, 120468.
7. Yamamoto, T.; Tezuka, Y. Topological Polymer Chemistry: A Cyclic Approach toward Novel Polymer Properties and Functions. *Polym. Chem.* **2011**, *2*, 1930–1941.
8. Yamamoto, T.; Tezuka, Y. Cyclic Polymers Revealing Topology Effects upon Self-Assemblies, Dynamics and Responses. *Soft Matter* **2015**, *11*, 7458–7468.
9. Jia, Z.; Monteiro, M. J. Cyclic Polymers: Methods and Strategies. *J. Polym. Sci. Part A Polym. Chem.* **2012**, *50*, 2085–2097.
10. Laurent, B. A.; Grayson, S. M. Synthetic Approaches for the Preparation of Cyclic Polymers. *Chem. Soc. Rev.* **2009**, *38*, 2202–2213.

11. Schappacher, M.; Deffieux, A. α-Acetal-ω-Bis(Hydroxymethyl) Heterodifunctional Polystyrene: Synthesis, Characterization, and Investigation of Intramolecular End-to-End Ring Closure. *Macromolecules* **2001**, *34*, 5827–5832.

12. Schäler, K.; Ostas, E.; Schröter, K.; Thurn-Albrecht, T.; Binder, W. H.; Saalwächter, K. Influence of Chain Topology on Polymer Dynamics and Crystallization. Investigation of Linear and Cyclic Poly(ε-Caprolactone)s by 1H Solid-State NMR Methods. *Macromolecules* **2011**, *44*, 2743–2754.

13. Zimm, B. H.; Stockmayer, W. H. The Dimensions of Chain Molecules Containing Branches and Rings. *J. Chem. Phys.* **1949**, *17*, 1301–1314.

14. Jeong, Y.; Jin, Y.; Chang, T.; Uhlik, F.; Roovers, J. Intrinsic Viscosity of Cyclic Polystyrene. *Macromolecules* **2017**, *50*, 7770–7776.

15. Poelma, J. E.; Ono, K.; Miyajima, D.; Aida, T.; Satoh, K.; Hawker, C. J. Cyclic Block Copolymers for Controlling Feature Sizes in Block Copolymer Lithography. *ACS Nano* **2012**, *6*, 10845–10854.

16. Honda, S.; Yamamoto, T.; Tezuka, Y. Topology-Directed Control on Thermal Stability: Micelles Formed from Linear and Cyclized Amphiphilic Block Copolymers. *J. Am. Chem. Soc.* **2010**, *132*, 10251–10253.

17. Cortez, M. A.; Godbey, W. T.; Fang, Y.; Payne, M. E.; Cafferty, B. J.; Kosakowska, K. A.; Grayson, S. M. The Synthesis of Cyclic Poly(Ethylene Imine) and Exact Linear Analogues: An Evaluation of Gene Delivery Comparing Polymer Architectures. *J. Am. Chem. Soc.* **2015**, *137*, 6541–6549.

18. Huang, K.; Rzayev, J. Well-Defined Organic Nanotubes from Multicomponent Bottlebrush Copolymers. *J. Am. Chem. Soc.* **2009**, *131*, 6880–6885.

19. Zhao, Y. L.; Cai, Q.; Jiang, J.; Shuai, X. T.; Bei, J. Z.; Chen, C. F.; Xi, F. Synthesis and Thermal Properties of Novel Star-Shaped Poly(L-Lactide)s with Starburst PAMAM-OH Dendrimer Macroinitiator. *Polymer.* **2002**, *43*, 5819–5825.

20. Van Aert, H. A. M.; Van Genderen, M. H. P.; Meijer, E. W. Star-Shaped Poly(2,6-Dimethyl-1,4-Phenylene Ether). *Polym. Bull.* **1996**, *37*, 273–280.

21. Pesek, S. L.; Li, X.; Hammouda, B.; Hong, K.; Verduzco, R. Small-Angle Neutron Scattering Analysis of Bottlebrush Polymers Prepared via Grafting-through Polymerization. *Macromolecules* **2013**, *46*, 6998–7005.

22. Tezuka, Y. Topological Polymer Chemistry by Dynamic Selection from Electrostatic Polymer Self-Assembly. *Chem. Rec.* **2005**, *5*, 17–26.

23. Tezuka, Y. Topological Polymer Chemistry for Designing Multicyclic Macromolecular Architectures. *Polym. J.* **2012**, *44*, 1159–1169.

24. Ebii, Y.; Ebe, M. Multicyclic Polymer Synthesis via a Consecutive Cyclization Approach. *Polym. J.* **2025**.

25. Ma, C.; Quan, Y.; Liao, X.; Sun, R.; Xie, M. Cyclic-Hanging-Multicyclic Polymer Synthesized by Ladderphane-Mediated Blocking-Cyclization Technique for the Direct Visualization of Cyclic Macromolecular Topology. *Polym. Chem.* **2023**, *14*, 2072–2079.

26. Lonsdale, D. E.; Monteiro, M. J. Various Polystyrene Topologies Built from Tailored Cyclic Polystyrene via CuAAC Reactions. *Chem. Commun.* **2010**, *46*, 7945–7947.

27. Hossain, M. D.; Reid, J. C.; Lu, D.; Jia, Z.; Searles, D. J.; Monteiro, M. J. Influence of Constraints within a Cyclic Polymer on Solution Properties. *Biomacromolecules* **2018**, *19*, 616–625.

28. Pipertzis, A.; Hossain, M. D.; Monteiro, M. J.; Floudas, G. Segmental Dynamics in

Multicyclic Polystyrenes. *Macromolecules* **2018**, *51*, 1488–1497.

29. Gavrilov, M.; Amir, F.; Kulis, J.; Hossain, M. D.; Jia, Z.; Monteiro, M. J. Densely Packed Multicyclic Polymers. *ACS Macro Lett.* **2017**, *6*, 1036–1041.
30. Yan, Z. C.; Hossain, M. D.; Monteiro, M. J.; Vlassopoulos, D. Viscoelastic Properties of Unentangled Multicyclic Polystyrenes. *Polymers* **2018**, *10*, 973.
31. Jeong, J.; Kim, K.; Lee, R.; Lee, S.; Kim, H.; Jung, H.; Kadir, M. A.; Jang, Y.; Jeon, H. B.; Matyjaszewski, K.; Chang, T.; Paik, H. J. Preparation and Analysis of Bicyclic Polystyrene. *Macromolecules* **2014**, *47*, 3791–3796.
32. Mohanty, A. K.; Ye, J.; Ahn, J.; Yun, T.; Lee, T.; Kim, K. S.; Jeon, H. B.; Chang, T.; Paik, H. J. Topologically Reversible Transformation of Tricyclic Polymer into Polyring Using Disulfide/Thiol Redox Chemistry. *Macromolecules* **2018**, *51*, 5313–5322.
33. Jung, J. H.; Kumar Mohanty, A.; Ye, J.; Lee, T.; Ahn, J.; Lim, Y. G.; Chang, T.; Paik, H. J. Covalent Fixed Multicyclic Polystyrene Conformers. *J. Polym. Sci. Part A Polym. Chem.* **2017**, *55*, 4020–4026.
34. Shi, G. Y.; Pan, C. Y. Synthesis of Well-Defined Figure-of-Eight-Shaped Polymers by a Combination of ATRP and Click Chemistry. *Macromol. Rapid Commun.* **2008**, *29*, 1672–1678.
35. Xue, X.; Chen, Y.; Li, Y.; Liang, K.; Huang, W.; Yang, H.; Jiang, L.; Jiang, Q.; Chen, F.; Jiang, T.; Lin, B.; Jiang, B.; Pu, H. Remarkable Untangled Dynamics Behavior of Multicyclic Branched Polystyrenes. *Chem. Commun.* **2021**, *57*, 399–402.
36. Mato, Y.; Honda, K.; Ree, B. J.; Tajima, K.; Yamamoto, T.; Deguchi, T.; Isono, T.; Satoh, T. Programmed Folding into Spiro-Multicyclic Polymer Topologies from Linear and Star-Shaped Chains. *Commun. Chem.* **2020**, *3*, 97.

37. Choi, T. L.; Grubbs, R. H. Controlled Living Ring-Opening-Metathesis Polymerization by a Fast-Initiating Ruthenium Catalyst. *Angew. Chem. Int. Ed.* **2003**, *42*, 1743–1746.

38. Xie, F.; Li, Z.; Li, Z.; Li, D.; Gao, Y.; Wang, B. Absolute Intensity Calibration and Application at BSRF SAXS Station. *Nucl. Instrum. Methods Phys. Res., Sect. A* **2018**, *900*, 64–68.

39. Blosch, S. E.; Alaboalirat, M.; Eades, C. B.; Scannelli, S. J.; Matson, J. B. Solvent Effects in Grafting-through Ring-Opening Metathesis Polymerization. *Macromolecules* **2022**, *55*, 3522–3532.

40. Fox, T. G., Jr.; Flory, P. J. Second-Order Transition Temperatures and Related Properties of Polystyrene. I. Influence of Molecular Weight. *J. Appl. Phys.* **1950**, *21*, 581–591.

41. Gao, L.; Oh, J.; Tu, Y.; Chang, T.; Li, C. Y. Glass Transition Temperature of Cyclic Polystyrene and the Linear Counterpart Contamination Effect. *Polymer* **2019**, *170*, 198–203.

42. Obukhov, S. P.; Rubinstein, M.; Duke, T. Dynamics of a Ring Polymer in a Gel. *Phys. Rev. Lett.* **1994**, *73*, 1263–1266.

43. Kulicke, W.-M.; Clasen, C. *Viscosimetry of Polymers and Polyelectrolytes*; Springer Science & Business Media, 2004.

44. Wagner, H. L. The Mark–Houwink–Sakurada Equation for the Viscosity of Atactic Polystyrene. *J. Phys. Chem. Ref. Data* **1985**, *14*, 1101–1106.

45. Li, Z.; Lee, N. S.; Wooley, K. L. Dynamic Cylindrical Assembly of Triblock Copolymers by a hierarchical process of covalent and supramolecular interactions. *J. Am. Chem. Soc.* **2011**, *133*, 1228–1231.

46. Hsu, H. P.; Paul, W.; Rathgeber, S.; Binder, K. Characteristic Length Scales and Radial

Monomer Density Profiles of Molecular Bottle-Brushes: Simulation and Experiment. *Macromolecules* **2010**, *43*, 1592–1601.

47. Li, Z.; Zhang, K. E.; Ma, J.; Chong, C.; Wooley, K. L. Facile Syntheses of Cylindrical Molecular Brushes by a Sequential RAFT and ROMP "Grafting-Through" Methodology. *J. Polym. Sci. Part A Polym. Chem.* **2009**, *47*, 5557–5563.
48. Dutta, S.; Wade, M. A.; Walsh, D. J.; Guironnet, D.; Rogers, S. A.; Sing, C. E. Dilute Solution Structure of Bottlebrush Polymers. *Soft Matter* **2019**, *15*, 2928–2941.
49. Porod, G. In Small Angle X-ray Scattering; Glatter, O.; Kratky, O., Eds.; Academic Press: London, 1982; pp 17–51.
50. SasView; https://www.sasview.org
51. Schmidt, P. W. Small-Angle Scattering Studies of Disordered, Porous and Fractal Systems. *J. Appl. Crystallogr.* **1991**, *24*, 414–435.
52. SasView; https://www.sasview.org/docs/user/models/flexible_cylinder.html
53. Rathgeber, S.; Pakula, T.; Wilk, A.; Matyjaszewski, K.; Lee, H. il; Beers, K. L. Bottle-Brush Macromolecules in Solution: Comparison between Results Obtained from Scattering Experiments and Computer Simulations. *Polymer* **2006**, *47*, 7318–7327.
54. Rathgeber, S.; Pakula, T.; Wilk, A.; Matyjaszewski, K.; Beers, K. L. On the Shape of Bottle-Brush Macromolecules: Systematic Variation of Architectural Parameters. *J. Chem. Phys.* **2005**, *122*,124904.
55. Zhang, B.; Gröhn, F.; Pedersen, J. S.; Fischer, K.; Schmidt, M. Conformation of Cylindrical Brushes in Solution: Effect of Side Chain Length. *Macromolecules* **2006**, *39*, 8440–8450.

Chapter 4

Synthesis of Deuterated Multicyclic Polystyrenes for A SANS Study to Explore the Structural Characteristics of Multicyclic Architectures in the Bulk

4.1 Introduction

Cyclic polymers are a class of macromolecules characterized by a closed-ring architecture devoid of chain ends. This distinctive topology gives rise to structural and physical properties that differ fundamentally from those of their linear counterparts.[1–8] Such properties include high density,[9] reduced hydrodynamic volume,[10] and an elevated glass transition temperature,[11] which arise from the topological constraints inherent to cyclic polymers, such as the absence of chain ends and reduced intermolecular entanglements. Both theoretical and experimental studies have consistently demonstrated that cyclic polymers exhibit distinct conformational and dynamic behaviors compared with their linear counterparts, spanning from a dilute solution to the bulk state.[12–20] Among these, the conformations of cyclic polymers in the bulk state constitute a fundamental problem, as they are complicated by topological constraints, which are absent in the structurally simpler linear chains. In this context, Takano et al. used small-angle neutron scattering (SANS) to quantify the bulk conformations of monocyclic polystyrenes (PS) over a wide molecular-weight range and showed that rings are globally more compact than linear chains. Specifically, they found that the radius of gyration follows $R_g \propto N^{0.47}$ for monocyclic PS rather than the linear-chain scaling of $R_g \propto N^{0.50}$.[21] Additionally, Suzuki et al.[22] and Vettorel et al.[23] independently employed Monte–Carlo simulations to demonstrate that the scaling exponent (ν) for a trivial ring polymer in a melt approaches 1/3 when the degree of polymerization of the ring polymer is extremely large. This value was later confirmed by a self-consistent field analysis.[24] Furthermore, both molecular dynamics (MD) simulations[25] and mean-field theory[26] have confirmed that the value of ν for a trivial ring polymer in a melt is also 1/3 if the molecular weight of the ring polymer is extremely large.

Building on the insights into neat ring melts and cyclic/linear blends summarized in Chapter 1, recent attention has increasingly focused on how topological constraints such as threading govern the structures and dynamics of cyclic polymers in mixtures with linear chains. Previous SANS and theoretical studies have shown that linear chains readily penetrate and thread cyclic polymers, leading to ring swelling and effectively attractive, entropically driven interactions that can be described by a negative effective Flory–Huggins parameter.[21,27,28] Building on these insights into the structural behaviors of multicyclic polymers, researchers have increasingly turned their attention to more complex cyclic architectures.

A particularly notable class of polymers is multicyclic polymers composed of two or more cyclic units within a single macromolecular backbone. Unlike monocyclic polymers, which are primarily characterized by their ring size, multicyclic polymers are characterized by two key topological parameters, namely the size of each cyclic unit and the number of such units. This dual-parameter system introduces a higher level of architectural complexity and allows for finer control over the macromolecular conformation and physical behavior.[29–32] Theoretical studies based on Gaussian chain models have provided fundamental insights into the conformational properties of multicyclic architectures. For example, Metzler et al. derived analytical expressions for the R_g and asphericity of rosette-type structures as functions of the number of loops and branches, demonstrating that increasing topological complexity leads to reduced coil dimensions and anisotropy compared with their star-like and linear counterparts.[33] More recently, Uehara et al. developed an exact formula for the R_g of arbitrary topological polymers using graph-theoretical methods, which allowed the rigorous evaluation of contraction factors for multicyclic topologies within the thermodynamic limit.[34] From a scattering perspective, Hammouda formulated form factors for star polymers with looping branches and

ring polymers, highlighting characteristic features in the Kratky plots that indicate loop-induced compaction and reduced chain extension.[35]

In parallel with these structural studies, increasing attention has been directed toward understanding how multicyclic polymers interact with linear chains in blends, where topological constraints lead to unique threading phenomena. In this context, the entanglement behavior between linear and multicyclic chains has been explored through MD simulations.[36–38] For example, Hagita et al. reported that when the degree of polymerization of a single cyclic unit in a multicyclic polymer is equivalent to that of a monocyclic polymer, multicyclic architectures exhibit a greater propensity for threading by linear chains[38]. Specifically, the number of linear chains penetrating each ring unit was demonstrated to increase with the number of cyclic units, indicating that more topologically complex architectures facilitate a higher degree of interpenetration.[38] These findings highlight the importance of the topological design in governing blend interactions, while underscoring the requirement for systematic structural investigations of multicyclic/linear polymer systems. In a previous study, Satoh et al. experimentally examined the effect of the ring topology on threading by synthesizing cyclic poly(dimethylsiloxane) (PDMS) containing various numbers of cyclic units. It was found that multicyclic PDMS showed a greater tendency to be trapped in linear PDMS networks than in monocyclic PDMS, indicating enhanced interpenetration.[39] Despite growing theoretical interest in this area, experimental studies remain limited, primarily because of the synthetic challenges associated with the preparation of structurally well-defined multicyclic polymers. In particular, the ability to independently vary the number and size of cyclic units is essential for deducing the effects of each topological parameter on the macromolecular behavior. It is therefore crucial to establish experimental platforms that enable the precise synthesis and structural

characterization of multicyclic polymers to advance our understanding of topology-driven phenomena in neat multicyclic systems, as well as in their blends with linear polymers.

In this study, SANS is employed to comprehensively investigate the structural characteristics of multicyclic polymers both in the neat bulk state and in blends with linear polymers. Initially, a series of multicyclic polystyrenes (mc-PS) and deuterated multicyclic polystyrenes (mc-dPS) with varying ring sizes and numbers of cyclic units are synthesized via the cyclopolymerization approach. Additionally, a new synthetic route to α,ω-norbornenyl-terminated PS macromonomers is established, enabling precise control over the molecular weight of the polymer precursors. Unlike earlier approaches that employed living anionic polymerization to prepare telechelic PS, the present work utilizes atom transfer radical polymerization (ATRP) as the initial polymerization step, yielding telechelic Br–PS–Br, which is subsequently converted to the α,ω-norbornenyl macromonomer. A key challenge associated with cyclopolymerization is that the resulting multicyclic polymers inherently exhibit a broad dispersion in the number of cyclic units. As described in chapters 2 and 3, previous studies employing preparative size exclusion chromatography (SEC) primarily aimed to remove catalysts and byproducts such as monocyclic PS. In the present study, preparative SEC is additionally employed to finely fractionate the generated mc-PS, thereby isolating samples with a significantly narrower distribution of cyclic units. This should enable reliable structural analyses of the well-defined mc-PS samples. Using these materials, SANS is employed to examine the global conformations of the neat mc-PS in the bulk to elucidate how an increasing topological complexity influences the chain dimensions in comparison with Gaussian statistics. Subsequently, the same set of samples is blended with linear PS to explore the interaction characteristics of the multicyclic/linear blends, such as through threading and swelling. To the

best of my knowledge, this work represents the first experimental study that systematically addresses both the bulk-state conformations of multicyclic polymers and their structural responses in blends with linear chains, providing new insights into how the multicyclic architectural complexity governs the polymer structure and interactions. For multicyclic polymers in the bulk, excluded-volume effects play a significant role not only in determining the mean-square radius of gyration, but also in shaping the Kratky plots. It is therefore suggested that the Flory theorem is violated, as was initially demonstrated for monocyclic polymers.[21]

4.2 Experimental section

4.2.1 Materials

Grubbs' 3rd generation catalyst (G3) and ethylene bis(bromoisobutyrate) (EBBiB) were prepared according to previously reported methods.[40,41] CuBr (99.999%, Sigma-Aldrich), $CuBr_2$ (99.999%, Sigma-Aldrich), neutral alumina (Sigma-Aldrich), silver(I) perchlorate ($AgClO_4$, >99.0%, Kanto Chemical Co., Inc.), *N*,*N*,*N*',*N*'',*N*''-pentamethyldiethylenetriamine (PMDETA; >99.0%, Tokyo Chemical Industry Co., Ltd. (TCI)), *N*,*N*-dimethyl-4-aminopyridine (DMAP; >99.0%, TCI), 1-ethyl-3-(3-(dimethylamino)-propyl)carbodiimide hydrochloride (EDC; >98.0%, TCI), ethyl vinyl ether (>98.0%, TCI), (±)-*exo*-5-norbornenecarboxylic acid (*exo*-NB–COOH; 97%, Sigma-Aldrich), CH_2Cl_2 (>99.0%, Junsei Chemical Co., Ltd.), methanol (>99.8%, Sigma-Aldrich), dry methanol (>99.5%, Kanto Chemical Co., Inc.), acetone (>99.5%, Kanto Chemical Co., Inc.), toluene (>99.8%, Junsei Chemical Co., Ltd.), tetrahydrofuran (>99.8%, Junsei Chemical Co., Ltd.), *sec*-butyllithium (*sec*-BuLi; Kanto Chemical Co., Inc., 1.23 mol L^{-1} in cyclohexane/*n*-hexane, v/v = 24:1), dry *N*,*N*-dimethylformamide (dry DMF; >99.5%, <0.001% H_2O, Kanto Chemical Co., Inc.), and dry CH_2Cl_2 (>99.5%, <0.001% H_2O, Kanto Chemical Co., Inc.) were used as received. Styrene (>99%, TCI), deuterated styrene (styrene-d_8; >98.0%, >98 atom% D, Sigma-Aldrich), and cyclohexane (>99.5%, Kanto Chemical Co., Inc.) were purified by vacuum distillation over CaH_2.

4.2.2 Instruments

The polymerization experiments were carried out in an MBRAUN stainless steel glovebox equipped with a gas purification system (molecular sieves and copper catalyst) in a dry argon atmosphere (H_2O, O_2<0.1 ppm). The moisture and oxygen contents in the glovebox were monitored by an MB-MO-SE 1 moisture sensor and an MB-OX-SE 1 oxygen sensor, respectively. The ^{1}H (600 MHz) and ^{13}C NMR (100 MHz) spectra were recorded using a JEOL JNM-ECZ600 at room temperature in $CDCl_3$. The phase-covariance weighted NMR technique was used tp acquire ^{13}C NMR spectra.[42] The size exclusion chromatography (SEC) was performed at 40 °C in THF (flow rate, 1.0 mL min^{-1}) using a Jasco high-performance liquid chromatography system (PU-4180 HPLC pump, AS-4550 auto sampler, and CO-4060 column oven) equipped with a Shodex K-800D guard column (8.0 mm × 100 mm; particle size, 10 μm), two Shodex columns (K-806L and K-804L; linear, 8.0 mm × 100 mm; particle size, 10μm). The absolute number-averaged molecular weight ($M_{n,MALS}$) and dispersity ($Đ_{MALS}$) of the samples were determined by SEC with multiangle light scattering detection (SEC-MALS-Visco) in $CHCl_3$ (flow rate, 1.0 mL min^{-1}) at 40 °C using a Jasco high-performance liquid chromatography system (PU-4180 HPLC pump, AS-4550 auto sampler, and CO-4060 column oven) equipped with a Shodex K-800D guard column (8.0 mm × 100 mm; particle size, 10 μm), two Shodex columns (K-806L and K-804L; linear, 8.0 mm × 100 mm; particle size, 10μm), a DAWN 8 multiangle laser light scattering detector (Wyatt Technology), a Viscostar viscosity detector (Wyatt Technology), and an RI-501 refractive index detector (Shodex). The preparative SEC was performed at room temperature in $CHCl_3$ (flow rate, 10.0 mL min^{-1}) using LaboACE LC-7080 plus II liquid chromatography system (Japan Analytical Industry Co. Ltd.) equipped with a P-LA80 pump, a RI-700LA RI detector, JAIGEL-HR-P guard column (8 mm × 40 mm;

Japan Analytical Industry Co. Ltd.), JAIGEL-2HR plus column (linear, 20.0 mm × 600 mm; exclusion limit, 5.0×10^3), JAIGEL-2.5HR plus column (linear, 20.0 mm × 600 mm; exclusion limit, 2.0×10^4), JAIGEL-3HR plus column (linear, 20.0 mm × 600 mm; exclusion limit, 7.0×10^4), and JAIGEL-4HR plus column (linear, 20.0 mm × 600 mm; exclusion limit, 5.0×10^5).

Matrix-assisted laser desorption ionization time-of-flight mass spectrometry (MALDI-TOF MS)

The MALDI-TOF MS measurement of the obtained products was performed using an Bruker Daltonics (Germany) Ultraflex MALDI-TOF/TOF mass spectrometer equipped with a 355-nm Nd:YAG laser. PS samples were prepared by depositing a mixture of the polymer, matrix, and cationic agent in THF onto a sample plate. A 10:10:1 (v/v) ratio of [PS (1 g L^{-1} in THF)]/[*trans*-2-[3-(4-tertbutylphenyl)-2-methyl-propenylidene]malononitrile (DCTB; 20 g L^{-1} in THF)]/[silver trifluoroacetate (2.0 g L^{-1} in THF)] was used.

Preparation of PS pellets for small-angle neutron scattering (SANS) measurements

A predetermined amount (total 153 mg) of mc-PS, mc-dPS, and *h*/*d*-linear PS were dissolved in toluene (2 mL). The resulting solution was casted onto a Teflon dish, and the solvent was evaporated under a stream of compressed air at 120 °C overnight. The dried film was then further dried under vacuum at 180 °C for two days. Finally, the obtained material was molded into pellets using a hot press.

SANS Measurements.

SANS measurements were performed at C1-2: SANS-U in JRR-3M, Japan. The incident beam wavelength was set to 0.70 nm. A detector was placed 1.0 m or 8.0 m from the

sample. The measurement setup provided the q range of 0.04–3.4 nm^{-1}, where q is the magnitude of the scattering vector defined by $q = 4\pi/\lambda \sin(\theta)$, with the incident beam length denoted as λ, and the scattering angle of 2θ. All measurements were conducted at 25 °C and the resulting two-dimensional SANS images was converted to one-dimensional $I(q)$ versus q profiles via circular averaging.

4.2.3 Synthetic details

Synthesis of polystyrene bearing *α*,*ω*-bromide end groups (Br–PS–Br) via atom transfer radical polymerization (ATRP)

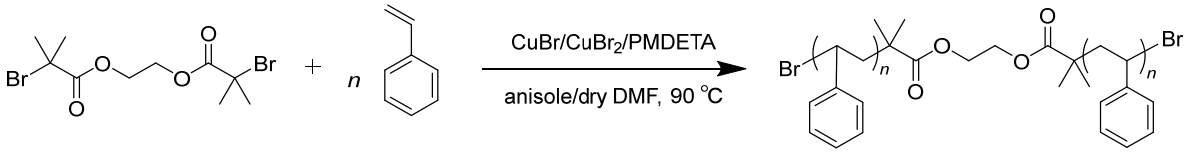

EBBiB Styrene Br–PS–Br

A typical procedure for the ATRP is as follows (Method A): CuBr (204.4 mg, 1.43 mmol, 0.95 eq.) was placed in a Schlenk flask A, and the flask was purged with argon. In a separate Schlenk flask B, styrene (30.0 g, 234 mmol, 68 eq.), EBBiB (540.1 mg, 1.50 mmol, 1.0 eq.), a premixed solution of $CuBr_2$ (16.8 mg, 75.0 μmol, 0.05 eq.), PMDETA (345 μL, 1.65 mmol, 1.1 eq.), and dry DMF (1.00 mL), as well as anisole (15.0 mL), were added. The solution in flask B was subjected to three freeze–pump–thaw cycles to remove dissolved gases. The degassed solution in flask B was then transferred to flask A under an argon atmosphere to initiate polymerization. The reaction mixture was stirred at 90 °C for 3 h and then exposed to air to terminate the polymerization. The resulting solution was diluted with THF and passed through a short column of neutral alumina to remove residual copper. After removal of the solvent under reduced pressure, the crude product was dissolved in CH_2Cl_2 and precipitated into methanol. The precipitated polymer was collected and dried under vacuum at 60 °C overnight to afford Br–PS_{6k}–Br as a white solid. Yield: 8.13 g (27.1%)

$M_{n,NMR}$ = 6,400, $M_{n,SEC}$ = 6,400 (THF), $Đ$ = 1.07 (THF)

^{1}H NMR ($CDCl_3$, 400 MHz): δ (ppm) 7.40–6.17 (m, *aromatic*), 4.59–4.34 (br, –C*H*Br), 3.44–3.01 (br, 4H, –(C*H*$_2$)$_2$OC(=O)–), 2.53–1.69 (m, –CH$_2$C*H*Ph–), 1.69–1.13 (m, –C*H*$_2$CHPh–), 0.99–0.74 (m, 12H, –OC(=O)C(C*H*$_3$)$_2$–).

Method A was used for the ATRP of styrene (80.0 g, 768 mmol, 480 eq.) with CuBr (218 mg, 1.52 mmol, 0.95 eq.), EBBiB (576 mg, 1.60 mmol, 1.0 eq.), a premixed solution of $CuBr_2$ (17.9 mg, 80.0 μmol, 0.05 eq.), PMDETA (368 μL, 1.76 mmol, 1.1 eq.), and dry DMF (1.00 mL), as well as anisole (22.4 mL) for 3 h to give Br–PS_{10k}–Br as a white solid. Yield: 8.22 g (10.3%)

$M_{n,NMR}$ = 9,900, $M_{n,SEC}$ = 9,400 (THF), $Đ$ = 1.07 (THF)

Method A was used for the ATRP of styrene (70.0 g, 672 mmol, 1057 eq.) with CuBr (86.7 mg, 604 μmol, 0.95 eq.), EBBiB (229 mg, 636 μmol, 1.0 eq.), a premixed solution of $CuBr_2$ (7.1 mg, 31.8 μmol, 0.05 eq.), PMDETA (146 μL, 699 μmol, 1.1 eq.), and dry DMF (1.00 mL), as well as anisole (20.0 mL) for 11 h to give Br–PS_{35k}–Br as a white solid. Yield: 20.0 g (28.5%)

$M_{n,NMR}$ = 31,900, $M_{n,SEC}$ = 33,500 (THF), $Đ$ = 1.16 (THF)

Synthesis of polystyrene bearing *α*,*ω*-hydroxy end groups (HO–PS–OH)

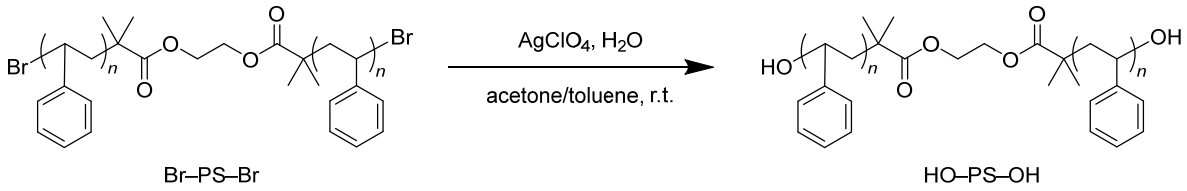

A typical procedure for the synthesis of HO–PS–OH is as follows (Method B): A two-necked flask equipped with a magnetic stir bar was charged with $AgClO_4$ (38.9 mg, 188 μmol) and subjected to argon purge. Separately, Br–PS_{6k}–Br ($M_{n,NMR}$ = 6,400, 500 mg, 78.1 μmol) was dissolved in a mixed solvent of acetone and toluene (8 mL, v/v = 5:3) and added to the flask under an argon atmosphere. After thorough mixing, distilated water (0.5 mL) was added, and the reaction mixture was stirred at room temperature overnight. The reaction mixture was passed through a short column of neutral alumina to remove silver residues. After evaporation of the solvents under reduced pressure, the residue was dissolved in CH_2Cl_2 and precipitated into methanol. The resulting solid was collected and dried under vacuum at 60 °C overnight to afford a white solid of HO–PS_{6k}–OH. Yield: 463 mg (92.6%)

$M_{n,NMR}$ = 6,400, $M_{n,SEC}$ = 6,300 (THF), $Đ$ = 1.07 (THF)

^{1}H NMR ($CDCl_3$, 400 MHz): δ(ppm) 7.40–6.17 (m, *aromatic*), 4.44–4.04 (br, –C*H*OH), 3.44–3.01 (br, 4H, –(CH_2)$_2$OC(=O)–), 2.53–1.69 (m, –CH_2C*H*Ph–), 1.69–1.13 (m, –CH_2CHPh–), 0.99–0.74 (m, 12H, –OC(=O)C(CH_3)$_2$–).

Method B was used for the reaction of Br–PS_{10k}–Br ($M_{n,NMR}$ =9,900, 5.30 g, 535 μmol, 1 eq.) with $AgClO_4$ (266 mg, 1.28 mmol, 2.4 eq.) in a mixed solvent of acetone and toluene (84.8 mL, v/v = 5:3) for overnight to give HO–PS_{10k}–OH as a white solid. Yield: 4.77 g (90.0%) $M_{n,NMR}$ = 10,300, $M_{n,SEC}$ = 9,500 (THF), $Đ$ = 1.07 (THF)

Method B was used for the reaction of Br–PS_{35k}–Br ($M_{n,NMR}$ =31,900, 5.00 g, 157 μmol, 1 eq.) with $AgClO_4$ (78.0 mg, 376 μmol, 2.4 eq.) in a mixed solvent of acetone and toluene (80.0 mL, v/v = 5:3) for overnight to give HO–PS_{35k}–OH as a white solid. Yield: 4.55 g (91.0%) $M_{n,NMR}$ = 32,000, $M_{n,SEC}$ = 33,700 (THF), $Đ$ = 1.17 (THF)

Synthesis of polystyrene bearing *α*,*ω*-norbornenyl end groups (NB–PS–NB)

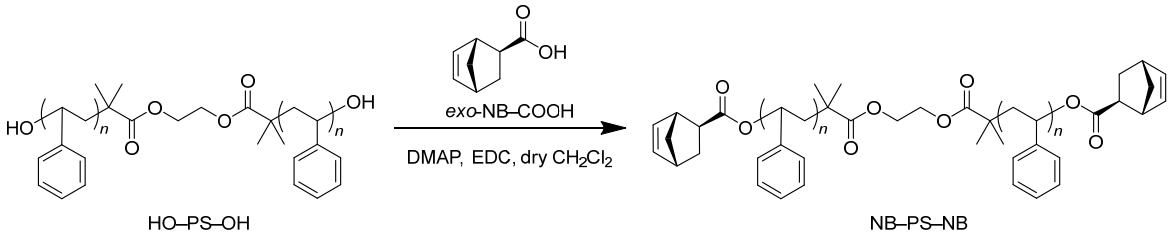

A typical procedure for the condensation reaction is as follows (Method C): In a round-bottom flask, HO–PS_{6k}–OH ($M_{n,NMR}$ = 6,400, 200 mg, 32.2 μmol, 1 eq.), *exo*-NB–COOH (17.7 mg, 125 μmol, 4 eq.), EDC (35.9 mg, 188 μmol, 6 eq.), and DMAP (22.9 mg, 188 μmol, 6 eq.) were dissolved in CH_2Cl_2 (2.0 mL), and the mixture was stirred at r.t. for 72 h. The polymer crude was purified by reprecipitation in methanol to give NB–PS_{6k}–NB as a white solid. Yield: 135 mg (67.5%)

$M_{n,NMR}$ = 6,600, $M_{n,SEC}$ = 6,200 (THF), $Đ$ = 1.06 (THF)

^{1}H NMR ($CDCl_3$, 400 MHz): δ (ppm) 7.40–6.17 (m, *aromatic*), 6.17–6.00 (m, 4H, –C*H*=C*H*– in norbornene ring), 4.44–4.04 (br, –C*H*OH), 3.44–2.76 (br, 8H, –(CH_2)$_2$OC(=O)–, –C*H*–CH_2–CH–CO– in norbornene ring, –C*H*–CH–CO– in norbornene ring), 2.53–1.69 (m, –CH_2C*H*Ph–, *endo*-C*H*– of –CH–CH_2–CH–C*H*CO– in norbornene ring, *exo*-C*H*– of –CH–C*H*$_2$–CH–CO– in norbornene ring), 1.69–1.13 (m, –C*H*$_2$CHPh–, –CH_2CC*H*$_3$(Ph)–, –C*H*$_2$CCH$_3$(Ph)–, –C*H*$_2$CH$_2$OCO–, *endo*-C*H*– of –CH–C*H*$_2$–CH–CO– in norbornene ring, bridge head –C*H*$_2$– in norbornene ring), 0.99–0.74 (m, 12H, –OC(=O)C(C*H*$_3$)$_2$–).

Method C was used for the reaction of HO–PS_{10k}–OH ($M_{n,NMR}$ = 10,300, 5.56 g, 540 μmol, 1 eq.) with *exo*-NB–COOH (298 mg, 2.16 mmol, 4 eq.), DMAP (396 mg, 3.24 mmol, 6 eq.), and EDC (621 mg, 3.24 mmol, 6 eq.) in CH_2Cl_2 (55.6 mL) for 90 h to give NB–PS_{10k}–NB as a white solid. Yield: 4.62 g (83.1%)

$M_{n,NMR}$ = 9,400, $M_{n,SEC}$ = 9,500 (THF), $Đ$ = 1.07 (THF), $M_{n,MALS}$ = 10,000, $Đ_{MALS}$ = 1.03

Method C was used for the reaction of HO–PS_{35k}–OH ($M_{n,NMR}$ = 32,200, 4.00 g, 124 μmol, 1 eq.) with *exo*-NB–COOH (68.7 mg, 497 μmol, 4 eq.), DMAP (91.1 mg, 745 μmol, 6 eq.), and EDC (143 mg, 745 μmol, 6 eq.) in CH_2Cl_2 (40.0 mL) for 142 h to give NB–PS_{35k}–NB as a white solid. Yield: 3.59 g (89.8%)

$M_{n,NMR}$ = 32,300, $M_{n,SEC}$ = 33,200 (THF), $Đ$ = 1.19 (THF), $M_{n,MALS}$ = 35,300, $Đ_{MALS}$ = 1.08

Synthesis of deuterated polystyrene bearing *α*,*ω*-bromide end groups (Br–dPS–Br) via ATRP

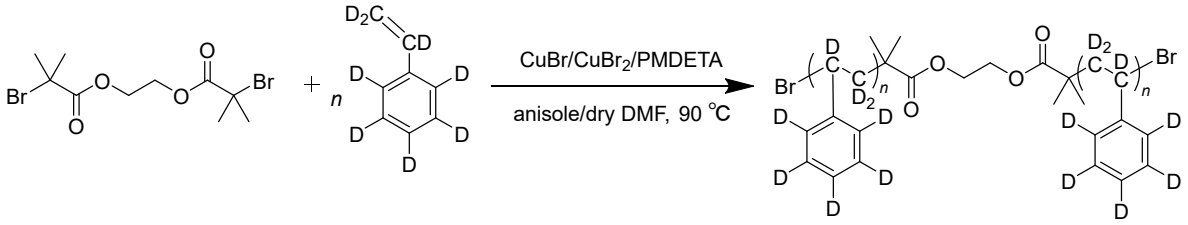

Method A was used for the ATRP of styrene-d_8 (16.0 g, 154 mmol, 240 eq.) with CuBr (87.2 mg, 608 μmol, 0.95 eq.), EBBiB (230 mg, 640 μmol, 1.0 eq.), a premixed solution of $CuBr_2$ (7.1 mg, 32.0 μmol, 0.05 eq.), PMDETA (147 μL, 704 μmol, 1.1 eq.), and dry DMF (1.00 mL), as well as anisole (5.0 mL) for 5.0 h to give Br–dPS_{10k}–Br as a white solid. Yield: 6.19 g (38.7%)

$M_{n,SEC}$ = 11,200 (THF), $Đ$ = 1.08 (THF)

^{1}H NMR ($CDCl_3$, 400 MHz): δ(ppm) 3.44–3.01 (br, 4H, –(CH_2)$_2$OC(=O)–), 0.99–0.74 (m, 12H, –OC(=O)C(CH_3)$_2$–).

Method A was used for the ATRP of styrene-d_8 (11.3 g, 108 mmol, 720 eq.) with CuBr (20.5 mg, 143 μmol, 0.95 eq.), EBBiB (54.3 mg, 151 μmol, 1.0 eq.), a premixed solution of $CuBr_2$ (1.7 mg, 7.54 μmol, 0.05 eq.), PMDETA (34.6 μL, 75.4 μmol, 1.1 eq.), and dry DMF (1.00 mL), as well as anisole (3.3 mL) for 34.0 h to give Br–dPS_{35k}–Br as a white solid. Yield: 4.72 g (41.8%)

$M_{n,SEC}$ = 32,600, $Đ$ = 1.10

Synthesis of deuterated polystyrene bearing *α*,*ω*-hydroxyl end groups (HO–dPS–OH)

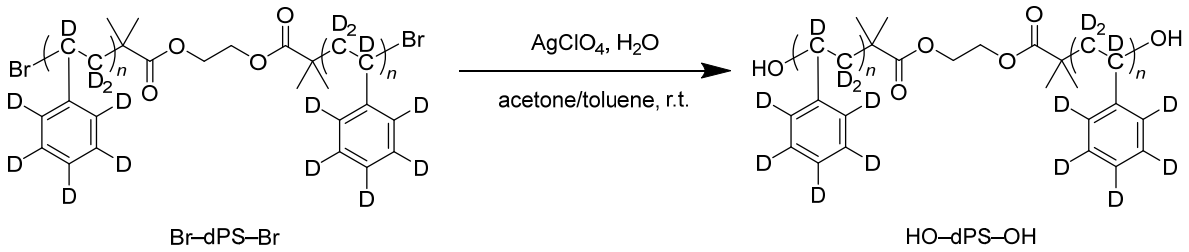

Method B was used for the reaction of Br–dPS$_{10k}$–Br ($M_{n,SEC}$ =11,200, 6.00 g, 536 μmol, 1 eq.) with $AgClO_4$ (267 mg, 1.29 mmol, 2.4 eq.) in a mixed solvent of acetone and toluene (96.0 mL, v/v = 5:3) for overnight to give HO–dPS$_{10k}$–OH as a white solid. Yield: 5.68 g (94.7%)

$M_{n,SEC}$ = 11,400 (THF), $Đ$ = 1.07 (THF)

^{1}H NMR ($CDCl_3$, 400 MHz): δ(ppm) 3.44–3.01 (br, 4H, –(CH_2)$_2$OC(=O)–), 0.99–0.74 (m, 12H, –OC(=O)C(CH_3)$_2$–).

Method B was used for the reaction of Br–dPS$_{35k}$–Br ($M_{n,SEC}$ =32,600, 4.46 g, 142 μmol, 1 eq.) with $AgClO_4$ (70.5 mg, 340 μmol, 2.4 eq.) in a mixed solvent of acetone and toluene (73.9 mL, v/v = 5:3) for overnight to give HO–dPS$_{35k}$–OH as a white solid. Yield: 4.55 g (98.5%)

$M_{n,SEC}$ = 32,800 (THF), $Đ$ = 1.10 (THF)

Synthesis of deuterated polystyrene bearing *α*,*ω*-norbornenyl end groups (NB–dPS–NB)

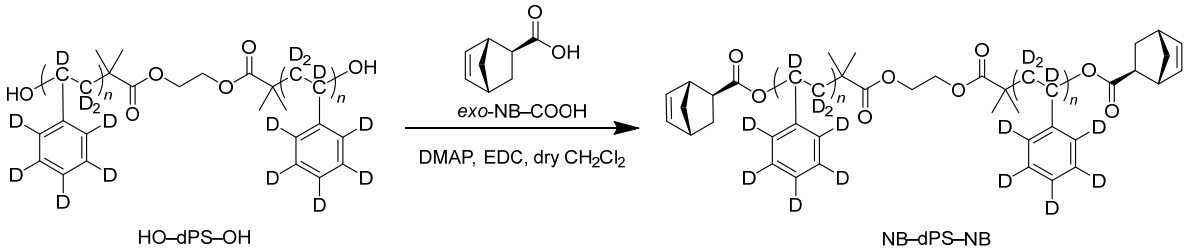

Method C was used for the reaction of HO–dPS$_{10k}$–OH ($M_{n,NMR}$ = 11,400, 5.50 g, 482 μmol, 1 eq.) with *exo*-NB–COOH (267 mg, 1.93 mmol, 4 eq.), DMAP (354 mg, 2.89 mmol, 6 eq.), and EDC (555 mg, 2.89 mmol, 6 eq.) in CH_2Cl_2 (55.0 mL) for 96 h to give NB–dPS$_{10k}$–NB as a white solid. Note that this sample was purified by preparative SEC in order to isolate a fraction of NB–dPS$_{10k}$–NB. Yield: 5.35 g (97.3%)

$M_{n,SEC}$ = 10,000 (THF), $Đ$ = 1.07 (THF), $M_{n,MALS}$ = 10,300, $Đ_{MALS}$ = 1.03

^{1}H NMR ($CDCl_3$, 400 MHz): δ(ppm) 6.17–6.00 (m, 4H, –C*H*=C*H*– in norbornene ring), 3.44–2.76 (br, 8H, –(C*H*$_2$)$_2$OC(=O)–, –C*H*–CH$_2$–CH–CO– in norbornene ring, –C*H*–CH–CO– in norbornene ring), 2.53–1.69 (m, –CH$_2$C*H*Ph–, *endo*-C*H*– of –CH–CH$_2$–CH–C*H*CO– in norbornene ring, *exo*-C*H*– of –CH–C*H*$_2$–CH–CO– in norbornene ring), 0.99–0.74 (m, 12H, –OC(=O)C(C*H*$_3$)$_2$–).

Method C was used for the reaction of HO–dPS$_{35k}$–OH ($M_{n,SEC}$ = 32,800, 4.40 g, 135 μmol, 1 eq.) with *exo*-NB–COOH (74.6 mg, 540 μmol, 4 eq.), DMAP (98.9 mg, 810 μmol, 6 eq.), and EDC (155 mg, 810 μmol, 6 eq.) in CH_2Cl_2 (44.0 mL) for 120 h to give NB–dPS$_{35k}$–NB as a white solid. Yield: 4.06 g (92.3%)

$M_{n,SEC}$ = 34,100 (THF), $Đ$ = 1.09 (THF), $M_{n,MALS}$ = 36,300, $Đ_{MALS}$ = 1.03

Synthesis of multicyclic polystyrene (mc-PS)

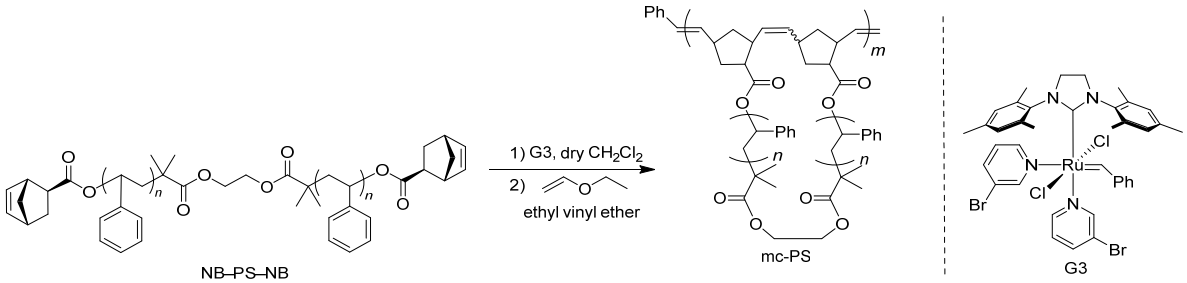

A typical procedure for the ring-opening metathesis polymerization (ROMP) is as follows (Method D): In a three-necked flask, a stock solution of Grubbs third-generation catalyst (G3; 6.25 mL, 50.0 μmol as a 8.0 mol L^{-1} in dry CH_2Cl_2, 1.0 eq.) was quickly added to a stirred mixture of NB–PS_{10k}–NB ($M_{n,MALS}$ = 10,000, 1.50 g, 150 μmol, 3.0 eq.) in dry CH_2Cl_2 (1.00 L) under an argon atmosphere. After 1.5 h, an excess amount of ethyl vinyl ether was added to the reacting mixture to terminate the ROMP. The crude product was purified by preparative SEC, affording 4c-PS_{10k} as a brown solid. Yield: 631 mg (42.1%)

$M_{n,SEC}$ = 25,200 (THF), $Đ$ = 1.07 (THF), $M_{n,SEC}$ = 21,700 ($CHCl_3$), $M_{n,MALS}$ = 35,700, $Đ_{MALS}$ = 1.05, average number of cyclic units = 3.6

Method D was used for the ROMP of NB–PS_{10k}–NB (2.00 g, 200 μmol, 9.0 eq.) with G3 (2.78 mL, 22.2 μmol as a 8.0 mol L^{-1} in dry CH_2Cl_2, 1.0 eq.) in dry CH_2Cl_2 (1.33 mL) for 9.0 h to give 7c-PS_{10k} as a brouwn solid. Yield: 551 mg (27.6%)

$M_{n,SEC}$ = 36,700 (THF), $Đ$ = 1.08 (THF), $M_{n,SEC}$ = 31,500 ($CHCl_3$), $M_{n,MALS}$ = 70,900, $Đ_{MALS}$ = 1.03, average number of cyclic units = 7.1

Method D was used for the ROMP of NB–PS_{35k}–NB ($M_{n,MALS}$ = 35,300, 3.98 g, 113 μmol, 3.0 eq.) with G3 (4.70 mL, 37.6 μmol as a 8.0 mol L^{-1} in dry CH_2Cl_2, 1.0 eq.) in dry CH_2Cl_2 (752 mL) for 4.5 h. The crude product was subjected to preparative SEC to fractionate the mixture based on molecular weight, affording three distinct fractions, designated as 3c-PS_{35k}, 4c-PS_{35k}, and 8c-PS_{35k}.

3c-PS_{35k}: $M_{n,SEC}$ = 77,500 (THF), $Đ$ = 1.07 (THF), $M_{n,SEC}$ = 58,600 ($CHCl_3$), $M_{n,MALS}$ = 88,800, $Đ_{MALS}$ = 1.05, average number of cyclic units = 2.5, yield = 556 mg

4c-PS_{35k}: $M_{n,SEC}$ = 130,400 (THF), $Đ$ = 1.08 (THF), $M_{n,SEC}$ = 86,800 ($CHCl_3$), $M_{n,MALS}$ = 155,000, $Đ_{MALS}$ = 1.02, average number of cyclic units = 4.4, yield = 632 mg

8c-PS_{35k}: $M_{n,SEC}$ = 220,900 (THF), $Đ$ = 1.17 (THF), $M_{n,SEC}$ = 130,300 ($CHCl_3$), $M_{n,MALS}$ = 279,300, $Đ_{MALS}$ = 1.05, average number of cyclic units = 7.9, yield = 519 mg

Synthesis of deuterated multicyclic polystyrene (mc-dPS)

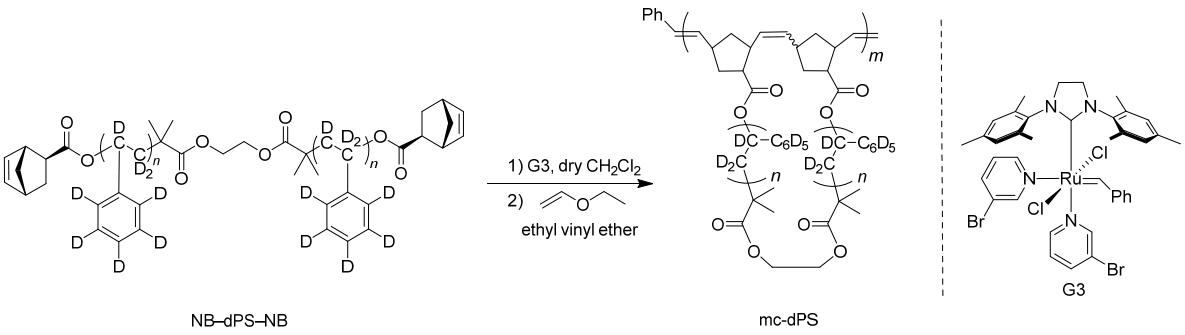

Method D was used for the ROMP of NB–dPS$_{10k}$–NB ($M_{n,MALS}$ = 10,200, 1.50 g, 147 μmol, 1.0 eq.) with G3 (6.10 mL, 43.4 μmol as a 8.0 mol L^{-1} in dry CH_2Cl_2, 1.0 eq.) in dry CH_2Cl_2 (980 mL) for 1.5 h to give 4c-dPS$_{10k}$ as a brown solid. Yield: 518 mg (34.5%)
$M_{n,SEC}$ = 26,000 (THF), $Đ$ = 1.07 (THF), $M_{n,SEC}$ = 23,000 ($CHCl_3$), $M_{n,MALS}$ = 35,700, $Đ_{MALS}$ = 1.01, average number of cyclic units = 3.5

Method D was used for the ROMP of NB–dPS$_{10k}$–NB (2.00 g, 190 μmol, 9.0 eq.) with G3 (2.65 mL, 21.1 μmol as a 8.0 mol L^{-1} in dry CH_2Cl_2, 1.0 eq.) in dry CH_2Cl_2 (1.27 L) for 9.0 h to give 7c-dPS$_{10k}$ as a brouwn solid. Yield: 771 mg (38.6%)
$M_{n,SEC}$ = 36,300 (THF), $Đ$ = 1.14 (THF), $M_{n,SEC}$ = 31,100 ($CHCl_3$), $M_{n,MALS}$ = 70,600, $Đ_{MALS}$ = 1.07, average number of cyclic units = 6.7

Method D was used for the ROMP of NB–dPS$_{35k}$–NB ($M_{n,MALS}$ = 36,300, 3.00 g, 82.6 μmol, 3.0 eq.) with G3 (3.44 mL, 27.5 μmol as a 8.0 mol L^{-1} in dry CH_2Cl_2, 1.0 eq.) in dry CH_2Cl_2 (551 mL) for 9.0 h. The crude product was subjected to preparative SEC to fractionate the mixture based on molecular weight, affording three distinct fractions, designated as 3c-dPS$_{35k}$, 4c-dPS$_{35k}$, and 8c-dPS$_{35k}$.

3c-dPS$_{35k}$: $M_{n,SEC}$ = 79,300 (THF), $Đ$ = 1.09 (THF), $M_{n,SEC}$ = 59,200 ($CHCl_3$), $M_{n,MALS}$ = 99,300, $Đ_{MALS}$ = 1.02, average number of cyclic units = 2.7, yield = 284 mg

4c-dPS$_{35k}$: $M_{n,SEC}$ = 137,500 (THF), $Đ$ = 1.10 (THF), $M_{n,SEC}$ = 91,800 ($CHCl_3$), $M_{n,MALS}$ = 158,000, $Đ_{MALS}$ = 1.02, average number of cyclic units = 4.4, yield = 325 mg

8c-dPS$_{35k}$: $M_{n,SEC}$ = 230,300 (THF), $Đ$ = 1.17 (THF), $M_{n,SEC}$ = 157,300 ($CHCl_3$), $M_{n,MALS}$ = 303,200, $Đ_{MALS}$ = 1.07, average number of cyclic units = 8.4, yield = 391 mg

Synthesis of *h*/*d*-random linear PS (*h*/*d*-linear PS)

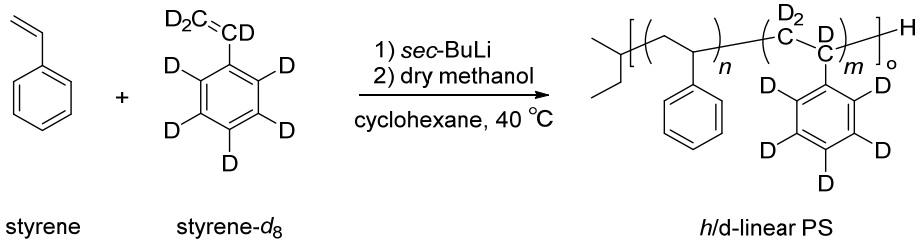

Under Ar atmosphere, cyclohexane (31.7 mL) was placed in a round-bottom flask equipped with a greaseless valve and then heated to 40 °C in an oil bath. *sec*-BuLi (55.0 μL, 66.0 μmol) was added to the solution. A mixture of styrene (2.04 mL, 17.4 mmol) and styrene-d_8 (2.04 mL, 17.4 mmol) was added to the solution, and the mixture was stirred for 2 h. Excess dry methanol was added to terminate the polymerization. The product was purified by reprecipitation in methanol to give *h*/*d*-linear PS as a white solid. Yield: 3.67 g (99.2%)

$M_{n,SEC}$ = 43,900 (THF), $Đ$ = 1.06 (THF)

^{1}H NMR ($CDCl_3$, 400 MHz): δ (ppm) 7.22–6.22 (m, *aromatic*), 2.23–1.66 (m, –CH_2CHPh–), 1.66–1.21 (m, –CH_2CHPh–), 0.89–0.77 (m, –*sec*-butyl).

4.3 Results and Discussion

4.3.1 Synthesis of the macromonomer

As outlined in **Scheme 4.1**, NB–PS–NB was synthesized as a macromonomer for use in the cyclopolymerization reaction. In the previous study describes in Chapter 2 and 3, commercially available HO–PS–OH, which was synthesized via living anionic polymerization followed by end-group transformation, was employed as the starting material. In contrast, in the current approach, ATRP (step A) was employed to access Br–PS–Br. This ATRP route provides precise control over the molecular weight and chain-end fidelity while dispensing with the rigorously anhydrous conditions and highly basic reagents that are commonly required for anionic polymerization. Moreover, this approach is readily scalable, broadly tolerant of functional groups, and translates directly to deuterated styrene under identical conditions.[43] The polymerization step was carried out in a mixture of anisole/dry DMF at 90 ºC, using EBBiB as a difunctional initiator and CuBr/$CuBr_2$/PMDETA as a catalyst. The reaction was stopped at a monomer conversion of ~30% to ensure the quantitative introduction of bromine groups at both chain ends. To obtain NB–PS–NB, the obtained Br–PS–Br was subjected to a two-step end-group modification protocol, including nucleophilic substitution with silver(I) perchlorate and water in acetone/toluene at room temperature to produce HO–PS–OH (step B), followed by esterification with *exo*-NB–COOH in CH_2Cl_2 in the presence of DMAP and EDC at room temperature (step C).

Scheme 4.1. The three-step synthetic route to NB–PS–NB

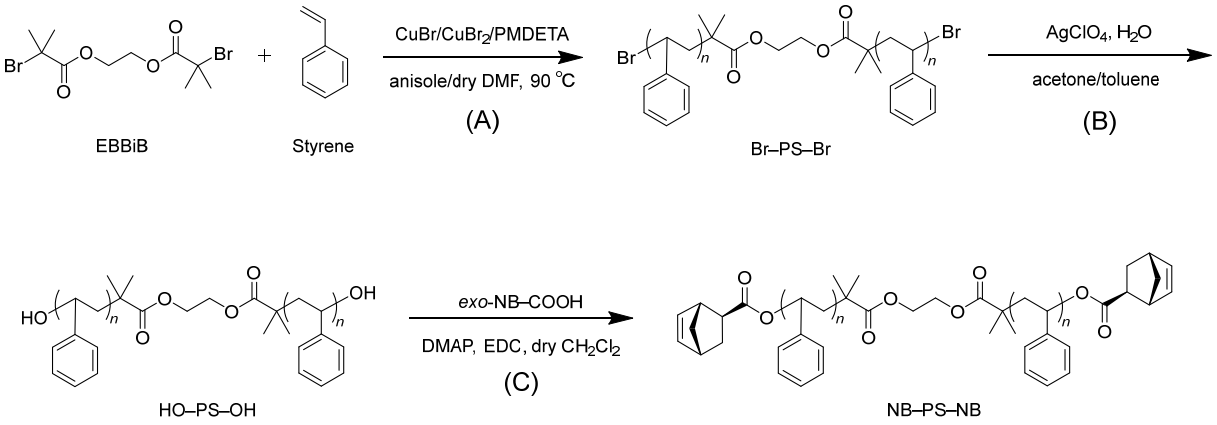

To confirm the end-group transformation reactions, NB–PS–NB with a number-average molecular weight of ~6,000 was initially synthesized as a model compound and subjected to structural characterization. The model macromonomer was intentionally designed with a suitable chain length to enable unambiguous tracking of each end-group transformation step using nuclear magnetic resonance (NMR) spectroscopy. In the ^{1}H NMR spectrum of Br–PS_{6k}–Br, in addition to the aromatic and benzylic protons arising from the main chain, characteristic signals corresponding to the bromine-adjacent protons at both the initiating and terminating ends were clearly observed (**Figure 4.1a**). Notably, the integral ratio of the ester methylene protons at the initiating end (δ = 3.4–3.0 ppm) to the ω-benzylic protons at the terminating end (δ = 4.6–4.3 ppm) was 1.96:4.00, which is in good agreement with the theoretical value of 2.00:4.00. This result demonstrates the efficient incorporation of bromine groups at both termini, confirming that the end-group structure was precisely controlled by ATRP. Transformations in the end-group structure caused by nucleophilic substitution and subsequent esterification were confirmed by the corresponding chemical shift changes in the benzylic protons. Specifically, upon conversion to HO–PS_{6k}–OH, the benzylic proton signals

shifted upfield (δ = 4.4–4.0 ppm), and after esterification to generate NB–PS_{6k}–NB, they shifted downfield (δ = 5.6–5.1 ppm). These stepwise changes indicated that each transformation proceeded selectively and quantitatively. Moreover, characteristic signals attributed to the olefinic protons of the norbornenyl groups were observed at δ = 6.3–5.9 ppm. The integral ratio between these signals and those of the initiator-derived protons was consistent with the theoretical value, indicating the complete introduction of norbornenyl groups at both chain ends. ^{13}C NMR spectroscopy also confirmed the quantitative nature of each reaction step, as evidenced by a shift in the benzylic carbon signal at the terminating end from 53.0–52.0 ppm in Br–PS_{6k}–Br to 73.5–72.5 ppm in HO–PS_{6k}–OH, and further to 74.0–73.5 ppm in NB–PS_{6k}–NB (Figure 4.1b). Matrix-assisted laser desorption/ionization time-of-flight mass spectrometry (MALDI-TOF MS) was used to verify the structure of the model macromonomer (Figure 4.1c). Due to potential end-group cleavage under laser irradiation, particularly in the case of the bromine-terminated (Br–PS_{6k}–Br) and norbornenyl-functionalized (NB–PS_{6k}–NB) species, structural analysis was conducted exclusively on HO–PS_{6k}–OH. The resulting spectrum displayed a series of repeated peaks with intervals of ~104 Da, corresponding to the repeating PS units. Among the observed peaks, the peak at m/z = 5960.64 closely matched the calculated mass for the HO–PS–OH with degree of polymerization n = 54 ($[M + Ag]^+$ = 5960.40). This excellent agreement strongly supports the structural assignment of the polymer as HO–PS_{6k}–OH. Collectively, these results demonstrated that the sequence of end-group transformation reactions, from bromination to hydroxylation, followed by esterification, proceeded in a highly selective and quantitative manner for the model macromonomer. The combination of ^{1}H and ^{13}C NMR analyses provided clear evidence of the successful introduction and transformation of functional end groups, whereas MALDI-TOF MS further confirmed the expected molecular

structure and the narrowly dispersed nature of the polymer. These findings validate the synthetic strategy and establish a robust foundation for the preparation of high-molecular-weight NB–PS–NB precursors for subsequent cyclopolymerization.

(a) ^{1}H NMR

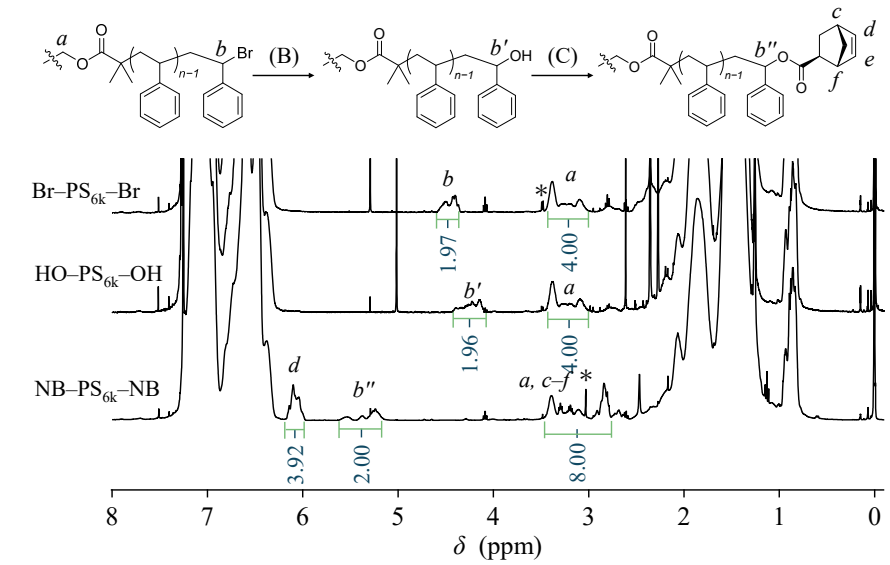

(b) ^{13}C NMR

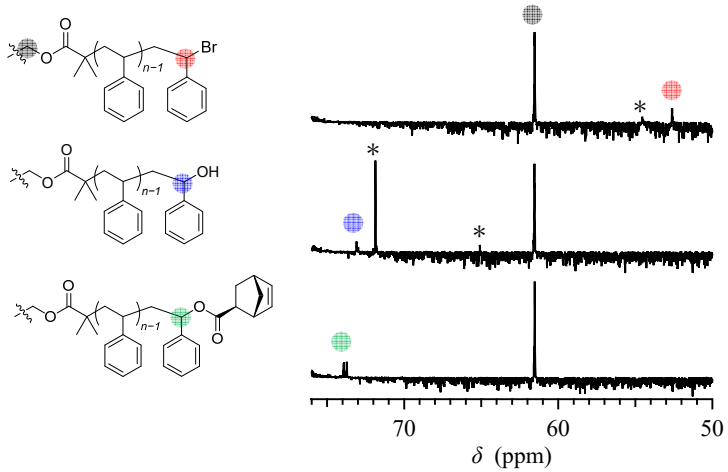

(c) MALDI-TOF MS

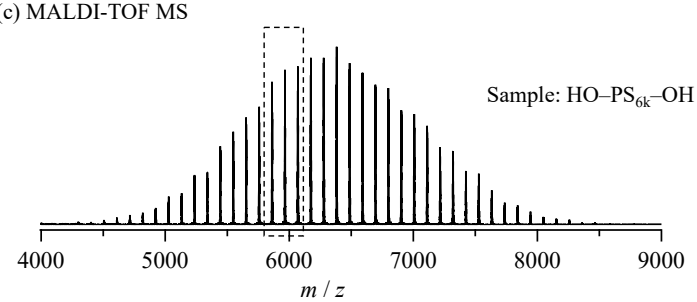

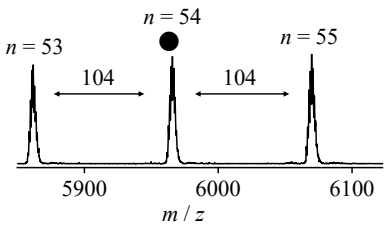

Calculated and observed M.W. $[M + Ag]^{+}$

	$n = 53$	$n = 54$	$n = 55$
Calculated M.W.	5856.33	5960.40	6064.46
Observed M.W.	5856.4	5960.6	6064.8

Figure 4.1. Structure analysis of NB–PS_{6k}–NB. (a) ^{1}H NMR spectra recorded for the Br–PS_{6k}–Br (upper), HO–PS_{6k}–OH (middle), and NB–PS_{6k}–NB (lower) species in $CDCl_3$ (400 MHz). (b) ^{13}C NMR spectra recorded for the Br–PS_{6k}–Br (upper), HO–PS_{6k}–OH (middle), and NB–PS_{6k}–NB (lower) species in $CDCl_3$ (100 MHz). The asterisks denote impurities. (c) MALDI-TOF MS analysis of HO–PS_{6k}–OH.

Building on these promising results, NB–PS–NB macromonomers with higher molecular weights (M_n = 10k and 35k) were subsequently synthesized for use in the cyclopolymerization reactions (**Table 4.1**). The introduction of norbornenyl groups at both termini was again confirmed to be quantitative by ^{1}H NMR spectroscopy (**Figures 4.2–4.7**), indicating that the optimized end-group transformation protocol could be reliably extended to higher molecular weight precursors. In addition, MALDI-TOF MS analysis was conducted on the 10k sample, and the observed molecular ion peak matched well with the theoretical mass of HO–PS_{10k}–OH, further supporting the successful synthesis and structural integrity of the macromonomer (**Figure 4.8**). However, MALDI-TOF MS analysis could not be performed for the 35k sample because of limitations in the ionization efficiency associated with its high molecular weight. These well-defined NB–PS_x–NB (x = 10k and 35k) macromonomers served as key building blocks for the synthesis of mc-PS with controlled ring sizes and architectures.

Table 4.1. Molecular characterization of the PS macromonomers

Sample	$M_{n,NMR}$	$M_{n,SEC}$ [a]	$Đ$ [a]	$M_{n,MALS}$ [b]
NB–PS_{10k}–NB	9,400	9,500	1.07	10,000
NB–dPS_{10k}–NB	-	10,000	1.07	10,300
NB–PS_{35k}–NB	32,300	33,200	1.19	35,300
NB–dPS_{35k}–NB	-	34,100	1.09	36,400

[a] Determined by SEC in THF using PS as the standard. [b] Determined using triple-detection SEC equipped with multiangle light scattering, viscosity and refractive index detectors (SEC-MALS-Visco) in chloroform.

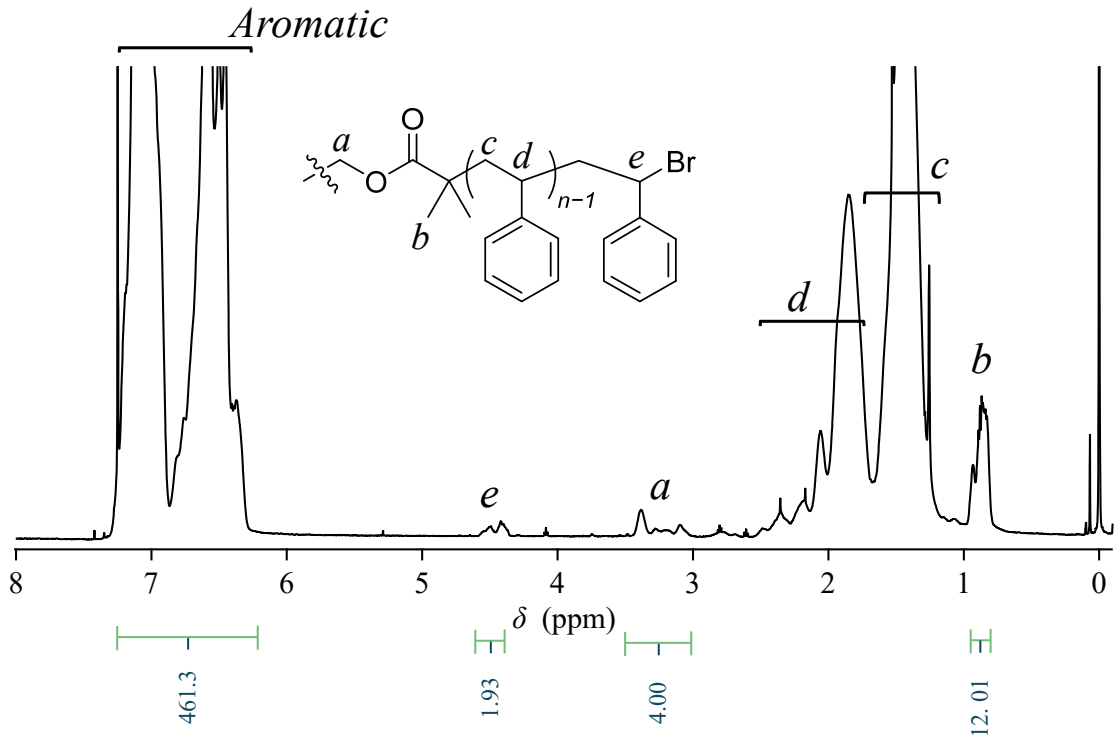

Figure 4.2. ^{1}H NMR spectrum of Br–PS_{10k}–Br in $CDCl_3$.

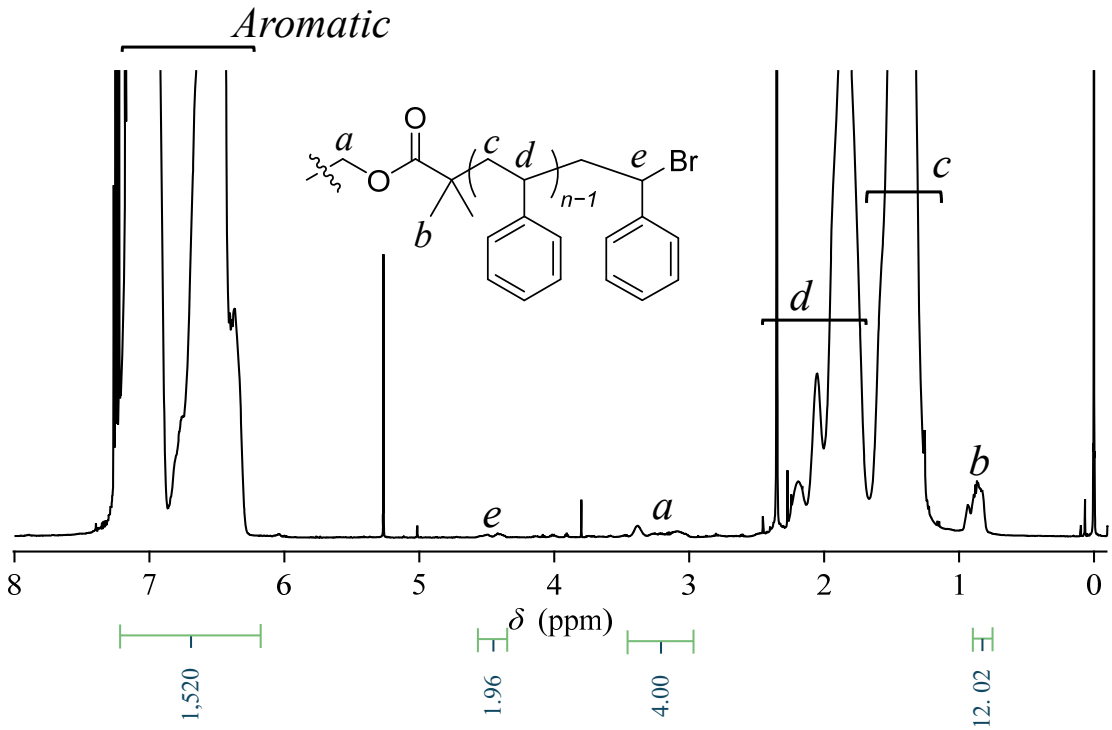

Figure 4.3. ^{1}H NMR spectrum of Br–PS_{35k}–Br in $CDCl_3$.

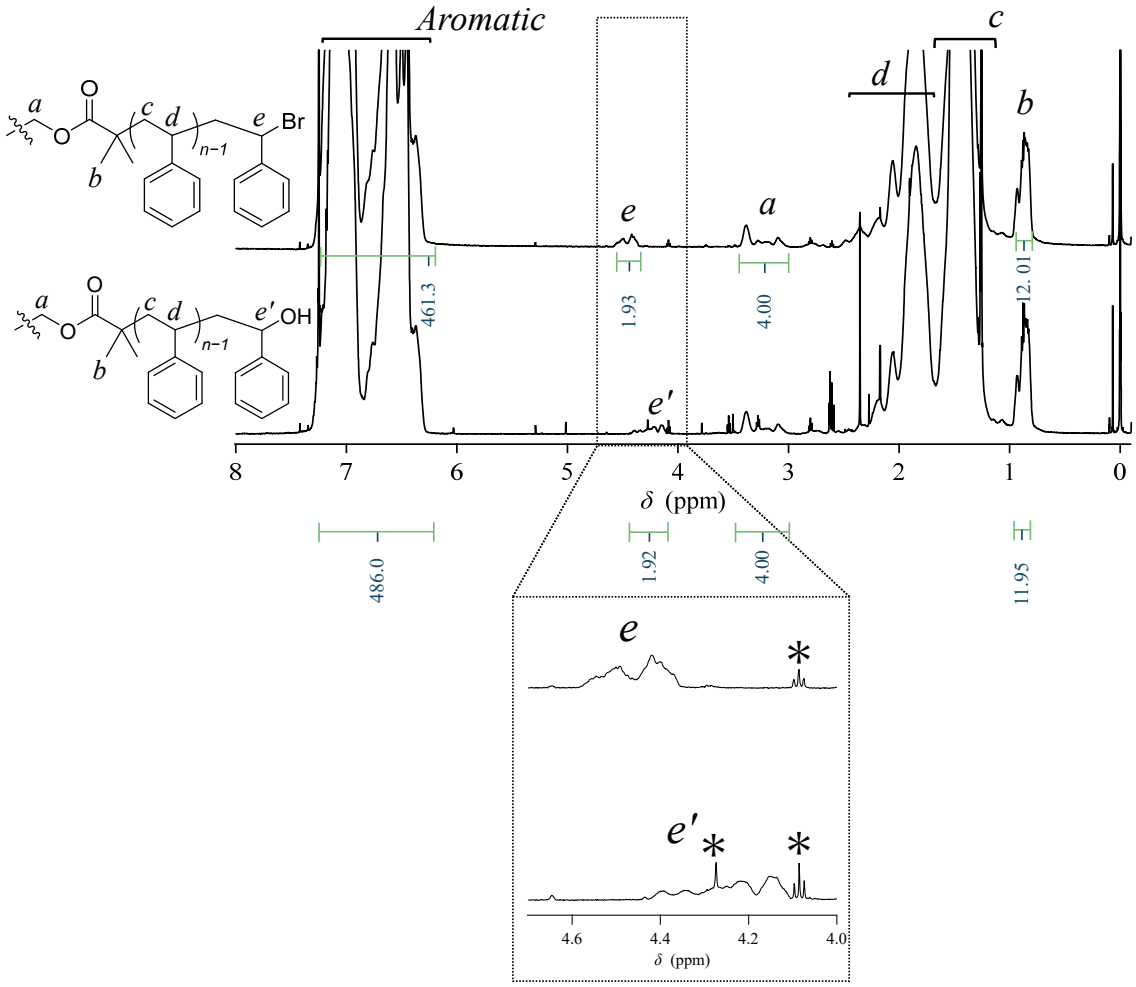

Figure 4.4. ^{1}H NMR spectra of Br–PS$_{10k}$–Br (upper) and HO–PS$_{10k}$–OH (lower) in $CDCl_3$. Astarisks denote impurities.

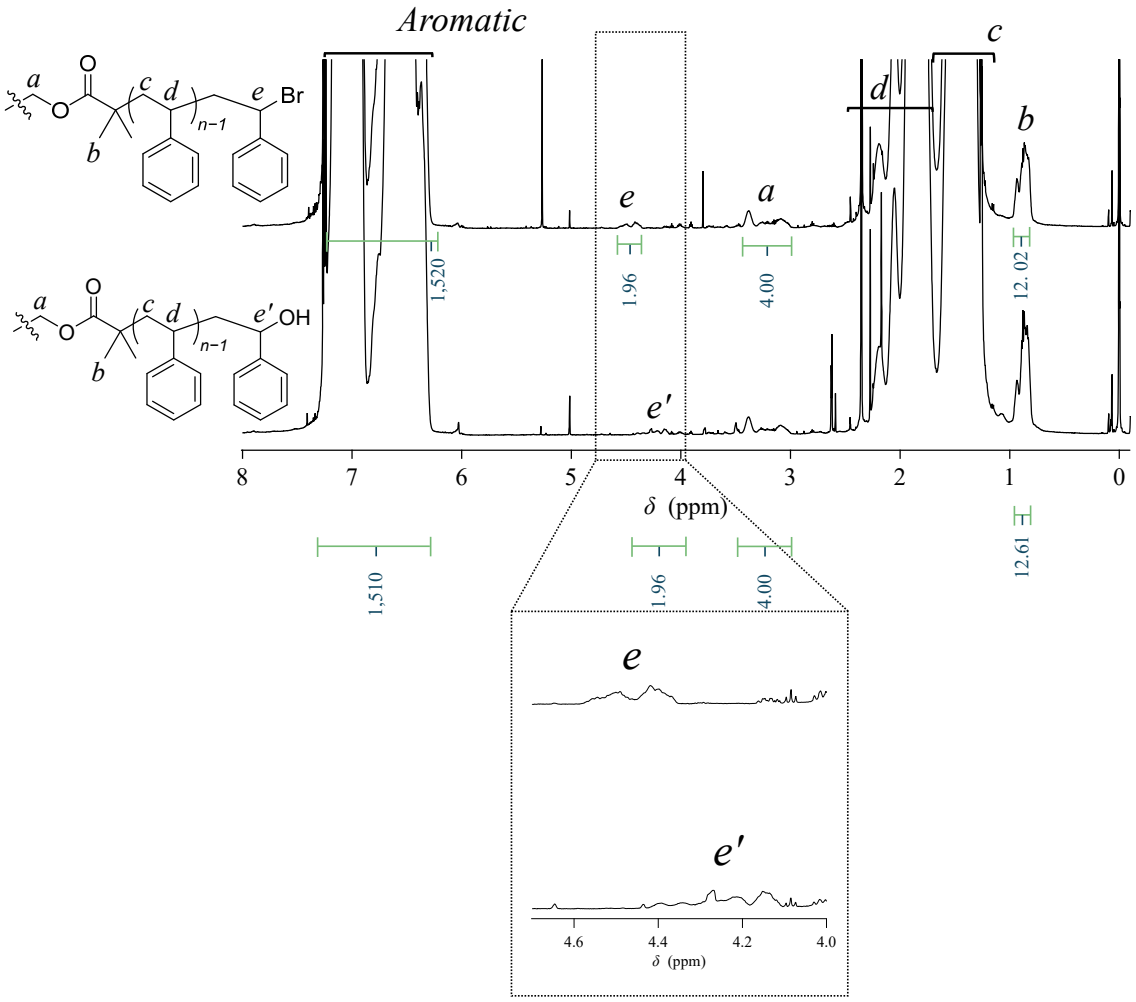

Figure 4.5. ^{1}H NMR spectra of Br–PS_{35k}–Br (upper) and HO–PS_{35k}–OH (lower) in $CDCl_3$. Astarisks denote impurities.

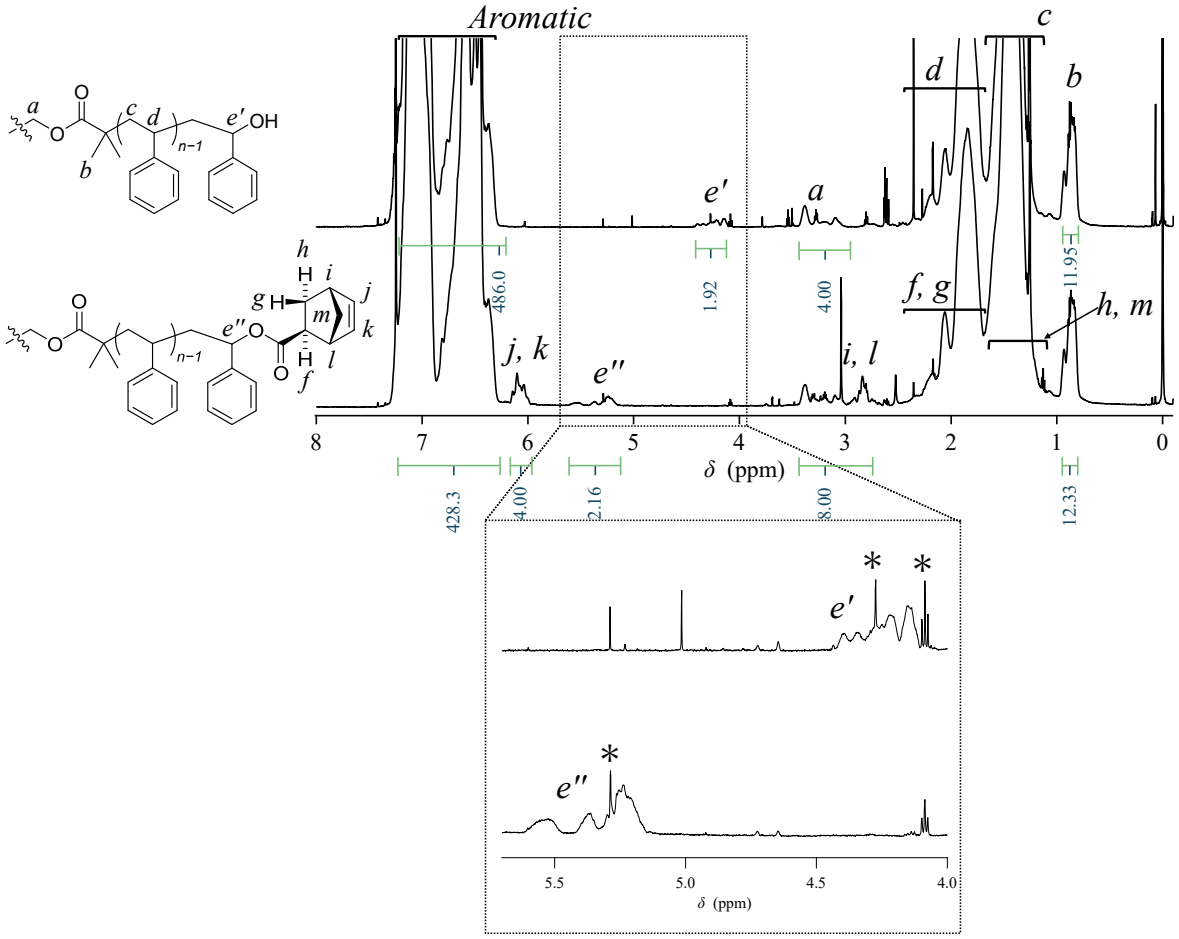

Figure 4.6. ^{1}H NMR spectra of HO–PS$_{10k}$–OH (upper) and NB–PS$_{10k}$–NB (lower) in $CDCl_3$. Asterisks denote impurities.

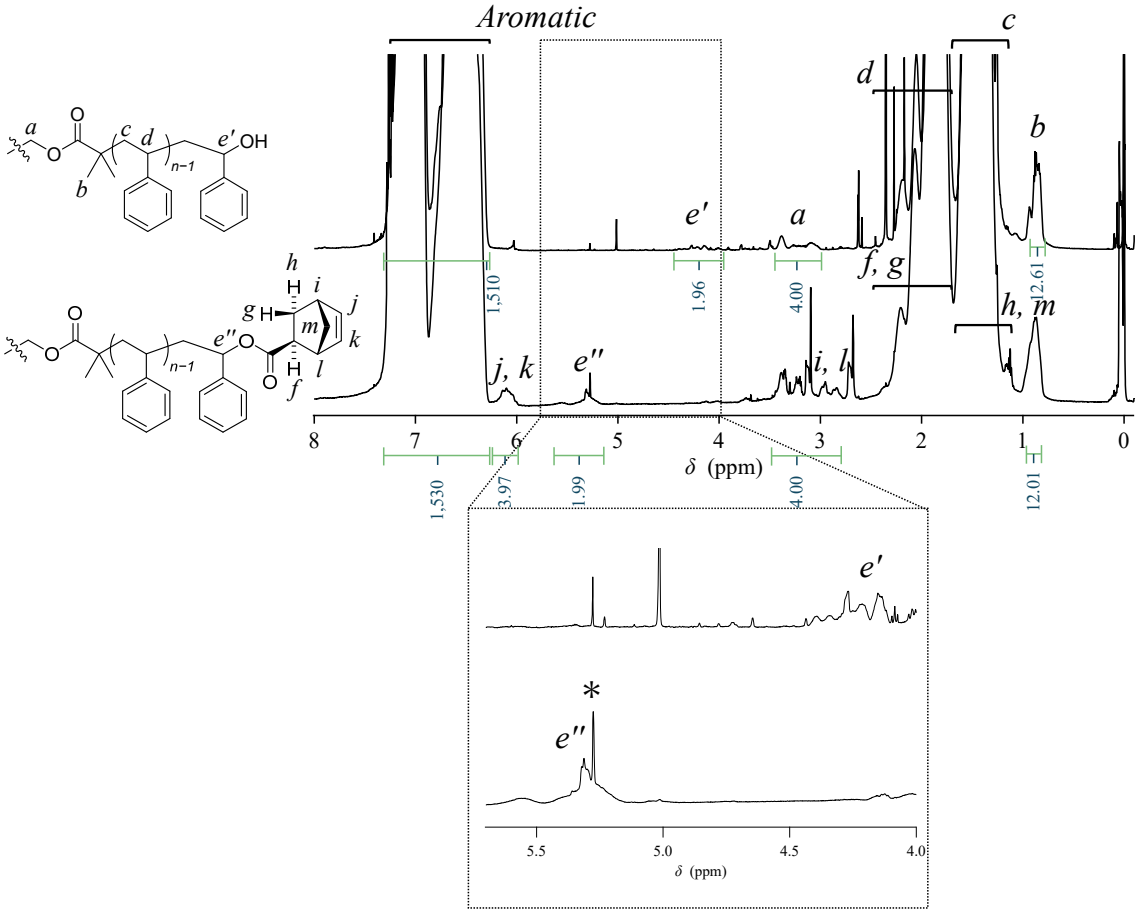

Figure 4.7. ^{1}H NMR spectra of HO–PS_{35k}–OH (upper) and NB–PS_{35k}–NB (lower) in $CDCl_3$. Asterisks denote impurities.

Sample: HO–PS_{10k}–OH

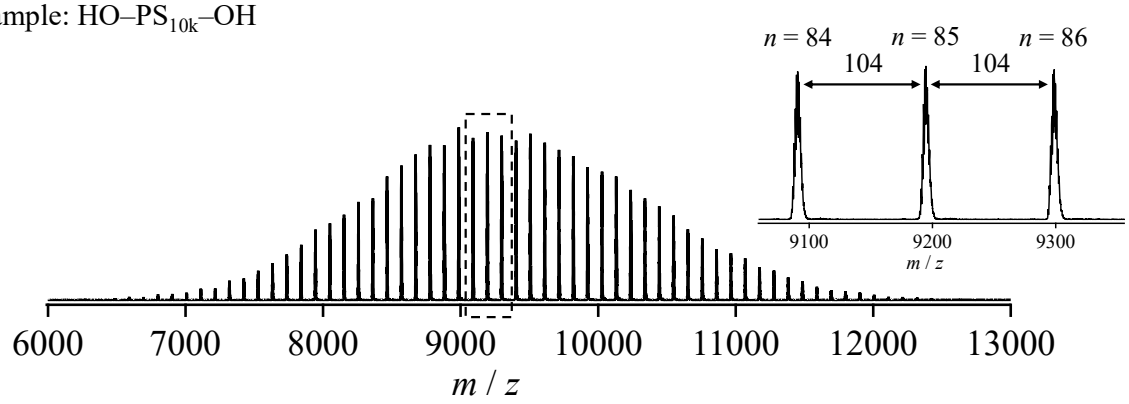

Calculated and observed M.W. $[M + Ag]^+$

	$n = 84$	$n = 85$	$n = 86$
Calculated M.W.	9082.27	9186.34	9290.40
Observed M.W.	9083.5	9188.3	9292.4

Figure 4.8. MALDI-TOF MS analysis of HO–PS_{10k}–OH.

The above synthetic strategy was subsequently applied to the deuterated PS macromonomers (NB–dPS–NB), which were designed to have molecular weights corresponding to those of NB–PS_x–NB (x = 10k and 35k). The preparation of these specimens was performed using styrene-d_8 as the monomer, whereas all other reagents and solvents were employed in their non-deuterated forms, following the same ATRP and end-group modification procedures optimized for the non-deuterated analogs. Structural analysis of the resulting NB–dPS–NB was performed using ^{1}H NMR spectroscopy (**Figures 4.9–4.10**). Although the bromobenzyl chain ends were not detectable due to deuterium substitution along the PS main chain, the integral ratio between the norbornenyl olefinic protons and the initiator-derived protons remained in close agreement with the theoretical value. This result confirms that the end-group transformations proceeded efficiently and quantitatively, even in the deuterated

system. In addition, MALDI-TOF MS analysis of the HO–dPS–OH sample (M_n = 10k) showed a series of repeated peaks with intervals of ~112 Da, consistent with the deuterated styrene repeat unit, and no discernible sub-peak series was observed, supporting high deuterium incorporation in the deuterated macromonomer (**Figure 4.11**). The remaining discrepancy between the calculated and observed masses is attributed primarily to a deuteration level lower than 100%, rather than to structural impurities. As in the non-deuterated case, MALDI-TOF MS could not be performed for the 35k sample because of the reduced ionization efficiency at high molecular weights.

Importantly, NB–PS–NB and NB–dPS–NB exhibited almost identical SEC retention times, suggesting that they possessed essentially equivalent molecular weights (**Figures 4.12–4.13**). Since hydrogenated and deuterated polymers with comparable degree of polymerization are known to show nearly identical SEC molecular weight[44] this result suggests that the two telechelic precursors prepared in this study possess essentially equivalent degrees of polymerization. This was corroborated by the absolute number-averaged molecular weights ($M_{n,MALS}$) obtained by multi-angle light scattering (MALS) analysis, which yielded comparable values for both samples. Accordingly, the mc-PS and mc-dPS specimens prepared from these macromonomers serve as appropriate model systems for accurately investigating the structural features by SANS, owing to their similar molecular weights per cyclic unit.

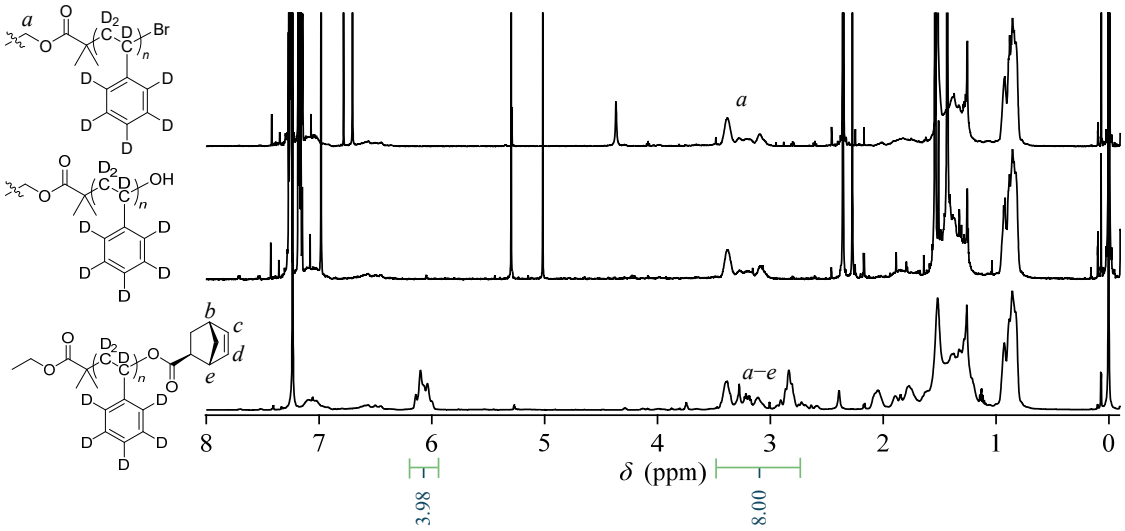

Figure 4.9. ^{1}H NMR spectra of Br–dPS$_{10k}$–Br (upper), HO–dPS$_{10k}$–OH (middle), and NB–dPS$_{10k}$–NB (lower) in $CDCl_3$.

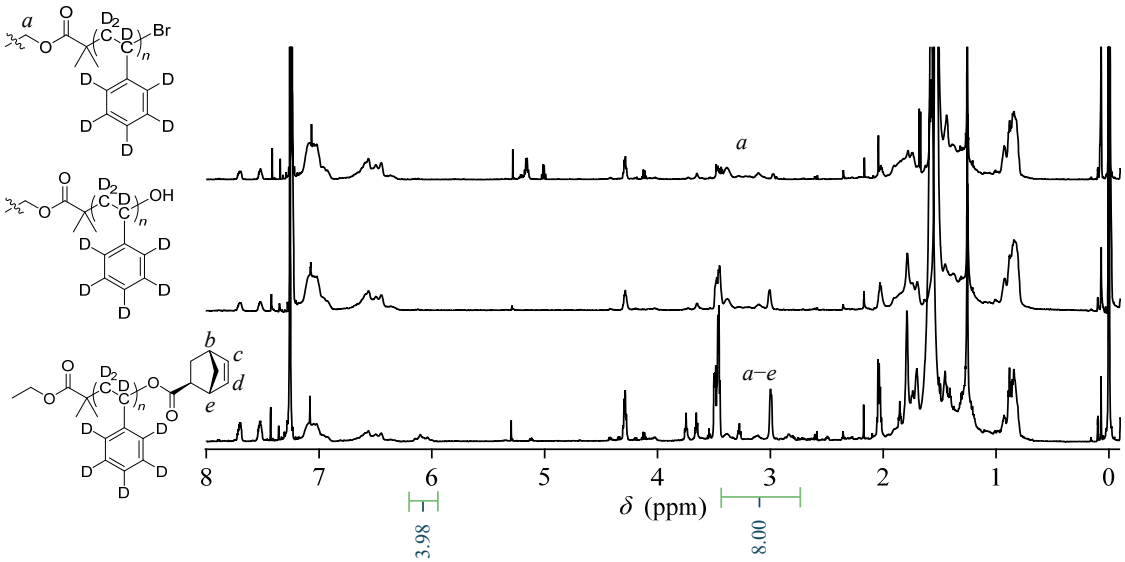

Figure 4.10. ^{1}H NMR spectra of Br–dPS$_{35k}$–Br (upper), HO–dPS$_{35k}$–OH (middle), and NB–dPS$_{10k}$–NB (lower) in $CDCl_3$.

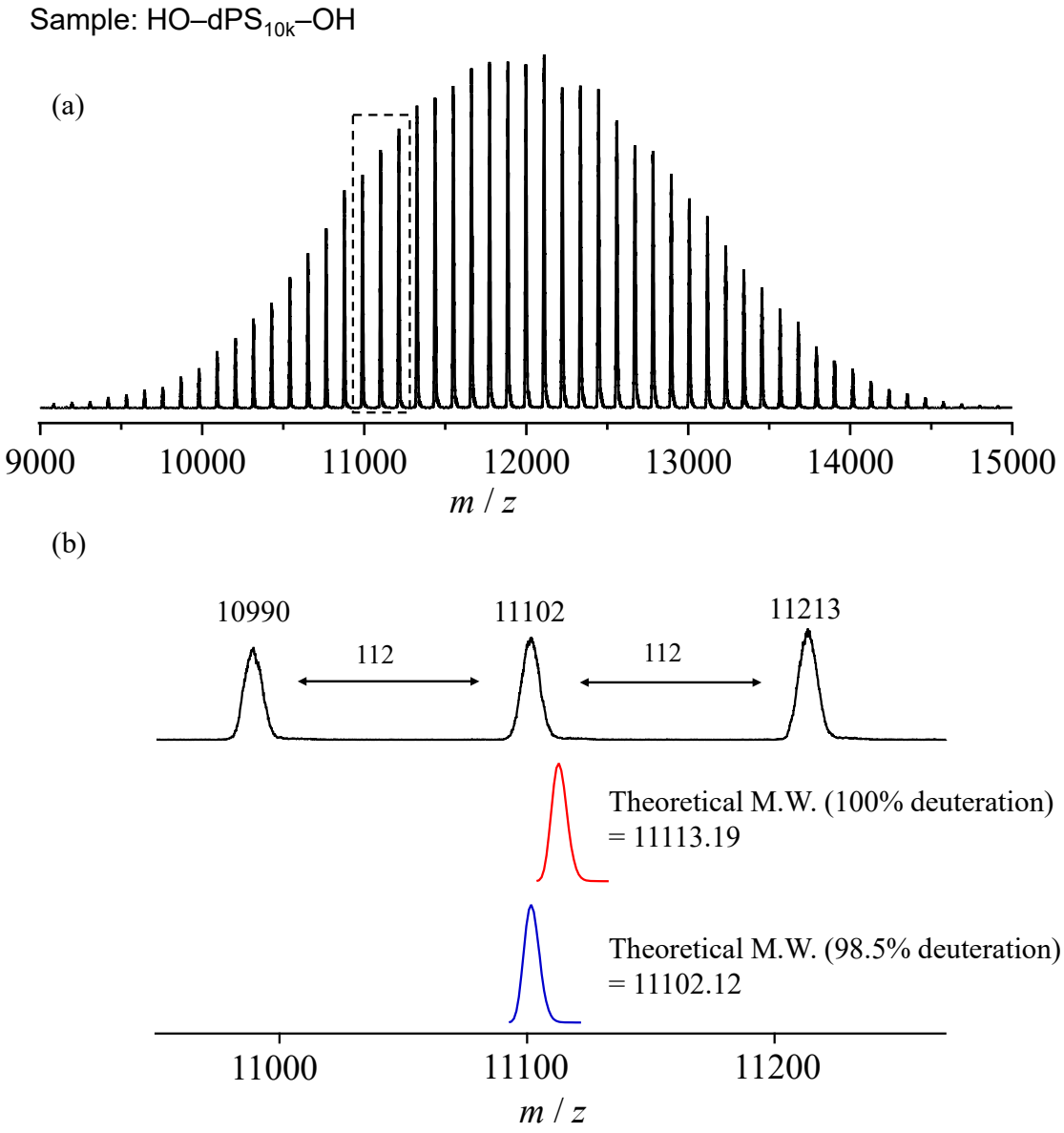

Figure 4.11. (a) MALDI-TOF MS analysis of HO–dPS$_{10k}$–OH. (b) The expanded spectrum overlaid with the theoretical isotopic distributions calculated for 100% ($C_{10}H_{18}O_6$–$(C_8D_8)_x$+Ag) (red) and 98.5% ($C_{10}H_{18}O_6$–$(C_8D_8)_x(C_8H_8)_{x-y}$+Ag) (blue) deuteration.

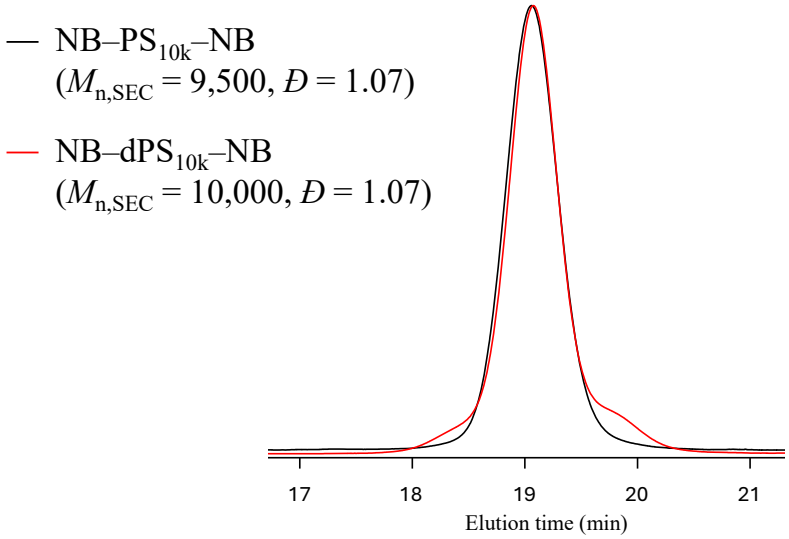

Figure 4.12. SEC traces of NB–PS$_{10k}$–NB (black) and NB–dPS$_{10k}$–NB (red) (refractive index (RI) detection; eluent, THF; flow rate, 1.0 mL min^{-1}).

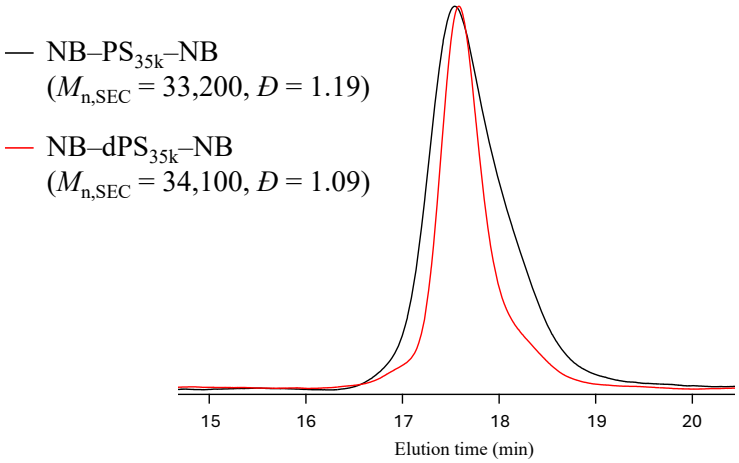

Figure 4.13. SEC traces of NB–PS$_{35k}$–NB (black) and NB–dPS$_{35k}$–NB (red) (refractive index (RI) detection; eluent, THF; flow rate, 1.0 mL min^{-1}).

4.3.2 Synthesis of hydrogenated multicyclic and deuterated multicyclic polystyrene

As outlined in **Scheme 4.2**, multicyclic polystyrene (mc-PS) was synthesized using a cyclopolymerization method established in Chapter 2. Specifically, the cyclopolymerization of NB–PS–NB was conducted in CH_2Cl_2 using the G3 catalyst to afford mc-PS. For the NB–PS–NB specimen with a molecular weight of ~10k, polymerization was carried out at initial concentration ratios of $[NB–PS_{10k}–NB]_0/[G3]_0$ = 3:1 or 6;1, whereas for the 35k macromonomer, a ratio of 3:1 was employed. One notable limitation of the cyclopolymerization method is that the resulting multicyclic polymers exhibit a broad distribution in the number of cyclic units, leading to relatively high dispersity (*Đ*). As shown in **Figure 4.14**, the SEC traces of the crude mc-PS show broad dispersity and multiple elution peaks. This heterogeneity was attributed to the presence of mc-PS species with different numbers of cyclic units. To address this issue, mc-PS was subjected to preparative SEC to fractionate the crude products into samples with a narrower distribution of cyclic units, thereby reducing the structural heterogeneity. Upon subjecting $NB–PS_{10k}–NB$ to cyclopolymerization under two the different initial concentration ratios defined above, preparative SEC yielded a single fraction with a relatively narrow distribution in the number of cyclic units in both cases, with *Đ* values of 1.05 and 1.08, respectively (**Figures 4.15a–4.15b** and **Table 4.2**). In the crude product obtained using a 3:1 ratio, the SEC trace indicated the presence of monocyclic by-products, which were completely removed during preparative SEC. In contrast, the crude product obtained using a 6:1 ratio contained unreacted macromonomers; however, SEC analysis confirmed that the isolated fraction was free of such unreacted species. In addition, $M_{n,MALS}$ indicated that these fractions contained, on average, approximately four and seven cyclic units, respectively. The average number of cyclic units in the obtained mc-PS was estimated by dividing the $M_{n,MALS}$ of mc-PS

by that of the corresponding macromonomer. In contrast, the cyclopolymerization of NB–PS_{35k}–NB under an initial $[NB–PS_{35k}–NB]_0/[G3]_0$ ratio of 3:1 afforded a single crude product, which was successfully separated by preparative SEC into three fractions that were estimated to contain approximately three, four, and eight cyclic units, respectively (**Figure 4.15c**). Each of these fractions was also confirmed to exhibit low dispersity ($Đ < 1.2$), further indicating that they possess a narrow distribution in the number of cyclic units and can be regarded as nearly monodisperse samples.

Scheme 4.2. Synthesis of (a) mc-PS and (b) mc-dPS via the cyclopolymerization approach

(a)

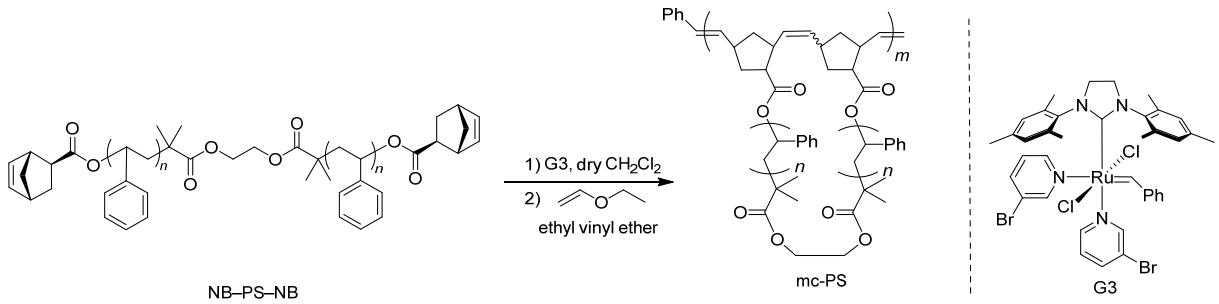

(b)

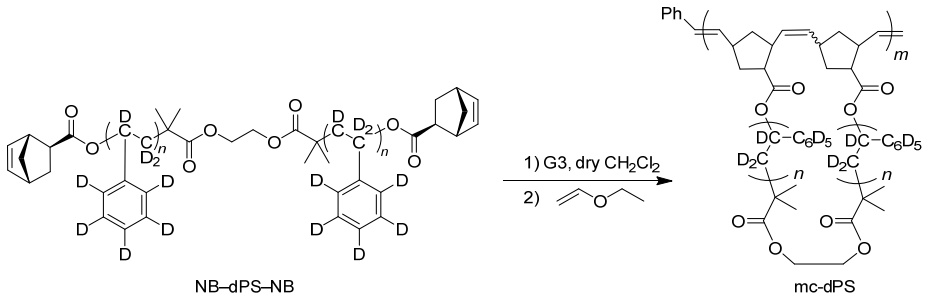

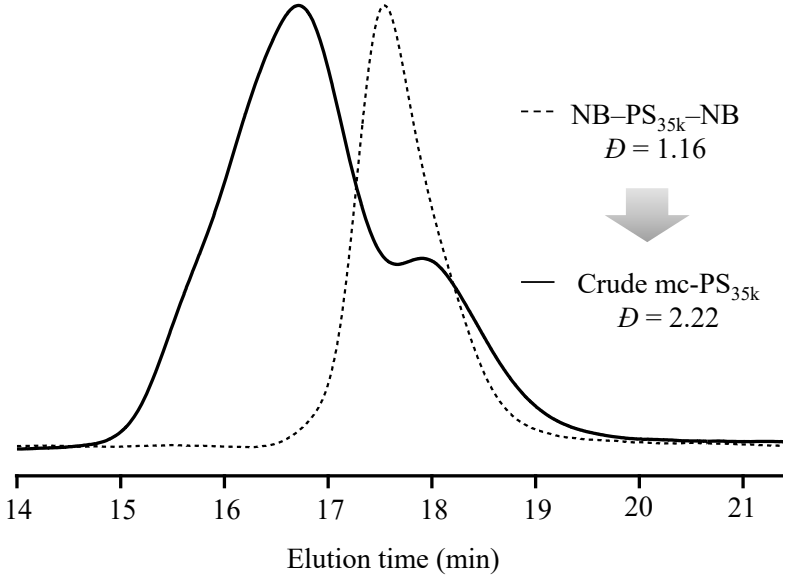

Figure 4.14. SEC traces recorded for the NB–PS_{35k}–NB (black solid line) and crude mc-PS_{35k} (black dotted line) specimens. The SEC measurements were performed using refractive index (RI) detection with THF as the eluent at a flow rate of 1.0 mL min^{-1}.

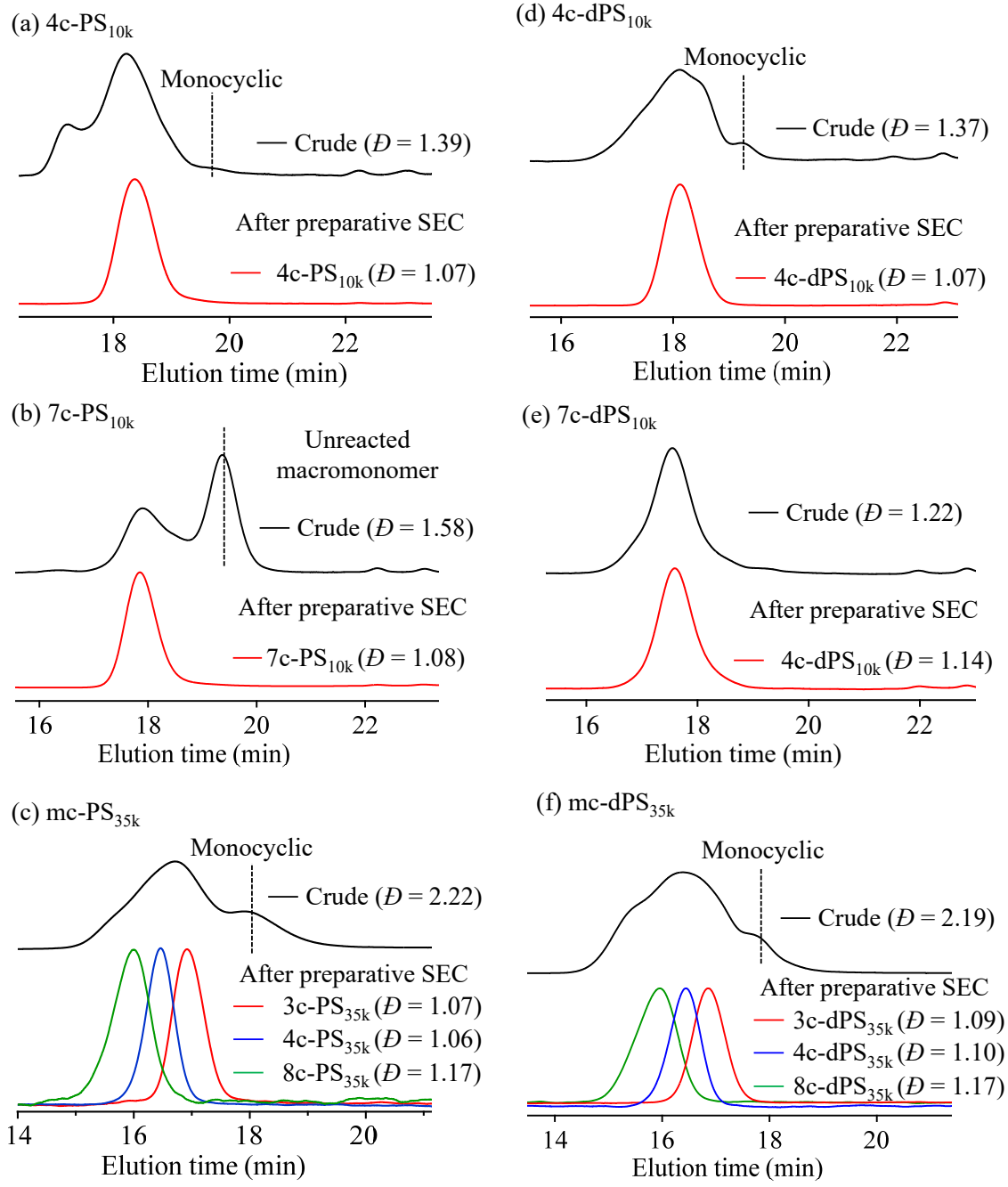

Figure 4.15. (a–c) SEC traces recorded for the crude mc-PS (upper) and mc-PS specimens after preparative SEC (lower). (d–f) SEC traces recorded for the crude mc-dPS (upper) and mc-dPS specimens after preparative SEC (lower). The SEC measurements were performed using RI detection with THF as the eluent at a flow rate of 1.0 mL min^{-1}.

Table 4.2. Molecular characterization of mc-PS and mc-dPS

Sample	$M_{n,SEC}$ [a]	$M_{n,MALS}$ [b]	$M_{n,MALS}$ for each ring [b]	Average number of cyclic units [c]	g_{sol} [d]
4c-PS$_{10k}$	21,700	35,700	10,000	3.6	0.61
4c-dPS$_{10k}$	23,000	35,700	10,300	3.5	0.64
7c-PS$_{10k}$	31,500	70,900	10,000	7.1	0.44
7c-dPS$_{10k}$	31,100	70,600	10,300	6.9	0.44
3c-PS$_{35k}$	58,600	88,800	35,300	2.5	0.66
3c-dPS$_{35k}$	59,200	99,300	36,300	2.7	0.60
4c-PS$_{35k}$	86,800	155,500	35,300	4.4	0.56
4c-dPS$_{35k}$	91,800	158,000	36,300	4.4	0.58
8c-PS$_{35k}$	130,300	279,300	35,300	7.9	0.47
8c-dPS$_{35k}$	157,300	303,200	36,300	8.4	0.52

[a]Determined by SEC in $CHCl_3$ using PS as the standard. [b]Determined using SEC-MALS-Visco in chloroform. [c]The average number of cycli c units in the obtained mc-PS was estimated as (M_n of mc-PS or mc-dPS)/(M_n of the corresponding macromonomer). [d]The apparent SEC-based contraction index (g_{sol}) was calculated as $g_{sol} = M_{n,\,SEC}$ ($CHCl_3$)/$M_{n,\,MALS}$ ($CHCl_3$).

It was subsequently considered that the obtained series of mc-PS may contain unexpected structural features, such as dangling chains arising from the reaction of only one norbornenyl group or crosslinked structures formed through intermolecular reactions involving such moieties. These structural irregularities are of concern because they may influence the physical properties of the resulting materials. Although the direct detection of such defect structures is challenging, indirect estimation is possible through careful analysis of the ^{1}H NMR spectrum. In fact, the ^{1}H NMR spectra of the samples after cyclopolymerization contained no signals corresponding to the norbornenyl groups, suggesting that the number of dangling chains

was negligible (**Figures 4.16–4.17**). In addition, the ^{1}H NMR spectra after cyclopolymerization exhibited signals assignable to (i) internal olefinic protons and (ii) terminal groups generated upon quenching of G3 with ethyl vinyl ether. These features are consistent with the progress of the underlying ROMP elementary steps during cyclopolymerization. Moreover, although the presence of dangling chains can eventually result in gelation during cyclopolymerization, all mc-PS samples were found to be completely soluble. These findings indicate that the use of highly dilute conditions selectively enables alternating intramolecular cyclization and subsequent intermolecular propagation, leading to a well-defined multicyclic architecture.

Additionally, deuterated mc-PS (mc-dPS) was also successfully synthesized using the deuterated macromonomer NB–dPS–NB via the same cyclopolymerization strategy (**Scheme 4.2b**). The resulting mc-dPS samples were subjected to preparative SEC, through which a total of five fractions with narrow dispersity ($Đ < 1.17$) were successfully obtained (**Figures 4.15d–4.15f**). Given that the resulting mc-dPS samples were fully soluble and the ^{1}H NMR signals originating from the norbornenyl group disappeared completely after cyclopolymerization, the presence of cross-links or dangling chains was considered to be highly unlikely (**Figures 4.18–4.19**). These results, in combination, are consistent with successful cyclopolymerization of NB–dPS–NB and with the structural regularity observed for mc-PS prepared under the same conditions. Comparison of the SEC traces of the corresponding mc-PS and mc-dPS samples revealed almost identical elution peak positions, indicating that their molecular weight distributions were virtually identical (**Figure 4.20**). Moreover, MALS analysis revealed that the absolute molecular weights of mc-PS and mc-dPS were comparable, further confirming similarities in their molecular characteristics.

To quantify the extent of topology-induced contraction in solution, the author compared SEC-calibrated and absolute molecular weights obtained under identical eluent conditions (**Figure 4.21**). Since SEC calibrated with linear PS standards primarily reflects hydrodynamic size under the specific eluent conditions, $M_{n,SEC}$ in $CHCl_3$ provides a direct basis for comparison with $M_{n,MALS}$ measured in the same solvent for architecturally compact polymers. The $M_{n,\,SEC}$ ($CHCl_3$) and apparent SEC-based contraction index (g_{sol}) defined as

$$g_{sol} = \frac{M_{n,SEC}\ (CHCl_3)}{M_{n,MALS}\ (CHCl_3)}$$

are summarized in Table 4.2 The resulting g_{sol} decreases monotonically with increasing the number of cyclic units for both protonated and deuterated series, consistent with progressively stronger topology-induced compaction. This trend is qualitatively consistent with prior observations that increasing topological constraints (e.g., higher arm numbers in star polymers or higher cyclic complexity in multicyclic polymers) leads to more compact conformations relative to linear chains, manifested as reduced hydrodynamic/structural size. [45–47] Taken together, these results confirm that structurally analogous multicyclic polystyrenes were obtained in both their deuterated and non-deuterated forms.

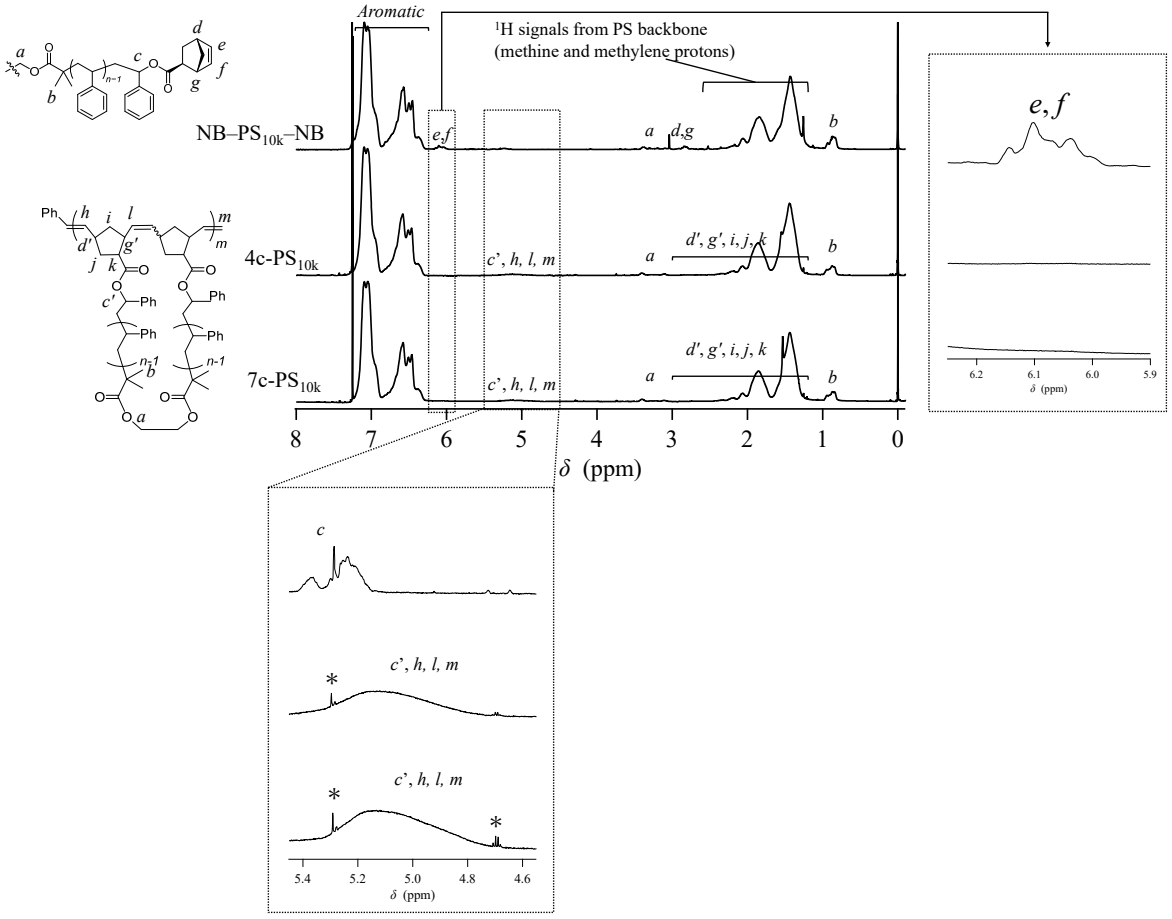

Figure 4.16. ^{1}H NMR spectra of NB–PS$_{10k}$–NB and mc-PS$_{10k}$s in $CDCl_3$.

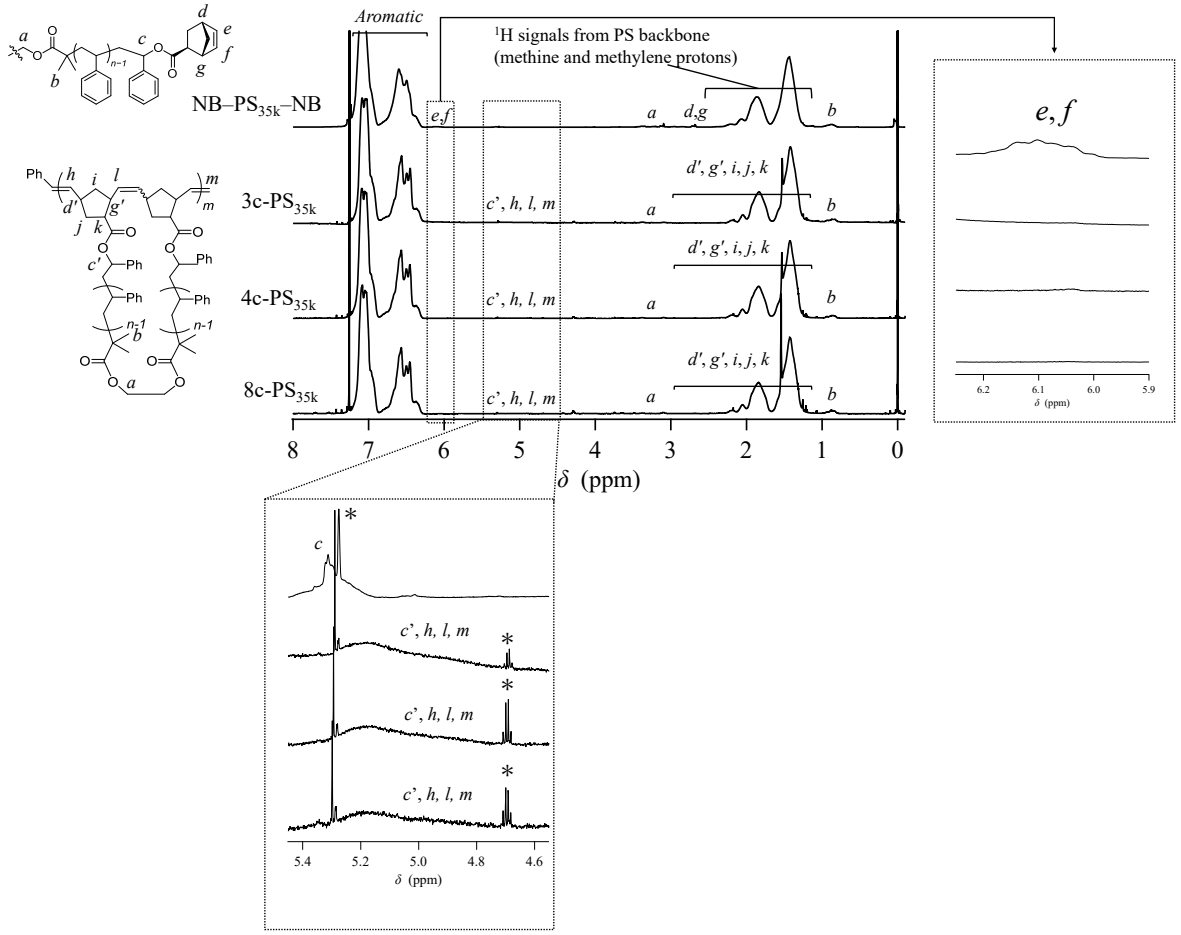

Figure 4.17. ^{1}H NMR spectra of NB–PS_{35k}–NB and mc-PS_{35k}s in $CDCl_3$.

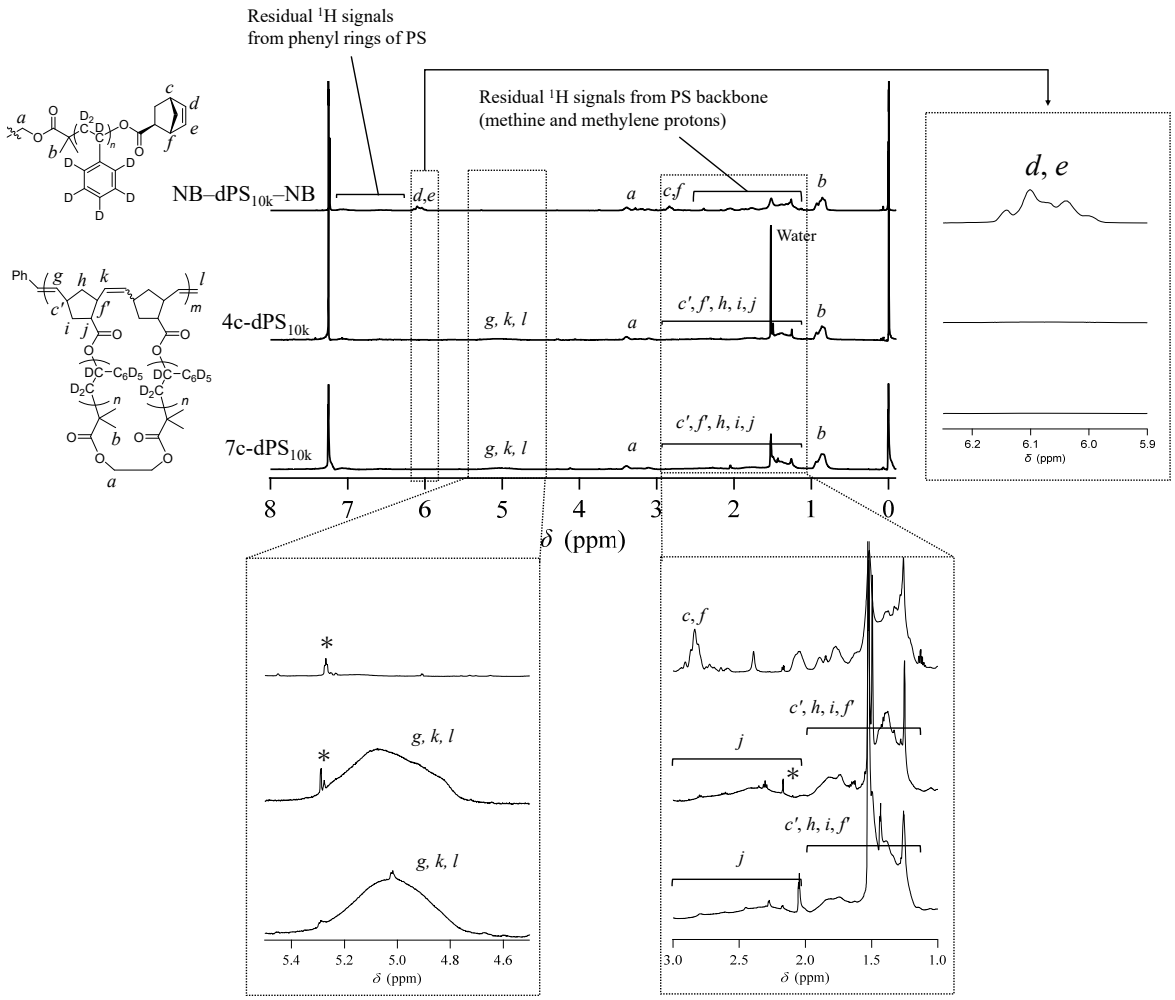

Figure 4.18. ^{1}H NMR spectra of NB–PS$_{10k}$–NB and mc-PS$_{10k}$s in $CDCl_3$.

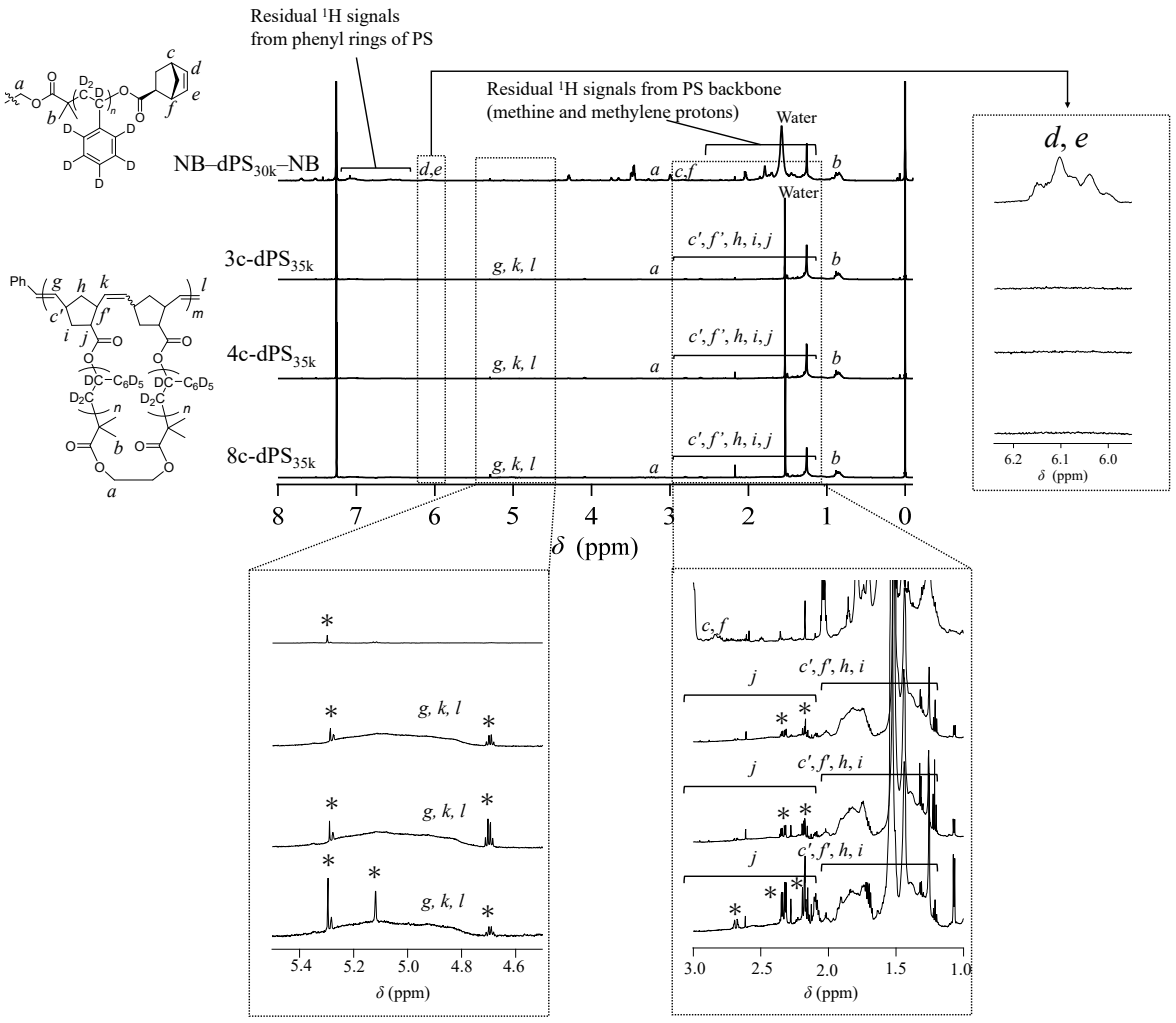

Figure 4.19. ^{1}H NMR spectra of NB–PS$_{35k}$–NB and mc-PS$_{35k}$s in $CDCl_3$.

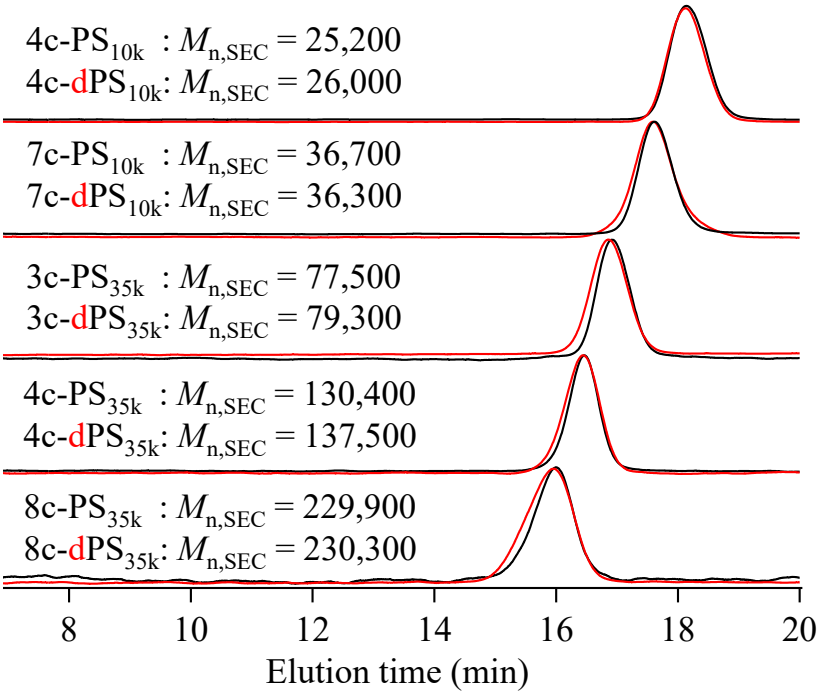

Figure 4.20. Comparison of the SEC traces recorded for the mc-PS (black) and mc-dPS (red) specimens. The SEC measurements were performed using RI detection with THF as the eluent at a flow rate of 1.0 mL min^{-1}.

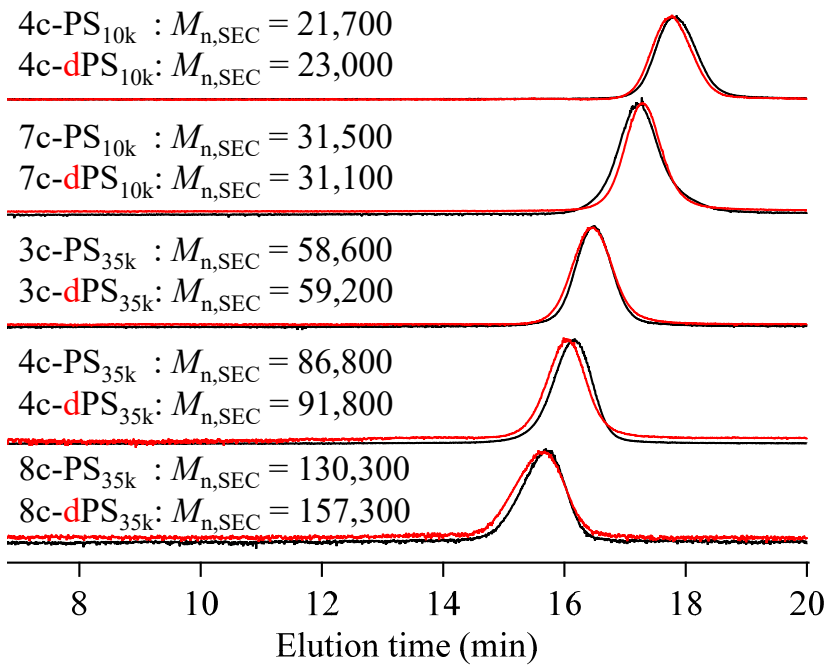

Figure 4.21. Comparison of the SEC traces recorded for the mc-PS (black) and mc-dPS (red) specimens. The SEC measurements were performed using RI detection with $CHCl_3$ as the eluent at a flow rate of 1.0 mL min^{-1}.

4.3.3 Evaluation of the radius of gyration for the neat mc-PS

The R_g values for the neat mc-PS samples listed in Table 4.2 were evaluated by SANS measurement. To perform these measurements, bulk blend samples were prepared by dispersing a low concentration of mc-PS ($\varphi_{mc\text{-}PS}$ = 10 wt%) in an mc-dPS matrix with the same ring architecture (e.g., 4c-PS_{10k}/4c-dPS_{10k}). This strategy enables the selective extraction of the scattering information from the target mc-PS component. For each sample, the scattering intensity ($I(q)$) was plotted as a function of the scattering vector (q), as shown in **Figure 4.22**. The $I(q)$ profiles in Figure 4.19 represent the raw scattering data after the subtraction of the background intensity. For all samples, a slight upturn was observed in the low-q region, which was attributed to nonspecific background scattering, likely arising from interfacial scattering with trace air bubbles or fine particulates in the samples.[48,49] As a precaution against such effects, degassing by thermal pressing was performed as much as possible prior to measurements.

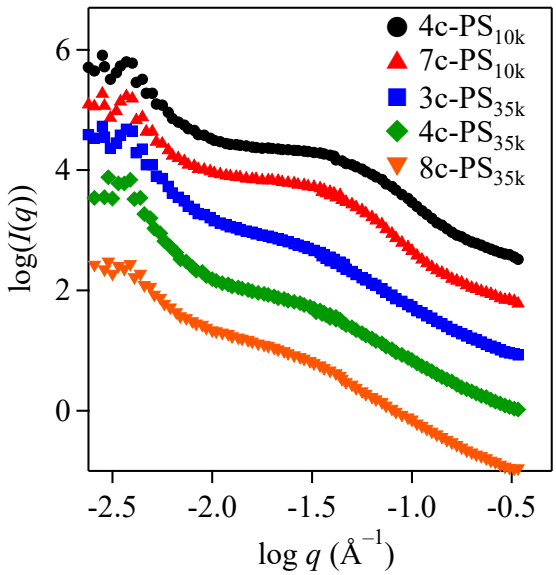

Figure 4.22. SANS profiles recorded at 25 ℃ for the mc-PS/mc-dPS bulk blend samples ($\varphi_{mc\text{-}PS}$ = 10 wt%). The curves are offset along the y-axis for clarity purposes.

The radius of gyration (R_g) values were determined using Guinier analysis, in which the low-q scattering data were fitted to the Guinier expression $\ln I(q) = \ln I(0) - q^2R_g^2/3$, where $I(0)$ denotes the extrapolated scattering intensity at the zero scattering vector ($q = 0$) (**Figure 4.23**). R_g and $I(0)$ were extracted from linear fits of the Guinier plots limited to $qR_g < 1.5$. As an initial step in evaluating the reliability of the present measurements and analytical methods, Guinier analysis was employed to determine R_g for a blend sample consisting of nondeuterated linear PS ($M_{w,MALS}$ = 46,500) dispersed in a deuterated linear PS matrix ($M_{w,MALS}$ = 53,000) (**Figures 4.24–4.25**). The resulting R_g value of 54.3±2.3 Å is consistent with the linear relationship between R_g and the molecular weight reported by Cotton et al. for a series of linear PS samples.[50] This agreement supports the reliability of SANS analysis and validates the subsequent R_g determinations for the mc-PS samples. **Figure 4.26** shows the R_g values determined for each mc-PS sample, plotted as a function of the overall degree of polymerization (N), with the numerical values provided in **Table 4.3**. For comparison, previously reported R_g values for linear and monocyclic PS are also shown.[21] Notably, across all the molecular weight regimes investigated herein, the mc-PS samples exhibited the smallest R_g values among the three topologies. Previous experimental and simulation-based studies have established that monocyclic polymers exhibit lower R_g values than linear polymers of the same molecular weight.[21,22,51] This behavior is generally attributed to chain compaction arising from the absence of chain ends. In the current evaluations, it was found that the mc-PS samples exhibited smaller R_g values than those of monocyclic PS. This further reduction in R_g can be attributed to the presence of multiple junction points in the multicyclic architecture, which restrict the local segmental motion and conformational freedom, thereby inducing a more compact molecular conformation compared with those of the linear and monocyclic counterparts with comparable

total molecular weights. However, Figure 4.26 also suggests that the R_g of 3c-PS_{35k} is close to that of monocyclic PS at a comparable molecular weight. This apparent proximity indicates that the bulk R_g of multicyclic architectures may be governed by an interplay of competing topological contributions, rather than by a single monotonic effect. In particular, the bulk R_g can reflect a balance between (i) compaction associated with junction-induced topological constraints and (ii) swelling arising from intramolecular excluded-volume interactions within the multicyclic architecture (see the following section for a detailed discussion). The latter contribution may become more pronounced as the segment length per cyclic unit increases, which can partially offset junction-induced compaction and yield an apparently modest net change in R_g in the higher-molecular-weight series, especially at lower cyclic-unit numbers. Nevertheless, the present dataset remains limited and does not allow an unambiguous separation of these competing contributions. In addition, subtle structural imperfections that are difficult to detect directly could potentially influence the measured coil dimensions. Further experimental and simulation studies by the community will be required to critically test this interpretation and to elucidate the origin of the observed R_g behavior in the bulk state.

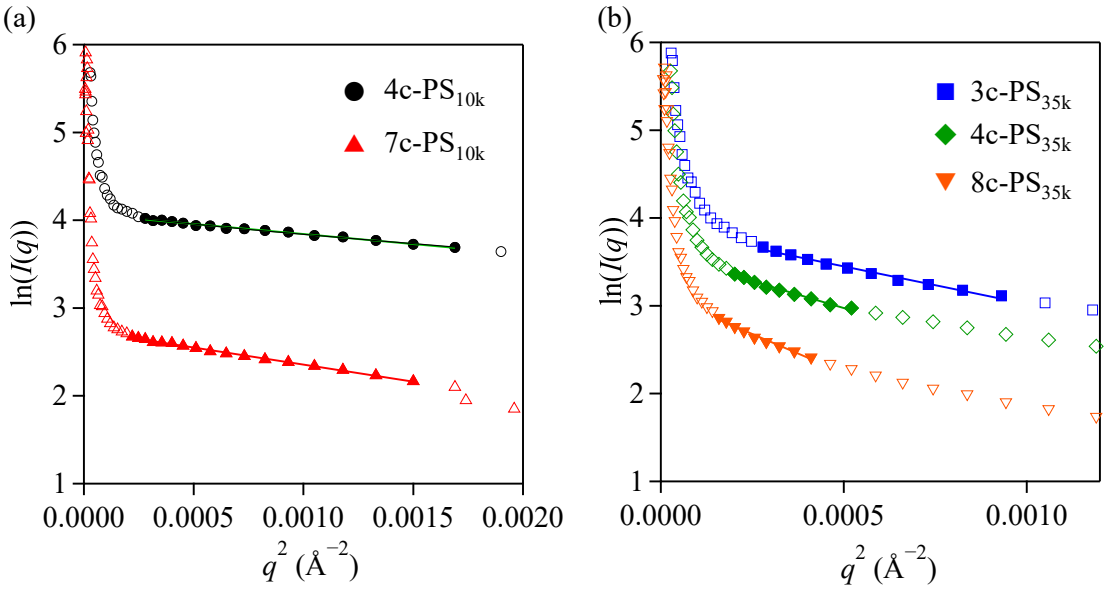

Figure 4.23. Guinier plots for the (a) mc-PS$_{10k}$/mc-dPS$_{10k}$ and (b) mc-PS$_{35k}$/mc-dPS$_{35k}$ bulk blend samples ($\varphi_{mc\text{-}PS}$ = 10 wt%) measured at 25 °C. The solid lines represent the optimal fits obtained from the Guinier equation. The curves are offset along the y-axis for clarity purposes.

Table 4.3. Summary of the molecular and conformational characteristics of mc-PS

Sample	$M_{n,MALS}$ [a]	$M_{w,MALS}$ [a]	$M_{n,MALS}$ of each ring [b]	Average number of cyclic units [b]	N [c]	R_g (Å) [d]	g_{bulk} [e]
4c-PS$_{10k}$	35,700	37,500	10,000	3.6	342	26.1±0.3	0.25
7c-PS$_{10k}$	70,900	73,000		7.1	680	34.2±0.4	0.22
3c-PS$_{35k}$	88,800	93,200	35,300	2.5	853	50.7±1.1	0.38
4c-PS$_{35k}$	155,500	158,100		4.4	1498	60.5±1.7	0.32
8c-PS$_{35k}$	279,300	293,300		7.9	2679	73.1±2.0	0.25

[a]Determined using SEC-MALS-Visco in chloroform. [b]The average number of cyclic units in the obtained mc-PS was estimated as (M_n of mc-PS)/(M_n of the macromonomers). [c]The overall degree of polymerization for the mc-PS/mc-dPS bulk blend samples was calculated by $N = N_h N_d (m_d d_h \varphi_h + m_h d_d \varphi_d)/(N_h m_d d_h \varphi_h + N_d m_h d_d \varphi_d)$, where N_h and N_d are the degree of polymerization, d_h and d_d are the density (i.e., 1.05 and 1.14 g cm^{-3}, respectively), φ_h and φ_d are the volume fractions of the hydrogenous and deuterated PS components, and m_h and m_d are the molecular weights for the hydrogenous and deuterated styrene monomers (i.e., 104.15 and 112.20 g mol^{-1}, respectively). [d]Calculated using the Guinier equation. [e]The size-reduction factor (g_{bulk}) was calculated as $g_{bulk} = \langle R_{g,\,mc\text{-}PS}^2 \rangle \,/\, \langle R_{g,\,linear}^2 \rangle$.

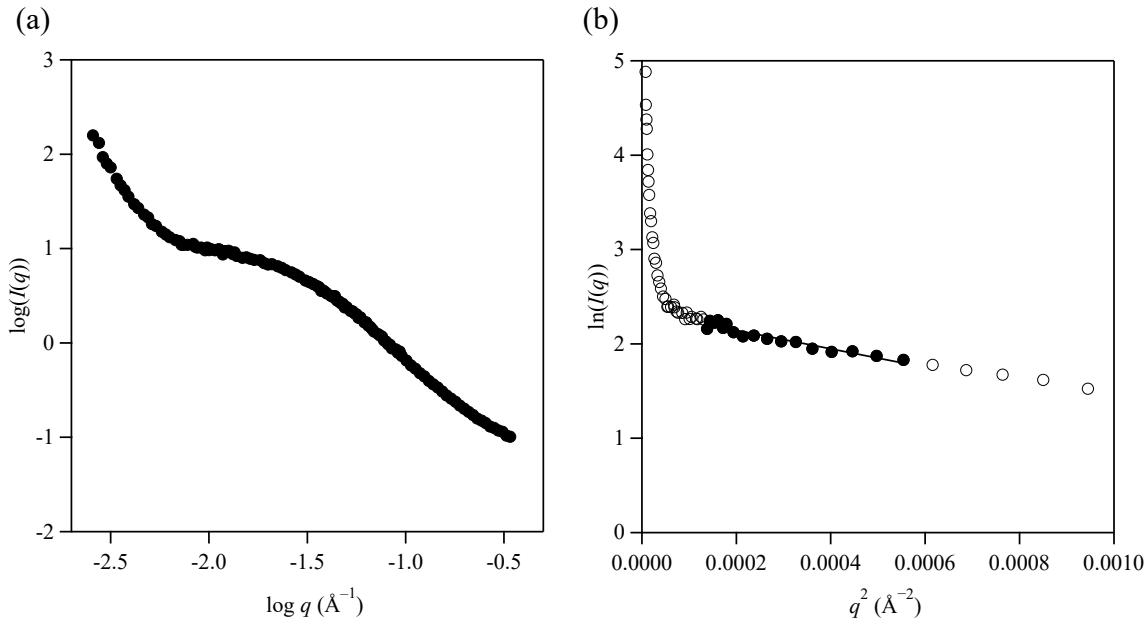

Figure 4.24 (a) SANS profiles for non-deuterated linear polystyrene/deuterated linear polystyrene (50wt%/50wt%) bulk blend sample measured at 25 ℃. (b) Guinier plot for the non-deuterated linear polystyrene/deuterated linear bulk blend sample.

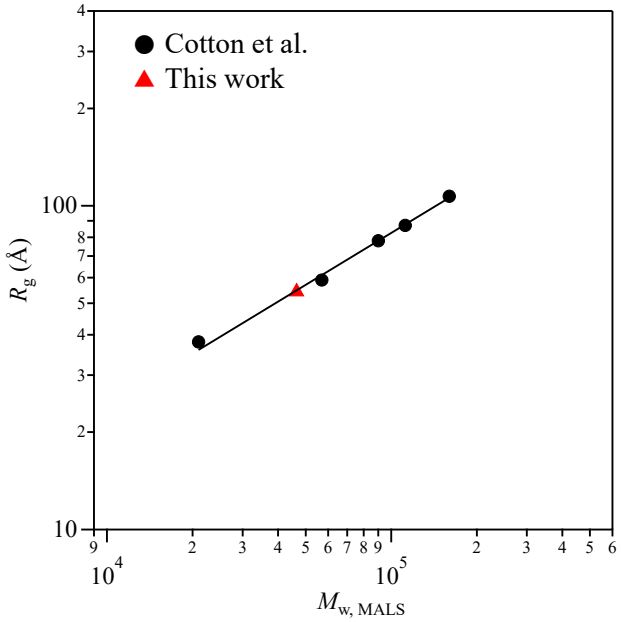

Figure 4.25. $M_{w,MALS}$ and dependence of R_g for the linear polystyrene samples. For comparison, the R_g values for linear polystyrene were taken from the literature reported by Cotton et al.[50] and plotted in the same panel. The solid lines represent the approximate straight fits.

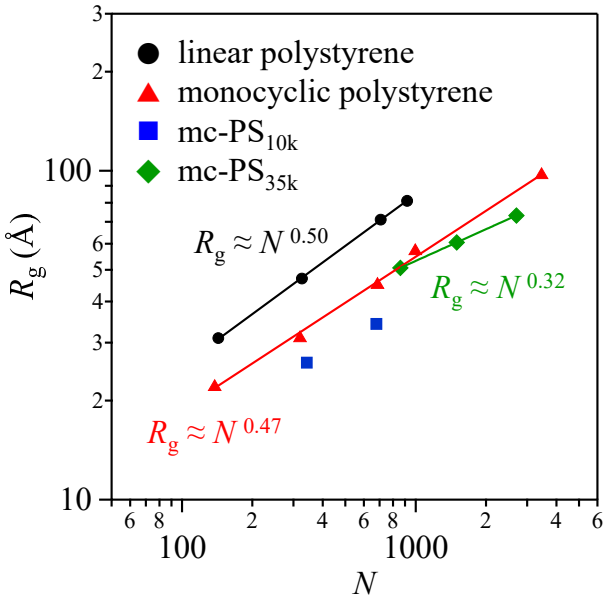

Figure 4.26. N dependence of R_g for the mc-PS samples. For comparison, the literature R_g values for linear and monocyclic PS and monocyclic PS are also shown.[21] The solid lines represent the approximate straight line fits of the data.

To gain further insight into the topological compaction of mc-PS relative to its linear counterparts, the size-reduction factor (g_{bulk}), $g_{bulk} = \langle R_{g,\,mc\text{-}PS}^2 \rangle / \langle R_{g,\,linear}^2 \rangle$ was evaluated for each sample (Table 4.3). Here, $\langle R_{g,\,linear}^2 \rangle$ denotes the mean-square radius of gyration of the corresponding linear PS having the same molecular weight as the mc-PS sample in the bulk, which can be estimated from the empirical bulk relation reported by Cotton et al.,[50] i.e., $R_{g,\,linear} = 0.27M^{0.5}$. The theoretical g_{bulk} value for an ideal ring relative to a linear chain of equal molecular weight is 0.5, and previous SANS analyses of monocyclic PS in θ solvents (i.e., solvent conditions under which excluded-volume effects are cancelled and the chain behaves as an ideal Gaussian coil) demonstrated experimental g_{bulk} values in the range of 0.5–0.7.[10,15,54] In contrast, the current mc-PS samples yielded $g_{bulk} < 0.5$, demonstrating a more compact

conformation than monocyclic PS and establishing a clear hierarchy of coil dimensions: linear > monocyclic > multicyclic. This is consistent with the progressive increase in topological constraints. Notably, within the mc-PS series, g_{bulk} tended to decrease with increasing number of cyclic units, suggesting progressively enhanced compactness with increasing multicyclic constraint. This tendency qualitatively resembles the systematic compaction reported for multi-arm star polymers with increasing arm numbers, implying that the accumulation of topological constraints could similarly promote coil contraction in the bulk.[45]

4.3.4 Comparison of the experimental radius of gyration values with the ideal rosette predictions

Having established the absolute chain dimensions of mc-PS in the bulk, the evolution of these dimensions relative to the ideal-chain expectations was examined with an increasing number of cyclic units. For this purpose, the expected fractional change in R_g upon varying the number of cyclic units was derived from a Gaussian chain rosette model (i.e., multiple rings joined at a single common junction) that neglected the excluded-volume and entanglement effects. Although the current mc-PS is not a true rosette, but rather a ring-grafted comb, a comparison with the Gaussian rosette model is informative when the number of rings is modest because the local environment near each junction is rosette-like. For a rosette composed of m rings, each containing n segments, the mean square R_g ($\langle R_{g,m}^2 \rangle$) can be expressed as follows:

$$\langle R_{g,m}^2 \rangle = \frac{Nb^2}{6m}\left(1 - \frac{1}{2m}\right) \qquad (1)$$

where N (= mn) represents the total number of segments in the rosette and b denotes the length of the segment. Equation (1) was initially derived by Blavatska and Metzler[33] with respect to the path integral, wherein they implicitly assumed that n is extremely large,[33] f_1 corresponds to m, and Sd corresponds to nb^2. This expression can also be derived in terms of the resistance distance by taking the limit of n to infinity.[53] Furthermore, the exact expression of $\langle R_{g,m}^2 \rangle$ can be derived for finite n values as described by Uehara et al.,[34] and its incorporation into Equation (1) gives Equation (2), as follows:

$$\langle R_{g,m}^2 \rangle = \frac{nb^2}{6}\left(1 - \frac{1}{2m}\right). \qquad (2)$$

Additionally, the ratio of $\langle R^2_{g,m} \rangle$ for m_2 rings to that for m_1 rings with the same number of segments n in each ring is given by Equation (3):

$$\langle R^2_{g,m2} \rangle / \langle R^2_{g,m1} \rangle = \left(1 - \frac{1}{2m_1}\right) / \left(1 - \frac{1}{2m_2}\right). \qquad (3)$$

For the mc-PS samples with smaller ring sizes (10k), the effect of increasing the number of cyclic units is already evident. Specifically, upon increasing the average number of cyclic units from 3.6 (4c-PS_{10k}) to 7.1 (7c-PS_{10k}), R_g increases from 26.1 to 34.2 Å, corresponding to a ~31 % increase, whereas the ideal Gaussian model based on Equation (3) predicted an increase of only ~4 % (**Table 4.4**). Despite the asymptotic screening of the excluded-volume effects in polymer melts, the observed increase in R_g with an increasing number of cyclic units far exceeded the ideal-chain baseline. As a reference, linear PS follows Gaussian coil expectations in the melt over a broad molecular weight range, wherein R_g agrees with the ideal chain scaling and absolute coil dimensions established by SANS.[54] This behavior likely reflects a unique manifestation of junction-localized excluded-volume effects, which are characteristic of multicyclic architectures. A similar but more pronounced trend was observed for the larger ring series (35k). Specifically, upon increasing m from 2.5 (3c-PS_{35k}) to 7.9 (8c-PS_{35k}), R_g increases from 50.7 to 73.1 Å (~44%), whereas the ideal model based on Equation (3) predicted an increase of only ~8%. Taken together, both series showed a clear enhancement of R_g relative to the ideal predictions, with the change becoming more evident for the 35k rings. This can be attributed to the fact that multiple cyclic units are covalently tethered through a limited number of junctions, leading to dense local packing and the strengthening of intramolecular excluded-volume interactions that are not fully screened in the bulk.

Table 4.4. Comparison of the changes in R_g with number of cyclic units between real and ideal chain values

	mc-PS$_{10k}$ (ring size: 10k)	mc-PS$_{35k}$ (ring size: 35k)
Change in the number of cyclic units	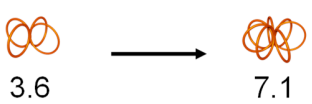 3.6 → 7.1	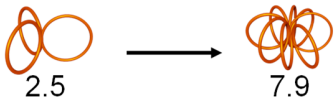 2.5 → 7.9
R_g change for ideal chains (Rosette model)	4% increase	8% increase
R_g change for real chains	31% increase	44% increase

To further quantify the change in ideal-chain behavior, the scaling relationship was analyzed between R_g and the total degree of polymerization, N. In the case of linear polymers, the scaling relationship between R_g and N follows $R_g \approx N^{0.5}$ in the melt state, consistent with ideal Gaussian chain behavior. In contrast, Takano et al. reported that for monocyclic PS in the bulk, the scaling exponent decreased to ~0.47, reflecting the topological constraint imposed by the absence of chain ends.[21] In the current work, the scaling behavior of multicyclic PS was examined for two mc-PS$_{10k}$ and three mc-PS$_{35k}$ samples (Figure 4.26). For mc-PS$_{10k}$, only two data points were available, precluding a reliable determination of the scaling exponent (v). Nevertheless, visual inspection of the R_g versus N plot suggests that mc-PS$_{10k}$ exhibits a v comparable to, or potentially smaller than, that of monocyclic PS. In contrast, analysis of the mc-PS$_{35k}$ data yielded v = 0.32. Equation (2) can therefore be rewritten as a function of the total degree of polymerization N by eliminating m, yielding:

$$R_g^2 = \frac{nb^2}{6}\left(1 - \frac{n}{2N}\right). \qquad (4)$$

When the ring size (n) is fixed, this relationship predicts that the mean-square radius of gyration should remain nearly constant with respect to N. In other words, for an ideal Gaussian chain, R_g is expected to saturate with increasing N. However, as shown in Figure 4.26, the R_g value of mc-PS appears to increase with N. This discrepancy provides direct experimental evidence that the excluded-volume effects in multicyclic architectures are not fully screened, even in the bulk, thereby serving as a counterexample to the Flory theorem, which assumes complete screening of excluded-volume interactions under melt conditions.[51]

4.3.5 Kratky analysis for the neat multicyclic polystyrene

To analyze the multicyclic conformations in greater detail, Kratky plots (q^2I(q) vs. q) were constructed (**Figures 4.27a–4.27b**). All mc-PS samples displayed a pronounced upturn from intermediate to high q, and the magnitude of the upturn increased systematically with the number of cyclic units. For direct comparison with ideal-chain behavior, ideal Kratky curves were calculated for rosette models with varying numbers of cyclic units (**Figure 4.28)**; the calculation procedure is described in the Supporting Information. In all cases, the ideal q^2I(q) approached a high-q plateau and did not display a systematic upturn with an increasing number of cyclic units. In contrast, the current mc-PS data showed a pronounced high-q upturn, the magnitude of which increased with the number of cyclic units. This deviation from the ideal-chain model suggests intramolecular excluded-volume effects that remain incompletely screened near the densely packed ring junctions. This interpretation aligns with the preceding R_g analysis, where the increase in R_g with the number of cyclic units markedly exceeds the ideal rosette predictions, indicating intramolecular excluded-volume effects. The high-q upturn in the Kratky plots represents a short-length-scale manifestation of the same junction-localized swelling. Notably, neither linear PS nor monocyclic PS exhibited the high-q upturn observed for mc-PS; the linear PS lost this high-q increase beyond a threshold molecular weight ($M_w \approx$ 30,000) and recovered the Gaussian high-q plateau, whereas the monocyclic PS showed no systematic increase at high q values across a wide molecular-weight range.[21] Taken together, the persistence of a high-q upturn, irrespective of the ring unit size, and its systematic strengthening with the number of cyclic units, identify this response as a distinctive feature of multicyclic architectures. The form factors were previously calculated for the ideal model of multicyclic polymers by Hammouda, considering that each looping branch is part of a long

single linear chain.[35] These values are derived in the Supporting Information based on the resistance distance of any corresponding simple graph.[55,56]

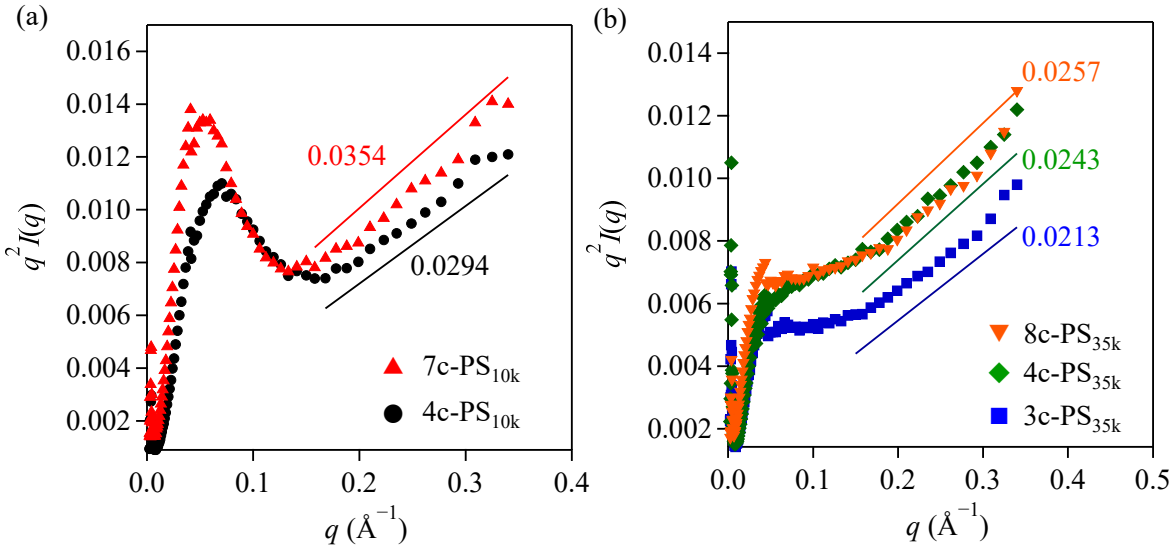

Figure 4.27. Kratky plots obtained for the (a) mc-PS_{10k} and (b) mc-PS_{35k} specimens. In panels (a) and (b), the straight lines represent linear fits to the high-q region, and the numbers adjacent to the lines indicate the corresponding fitted slopes.

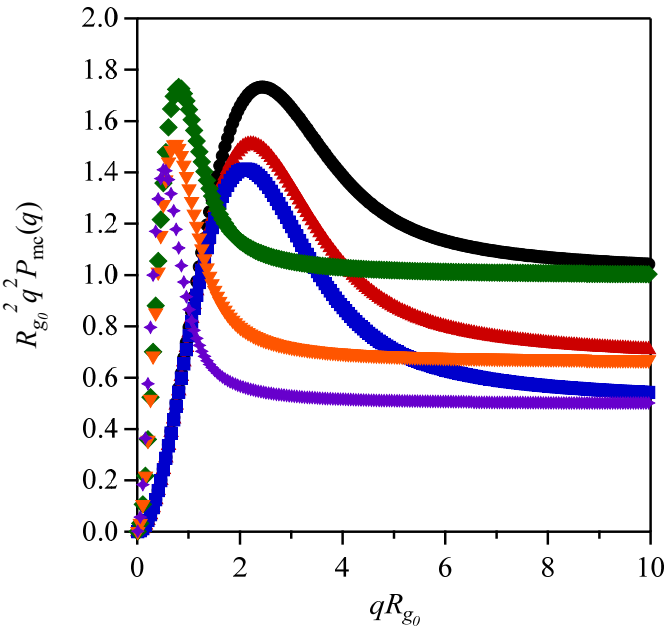

Figure 4.28. Kratky plots of Gaussian multicyclic polymers consisting of chains of n segments and those of $9n$ segments for m = 2, 3, and 4: $R_{g0}^2 q^2 P_{mc}(q)$ versus qR_{g0} for ring chains of n segments with m = 2 (black) , 3 (red) and 4 (blue), and for ring chains of $9n$ segments with m=2 (green), 3 (orange), and 4 (purple). Here, R_{g0}^2 is given by $R_{g0}^2 = nb^2/6$.

Focusing next on the Kratky peak appearing in the range $0 < q < 0.1$ Å^{-1}, a systematic increase in the peak height was observed upon increasing the number of cyclic units at fixed ring size. This trend was also evident in the normalized representation (**Figure 4.29**). Within the ideal Gaussian framework for rosette polymers, assuming that the rings scatter independently, the total intramolecular form factor can be decomposed as follows (a detailed derivation is provided in the Supporting Information):

$$P_{\mathrm{mc}}(q)=\frac{1}{m}P_{\mathrm{sc}}(q)+\frac{m-1}{m}P_{\mathrm{ic}}(q). \qquad (5)$$

where m is the number of cyclic units per macromolecule, $P_{\mathrm{sc}}(q)$ denotes the single-ring contribution, and $P_{\mathrm{ic}}(q)$ represents the inter-ring cross-terms. In the peak region, the response is governed predominantly by the single-ring term $(1/m)P_{\mathrm{sc}}(q)$; hence, theory predicts that the peak intensity should decrease as the number of cyclic units increases (Figure 4.29). Contrary to this prediction, the current experiments showed that the peak intensity increased with increasing m. This finding indicates that the ring contributions are not independent, but are positively correlated, such that the inter-ring term $P_{\mathrm{ic}}(q)$ imparts a non-negligible constructive contribution, even in the peak regime. These observations suggest that the cyclic units are not statistically independent; rather, positive inter-ring correlations emerge within a macromolecule, consistent with the strengthening of the high-q response. Overall, multicyclic polymers do not conform to the ideal-rosette independent-ring picture, and pronounced junction-localized swelling reveals intramolecular excluded-volume effects.

Taken together, the above discussion suggests that, in the bulk, the chain size of mc-PS reflects a balance between two competing topology-related contributions. On one hand, the formation of multiple junction points introduces additional constraints that tend to compact the overall conformation. On the other hand, the intramolecular excluded-volume interactions can

promote chain swelling. Returning to Figure 4.26, 3c-PS$_{35k}$ exhibits an R_g comparable to that of monocyclic PS at a similar total molecular weight. This observation suggests that mc-PS does not necessarily exhibit a smaller R_g than the monocycle across all architectures.

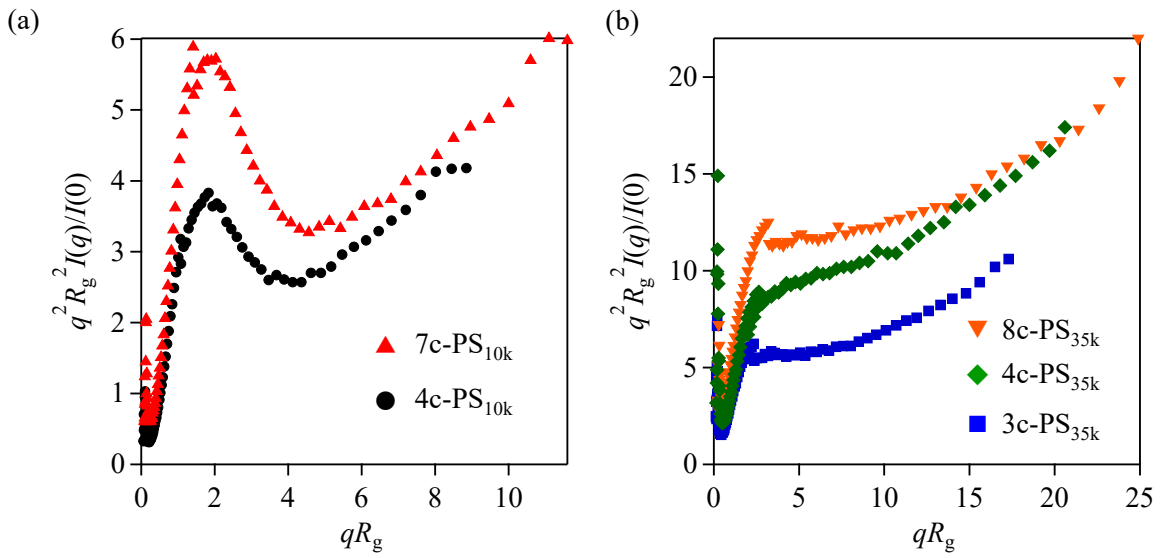

Figure 4.29. Normalized Kratky plots for (a) mc-PS$_{10k}$ and (b) mc-PS$_{35k}$.

4.3.6 Structural analysis of multicyclic polystyrene in the linear matrix

To investigate how the presence of linear chains influences the global chain dimensions of mc-PS, the variation in R_g was examined for a series of mc-PS samples with different numbers and sizes of cyclic units upon blending with linear PS (**Table 4.5**). The bulk blend samples were prepared with linear PS volume fractions (φ_{linear}) of 35, 80, and 90 wt%, while maintaining the mc-PS/mc-dPS ratio fixed at 10:90 (w/w), consistent with the neat mc-PS measurements described in the previous section. The linear PS component was a random copolymer of non-deuterated and deuterated styrenes with a volume fraction of 50:50 (*h*/*d*-linear PS; $M_{n,MALS}$ = 43,900), which was designed to exhibit negligible coherent scattering contrast in SANS.[57–59] Preparation of the *h*/*d*-linear PS is detailed in the Supporting Information (**Figure 4.30**), and the resulting R_g values for each blend composition are summarized in **Table 4.5**, together with the calculated swelling ratio (SR), defined as SR = 100×(R_g in blend−R_g in neat mc-PS)/(R_g in neat mc-PS) (%). Representative scattering profiles and Guinier plots are shown in **Figure 4.31–4.35**.

Table 4.5. R_g values for the mc-PS specimen in a linear matrix with different φ_{linear} values [a]

Sample	φ_{linear}	$M_{n,MALS}$ [b]	M_n of each ring [b]	Average number of cyclic units [c]	R_g (Å) [d]	SR (%) [e]
4c-PS$_{10k}$	0 (neat)	35,700	10,000	3.6	26.8±0.6	-
	65				28.7±0.5	6.78
	80				26.7±0.5	−0.421
	90				26.8±0.5	0.00
7c-PS$_{10k}$	0 (neat)	70,900		7.1	34.2±0.4	-
	65				34.3±0.5	0.256
	80				33.3±0.4	−2.67
	90				31.7±0.3	−8.06
3c-PS$_{35k}$	0 (neat)	88,800	35,300	2.5	50.7±1.1	-
	65				50.8±1.0	0.116
	80				51.7±1.7	1.87
	90				52.2±1.5	2.88
4c-PS$_{35k}$	0 (neat)	155,500		4.4	60.5±1.7	-
	65				64.0±1.6	0.265
	80				62.4±1.0	3.01
	90				64.0±0.7	5.45
8c-PS$_{35k}$	0 (neat)	279,300		7.9	73.1±2.0	-
	65				81.0±1.5	9.72
	80				81.2±1.5	9.93
	90				83.3±3.9	12.2

[a]All SANS measurements were performed for the mc-PS/mc-dPS blends in the linear matrix with a fixed weight ratio of 10:90 (w/w), wherein the linear matrix consisted of a random copolymer of non-deuterated and deuterated styrenes with a volume fraction of 50:50 (*h*/*d*-linear PS; $M_{n,MALS}$ = 43,900) [b]Determined by SEC-MALS-Visco in chloroform. [c]The average number of cyclic units in the obtained mc-PS was estimated according to (M_n of mc-PS)/(M_n of the macromonomers). [d]Calculated using the Guinier equation. [e]The swelling ratio of mc-PS was calculated as 100×(R_g in blend−R_g in neat mc-PS)/(R_g in neat mc-PS) (%).

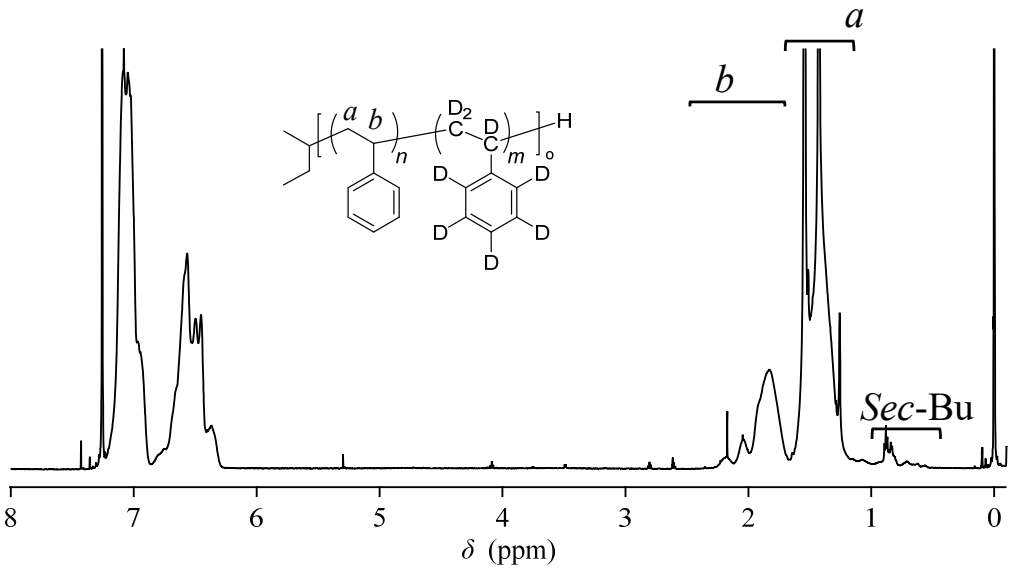

Figure 4.30 ^{1}H NMR spectrum of *h*/*d*-linear PS in $CDCl_3$.

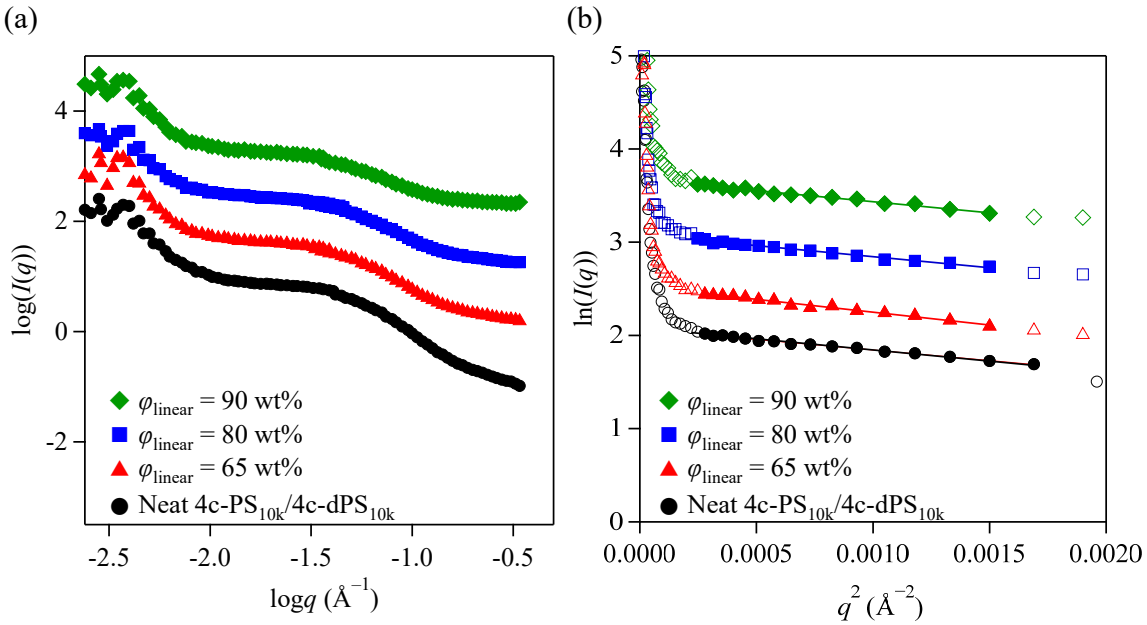

Figure 4.31. (a) SANS profiles for 4c-PS$_{10k}$/4c-dPS$_{10k}$ bulk blend sample ($\varphi_{mc\text{-}PS}$ = 10 wt%) and their blends with *h*/*d*-linear PS measured at 25 °C. (b) Guinier plots for 4c-PS$_{10k}$/4c-dPS$_{10k}$ bulk blend samples and their blends with *h*/*d*-linear PS. The curves are shifted along the y-axis for better visibility.

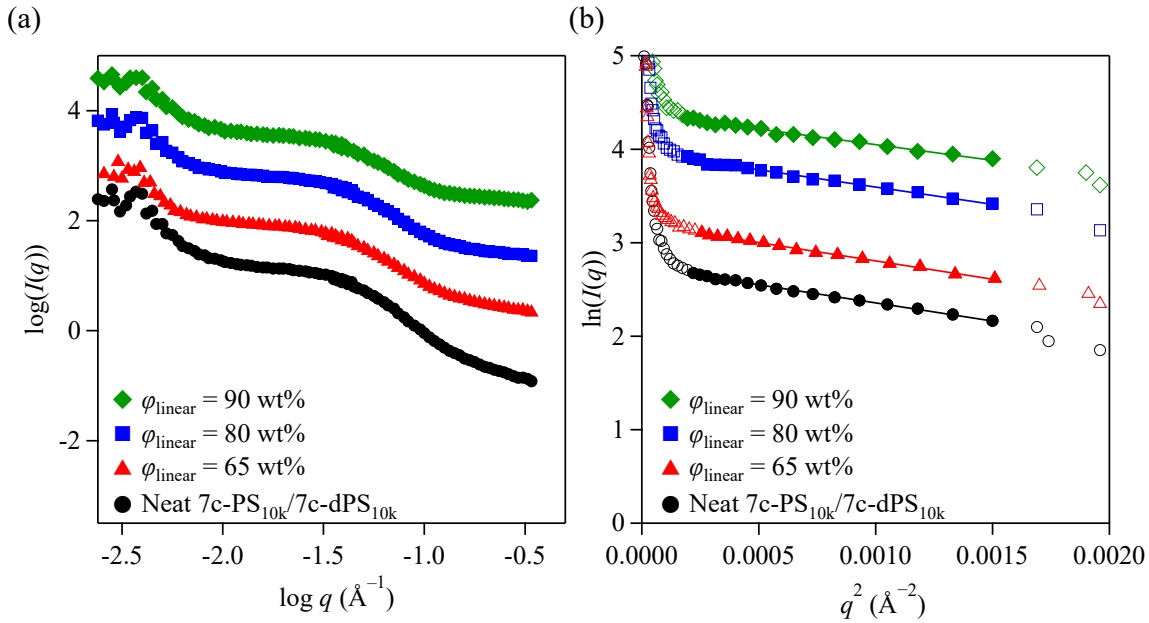

Figure 4.32. (a) SANS profiles for 7c-PS_{10k}/7c-dPS_{10k} bulk blend sample ($\varphi_{mc\text{-}PS}$ = 10 wt%) and their blends with *h*/*d*-linear PS measured at 25 °C. (b) Guinier plots for 7c-PS_{10k}/7c-dPS_{10k} bulk blend samples and their blends with *h*/*d*-linear PS. The curves are shifted along the y-axis for better visibility.

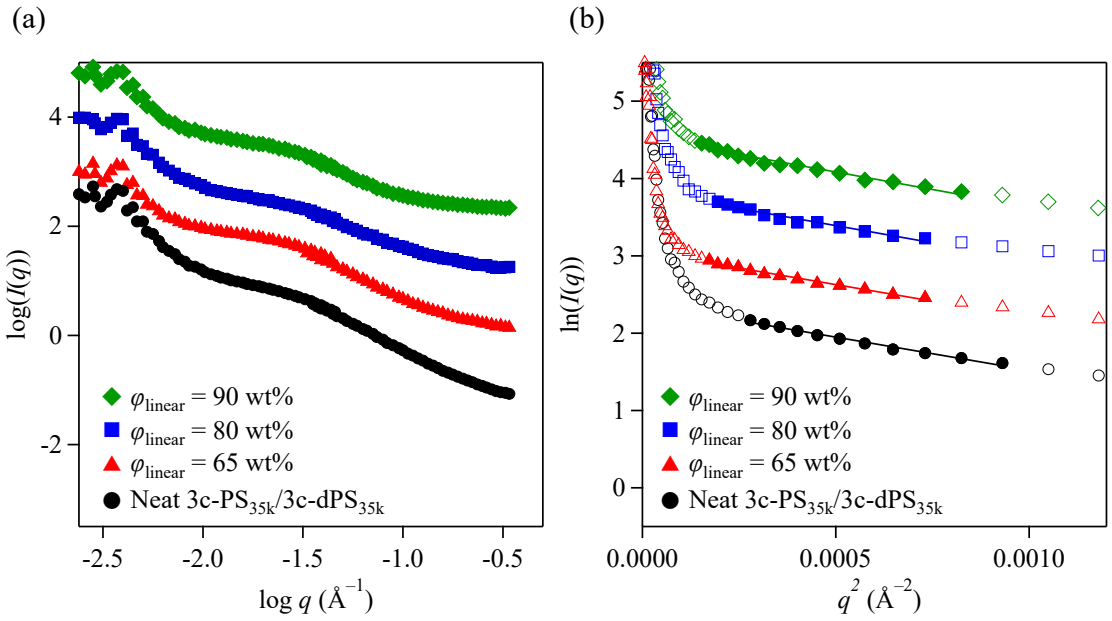

Figure 4.33. (a) SANS profiles for 3c-PS$_{35k}$/3c-dPS$_{35k}$ bulk blend sample ($\varphi_{mc\text{-}PS}$ = 10 wt%) and their blends with *h*/*d*-linear PS measured at 25 °C. (b) Guinier plots for 3c-PS$_{35k}$/3c-dPS$_{35k}$ bulk blend samples and their blends with *h*/*d*-linear PS. The curves are shifted along the y-axis for better visibility.

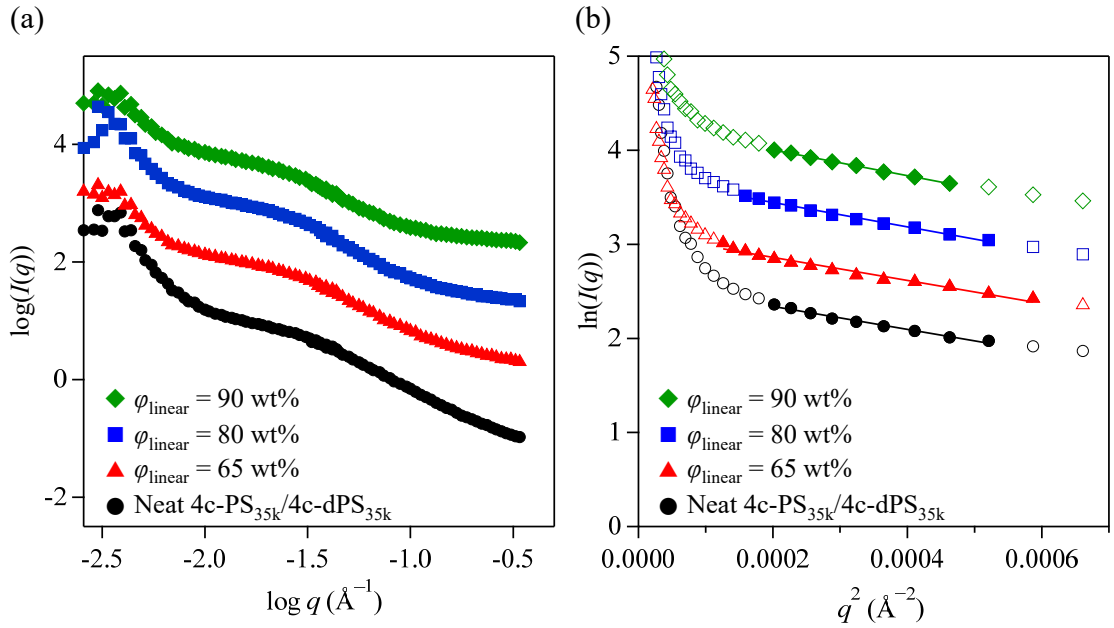

Figure 4.34. (a) SANS profiles for 4c-PS$_{35k}$/4c-dPS$_{35k}$ bulk blend sample ($\varphi_{mc\text{-}PS}$ = 10 wt%) and their blends with *h*/*d*-linear PS measured at 25 °C. (b) Guinier plots for 4c-PS$_{35k}$/4c-dPS$_{35k}$ bulk blend samples and their blends with *h*/*d*-linear PS. The curves are shifted along the y-axis for better visibility.

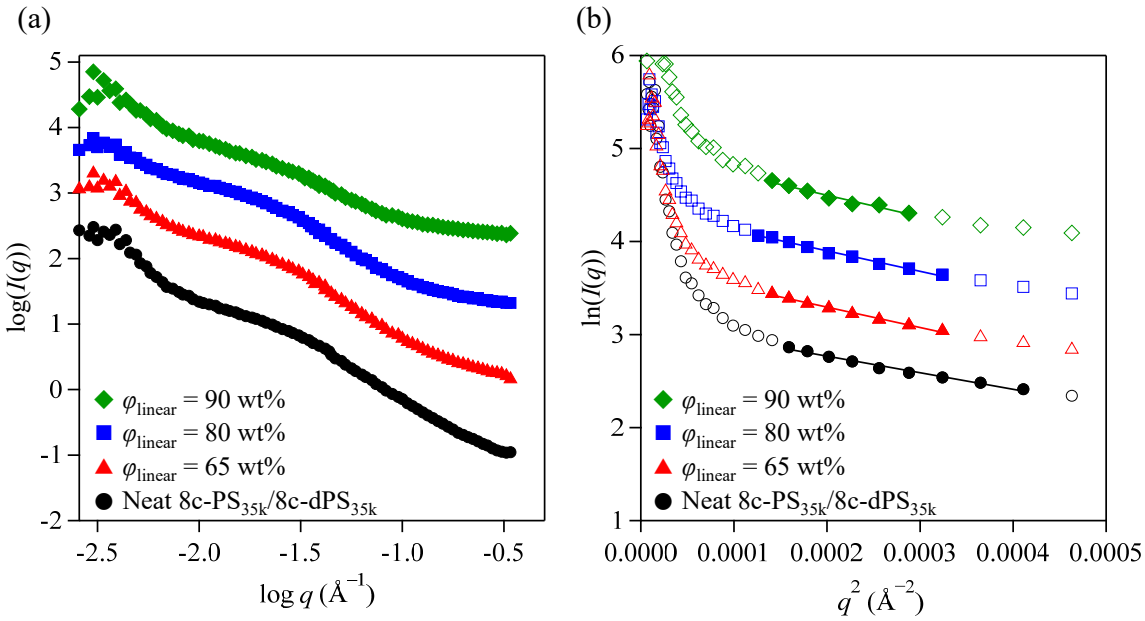

Figure 4.35. (a) SANS profiles for 8c-PS$_{35k}$/8c-dPS$_{35k}$ bulk blend sample ($\varphi_{mc\text{-}PS}$ = 10 wt%) and their blends with *h*/*d*-linear PS measured at 25 °C. (b) Guinier plots for 8c-PS$_{35k}$/8c-dPS$_{35k}$ bulk blend samples and their blends with *h*/*d*-linear PS. The curves are shifted along the y-axis for better visibility.

For the mc-PS$_{10k}$ samples (4c-PS$_{10k}$ and 7c-PS$_{10k}$), R_g exhibited little or no decrease upon blending with *h*/*d*-linear PS, with the SR values remaining close to, or slightly below, unity. In particular, 7c-PS$_{10k}$ exhibited a modest decrease in R_g at higher φ_{linear} values, indicating a possible contraction of the multicyclic structure. For the mc-PS$_{35k}$ samples (3c-PS$_{35k}$, 4c-PS$_{35k}$, and 8c-PS$_{35k}$), R_g increased upon blending with the linear PS, especially in the cases of the 4c-PS$_{35k}$ and 8c-PS$_{35k}$ samples. This contrasting behavior between mc-PS$_{10k}$ and mc-PS$_{35k}$ can be rationalized in terms of the entanglement molecular weight (M_e) of PS, which is ~18,000.[60] In mc-PS$_{10k}$, the molecular weight of each cyclic unit ($M_{n,ring}$ = 10,000) was below M_e, rendering it difficult for the *h*/*d*-linear PS chains to form stable topological interpenetrations with a multicyclic architecture. Consequently, the presence of the linear chains did not lead to appreciable swelling. In contrast, the molecular weight of each cyclic unit in mc-PS$_{35k}$ ($M_{n,ring}$ = 35,300) exceeded M_e, thereby allowing the *h*/*d*-linear PS chains to penetrate and topologically interact with the cyclic units. Such threading interactions are expected to increase the effective volume and promote expansion of the multicyclic conformation, resulting in the observed R_g increase. This interpretation is further supported by the coarse-grained MD simulations of ring–linear blends conducted by Hagita et al., who demonstrated that persistent threading rarely occurs for small rings, whereas larger rings accommodate multiple penetrations and undergo expansion.[61] This threshold-like behavior rationalizes the absence of swelling in mc-PS$_{10k}$ and the pronounced R_g increase for in mc-PS$_{35k}$. To the best of my knowledge, prior studies on monocyclic polymers have not examined rings with sufficiently low molecular weights (e.g., $M_{n,ring} < M_e$). Therefore, this threshold-like trend is reported here for the first time.

Furthermore, for mc-PS$_{35k}$, the SR increased with increasing φ_{linear}. This trend can be attributed to the greater number of *h*/*d*-linear PS chains penetrating each multicyclic molecule

as the proportion of *h*/*d*-linear PS in the blend increases, thereby promoting swelling of the mc-PS_{35k} chains. A similar dependence of swelling on the linear chain content has been reported for monocyclic polymers, and the present results are consistent with these findings.[21,27]

The effect of the number of cyclic units on the swelling behavior was further examined by focusing on the samples at φ_{linear} = 90%. The SR values of 3c-PS_{35k}, 4c-PS_{35k}, and 8c-PS_{35k} were 2.88%, 5.45%, and 12.2%, respectively, indicating a clear increasing trend with the number of cyclic units. This trend can be rationalized by considering that as the number of cyclic units within a single mc-PS molecule increases, the number of *h*/*d*-linear PS chains capable of penetrating the molecule also increases. The accumulation of such threading events per molecule led to a pronounced expansion of the multicyclic conformation. Indeed, Hagita et al. demonstrated through MD simulations that the number of linear chains penetrating each ring unit increases with the total number of cyclic units.[38] The present study experimentally confirms this trend for the first time, providing direct evidence for the influence of the number of cyclic units on the cyclic swelling behavior in multicyclic polymers.

4.4 Conclusions

In this chapter, a versatile experimental platform was established for the synthesis of well-defined multicyclic polystyrenes (mc-PS) by combining atom radical transfer polymerization-based macromonomer synthesis and ring-opening metathesis polymerization (ROMP)-based cyclopolymerization. This robust strategy was readily extended to deuterated multicyclic polystyrenes (mc-dPS). Using small-angle neutron scattering, the structural characteristics of these samples were systematically investigated, both in the neat bulk state and in blends with linear polystyrene. In the neat bulk state, the mc-PS exhibited smaller radii of gyration than the linear and monocyclic analogs of comparable molecular weights, demonstrating enhanced chain compaction arising from the multicyclic topology. Relative to a Gaussian chain rosette model, the experimental results imply that the excluded-volume interactions remain partially unscreened in the bulk; Kratky analysis provided consistent evidence for this behavior. In the linear polymer blends, mc-PS showed ring-size-dependent swelling behavior. Specifically, expansion was observed only when the ring size exceeded the entanglement molecular weight, and the degree of swelling increased with the number of cyclic units. These findings highlight that multicyclic topological complexity governs both the intrinsic conformations and interactions in blends with linear polymers, offering new opportunities for designing polymer materials with tunable properties and functions through architectural control.

4.5. References

(1) Haque, F. M.; Grayson, S. M. The Synthesis, Properties and Potential Applications of Cyclic Polymers. *Nat. Chem.* **2020**, *12*, 433–444.

(2) Golba, B.; Benetti, E. M.; De Geest, B. G. Biomaterials Applications of Cyclic Polymers. *Biomaterials* **2021**, *267*, 120468.

(3) Yamamoto, T.; Tezuka, Y. Topological Polymer Chemistry: A Cyclic Approach toward Novel Polymer Properties and Functions. *Polym. Chem.* **2011**, *2*, 1930–1941.

(4) Yamamoto, T.; Tezuka, Y. Cyclic Polymers Revealing Topology Effects upon Self-Assemblies, Dynamics and Responses. *Soft Matter* **2015**, *11*, 7458–7468.

(5) Jia, Z.; Monteiro, M. J. Cyclic Polymers: Methods and Strategies. *J. Polym. Sci. Part A Polym. Chem.* **2012**, *50*, 2085–2097.

(6) Laurent, B. A.; Grayson, S. M. Synthetic Approaches for the Preparation of Cyclic Polymers. *Chem. Soc. Rev.* **2009**, *38*, 2202–2213.

(7) Chen, C.; Weil, T. Cyclic Polymers: Synthesis, Characteristics, and Emerging Applications. *Nanoscale Horizons* **2022**, *7*, 1121–1135.

(8) Liénard, R.; De Winter, J.; Coulembier, O. Cyclic Polymers: Advances in Their Synthesis, Properties, and Biomedical Applications. *J. Polym. Sci.* **2020**, *58*, 1481–1502.

(9) Clarson, S. J.; Semlyen, J. A. Cyclic Polysiloxanes: 1. Preparation and Characterization of Poly(Phenylmethylsiloxane). *Polymer* **1986**, *27*, 1633–1636.

(10) Zimm, B. H.; Stockmayer, W. H. The Dimensions of Chain Molecules Containing Branches and Rings. *J. Chem. Phys.* **1949**, *17*, 1301–1314.

(11) Schappacher, M.; Deffieux, A. α-Acetal-ω-Bis(Hydroxymethyl) Heterodifunctional Polystyrene: Synthesis, Characterization, and Investigation of Intramolecular End-to-End Ring Closure. *Macromolecules* **2001**, *34*, 5827–5832.

(12) Ge, T.; Panyukov, S.; Rubinstein, M. Self-Similar Conformations and Dynamics in Entangled Melts and Solutions of Nonconcatenated Ring Polymers. *Macromolecules* **2016**, *49*, 708–722.

(13) Rubinstein, M. Dynamics of Ring Polymers in the Presence of Fixed Obstacles. *Phys. Rev. Lett.* **1986**, *57*, 3023–3026.

(14) Takano, A.; Kushida, Y.; Ohta, Y.; Masuoka, K.; Matsushita, Y. The Second Virial Coefficients of Highly-Purified Ring Polystyrenes in Cyclohexane. *Polymer* **2009**, *50*, 1300–1303.

(15) Takano, A.; Ohta, Y.; Masuoka, K.; Matsubara, K.; Nakano, T.; Hieno, A.; Itakura, M.; Takahashi, K.; Kinugasa, S.; Kawaguchi, D.; Takahashi, Y.; Matsushita, Y. Radii of Gyration of Ring-Shaped Polystyrenes with High Purity in Dilute Solutions. *Macromolecules* **2012**, *45*, 369–373.

(16) Arrighi, V.; Gagliardi, S.; Dagger, A. C.; Semlyen, J. A.; Higgins, J. S.; Shenton, M. J. Conformation of Cyclics and Linear Chain Polymers in Bulk by SANS. *Macromolecules* **2004**, *37*, 8057–8065.

(17) Brás, A. R.; Pasquino, R.; Koukoulas, T.; Tsolou, G.; Holderer, O.; Radulescu, A.; Allgaier, J.; Mavrantzas, V. G.; Pyckhout-Hintzen, W.; Wischnewski, A.; Vlassopoulos, D.; Richter, D. Structure and Dynamics of Polymer Rings by Neutron Scattering: Breakdown of the Rouse Model. *Soft Matter* **2011**, *7*, 11169–11176.

(18) Richter, D.; Gooßen, S.; Wischnewski, A. Celebrating Soft Matter's 10th Anniversary: Topology Matters: Structure and Dynamics of Ring Polymers. *Soft Matter* **2015**, *11*, 8535–8549.

(19) McKenna, G. B.; Hostetter, B. J.; Hadjichristidis, N.; Fetters, L. J.; Plazek, D. J. A Study of the Linear Viscoelastic Properties of Cyclic Polystyrenes Using Creep and Recovery Measurements. *Macromolecules* **1989**, *22*, 1834–1852.

(20) Doi, Y.; Matsubara, K.; Ohta, Y.; Nakano, T.; Kawaguchi, D.; Takahashi, Y.; Takano, A.; Matsushita, Y. Melt Rheology of Ring Polystyrenes with Ultrahigh Purity. *Macromolecules* **2015**, *48*, 3140–3147.

(21) Iwamoto, T.; Doi, Y.; Kinoshita, K.; Ohta, Y.; Takano, A.; Takahashi, Y.; Nagao, M.; Matsushita, Y. Conformations of Ring Polystyrenes in Bulk Studied by SANS. *Macromolecules* **2018**, *51*, 1539–1548.

(22) Suzuki, J.; Takano, A.; Matsushita, Y. Topological Effect in Ring Polymers Investigated with Monte Carlo Simulation. *J. Chem. Phys.* **2008**, *129*, 034903.

(23) Vettorel, T.; Reigh, S. Y.; Yoon, D. Y.; Kremer, K. Monte-Carlo Method for Simulations of Ring Polymers in the Melt. *Macromol. Rapid Commun.* **2009**, *30*, 345–351.

(24) Suzuki, J.; Takano, A.; Deguchi, T.; Matsushita, Y. Dimension of Ring Polymers in Bulk Studied by Monte-Carlo Simulation and Self-Consistent Theory. *J. Chem. Phys.* **2009**, *131*, 144902.

(25) Halverson, J. D.; Lee, W. B.; Grest, G. S.; Grosberg, A. Y.; Kremer, K. Molecular Dynamics Simulation Study of Nonconcatenated Ring Polymers in a Melt. I. Statics. *J. Chem. Phys.* **2011**, *134*, 204904.

(26) Sakaue, T. Ring Polymers in Melts and Solutions: Scaling and Crossover. *Phys. Rev. Lett.* **2011**, *106*, 1–4.

(27) Kruteva, M.; Monkenbusch, M.; Allgaier, J.; Pyckhout-Hintzen, W.; Porcar, L.; Richter, D. Structure of Polymer Rings in Linear Matrices: SANS Investigation. *Macromolecules* **2023**, *56*, 4835–4844.

(28) Grest, G. S.; Ge, T.; Plimpton, S. J.; Rubinstein, M.; O'Connor, T. C. Entropic Mixing of Ring/Linear Polymer Blends. *ACS Polym. Au* **2023**, *3*, 209–216.

(29) Mato, Y.; Honda, K.; Ree, B. J.; Tajima, K.; Yamamoto, T.; Deguchi, T.; Isono, T.; Satoh, T. Programmed Folding into Spiro-Multicyclic Polymer Topologies from Linear and Star-Shaped Chains. *Commun. Chem.* **2020**, *3*, 1–7.

(30) Hossain, M. D.; Reid, J. C.; Lu, D.; Jia, Z.; Searles, D. J.; Monteiro, M. J. Influence of Constraints within a Cyclic Polymer on Solution Properties. *Biomacromolecules* **2018**, *19*, 616–625.

(31) Pipertzis, A.; Hossain, M. D.; Monteiro, M. J.; Floudas, G. Segmental Dynamics in Multicyclic Polystyrenes. *Macromolecules* **2018**, *51*, 1488–1497.

(32) Gavrilov, M.; Amir, F.; Kulis, J.; Hossain, M. D.; Jia, Z.; Monteiro, M. J. Densely Packed Multicyclic Polymers. *ACS Macro Lett.* **2017**, *6*, 1036–1041.

(33) Blavatska, V.; Metzler, R. Conformational Properties of Complex Polymers: Rosette versus Star-like Structures. *J. Phys. A Math. Theor.* **2015**, *48*, 135001.

(34) Cantarella, J.; Deguchi, T.; Shonkwiler, C.; Uehara, E. An Exact Formula for the Contraction Factor of a Subdivided Gaussian Topological Polymer. *J. Phys. A Math. Theor.* **2025**, *58*, 355201.

(35) Hammouda, B. Form Factors for Branched Polymers with Excluded Volume. *J. Res. Natl. Inst. Stand. Technol.* **2016**, *121*, 139–164.

(36) Murashima, T.; Hagita, K.; Kawakatsu, T. Topological Transition in Multicyclic Chains with Structural Symmetry Inducing Stress-Overshoot Phenomena in Multicyclic/Linear Blends under Biaxial Elongational Flow. *Macromolecules* **2022**, *55*, 9358–9372.

(37) Hagita, K.; Murashima, T.; Ebe, M.; Isono, T.; Satoh, T. Trapping Probabilities of Multiple Rings in End-Linked Gels. *Polymer* **2022**, *245*, 124683.

(38) Hagita, K.; Murashima, T. Multi-Ring Configurations and Penetration of Linear Chains into Rings on Bonded Ring Systems and Polycatenanes in Linear Chain Matrices. *Polymer* **2021**, *223*, 123705.

(39) Ebe, M.; Soga, A.; Fujiwara, K.; Ree, B. J.; Marubayashi, H.; Hagita, K.; Imasaki, A.; Baba, M.; Yamamoto, T.; Tajima, K.; Deguchi, T.; Jinnai, H.; Isono, T.; Satoh, T. Rotaxane Formation of Multicyclic Polydimethylsiloxane in a Silicone Network: A Step toward Constructing "Macro-Rotaxanes" from High-Molecular-Weight Axle and Wheel Components. *Angew. Chem. Int. Ed.* **2023**, *62*, e202304493.

(40) Choi, T. L.; Grubbs, R. H. Controlled Living Ring-Opening-Metathesis Polymerization by a Fast-Initiating Ruthenium Catalyst. *Angew. Chem. Int. Ed.* **2003**, *42*, 1743–1746.

(41) Kavitha, A. A.; Singha, N. K. Smart "All Acrylate" ABA Triblock Copolymer Bearing Reactive Functionality via Atom Transfer Radical Polymerization (ATRP): Demonstration of a "Click Reaction" in Thermoreversible Property. *Macromolecules* **2010**, *43*, 3193–3205.

(42) Fukazawa, J.; Takegoshi, K. Phase Covariance in NMR Signal. *Phys. Chem. Chem. Phys.* **2010**, *12*, 11225–11227.

(43) Harrisson, S.; Whitfield, R.; Anastasaki, A.; Matyjaszewski, K. Atom Transfer Radical Polymerization. *Nat. Rev. Methods Prim.* **2025**, *5*, 2.

(44) Chang, D.; Li, T.; Li, L.; Jakowski, J.; Huang, J.; Keum, J. K.; Lee, B.; Bonnesen, P. V.; Zhou, M.; Garashchuk, S.; Sumpter, B. G.; Hong, K. Selectively Deuterated Poly(ε-caprolactone)s: Synthesis and Isotope Effects on the Crystal Structures and Properties. *Macromolecules* **2018**, *51*, 9393–9404.

(45) Chremos, A.; Jeong, C.; Douglas, J. F. Influence of polymer architectures on diffusion in unentangled polymer melts. *Soft Matter* **2017**, *13*, 5778–5784.

(46) Daoud, M.; Cotton, J. P. Star shaped polymers: a model for the conformation and its concentration dependence. *J. Phys. (Paris)* **1982**, *43*, 531–538.

(47) Suzuki, T.; Yamamoto, T.; Tezuka, Y. Constructing a Macromolecular K3,3 Graph through Electrostatic Self-Assembly and Covalent Fixation with a Dendritic Polymer Precursor. *J. Am. Chem. Soc.* **2014**, *136*, 10148–10155.

(48) Hayashi, H.; Flory, P. J.; Wignall, G. D. Configuration of the Polyisobutylene Chain according to Neutron and X-ray Scattering *Macromolecules* **1983**, *16*, 1328–1335

(49) Brown, H. R.; Wignall, G. D. A SANS Study of the Dimensions of Polystyrene Formed by Freeze-Drying from Dilute Solution. *Macromolecules* **1990**, *23*, 683–685.

(50) Cotton, J. P.; Farnoux, B.; Jannink, G.; Decker, D.; Benoit, H.; Picot, C.; Higgins, J.; Ober, R.; des Cloizeaux, J. Conformation of Polymer Chain in the Bulk. *Macromolecules* **1974**, *7*, 863–872.

(51) Hur, K.; Jeong, C.; Winkler, R. G.; Lacevic, N.; Gee, R. H.; Yoon, D. Y. Chain Dynamics of Ring and Linear Polyethylene Melts from Molecular Dynamics Simulations. *Macromolecules* **2011**, *44*, 2311–2315.

(52) Deguchi, T.; Uehara, E. Statistical and Dynamical Properties of Topological Polymers with Graphs and Ring Polymers with Knots. *Polymers* **2017**, *9*, 13–15.

(53) Cantarella, J.; Deguchi, T.; Shonkwiler, C.; Uehara, E. Radius of Gyration, Contraction Factors, and Subdivisions of Topological Polymers. *J. Phys. A Math. Theor.* **2022**, *55* 475202.

(54) Fetters, L. J.; Lohse, D. J.; Richter, D.; Witten, T. A.; Zirkel, A. Connection between Polymer Molecular Weight, Density, Chain Dimensions, and Melt Viscoelastic Properties. *Macromolecules* **1994**, *27* , 4639–4647.

(55) Cantarella, J.; Deguchi, T.; Shonkwiler, C.; Uehara, E. Factoring the Laplacian to Understand Topological Polymers. *Europhys. Lett.* **2025**, *152*, 12001.

(56) Tomiyoshi, Y.; Honda, T.; Kawakatsu, T.; Murashima, T.; Uehara, E.; Deguchi, T. Density Functional Theory for Cyclic Block Copolymer Melts. *Macromolecules* **2024**, *57*, 10704–10716.

(57) Torikai, N.; Takabayashi, N.; Noda, I.; Suzuki, J.; Matsushita, Y. Chain Dimensions of Polystyrenes Diluted with Low Molecular Weight Homologues. *J. Phys. Chem. Solids* **1999**, *60*, 1325–1328.

(58) Torikai, N.; Takabayashi, N.; Suzuki, J.; Noda, I.; Matsushita, Y. SANS Study on Chain Dimension of Polystyrenes Diluted with Low Molecular-Weight Homologues in Semi-Dilute Solutions. *Polymer* **2013**, *54*, 929–934.

(59) Quan, X.; Koberstein, J. T. Theoretical Aspects of Small-angle Neutron Scattering from Multiphase Polymers. *J. Polym. Sci. Part B Polym. Phys.* **1987**, *25*, 1381–1394.

(60) Ferry, J. D. *Viscoelastic Properties of Polymers*; John Wiley & Sons, 1980.

(61) Hagita, K.; Murashima, T.; Jinnai, H. Demonstration of Reinforcement in Polymer Composite with Rings Penetrating the Diamond-Lattice Network. *Polymer* **2022**, *243*, 124637.

4.6. Supporting information

Kratky plots for the Gaussian model of rosette polymer

Form factor of a polymer expressed with resistance distance

The author defines the form factor $P(q)$ of a topological polymer consisting of N segments by

$$P(q)= \frac{1}{N^2} \sum_{j,\,k=1}^{N} \langle \exp(iq\cdot r_{jk}) \rangle$$

The symbol $\langle A \rangle$ denotes the ensemble average quantity A over the conformations of the polymer and r_{jk} the difference of position vectors R_j and R_k as $r_{jk} = R_k - R_j$, where R_j and R_k are the position vectors of the jth and kth segments, respectively. For Gaussian chains, the author calculates the expectation value of the exponential of the inner product between wave vector q and the deviation of the difference of position vectors Δr_{jk} as

$$\langle \exp\left(iq\cdot r_{jk}\right) \rangle = \langle \exp\left(iq\cdot \Delta r_{jk}\right) \rangle$$

$$= \exp\left(-\frac{1}{2}\sum_{\alpha} q_{\alpha}^2 \langle (\Delta r_{jk}^{\alpha})^2 \rangle\right.$$

Here r_{jk}^{α} denotes the α-component of r_{jk}: $(r_{jk})^{\alpha} = r_{jk}^{\alpha}$ for $\alpha = x, y$ and z.

The author can show that the mean-square deviations of the difference of position vectors is expressed in terms of resistance distance Ω_{jk} between the jth and kth segments

$$\langle (\Delta r_{jk}^{\alpha})^2 \rangle = \frac{b^2}{3} \Omega_{jk} \text{ for } x, y, z,$$

where b_i^2 the mean square of bond length. Thus, the author expresses the ensemble average of the exponential in terms of the resistance distance

$$\langle \exp\left(iq\cdot \mathrm{r_{jk}}\right) \rangle = \exp\left(-\frac{1}{6} q^2 b^2 \Omega_{jk}\right)$$

And the author obtains the following formula (see references (1) and (2))

$$P(q)= \frac{1}{N^2} \sum_{j,k=1}^{N} (-\frac{1}{6} q^2 b^2 \Omega_{jk})$$

Form factor of multicyclic polymers

The author denotes by $P_{sc}(q)$ the form factor of monocycle polymer.

$$P_{sc}(q)= \int_0^1 \int_0^1 dxdy \exp(-\frac{q^2}{6} nb^2 |x\text{-}y|(1-|x\text{-}y|))$$

The author denote by $P_{ic}(q)$ the contribution from two different loops to the form factor. It is expressed as follows.

$$P_{ic}(q) = \int_0^1 \int_0^1 dxdy \exp(-\frac{q^2}{6} nb^2 (x(1-x) + y(1-y))$$

The form factor of the multicyclic polymer with m loops is given by

$$P_{mc}(q) = \frac{1}{m} P_{sc}(q) + \frac{m-1}{m} P_{ic}(q)$$

References

(1) Cantarella, J.; Deguchi, T.; Shonkwiler, C.; Uehara, E. Factoring the Laplacian to Understand Topological Polymers. *Europhys. Lett.* **2025**, *152*, 12001. https://doi.org/10.1209/0295-5075/ae082a.

(2) Tomiyoshi, Y.; Honda, T.; Kawakatsu, T.; Murashima, T.; Uehara, E.; Deguchi, T. Density Functional Theory for Cyclic Block Copolymer Melts. *Macromolecules* **2024**, *57*, 10704–10716. https://doi.org/10.1021/acs.macromol.4c02003.

Chapter 5

Conclusions

In this dissertation, the author established a cyclopolymerization-based synthetic platform that enables precise and systematic preparation of multicyclic polystyrenes (mc-PS) and PS-containing multicyclic copolymers, in which both the ring size and the number of cyclic units can be independently controlled. Using this platform, the author systematically synthesized a series of mc-PS samples that significantly extend the accessible range of both the number and size of cyclic units beyond those reported previously. Compared to earlier approaches that rely on multistep synthetic sequences, the present method affords these multicyclic architectures in a highly efficient and straightforward manner. PS itself is a benchmark material in polymer physics and an industrially important polymer species, underscoring the broad relevance of the developed synthetic platform. Consequently, this platform provides a robust basis for systematic investigations of structure–property relationships in multicyclic architectures, a regime that has remained largely unexplored due to the lack of well-defined samples with independently tunable topological parameters. In a broader context, the insights obtained in this work are expected to facilitate the rational design and development of functional materials that exploit the unique topological features of multicyclic polymers. A summary of the important achievements and findings in the present study is as follows:

Chapter 2 established systematic synthesis of mc-PS and PS-containing multicyclic copolymers via the cyclopolymerization of α,ω-dinorbornenyl end-functionalized macromonomers. Owing to the high efficiency of the cyclopolymerization reaction, the author systematically synthesized a series of mc-PSs, achieving the highest reported number of cyclic units (239) and molecular weight of cyclic units (52 100). Furthermore, the author successfully

synthesized multicyclic copolymers composed of PS and poly(*rac*-lactide) with various architectures via the cyclopolymerization of block copolymer-type macromonomers or the cyclocopolymerization of two macromonomers.

Chapter 3 investigated how multicyclic polymer topology influences the structural and physical properties of materials by systematically comparing mc-PS with its acyclic counterpart, graft PS (g-PS). It was found that mc-PS exhibits a higher glass transition temperature and degradation temperature, a smaller hydrodynamic volume, a lower intrinsic viscosity, and a larger apparent Kuhn length than g-PS. Moreover, solution scattering analyses revealed that, as the number of cyclic units increases, the coil conformation of mc-PS undergoes a characteristic transition from a more spherical to a more cylindrical shape, and this topology-dependent trend is essentially the same as that observed for g-PS.

Chapter 4 first examined the improvement in the macromonomer synthesis protocol, which lowered the experimental barrier to producing mc-PS samples and thus enabled a more extensive and systematic investigation of topology-dependent physical properties. On the basis of this advance, Chapter 4 established a versatile experimental platform combining cyclopolymerization and structural analysis to prepare both hydrogenated mc-PS and deuterated multicyclic polystyrenes (mc-dPS). Their structural characteristics were then systematically examined by small-angle neutron scattering in both the neat bulk state and blends with linear PS. In the neat bulk state, mc-PS exhibited smaller radii of gyration than linear and monocyclic analogues of comparable molecular weight, demonstrating enhanced chain compaction arising from the multicyclic topology. Comparison with a Gaussian-chain rosette model indicated that

excluded-volume interactions remain partially unscreened in the bulk. In blends with linear polymers, mc-PS showed ring-size-dependent swelling: expansion was observed only when the ring size exceeded the entanglement molecular weight of linear PS, and the degree of swelling increased with the number of cyclic units.

Chapters 3 and 4 examine complementary regimes of the number of cyclic units in mc-PS. Chapter 3 focuses on the high-cyclic-unit regime, in which mc-PS adopts a more cylindrical coil conformation, whereas Chapter 4 centers on the low-cyclic-unit regime, where mc-PS remains essentially spherical. Taken together, these chapters provide a unified understanding of how multicyclic topology governs both the chain structure and physical properties of mc-PS across the entire range of cyclic-unit numbers.

In conclusion, the author established a systematic synthetic platform for well-defined PS-based multicyclic polymers and elucidated how their multicyclic topology governs the structure and physical properties of the resulting materials. To date, most studies on multicyclic polymers have remained largely at the level of academic curiosity. In particular, despite the central role of PS as both a benchmark material in polymer physics and an industrially important commodity polymer, no systematic synthetic framework had been available for well-defined PS-based multicyclic polymers, nor had there been any comprehensive investigation of how their physical properties depend on the number and size of the cyclic units. This study established a new fundamental foundation for both the synthesis and characterization of multicyclic polymers, while also providing a practical pathway toward the development of advanced functional materials that actively exploit multicyclic topology as a design parameter.

From a materials perspective, Chapter 3 found that multicyclic topology offers a practical handle to tune key thermal and solution properties within an identical polystyrene chemistry. In particular, mc-PS exhibits an elevated glass-transition temperature and enhanced resistance to the onset of thermal degradation. Moreover, the lower intrinsic viscosity suggests potential advantages for solution-based processes that require low viscosity at a given polymer concentration, such as coating applications. Multicyclic–linear chain threading observed in Chapter 4 suggests that multicyclic polymers could serve as topology-defined physical crosslinkers in polymer matrices. In particular, Chapter 4 further demonstrated that the number of linear chains penetrating each ring unit was demonstrated to increase with the number of cyclic units, implying that the effective density of physical crosslinks may be tunable via the number of cyclic units, providing a practical handle to adjust network-like constraints without changing chemical composition. Overall, the author believes that the concepts and methodologies developed in this dissertation will provide a versatile platform for future explorations of topology-driven phenomena in polymers and for translating multicyclic architectures into practical applications.